Entomology in Focus 1

Cláudia P. Ferreira
Wesley A.C. Godoy *Editors*

Ecological Modelling Applied to Entomology

Entomology in Focus

Volume 1

Series Editor

Fernando L. Cônsoli
Piracicaba, Brazil

This series features volumes of selected contributions from workshops and conferences in all areas of current research activity in applied mathematics. Besides an overall evaluation, at the hands of the publisher, of the interest, scientific quality, and timeliness of each proposal, every individual contribution is refereed to standards comparable to those of leading mathematics journals. This series thus proposes to the research community well-edited and authoritative reports on newest developments in the most interesting and promising areas of mathematical research today.

More information about this series at http://www.springer.com/series/10465

Cláudia P. Ferreira • Wesley A.C. Godoy
Editors

Ecological Modelling Applied to Entomology

Springer

Editors
Cláudia P. Ferreira
Departamento de Bioestatistica
Instituto de Biociências
Universidade Estadual Paulista
Botucatu, São Paulo, Brazil

Wesley A.C. Godoy
Departamento de Entomologia e Acarologia
Escola Superior de Agricultura
"Luiz de Queiroz"
Universidade de São Paulo
Piracicaba, São Paulo, Brazil

Additional material to this book can be downloaded from http://extras.springer.com

ISBN 978-3-319-06876-3 ISBN 978-3-319-06877-0 (eBook)
DOI 10.1007/978-3-319-06877-0
Springer Cham Heidelberg New York Dordrecht London

Library of Congress Control Number: 2014953586

Printed on acid-free paper

Springer is part of Springer Science+Business Media (www.springer.com)

Preface

In recent decades, entomologists have expanded their analytical tools to improve the interface between population theory and ways to analyse and interpret results in research programs that emphasise mathematical modelling. Entomology is a fruitful area for investigating complex processes and dynamic systems due to the biological characteristics exhibited by insects. They experience different life phases, frequent notable interactions, and are classified by intraspecific to trophic relationships with different degrees of association. The Neotropical ecozone is one of the eight major zoogeographical areas of the world, which contains about a third of the world's insects that live in complex topographical environments. This condition likely allowed these organisms to experience different levels of adaptation to face the diversity of factors influencing their demography. The changes that occurred in these environments have substantially altered the resource sources for insects, especially food availability. The predominance of monocultures in Neotropical areas has remarkably impacted the environment and substantially changed the structure of insect fauna by providing suitable conditions for infestation by pests. Accelerated urbanisation processes have also negatively impacted the urban scenarios, including giving rise to the emergence of infra-structural problems in the metropolis and inducing the proliferation of vector insects of serious diseases. Given the extensive problems facing humanity, we live in what could be called the era of challenge and exploding information. Concurrently, thanks to growing interest in developing models, ample opportunities to generate and explore data have quickly been created by theorists, statisticians and entomologists, who can analyse data with precise tools, particularly when ecological methodologies are applied to entomology. The computational resources currently available are far superior to what was available in the past, thus allowing bold designs that can consider space and time simultaneously, especially in interface areas such as ecological modelling. The use of mathematical models to describe ecological processes and predict tendencies has been increasing in the last decades in response to growing demand for analytical tools that are compatible with emerging issues in the previous

and current centuries. Comprehending basic population or community functions using ecological formalism can lead to useful models embedded in ecological theory that are capable of covering a wide spectrum of issues, ranging from spatio-temporal ecological patterns of populations and/or communities to epidemiological aspects or trophic webs. This is a pioneering work in a specific area with interesting interfaces for people interested in interdisciplinary studies. We hope that it will be useful for a significant number of researchers and students involved with insect population dynamics emphasising pest management and conservation. The authors of this book thank Fundação de Amparo à Pesquisa do Estado de São Paulo FAPESP and Conselho Nacional de Desenvolvimento Científico e Tecnológico CNPq for the support with the research projects.

Botucatu, SP, Brazil Claudia P. Ferreira
Piracicaba, SP, Brazil Wesley A.C. Godoy

Contents

1 Insects and the Ecological Basis for Mathematical Modelling 1
Claudia P. Ferreira and Wesley A.C. Godoy

2 Demographic Processes in Spatially Structured Host-Parasitoid Systems 11
Carolina Reigada, Marcus Aloizio Martinez de Aguiar, and Lucas Dias Fernandes

3 Abiotic Effects on Population Dynamics of Mosquitoes and Their Influence on Dengue Transmission 39
Hyun Mo Yang, José Luiz Boldrini, Artur Cesar Fassoni, Karla Katerine Barboza de Lima, Luiz Fernando Souza Freitas, Miller Ceron Gomez, Valmir Roberto Andrade, and André Ricardo Ribas Freitas

4 Modelling the Implications of Temperature on the Life Cycle of *Aedes aegypti* Mosquitoes 81
Marcelo Margon Rossi, Lêuda Ólivêr, and Eduardo Massad

5 Predictive Modelling of Insect Metacommunities in Biomonitoring of Aquatic Networks 109
Tadeu Siqueira, Lucas Danilo Durães, and Fabio de Oliveira Roque

6 Modeling Trophic Interactions in Insect Population Dynamics 127
Michel Iskin da Silveira Costa and Lucas Del Bianco Faria

7 Coupled Map Lattice Model for Insects and Spreadable Substances 141
Luiz Alberto D. Rodrigues, Maria C. Varriale, Wesley A.C. Godoy, and Diomar C. Mistro

8 Computational Methods for Accurate Evaluation of Pest Insect Population Size 171
Natalia Petrovskaya and Nina Embleton

9 Models for Overdispersed Data in Entomology 219
Clarice G.B. Demétrio, John Hinde, and Rafael A. Moral

Index 261

Chapter 1
Insects and the Ecological Basis for Mathematical Modelling

Claudia P. Ferreira and Wesley A.C. Godoy

Abstract This book brings together nine chapters that aim to present the most recent research on the interface between ecological modelling and entomology. The chapters are summaries of research performed in different Brazilian institutions, UK and Ireland universities. The idea of the book is to present different focuses of study by aggregating theoretical ecology and applications in agricultural and medical entomology, also emphasising pest management and conservation. This chapter briefly summarises a history of the population theory applied to entomology and will introduce the reader to the topics developed in the following chapters.

Keywords Entomology • Insect population modelling

1.1 Introduction

Insects are fascinating organisms that have suffered evolutionary adaptations over geologic periods. Their extraordinary stages of evolution have provided them with special characteristics to occupy different habitats and to face a variety of environmental conditions (Carpenter 1953). Due to this flexibility, insects have been able to develop specific abilities and strategies for exploiting resources to guarantee their survival even in adverse conditions. They are advantageous to humans in various contexts. For example, there are insect species that act as natural enemies of pests, that yield products beneficial to humans, such as the honey bee and silkworm, and that can be used as forensic indicators, biotherapy and food (Goldsmith et al. 2005; Parnés and Lagan 2007; Wells and Stevens 2008; Srinivasan 2010; van Huis 2012). However, although these organisms exhibit interesting mechanisms of

C.P. Ferreira
Departamento de Bioestatistica, Instituto de Biociências, Universidade Estadual Paulista, Botucatu, São Paulo, Brazil
e-mail: pio@ibb.unesp.br

W.A.C. Godoy (✉)
Departamento de Entomologia e Acarologia, Escola Superior de Agricultura "Luiz de Queiroz", Universidade de São Paulo, Piracicaba, São Paulo, Brazil
e-mail: wacgodoy@usp.br

C.P. Ferreira, W.A.C. Godoy (eds.), *Ecological Modelling Applied to Entomology*, Entomology in Focus 1, DOI 10.1007/978-3-319-06877-0_1

adaptation that have important ecological roles and are beneficial for humans, they have also displayed a high capacity for increasing their population sizes, mainly in systems with a high food availability, such as forests, crops, terrestrial and aquatic environments, or even animal hosts. A high density of insects could severely damage growing crops and cause epidemics, host infestations and a trophic imbalance with negative consequences for conservation (Lima et al. 2009).

1.2 Insects and Their Evolutionary Strategies

Evolutionary strategies in insects have been classified according to the bioecological characteristics, which involve relevant factors such as body size, egg size, development rate, fecundity, longevity, sex ratio, dispersal ability and density dependence (Speight et al. 2008). These strategies could be understood as responses to evolutionary pressures to attain the best species performance and involves striking a balance between costs and benefits (Harrison et al. 2010). The best performance usually involves a high magnitude of fecundity (Awmack and Leather 2002) which is mediated nevertheless by density-dependent mechanisms. This observation could be understood as optimisation, ecologically expressed by *r*- or *K*-strategy. This is a theory that describes different strategies by combining traits in an attempt to obtain the best advantage by confronting parental investment and the quantity and quality of offspring (Pianka 1970). Generally, species governed by *r*-selection invest in many offspring, whereas *k*-strategists focus theirs on a few (Pianka 1970). Conversely, *r*-selected insect populations are unpredictable in their ecological trends, where the cycles they experience over time depend on the demographic parameters of fecundity and survival. Occasionally, an overexploitation of resources will encourage populations to invade new areas (Davis et al. 2005). Insects viewed as *k*-strategists are frequently regulated by density-dependent factors and have a low fecundity (Matthews and Matthews 1978).

The movement of insects among different areas may be viewed according to different perspectives and perhaps more appropriately classified into two basic types: passive and active (Yates and Boyce 2012). The passive type has highlighted the need for studies that emphasise phytogeography history, demography and population dynamics mainly due to changing dynamic patterns in human movement (Jones 2001; Bentley et al. 2012; Fresia et al. 2013). The benefits of modern transportation, the economic growth of emerging countries and globalisation have facilitated the transport of several items for human consumption, including organic products, such as seeds, seedlings, cereal, fruits, meat, and many others (Bentley et al. 2012; Hu et al. 2013). In response to this increasing transport of items, several pest species have invaded new areas and frequently cause problems for the new environments or hosts (Mazzi and Dorn 2012).

1.3 Insects and the Climate Changes

Global warming has also exerted a significant influence on the distribution of species around the world, with negative impacts on conservation, agriculture and public health (Ferron and Deguine 2005; Kiritani 2006; Andrew and Hughes 2007). Noticeably, insect species living in areas with predominantly high temperatures are stimulated to leave their origin regions to new areas, with similar temperatures, that were previously not inhabited by these species (Ammunet et al. 2011). The implications of climate change for people and the environment are unpredictable, but the dynamics of diseases transmitted by insects is a relevant concern that is shared among nations worldwide. Malaria afflicts more than a billion of people and causes 2 million deaths per year (WHO 2011a, b). Dengue fever infects 100 million people annually (WHO 2011a). Vector mosquitoes have developed a significant resistance to insecticides, which decreases the efficiency of the methods used to control these disease vectors (Zaim and Guillet 2002). All of these factors underscore serious concerns about the future of global public health.

1.4 Insects and Their Responses

Resistance to insecticides is an increasing challenge currently faced by chemical manufacturers. The use of chemical products without criteria, as well as the widespread use of insecticides throughout the world, has increased the resistance to different product classes (Carvalho et al. 2013). New chemical formulations have been proposed as an attempt to increase the efficiency of products (Casida and Durkin 2013). However, product toxicity for the environment, animals and humans is a serious consequence for social welfare in addition to the high costs for growers (Isman 2006). Transgenic crops represent a part of the modern agricultural strategy to combat pest attacks (Kos et al. 2009) and consist of plants that are genetically engineered to produce insecticidal proteins encoded by *Bacillus thuringiensis* (Bt) genes (Shelton et al. 2002). More Bt crops are employed worldwide today than 15 years ago and are housed on more than 420 million hectares (Tabashnik et al. 2013). These observations are interesting, but their implications for an invasion of secondary pests over time remains to be evaluated (Qiu 2010). Perhaps the greatest challenge for the coming decades is to reconcile the rising needs of the fight against vector-borne disease and devastating agricultural pests with biological conservation. This would open new perspectives for optimising technology and various strategies to appropriately apply modern synthetic insecticides, biological control agents, botanical insecticides, pheromones, insect growth regulators, genetic manipulation of pest species, host-plant resistance, and cultural techniques for organic farming and intercropping (Kogan and Jepson 2007; Thacker 2002).

1.5 Insects and the Numbers

The population pest density frequently reaches outbreak levels that pose considerable economic and environmental impacts to agriculture, forests and to human health around the world (Perveen 2012). Much of the variability in insect pest population density may be attributed to several density-dependent or independent mechanisms, including interacting effects with weather or natural enemies (Bommarco et al. 2007). Despite the considerable number of recent studies on ecology and population dynamics in insects (Liebhold and Tobin 2008), more quantitative and qualitative information is required to generate different possible analytical approaches. Empirical approaches may increase the knowledge about ecological patterns implicit in population dynamics of pest species and create a database of proposed strategies for control that consider the risks arising from the previously mentioned factors (Ives and Schellhorn 2011).

Dealing with quantitative data requires appropriate analytical tools that come mainly from computation, mathematics and statistics. Ecological modelling is an essential part of both research and management of pest insects and is the major tool for predicting population dynamics. The history of mathematical modelling in insects begins with the conventional steps that exist for biological scenarios, i.e., abstraction and subsequent proposition of theoretical models, which, although considered simple, are capable of retaining the most important ingredients of population change (Murray 2001). Models of this nature, which have existed for more than a century, express mathematical functions capable of describing the shape of the ecological patterns of time series, such as the paper by Benjamin Gompertz that emphasises the law of human mortality (Gompertz 1825). Simple models, such as the Verhulst model (Verhulst 1838) for population growth, have bolstered more sophisticated formulations, which have improved by adding important mechanisms that make the model more realistic by including delayed density-dependence, interspecific and trophic interactions, age or stage structure, spatial dimension, stochasticity and control strategies (Bascompte and Sole 1998; Murray 2001; Lima et al. 2009; Rosenheim 2011).

1.6 Insects and Their Interactions

The structure of insect populations and communities includes complex relationships that express different types of interactions, such as intra and interspecific competition, cannibalism, predation, parasitism, commensalism, and a variety of relationships with the environment (Felton and Tumlinson 2008; Polis 1991). On one hand, modelling insect populations is a challenge because life cycles are complex and involve lags that produce a strong dependence between life stages

mainly in species that exhibit non-overlapping generations (Hassell et al. 1976). On the other hand, there are species that overlap generations, and thus, the systems exhibit reproductive patterns similar to mammals. In both cases, two different types of equations are required to describe the system dynamics: one for non-overlapping populations and one for overlapping populations (Edelstein-Keshet 1978). However, insect life cycles are shorter than those of vertebrates or even perennial plants, and some of them are easily reared in the laboratory, which encourages experimentation and mathematical modelling (Cushing et al. 2003).

1.7 Insects and the Models

Verhulst (1838), Thompson (1924), Lotka (1925) and Volterra (1926) are the precursors of ecological theory, which was the basis for the first mathematical models presented to study populations and interactions between species of arthropods (Hassel 1978). Subsequently, Nicholson (1933) and Nicholson and Bailey (1935) proposed the first models to investigate prey-predator interactions, which served as a great foundation for host-parasitoid models. The studies performed by Nicholson (1954, 1957) provided long-term laboratory series that focused on the population dynamics of *Lucilia cuprina* (Diptera: Calliphoridae) to investigate effects of resource scarcity at different life stages. The results obtained described a series with quasi-cycles and have been widely revisited by ecologists, such as the paper by Gurney et al. (1980) entitled "Nicholson's blowflies revisited".

In 1985, Prout and McChesney (1985) published an interesting and useful discrete time mathematical formulation that considered the delay effect on fecundity and survival of competition during the larval stage of *Drosophila melanogaster* to demonstrate how the functions of larval density, fecundity and survival can influence the dynamic behaviour of populations in the laboratory (Prout and McChesney 1985). This theory has been widely used to model blowfly populations in a biological invasion scenario (Serra et al. 2007; Coutinho et al. 2012; Moretti et al. 2013).

James Carey (1993) provided an extremely important contribution for the application of statistics and ecological theory to entomology. Carey presented important demographic methods to study life tables in insect populations. Dennis et al. (1995) initiated an era of notable papers by proposing the LPA model, which is designed to combine theory and experimentation to investigate ecological equilibrium patterns in *Tribolium castaneum* by considering different life stages, such as larva, pupa and adult. A textbook entitled "Chaos in ecology: experimental nonlinear dynamics" is a nice compilation of the mechanisms of population growth, nonlinear stage-structured population models, and chaos in ecology.

1.8 This Book

In the current book, we present a compilation of studies that are at the interface between mathematical modelling and entomology. Our proposal presents models constructed to study different types of insects in distinct habitats and scenarios to demonstrate how the theory can be used as a powerful tool to describe ecological patterns and project tendencies. The next eight chapters will present an overview of different ecological modelling applications, emphasising agricultural, medical entomology and conservation.

The chapters describe a synthesis of the most recent research developed in several Brazilian research institutions and also in three universities in the United Kingdom and Ireland. A spatially explicit model is presented in Chap. 2 that assumes density-dependent effects during pre- and post-dispersal in a host-parasitoid system. The model reveals that behaviour may influence the spatial distribution and the abundance of species in the landscape. Chapters 3 and 4 focus on how abiotic factors affect the life cycle and population dynamics of mosquitoes with consequences for dengue transmission. Chapter 3 presents a mathematical model to evaluate parameters dependent on temperature and that are significantly influenced by rainfall. The model assumes that seasonality causes the varying population size and simulates a coupling of mosquitoes and humans to assess the transmission of dengue virus. In the fourth chapter, a mathematical model describes the influences of temperature on *A. aegypti* life stages by characterising transitions and death rates as a function of temperature. With this formalism, they also describe the influence of the temperature on dengue transmission.

In the fifth chapter, metacommunity models are used to investigate the geometry of riverine networks, emphasising aquatic insects. The authors show that the strength of the environmental impact, the spatial position of the impact within the network and the degree of dispersal among local communities can severely affect the performance of statistical models regularly employed in biomonitoring programs. Chapter 6 provides insights into how to represent trophic interactions by using different models that consider semelparity and iteroparity and demonstrate the relevance of the interaction strength in determining food web dynamics. Chapter 7 presents coupled map lattices to study the spatio-temporal insect dynamics. The lattices consider natural degradation as well as dynamics affected by chemical substances or volatiles that move by diffusion and advection due to the wind. The proposal to use coupled map lattices aimed to analyse the effects of the insect behavioural response on their density, distribution and persistence. Chapter 8 proposes an important strategy for pest management programs by presenting a mathematical formalism for monitoring pest abundance in agricultural fields. A mathematical background for methods of numerical integration is provided and application of numerical integration in the pest monitoring procedure is discussed to demonstrate this proposal. The ninth chapter delineates how to model overdispersed data in typical entomological scenarios, mainly when outcomes of interest are in the

form of counts or proportions. As a foundation for the model, the authors discuss possible causes for overdispersion in insects and use different approaches to analyse distinct ecological patterns of distribution.

References

Ammunet T, Klemola T, Saikkonen K (2011) Impact of host plant quality on geometrid moth expansion on environmental and local population scales. Ecography 34:848–855

Andrew NR, Hughes L (2007) Potential host colonization by insect herbivores in a warmer climate: a transplant experiment. Glob Change Biol 13:1539–1549

Awmack CS, Leather SR (2002) Host plant quality and fecundity in herbivorous insects. Annu Rev Entomol 47:817–844

Bascompte J, Sole RV (1998) Spatiotemporal patterns in nature. Trends Ecol Evol 13:173–174

Bentley JW, Robson M, Sibale BB et al (2012) Travelling companions: emerging diseases of people, animals and plants along the Malawi-Mozambique border. Hum Ecol 40:557–569

Bommarco R, Firle SO, Ekbom B (2007) Outbreak suppression by predators depends on spatial distribution of prey. Ecol Model 201:163–170

Carey JR (1993) Applied demography for biologists: with special emphasis on insects. Oxford University Press, New York

Carpenter FM (1953) The geological history and evolution of insects. Am Sci 41:256–270. Annu Rev Entomol 47:817–844

Carvalho RA, Omoto C, Field LM et al (2013) Investigating the molecular mechanisms of organophosphate and pyrethroid resistance in the fall armyworm *Spodoptera frugiperda*. Plos One 8:e62268. doi:10.1371/journal.pone.0062268

Casida JE, Durkin KA (2013) Neuroactive insecticides: targets, selectivity, resistance, and secondary effects. Annu Rev Entomol 58:99–117

Coutinho RM, Godoy WAC, Kraenkel RA (2012) Integrodifference model for blowfly invasion. Theor Ecol 5:363–371

Cushing JM, Costantino RF, Dennis B et al (2003) Chaos in ecology: experimental nonlinear dynamics. Academic, San Diego

Davis MA, Thompson K, Grime JP (2005) Invasibility: the local mechanism driving community assembly and species diversity. Ecography 28:696–704

Dennis BR, Desharnais A, Cushing JM et al (1995) Nonlinear demographic dynamics: mathematical models, statistical methods and biological experiments. Ecol Monogr 65:261–281

Edelstein-Keshet L (1978) Mathematical models in biology. Princeton University Press, Princeton

Felton GW, Tumlinson JH (2008) Plant-insect dialogs: complex interactions at the plant-insect interface. Curr Opin Plant Biol 11:457–463

Ferron P, Deguine JP (2005) Crop protection, biological control, habitat management and integrated farming, a review. Agron Sustain Dev 25:17–24

Fresia P, Azeredo-Espin AML, Lyra ML (2013) The phylogeographic history of the new world screwworm fly, inferred by approximate Bayesian computation analysis. Plos One 8:e76168. doi:10.1371/journal.pone.0076168

Goldsmith MR, Shimada T, Abe H (2005) The genetics and genomics of the silkworm, *Bombyx mori*. Annu Rev Entomol 50:71–100

Gompertz B (1825) On the nature of the function expressive of the law of human mortality, and on a new mode of determining the value of life contingencies. Philos Trans R Soc Lond 115:513–585

Gurney WSC, Blythe SP, Nisbet RM (1980) Nicholson's blowflies revisited. Nature 287:17–21

Harrison JF, Kaiser A, VandenBrooks JM (2010) Atmospheric oxygen level and the evolution of insect body size. Proc R Soc B 277:1937–1946
Hassel MP (1978) The dynamics of arthropod predator-prey systems, Monographs in population biology. Princeton University Press, Princeton
Hassell MP, Lawton JH, May RM (1976) Patterns of dynamical behaviour in single species populations. J Anim Ecol 45:471–486
Hu SJ, Ning T, Fu DY et al (2013) Dispersal of the Japanese pine sawyer, *Monochamus alternatus* (Coleoptera: Cerambycidae), in mainland China as inferred from molecular data and associations to indices of human activity. Plos One 8:e57568. doi:10.371/journal.pone.0057568
Isman MB (2006) Botanical insecticides, deterrents, and repellents in modern agriculture and an increasingly regulated world. Annu Rev Entomol 51:45–66
Ives AR, Schellhorn NA (2011) Novel pests and technologies: risk assessment in agroecosystems using simple models in the face of uncertainties. Curr Opin Environ Sustain 3:100–104
Jones RE (2001) Mechanisms for locating resources in space and time: impacts on the abundance of insect herbivores. Austral Ecol 26:518–524
Kiritani K (2006) Predicting impacts of global warming on population dynamics and distribution of arthropods in Japan. Popul Ecol 48:5–12
Kogan M, Jepson P (2007) Perspectives in ecological theory and integrated pest management. Cambridge University Press, Cambridge
Kos M, van Loon JJ, Dicke M et al (2009) Transgenic plants as vital components of integrated pest management. Trends Biotechnol 27:621–627
Liebhold AM, Tobin PC (2008) Population ecology of insect invasions and their management. Annu Rev Entomol 53:387–408
Lima EABF, Ferreira CP, Godoy WAC (2009) Ecological modeling and pest population management: a possible and necessary connection in a changing world. Neotrop Entomol 38:699–707
Lotka AJ (1925) Elements of physical biology. Williams & Williams Company, Baltimore
Matthews RW, Matthews JR (1978) Insect behaviour. Wiley, New York
Mazzi D, Dorn S (2012) Movement of insect pests in agricultural landscapes. Ann Appl Biol 160:97–113
Moretti AC, Coutinho RM, Moral RA et al (2013) Quantitative and qualitative dynamics of exotic and native blowflies (Diptera: Calliphoridae) with migrations among municipalities. Community Ecol 14:249–257
Murray JD (2001) Mathematical biology, an introduction. Springer, New York
Nicholson AJ (1933) The balance of animal populations. J Anim Ecol 2:131–178
Nicholson AJ (1954) An outline of the dynamics of animal populations. Aust J Zool 2:9–65
Nicholson AJ (1957) The self adjustment of populations to change. Cold Spring Harb Symp Quant Biol 22:153–173
Nicholson AJ, Bailey VA (1935) The balance of animal populations. Part 1. Proc Zool Soc London 3:551–598
Parnés A, Lagan KM (2007) Larval therapy in wound management: a review. Int J Clin Pract 61:488–493
Perveen F (2012) Insecticides, advances in integrated pest management. InTech, Rijeka
Pianka ER (1970) On r and K selection. Am Nat 104:592–597
Polis GA (1991) Complex trophic interactions in deserts: an empirical critique of food-web theory. Am Nat 138:123–155
Prout T, McChesney F (1985) Competition among immatures affects their adult fertility: population dynamics. Am Nat 126:521–558
Qiu J (2010) GM crop use makes minor pests major problem. Nature. doi:10.1038/news.2010.242
Rosenheim JA (2011) Stochasticity in reproductive opportunity and the evolution of egg limitation in insects. Evolution 65:2300–2312
Serra H, Silva ICR, Mancera PFA et al (2007) Stochastic dynamics in exotic and native blowflies: an analysis combining laboratory experiments and a two-patch metapopulation model. Ecol Res 22:686–695

Shelton AM, Zhao JZ, Roush RT (2002) Economic, ecological, food safety, and social consequences of the deployment of Bt transgenic plants. Annu Rev Entomol 47:845–881
Speight MR, Hunter MD, Watt AD (2008) Ecology of insects: concepts and applications. Wiley-Blackwell, Oxford
Srinivasan MV (2010) Honey bees as a model for vision, perception, and cognition. Annu Rev Entomol 55:267–284
Tabashnik BE, Brévault T, Carrière Y (2013) Insect resistance to Bt crops: lessons from the first billion acres. Nat Biotechnol 31:510–521
Thacker JRM (2002) An introduction to arthropod pest control. Cambridge University Press, Cambridge
Thompson WR (1924) La theory mathematique de l'action des parasites entomophages et le facteur du hassard. Annales Faculte des Sciences de Marseille 2:69–89
van Huis A (2012) Potential of insects as food and feed in assuring food security. Annu Rev Entomol 58:563–583
Verhulst PF (1838) Notice sur la loi que la population poursuit dans son accroissement. Correspondance mathématique et physique 10:113–121
Volterra V (1926) Fluctuations in the abundance of a species considered mathematically. Nature 118:558–560
Wells JD, Stevens R (2008) Application of DNA-based methods in forensic entomology. Annu Rev Entomol 53:103–120
WHO (2011a) Global health observatory. Available at: http://apps.who.int/ghodata/?vid=110001
WHO (2011b) Malaria fact sheet. Available at: http://www.who.int/mediacentre/factsheets/fs094/en/
Yates G, Boyce MS (2012) Dispersal, animal. In: Hastings A, Gross LJ (eds) Encyclopedia of theoretical ecology. University of California Press, Berkeley
Zaim M, Guillet R (2002) Alternative insecticides: an urgent need. Trends Parasitol 18:161–163

Chapter 2
Demographic Processes in Spatially Structured Host-Parasitoid Systems

Carolina Reigada, Marcus Aloizio Martinez de Aguiar, and Lucas Dias Fernandes

Abstract We explore the demographic control effects that arise from the foraging behaviour and reproductive strategies of host-parasitoid metapopulation systems under the influence of spatio-temporal variations in patch quality. Parasitoid populations are characterised by different levels of density-dependent sex ratio adjustments and interference competition. Using a spatially explicit mathematical model, in which the habitats are described by the frequency and distribution of host resources, we assume that the species are subjected to density-dependent effects in two different periods of their life cycles: pre- and post-dispersal. During the pre-dispersal period, the number of individuals that disperse or remain in each patch depends on the species "optimal decision" to explore or to leave the current patch, which is affected by the local number of individuals. After dispersal, individuals arriving in a new patch are influenced by the local densities, which define the host survival rate and reproductive success of parasitoids. We show that different demographic control levels, which arise from species behaviour and ecological processes in response to changes in patch quality, lead to different spatial distributions and species abundance in the landscape. The results elucidate how host-parasitoid life history affects species establishment and the efficiency of parasitoids as biological control agents.

Keywords Spatial structure • Host-parasitoid dynamics • Demography • Metapopulation • Patch dynamics • Biological control • Foraging behaviour • Landscape structure • Sex ratio • Density- dependence

C. Reigada (✉) • M.A.M. de Aguiar
Universidade Estadual de Campinas, Unicamp, 13083-970 Campinas, SP, Brazil
e-mail: ca.reigada@gmail.com; aguiar@ifi.unicamp.br

L.D. Fernandes
Department of Physics, University of Aberdeen, AB24 3UE Aberdeen, UK
e-mail: lucasfernandes@abdn.ac.uk

C.P. Ferreira, W.A.C. Godoy (eds.), *Ecological Modelling Applied to Entomology*, Entomology in Focus 1, DOI 10.1007/978-3-319-06877-0_2

2.1 General Introduction

Entomologists' interest in host-parasitoid interactions increased in the beginning of the twentieth century with the possibility of using parasitoids to control insect pests (Godfray and Shimada 1999). The research developed to include several important aspects of species life history, behaviour and communities of host-parasitoid systems. More recently, efforts have also been directed to model and understand these many characteristics theoretically, guided by data obtained from experimental and field studies (Godfray and Shimada 1999; Hassell 1978, 2000).

Parasitoids depend strongly on their hosts to complete their life cycle. This vital dependence paints an extremely complex ecological interaction, and elucidating its intricacies requires understanding ecological and behavioural aspects. The density of hosts in a patch and the way they are exploited by parasitoids are governed by complex chemical, visual and tactile cues in the localisation of hosts and in the parasitoid's adaptive behaviour through learning, aiming at increasing efficiency. This complex behaviour also involves the evolution of searching strategies, clutch size and sex ratios (Godfray 1994; Bernstein and Driessen 1996; Godfray and Shimada 1999; Wajnberg 2006; Amat et al. 2009). Due to the complexity involved in host-parasitoid interactions and the difficulties in acquiring large amounts of data to test many of these processes on species dynamics, numerous mathematical models have been developed to provide insights into several aspects of parasitoid biology.

Nicholson and Bailey (1935) pioneered a simple theoretical model that describes the host-parasitoid dynamics. Although this Nicholson and Bailey (NB) model displays unstable dynamics, where host and parasitoid populations cannot coexist, the NB model is frequently used as a starting point for many theoretical studies to add more realistic aspects to host-parasitoid models (Hassell 2000). The inclusion of biological realism in the NB model involves modifications to several aspects of the problem, such as the specific way parasitism is described, the inclusion of spatial structure and forms of demographic control in host and parasitoid populations (Chesson and Murdoch 1986; Pacala and Hassel 1991; Hassell 2000).

Generally, the high rates of attack observed for many parasitoid species lead to an over-exploitation of hosts and to their local extinction, which causes the subsequent extinction of parasitoid populations. Many theoretical and empirical works have suggested that the existence of an underlying spatial structure can stabilise the host-parasitoid dynamics (Briggs and Hoopes 2004; Cronin and Reeve 2005; Kerr et al. 2006; Rauch and Bar-Yam 2006; Arashiro and Tome 2007). Other stabilising factors include processes of demographic control (e.g., host carrying capacity, parasitoid interference, invulnerable age classes, different types of functional response and non-random parasitoid attack) (Murdoch and Oaten 1975; Hassell 1978, 2000; Briggs and Hoopes 2004) and food web structure (Price 1991; Hawkins 1992). This chapter focuses on the effects of spatial structure for host-parasitoid dynamics and considers the effects of some demographic processes on species dispersal rates.

Numerous spatial models have been developed to consider spatial structure in the host-parasitoid interaction (Murray 1993; Briggs and Hoopes 2004; Hassell and May 1973; Diekmann et al. 1988; Jongejans et al. 2008). These models describe

how dispersal can change the stability and persistence of otherwise unstable host-parasitoid dynamics (Briggs and Hoopes 2004; Cronin and Reeve 2005) and how a spatial structure can lead to different spatial patterns of species distribution (Hassel et al. 1991; Briggs and Hoopes 2004; Stacey et al. 2012). However, the species response to spatial subdivision and habitat connectivity can vary according to the behaviour of the species considered. In this context, few theoretical studies have made biological contributions, such as species foraging and reproductive behaviour, on species movements across a landscape (Hassell et al. 1983; Comins and Wellings 1985; Lozano et al. 1997; Meunier and Bernstein 2002; Reigada et al. 2012).

In this study, we consider foraging behaviour, reproductive strategies and population dynamics. Specifically, we consider an adjustment in the sex ratio of offspring and mutual interference among foragers as effects of demographic control in parasitoid populations and build our model on a spatially structured framework. In Sect. 2.2, we describe our mathematical model by detailing the landscape structure, the interaction functions and the dispersal mechanisms. We started from the NB approach and then go on to show how many biological aspects can be included, such as parasitoid sex ratio control and mutual interference and density-dependent species dispersal for host-parasitoid dynamics. In Sects. 2.3 and 2.4, we review and explore the results of previous works (Reigada and de Aguiar 2012; Reigada et al. 2012) by describing the influences of habitat quality, reproductive and foraging behaviour on species demography and dispersal rates. More specifically, in Sect. 2.3, we explore the effects of landscape patches in terms of frequency and distribution of host resources on species persistence and spatial distribution. In Sect. 2.4, we analyse how sex ratio adjustment and mutual interference in parasitoid populations can result in different patterns of species distribution on the landscape. We end the chapter by discussing possible future directions in this area of research, particularly considering more complex spatial structures with different spatial arrangements of patches and their interconnections. We also comment on the inclusion of co-evolution in reproductive and foraging response dynamics, which would allow researchers to understand how species adapt to different environmental conditions.

2.2 Modelling Host-Parasitoid Dynamics with Spatial Structure

2.2.1 The Nicholson Bailey Model

One of the first mathematical models that described host-parasitoid systems was provided by Nicholson and Bailey (1935). To situate our own model within the literature, we present a brief review of this classic model in this subsection. The Nicholson Bailey (NB) model describes the evolution of populations of hosts and parasitoids at discrete generations in the form of a finite differences system of equations:

$$\begin{aligned} N_{t+1} &= F(N_t, P_t) \\ P_{t+1} &= G(N_t, P_t) \end{aligned}. \tag{2.1}$$

The subscript is an integer that indicates the generation, and it is assumed that the populations at time $t+1$ can be completely determined from the populations at time t. The functions F and G control the growth of the populations and how they interact with each other.

The most general aspect of the host-parasitoid interaction is that the adult female parasitoid lays its eggs on or in the bodies of other insects, their hosts. The parasitoid eggs hatch, and the larvae consume its host either immediately or after a delay during which the host continues to feed and grow in size. In either case, the parasitised hosts die. The three basic assumptions of the NB model are:

1. The hosts that are not parasitised give rise to the next generation of hosts;
2. The parasitised hosts die and give rise to the next generation of parasitoids;
3. The proportion of parasitised hosts depends on the encounter rate between individuals of the two populations and might also depend on the density of each population.

These assumptions allow us to write the following dynamical equations:

$$\begin{aligned} N_{t+1} &= \lambda N_t f(N_t, P_t) \\ P_{t+1} &= c P_t (1 - f(N_t, P_t)) \end{aligned}, \tag{2.2}$$

where λ is the reproduction rate of hosts, c is the number of parasitoid eggs laid per host and $f = f(N_t, P_t)$ the fraction of hosts that are not attacked. Notably, in the absence of parasitoids, $f(N_t, P_t) = 1$, and the host population increases or decreases exponentially fast if $\lambda > 1$ or $\lambda < 1$, respectively.

To complete the dynamical equations, we still have to make assumptions about the form of the term $f(N_t, P_t)$. The NB model makes the following extra assumptions:

4. The encounters between hosts and parasitoids are random and independent. They are directly proportional to each of the population densities as:

$$N_e = \alpha N_t P_t, \tag{2.3}$$

where α is a parameter related to the efficiency of parasitoid searches. The mean number of effective encounters per host is then

$$\mu = \frac{N_e}{N_t} = \alpha P_t. \tag{2.4}$$

5. The only significant encounter is the first one, and it always results in a successful attack. Subsequent encounters do not affect the host's state.

The probability of n encounters is approximated by a Poisson distribution with characteristic parameter μ, and the probability of no encounters is given by $e^{-\mu}$, which is precisely the proportion of hosts that are not attacked. The model is then given by the following equations:

$$\begin{aligned} N_{t+1} &= \lambda N_t e^{-\alpha P_t} \\ P_{t+1} &= c P_t \left(1 - e^{-\alpha P_t}\right) \end{aligned} \tag{2.5}$$

The above equations are known as the NB model, which was developed in 1935 by the biologist AJ Nicholson and the physicist VA Bailey. This system presents a non-trivial equilibrium point (non-zero population densities), which is unstable for $\lambda > 1$ and any values of the parameters α and c. Because a model in which the only equilibrium point is unstable may not be appropriate to describe realistic data, many modifications have been proposed to the NB equations, which add more accurate biological aspects to the population growth and interaction terms. Some of these aspects, such as the carrying capacity for the host's growth, presence of refuges for hosts, demographic processes operating within the interaction patches and the addition of spatial structure, can stabilise the equilibrium point. For a more detailed description of these aspects, see (Briggs and Hoopes 2004; Edelstein-Keshet 2005).

2.2.2 *Extended Spatial Model*

We now turn to the construction of a more detailed model that will allow researchers to study different aspects of the host-parasitoid interaction, including the spatial distribution of populations. The species distribution patterns in a landscape depend strongly on the fraction of emigrants and on the dispersal rates of the species among patches. Therefore, we include two processes of demographic control in our model that are provided by the interference competition and control of the offspring sex ratio. Although a more complex mathematical treatment will be required, our approach will hopefully be more realistic. By describing a larger set of species behaviours and interaction details, the equations of this new model will be constructed following the reasoning of the NB model.

The three main aspects to be explored by the new model are:

1. Space. The equations of the NB model are finite difference equations that do not describe any underlying spatial structure. These types of models, also called spatially implicit models, are useful to describe well mixed populations or interactions that are localised in one or a few small patches. In cases where the geographical distance between individuals plays a major role in the way the species interact with each other, it is important to consider the range of action and dispersal of individuals, which might be related both to the physical limitations of the landscape and to intrinsic strategies of each species. These models are typically called spatially explicit models.

2. Sex allocation. In nature, most parasitoid species exhibit a type of haplodiploid reproduction called arrhenotoky, where females are born from fertilised eggs and males from unfertilised eggs, and thus, females control the sex ratio of their offspring (Charnov 1982). In our model, we considered that arrhenotokous parasitoid populations can adjust the progeny sex ratio according to the conditions of the exploited patch. The control of the sex ratio is intrinsically connected to the patch quality, which is related to the number of conspecific foragers and to the host abundance. This is an important concept and plays a crucial role in the dynamics of the interaction, as only female parasitoids attack hosts.
3. Interference competition. Another important aspect in host density fluctuations is the way parasitoids interact with each other. Female parasitoids may detect hosts that are already parasitised and keep searching for healthy hosts. In a population with a high parasitoid density, the ability of a female to detect parasitised hosts affects its probability of laying eggs and thus introduces interference competition.

With these three aspects in mind, we define the overall habitat as a set of connected patches, where host growth is limited by the carrying capacity. The dynamics are divided into two phases: first, hosts and parasitoids interact within every patch, and subsequently, a fraction of the emerging adult hosts and female parasitoid disperse to other patches.

2.2.2.1 The Interaction Phase

$H_{i,t}$, $F_{i,t}$ and $M_{i,t}$ represent populations of hosts, female and male parasitoids in patch i at time t. The following equations represent the in-patch interactions:

$$\begin{aligned} h_{i,t+1} &= H_{i,t}\left(\frac{\lambda k}{H_{i,t}(\lambda-1)+k}\right)\left[1-p\left(H_{i,t},F_{i,t}\right)\right] \\ f_{i,t+1} &= cH_{i,t}\,p\left(H_{i,t},F_{i,t}\right)s\left(H_{i,t},F_{i,t}\right) \\ m_{i,t+1} &= cH_{i,t}\,p\left(H_{i,t},F_{i,t}\right)\left[1-s\left(H_{i,t},F_{i,t}\right)\right] \end{aligned} \quad , \tag{2.6}$$

where the lower case letters for the populations in generation $t+1$ represent the pre-dispersal populations.

For small populations, the hosts grow exponentially fast, but the growth slows down when it approaches the limit defined by the carrying capacity k. The carrying capacity represents the limited amount of resources (both food and space) available in each patch, and that prevents the populations from growing indefinitely. If resources were unlimited, $k \to \infty$ and would recover the term $\lambda H_{i,t}$, for host growth. The growth term is multiplied by $(1-p(H, F))$, where $p(H, F)$ is the fraction of hosts that are attacked by female parasitoids and might depend on the densities of both hosts and female parasitoids.

The population of parasitoids in the next generation depend on the product $H_{i,t}$ $p(H_{i,t}, F_{i,t})$ and is multiplied by c, the mean number of adult parasitoids emerging from each host (the parasitoids are assumed to be gregarious).

Finally, the function $s(H, F)$ defines the proportion of female parasitoids in the progeny and is adjusted according to the patch quality. The proportion of male parasitoids is then represented by $(1-s(H, F))$.

Starting with these general equations, we must make assumptions on the forms of the functions $p(H, F)$ and $s(H, F)$. For the fraction of parasitised hosts $p(H, F)$, we define:

$$p\left(H_{i,t}, F_{i,t}\right) = \begin{cases} 1, & \text{if} \quad \upsilon\left(H_{i,t}, F_{i,t}\right) > 1 \\ \upsilon\left(H_{i,t}, F_{i,t}\right) & \text{if} \quad \upsilon\left(H_{i,t}, F_{i,t}\right) \leq 1 \end{cases}, \tag{2.7}$$

where

$$\upsilon\left(H_{i,t}, F_{i,t}\right) = \frac{32\alpha F_{i,t}}{H_{i,t} + \beta F_{i,t}^2} \tag{2.8}$$

and α is the parasitoid attack rate.

We assume that no host can be parasitised by more than one parasitoid (superparasitism), as female parasitoids can differentiate between healthy and parasitised pupae. The parameter β controls the efficiency with which they search and recognise healthy pupae. The interference among conspecific parasitoids is classified as low ($\beta = 0.01$), medium ($\beta = 0.03$) or high ($\beta = 0.05$). A low degree of interference characterises parasitoid populations that can detect healthy hosts in a parasitoid-crowded patch efficiently, consequently causing higher host mortality than parasitoid populations with medium and high levels of response to conspecifics. The consequences of different levels of interference competition for the host population are presented in Fig. 2.1. The smaller the β value, the lower the degree of interference among conspecifics. The number 32 represents the maximum number of hosts that can be parasitised by one parasitoid in the absence of parasitoid competition.

The proportion of female parasitoids in the progeny, $s(H, F)$, is defined as

$$s\left(H_{i,t}, F_{i,t}\right) = \exp\left(-\frac{\gamma F_{i,t}}{H_{i,t}}\right), \tag{2.9}$$

where γ controls how the ratio of females to hosts affects the sex ratio adjustment. If F/H is high, a female tends to increase the proportion of males in its progeny to increase the probability that her male offspring mate with the other females in the next generation. Thus, the parameter γ is related to the sensitivity of the sex ratio control to the F/H ratio, which is related to the patch quality. In our model, parasitoid populations can exhibit three different responses to fluctuations in patch

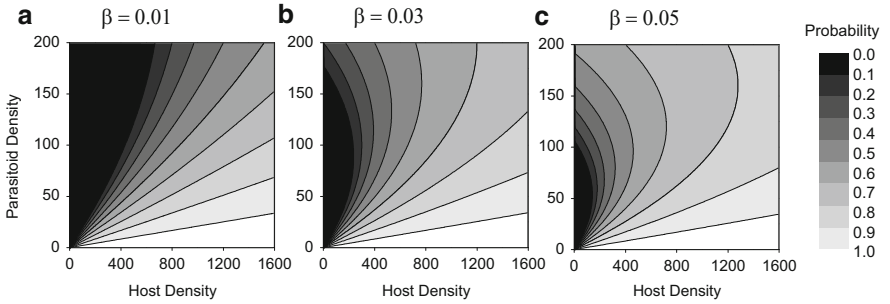

Fig. 2.1 Probability of survival for host populations interacting with a parasitoid population under different levels of interference competition in a patch. The contour plots are drawn for (**a**) low effect ($\beta = 0.01$), (**b**) medium effect ($\beta = 0.03$) and (**c**) high effect ($\beta = 0.05$) of interference competition (Reprinted from Ecological Modelling: Reigada et al. (2012), Copyright (2012), with permission from Elsevier [3136490533560])

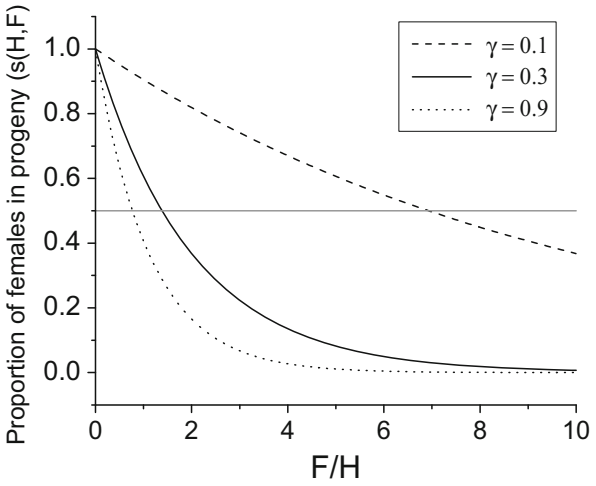

Fig. 2.2 Proportion of female offspring (decrease in the sex ratio) in parasitoid populations with different levels of sex ratio adjustment as a function of change in the quality of local conditions (*F/H*). An increase in the *F/H* represents a decrease in the patch quality. A sex ratio adjustment in the parasitoid population can be translated as the *F/H* proportion necessary to provoke changes in the ratio of a female parasitoid's progeny. The *dashed line* represents low ($\gamma = 0.1$), the *solid line* medium ($\gamma = 0.5$) and the *dotted line* high ($\gamma = 0.9$) degrees of sex ratio adjustment. More than 50 % of the offspring will be female for the following patch qualities: $F/H < 6.93$ for $\gamma = 0.1$, $F/H < 1.39$ for $\gamma = 0.5$ and $F/H < 0.77$ for $\gamma = 0.9$ (Reprinted from Ecological Modelling: Reigada et al. (2012), Copyright (2012), with permission from Elsevier [3136490533560])

quality: low ($\gamma = 0.1$), medium ($\gamma = 0.5$) and high ($\gamma = 0.9$) variations in the sex ratio. Parasitoid populations with larger values of γ respond more effectively to variations in the exploited patch. Patches with low γ values are expected to have a high female density (Fig. 2.2).

2.2.2.2 Dispersal Phase

After reproduction and parasitism occur in each patch, the populations may disperse to other patches representing habitats for local subpopulations. The set of patches that constitute the overall environment are placed on a two-dimensional square grid of L x L sites with reflective boundary conditions. However, not every site on the regular grid is necessarily a patch, as some sites may have no resources and, therefore, may not be useful for colonisation. Additionally, not every patch is connected to each other. Labeling the actual patches from 1 to N, we introduce the adjacency matrix A with elements $A_{ij} = 1$ if patches i and j are connected (and direct migration from one to the other is possible) and $A_{ij} = 0$ if not (Fig. 2.3). The introduction of the adjacency matrix allows us to generalise the form in which the patches are connected and consider landscapes of different topographies.

Adult hosts and female parasitoids can either disperse to other patches or remain on their home patch, depending on the local conditions. The number of hosts that leave the original patch, $h^{out}_{i,t+1}$, is represented by the following equation:

$$h^{out}_{i,t+1} = \frac{\mu_H h^2_{i,t+1}}{h_{i,t+1} + h^0}. \tag{2.10}$$

where, μ_H is the maximum dispersal rate of hosts in highly populated patches, and h^0 is the tolerance to conspecifics. In this manner, the number of hosts that leave the patch depends on the local host density; if the density is low, then a large fraction of hosts stay in the patch. The dispersing hosts $h^{out}_{i,t+1}$ are divided among the neighbouring connected patches *j, (j ≠ i)*. The number of hosts arriving on patch j coming from patch i is represented by the following equation:

$$\Psi^i_{j,t+1} = \frac{0.05}{r_{i,j}} h^{out}_{i,t+1}, \tag{2.11}$$

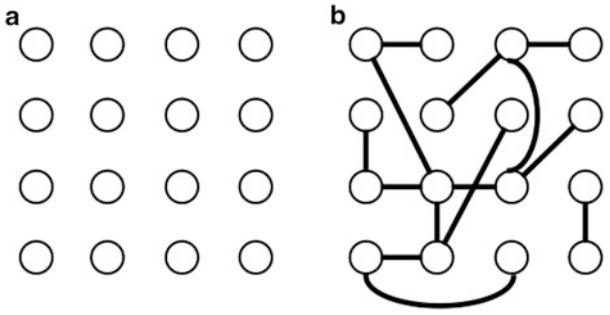

Fig. 2.3 (**a**) The two-dimensional square grid of sites determines the position of each site, whereas (**b**) the adjacency matrix displays how the sites are connected to each other. This approach permits assessment of non-trivial patterns of connection

where $r_{i,j}$ is the distance between the current patch and the destination patch measured in units of the lattice parameter so that $r = 1$ for patches located on adjacent sites.

After dispersal, the new generation of hosts is updated to

$$H_{i,t+1} = h_{i,t+1} + \sum_{j=1}^{L^2} A_{i,j} \left(\Psi^j_{i,t+1} - \Psi^i_{j,t+1} \right), \tag{2.12}$$

where A is the adjacency matrix as defined above. This accounts for the local population minus the amount that dispersed to neighbouring patches and plus the hosts that arrived from the same patches.

Because the parasitoids experience a longer period of maturation to reach the adult stage, their dispersal occurs after the dispersal of the hosts. The number of dispersing female parasitoids (male parasitoids do not disperse) depends on the number of parasitoids as well as on the number of hosts in the originating patch and is represented by

$$f^{out}_{i,t+1} = \begin{cases} \mu_F \dfrac{H^0}{H^0 + H_{i,t+1}} \dfrac{f^2_{i,t+1}}{f_{i,t+1} + f^0}, & \text{if} \quad H_{i,t+1} > 0 \\ f_{i,t+1}, & \text{if} \quad H_{i,t+1} = 0 \end{cases}, \tag{2.13}$$

where μ_F is the maximum parasitoid dispersal if the host density is small and the female density is high (low quality patch). The constant factors H^0 and f^0 represent the number of hosts needed to keep the female parasitoids from dispersing and the tolerance to other female parasitoids, respectively. The number of dispersing females that arrive at patch j coming from patch i is represented by the following equation:

$$\phi^i_{j,t+1} = \begin{cases} \dfrac{0.25}{r_{i,j}} f^{out}_{i,t+1}, & \text{if} \quad H_{i,t+1} > 0 \\ 0, & \text{if} \quad H_{i,t+1} = 0 \end{cases} \tag{2.14}$$

Comparing this expression with the corresponding equation for the hosts, we note that hosts may disperse to more distant patches than the parasitoids, as has been documented in field observations (Tscharntke et al. 2005). The final population of female parasitoids in each patch at generation $t + 1$ is provided by the following equation:

$$F_{i,t+1} = f_{i,t+1} + \sum_{j=1}^{L^2} A_{i,j} \left(\phi^j_{i,t+1} - \phi^i_{i,t+1} \right). \tag{2.15}$$

2.3 Resources Quality, Frequency and Duration

2.3.1 General Overview

In nature, it is common to find a high aggregation of consumer individuals in landscape areas where resource quality is high. However, the quality and duration of a resource in the landscape can change over time and affect the distribution and abundance of species. In this section, we study this situation by considering changes in location and lifetime of resource patches and explore the consequences of ephemeral resource patches for the persistence of host-parasitoid metapopulations and the spatial distribution of individuals in the landscape.

The main purpose of this section is to compare host-parasitoids dynamics in landscapes where host resources can be either constant or ephemeral. We investigated how the frequency with which ephemeral resources occur in the landscape affects the populations by progressively reducing its likelihood. In communities structured in metapopulations consisting of ephemeral local patches, the extinction of local populations depends on the resource lifetime, their distribution and their frequency in the landscape, as the persistence of species is related to the production of emigrants in a patch and on their inter-patch dispersal. In these landscapes, the recolonisation of a patch is conditioned to the appearance of new resources at the same site in the next time step, which makes it a new ephemeral patch. We also quantified the effects of variation in the quality of the resource patch, which was measured in terms of host carrying capacity (k).

The spatial structure was modelled using a regular square network with 2,500 (50×50) sites (or nodes) that are connected to neighbour sites by potential migration. The dispersion patterns follow the Eqs. 2.10, 2.11, 2.12, 2.13, 2.14 and 2.15 provided in Sect. 2.2, and migration is possible to all neighbours within a radius R_H for hosts and R_F for parasitoids. In this manner, considering sites i and j, we determined the elements of the Adjacency matrix, $A_{ij} = 1$, if $r_{i,j} \leq R_H$, for hosts, or $r_{i,j} \leq R_F$, for parasitoids. In this study, $R_H = 3.61$ and $R_F = 3$. After accounting for the fraction of migrant hosts and parasitoids in each site (Eqs. 2.10 and 2.13), dispersing populations were allocated in neighbour sites until all of the migrant fraction was distributed, with the closest neighbours receiving first (if two or more neighbour sites are the same distance away from the considered site, they are chosen in a random order) or until the maximum distance is achieved.

To clearly distinguish between locations with and without resources, we use the term patch for the former and site for the latter. Therefore, a patch is a site with resources. We started the simulations with 300 hosts and 4 parasitoids at a single patch located in the centre of the landscape. Resources were randomly distributed with a probability pr for each site at the beginning of each generation and removed at the end of the generation following a new allocation of resources. The distribution of resources at each generation is independent of the previous distributions. Notably, although the presence of resources at a site makes it available to receive hosts, the

actual occupation is only possible through migration of individuals from neighbour patches. For simulating landscapes with a continuous presence of resources, $pr = 1$.

For the dynamical model, we assumed high interference competition ($\beta = 0.06$) and an intermediary sex ratio adjustment ($\gamma = 0.5$). The details of the host-parasitoid dynamical model and the complete set of parameters used are described in Sect. 2.2. To study the effects of resource quality, we used two values for the carrying capacity: (i) a fixed size for the ephemeral basal resources ($k = 1{,}600$ host individuals per patch) and (ii) variable sizes for ephemeral basal resources (the carrying capacity assigned to a patch was uniformly selected in the interval $1{,}600 \leq k_{rand} \leq 8{,}000$ host individuals). For each simulation, we ran the host-parasitoid dynamic for 10,000 time-steps.

2.3.2 Simulation Results

We explored the effects of fixed and random carrying capacities ($k = 1{,}600$ and $1{,}600 \leq k_{rand} \leq 8{,}000$ host individuals). In both cases, the allocation probability (pr) had important implications for species persistence and distribution in the landscape. For $pr < 0.4$, hosts and parasitoids were extinct in both scenarios. For $pr = 0.5$, host populations persisted, and parasitoid populations became extinct. Coexistence was observed only for $pr \geq 0.6$ (Fig. 2.4), where large values of pr increased host-parasitoid abundance and changed the dynamics and the spatial pattern distribution.

Although the frequency of resource allocation (pr) affected the persistence of hosts and parasitoids equally in both fixed and variable resource quality conditions, the resulted fluctuation dynamics were different. In landscapes comprised by low quality patches ($k = 1{,}600$), host and parasitoid population sizes fluctuated with low abundances (Fig. 2.4a). Conversely, the size and fluctuation of species populations in a landscape composed by patches of different quality ($1{,}600 \leq k_{rand} \leq 8{,}000$) was systematically higher (Fig. 2.4b), indicative of the importance of the resource dynamics for species occupancy and global abundance distribution.

For fixed low resource sizes, the parasitoids could not occupy all patches in the landscape, and patches with hosts but no parasitoids were observed at all values of pr (Fig. 2.4a). In these cases, the dynamics converged to a regime of large population fluctuations, where host and parasitoid abundances were largely variable in space and time as shown in Fig. 2.5a for times 9,990, 9,995 and 10,000. For $t = 9{,}990$, patches with a high density of hosts were clearly observed, whereas for $t = 9{,}995$, the parasitoid population in these patches increased significantly due to overexploitation. For $t = 10{,}000$, the parasitoid population decreased again due to a lack of hosts because of the intense parasitism at previous times.

For variable resource sizes, host populations occupied all available patches in the landscape, but the parasitoids did not occupy all patches with hosts when the frequency of resource occurrence was low ($pr = 0.6$), and the population fluctuations resulted in oscillatory host and parasitoid abundances (Fig. 2.5b). For $pr \geq 0.6$, all patches were occupied by hosts and parasitoids, with the parasitoid metapopulation

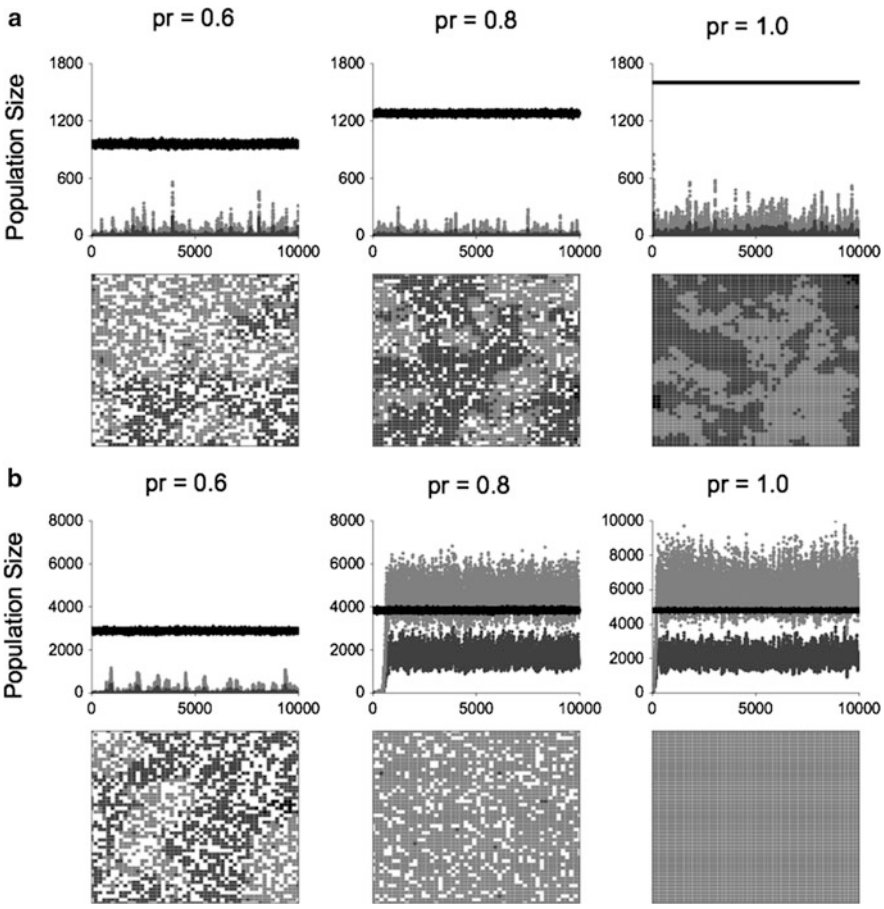

Fig. 2.4 Spatial occurrence and persistence of hosts and parasitoids after 10,000 time-steps as a function of time. The landscape has 50×50 sites with reflective boundary conditions. The results are displayed for different probabilities of ephemeral resource occurrence (*pr*). (**a**) A fixed size of the ephemeral resource ($k = 1{,}600$ host individuals) and (**b**) variable ephemeral resource size ($1{,}600 \leq k_{rand} \leq 8{,}000$ host individuals). *Black*, *dark gray* and *light gray* symbols represent, respectively, the basal ephemeral resource, host and parasitoid abundances. Parameter values: $\lambda = 1.5$; $\alpha = 0.34$; $\beta = 0.06$; $c = 20$; $\gamma = 0.5$; $\mu_H = 0.85$; $\mu_F = 0.4$ (Reprinted with minor adaptations from Oikos: Reigada and de Aguiar (2012), Copyright (2012), with permission from John Wiley and Sons [3117141225588])

divided into two subgroups, where abundances oscillated synchronously (Fig. 2.5b). We also simulated landscapes with a stable level of high-quality resource patches ($k = 8{,}000$). The same qualitative patterns displayed in Fig. 2.4b were observed, suggesting that the existence of high-quality patches increases the number of dispersal individuals so that host populations exist in all areas of the landscape where resources are available.

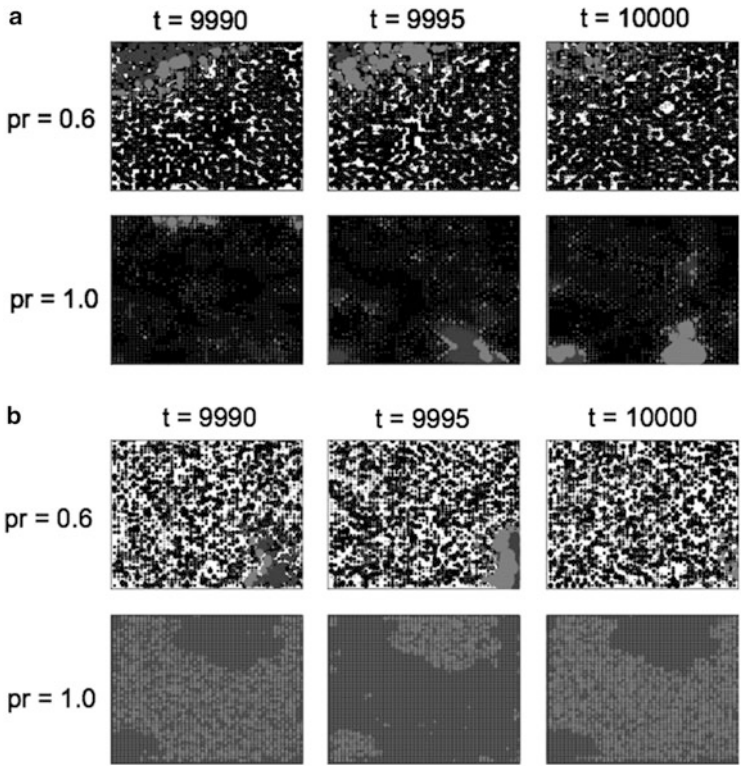

Fig. 2.5 Snapshots of the basal resource, host and parasitoid spatial occupancy for $t = 9{,}990$, $t = 9{,}995$ and $t = 10{,}000$ time-steps. *Black*, *dark gray* and *light gray* symbols represent, respectively, the basal ephemeral resource, host and parasitoid abundances within each patch. The sizes of the *dots* are proportional to the population at each site. The results are displayed for two values of the basal resource occurrence ($pr = 0.6$ and $pr = 1.0$). (**a**) $k = 1{,}600$ and (**b**) $1{,}600 \leq k_{rand} \leq 8{,}000$. Parameter values $\lambda = 1.5$; $\alpha = 0.34$; $\beta = 0.06$; $c = 20$; $\gamma = 0.5$; $\mu_H = 0.85$; $\mu_F = 0.4$. The number of sites and boundary conditions are the same as in Fig. 2.4 (Reprinted from Oikos: Reigada and de Aguiar (2012), Copyright (2012), with permission from John Wiley and Sons [3117141225588])

2.3.3 Discussion

The spatial structure has been postulated as the principal mechanism for increasing the persistence time of host-single parasitoid interactions, as the likelihood that an individual host is parasitised depends on its spatial location and on the overall host distribution (Bailey et al. 1962; Hassell and May 1974; Hassell et al. 1991). However, the persistence of a metapopulation occurs only if the species display limited dispersal and if the subpopulation dynamics is asynchronous (Levins 1969, 1970; Gilpin and Hanski 1991; Hanski and Gilpin 1997). Our results demonstrated that variations in resource frequency and quality affected the number of dispersing

individuals and species colonisation rates with important consequences for species occupancy and distribution over the landscape. Different resource qualities lead to different fluctuation patterns of host and parasitoid populations.

Previous studies have argued that density fluctuations increase the extinction risk of local populations, especially when the populations are small and the patches ephemeral (Lande 1993; Legendre et al. 1999). Several studies have also reported that high carrying capacities can cause instability that may lead to the extinction of the metapopulation (Lande 1993; Saether et al. 1998). Even narrow density fluctuations can disrupt the regulation within local patches and lead to the extinction of the metapopulation (Bonsall et al. 2002).

In our simulations, host-parasitoid interactions occurring in poor-quality environments ($k = 1{,}600$) produced a low host density that lead to an increase in the number of males in the parasitoid progeny and consequently a decrease in the parasitoid dispersers (females). This relatively low number of female parasitoids, combined with the higher dispersal rate of hosts compared to parasitoids, led to the development of large changes in species distribution over time. Landscapes with high-quality resources had smaller fluctuations in the populations and higher number of dispersed parasitoids, which spread to all available patches in the landscape. In simulations with higher carrying capacities, we observed a small probability of local extinctions, and parasitoids were present in all patches with hosts.

Although several studies have considered the influence of the carrying capacity on the persistence of populations, much less effort has been made towards understanding communities that depend on ephemeral basal resources. Our results have demonstrated how species abundance and distribution can change depending on the characteristics of the basal resource for a host-parasitoid trophic interaction. Bottom-up effects are important to the parasitoid community (Price 1991; Hawkins 1992), and the lower trophic level (host resources) can constrain the number and strength of trophic links in host-parasitoid webs (Price 1991). We observed that resource sizes and their spatial distributions are important for determining the number of host and parasitoid migrants. The variability in ephemeral resource sizes (fixed or random) affected the species' spatial distribution pattern, and coexistence was possible only for high probabilities of ephemeral resources in the landscape.

Host-parasitoid persistence was negatively affected by the presence of ephemeral patches because of the isolation of ephemeral subpopulations (due to a low occurrence of resources in these sites) and due to the low total resources. The results demonstrated that host-parasitoid persistence requires a minimum number of patches in the landscape, which in turn depends upon the probability of resource allocation. A low occurrence of resources caused the isolation of patches in the landscape. Conversely, landscapes with a high density of patches yielded a formation of clusters of host-parasitoid populations. The clusters were linked by dispersion and helped to ensure the persistence of both species.

We demonstrated that increasing the carrying capacity leads to a higher number of migrants that spread and colonise new patches in the spatial structure. When

the resources were low, coexistence was not observed. These results highlight the importance of demographic fluctuations, environmental factors and patch connectivity for the density of migrants and host-parasitoid persistence in landscapes with ephemeral resources.

In this section, we demonstrated that landscapes composed by ephemeral patches can lead to the persistence of host and parasitoid species depending on the number of sites with resources. Our results have the potential to provide broad management guidelines for host-parasitoid and other insect interactions with stochastic environmental characteristics (e.g., ephemeral resources, fragmented habitats, crop rotations in agricultural ecosystems or schedules of harvest in managed cultures) and demographic processes (e.g., arising from behaviour, genetic and physiological factors). The results presented here are also relevant to the control of patchily distributed pests, which can be maintained by the occurrence of ephemeral resources in the landscape.

2.4 Foraging and Reproductive Strategies

2.4.1 General Overview

Production of dispersers is essential for colonising empty patches and for promoting the global persistence of a metapopulation (Levins 1970; Hanski 1999). The dispersal of parasitoids from their current patch to a new patch occupied by hosts is the fundamental process that determines coexistence in these systems. Dispersion also affects their spatial distribution and metapopulation structure, as parasitoid aggregation is lower in patches with a low host density, which allows hosts in these patches to escape extinction and contributes to the coexistence of hosts and parasitoids (Hassell 2000). We demonstrated in the previous section that within-patch dynamics are essential to promote emigration and directly impact species movement. In this section, we explore how the effects of sex ratio adjustment and interference competition contribute to controlling the demography, species movement and the coexistence probability of host-parasitoid systems.

Parasitoid reproductive success is directly related to host abundance and the way hosts are exploited (Godfray 1994; Outreman et al. 2005). However, successful parasitism depends not only on host density but also on parasitoid density, given that higher numbers of parasitised hosts in an exploited patch can decrease the reproductive success of a female parasitoid. Depending on the density of conspecifics and on the host density in the patch, a female parasitoid can adopt different patch exploitation strategies thereby "optimising" its results. These conditions determine the "quality" of the exploited patch and can be measured by the ratio of non-parasitised host per parasitoid, H/F (Fauvergue et al. 2006; Reigada et al. 2012; Reigada and de Aguiar 2012).

The profitability of host patches changes over space due to competition by hosts and over time due to host depletion (Fauvergue et al. 2006). A decrease

in patch quality reduces the reproductive success of female parasitoids and can stimulate them to leave the patch and search for a better one, which increases the species dispersal rate among patches in the landscape. To maximise its chances for reproduction, a foraging female parasitoid needs to decide whether to leave its natal patch in search of better conditions or to stay. The choice is determined by the patch quality required by the species (Fretwell and Lucas 1970; Charnov 1976) and by their dispersal capability. Once a patch is selected, the female parasitoid must optimise her reproductive potential to ensure that her genes are passed on.

In nature, arrhenotokous parasitoid species usually mate in isolated groups before dispersing to new host patches and frequently show female-biased sex ratios. Hamilton (1967) observed this characteristic and proposed the theory of Local Mate Competition (LMC). This theory has been the basis for numerous studies about adaptive sex ratio adjustment in parasitoid species (Hassell et al. 1983; Godfray 1994; Godfray and Werren 1996; Santolamazza-Carbone and Rivera 2003; Shuker et al. 2006; Reigada et al. 2012) and assumes that females can control the sex ratio of their offspring in an haplodiploid population. Therefore, females can reduce the mating competition between their male offspring in response to foundress numbers (female that lay eggs) and the number of parasitised hosts in the patch (Hamilton 1967; Shuker et al. 2006; Grillenberger et al. 2009).

The adjustment of the progeny sex ratio can be understood as a strategy of female parasitoids to control sib-mating in patches of parasitised hosts. In addition to inbreeding control, arrhenotoky also influences the population growth within patches. In fact, the variation of the parasitoid sex ratio as a function of host and parasitoid densities observably affects the host-parasitoid dynamics, given that only mated females are able to produce female offspring capable of parasitising hosts. This method of population control prevents the overexploitation of hosts and consequently increases the stability of the host-parasitoid interaction (Hassell et al. 1983; Comins and Wellings 1985; Meunier and Bernstein 2002; Reigada et al. 2012; Reigada and de Aguiar 2012).

In this section, we explore how variations in patch quality influence the host-parasitoid coexistence, their dispersal and spatial distribution over the landscape. In addition, we will analyse the effects of different levels of parasitoid responsiveness to patch quality on species persistence and distribution on the landscape.

Throughout this section, the landscape is represented by a regular grid with 1,600 connected patches (40×40), where host resources are permanent, but host populations are limited by a carrying capacity. Only hosts and female parasitoids are allowed to disperse to other patches, and because male parasitoids are unable to disperse, we assume that mating occurs in their native patch. We also define the parasitoid foraging behaviour by their competitive abilities and by their ability to change the sex ratio of the progeny according to variations in patch quality. Competitive ability is a measure of the parasitoid efficiency in recognising parasitised hosts and laying their eggs on healthy hosts (interference competition). We consider parasitoid populations with three different levels of competitive ability, classified as low, medium and high, according to three different values of the parameter β (Fig. 2.1). The three degrees of sex ratio adjustment, which are also classified as low, medium or high, refer to the values of parameter γ (Fig. 2.2).

2.4.2 Simulation Results

2.4.2.1 Effects of Interference Competition and Sex Ratio Adjustments

In this sections, all simulations were initialised with 300 hosts and 4 female parasitoids at a single patch located at the centre of the landscape, where all other patches were empty. The host and parasitoid populations evolved according to the model described in Sect. 2.2, where the response of parasitoids to patch quality is based on three different foraging behaviours: (i) the decision to remain in or leave the current patch; (ii) the control of the progeny's sex ratio and (iii) the competitive abilities of the female parasitoids. Sex ratio control occurs in response to spatio-temporal fluctuations of host density, and competitive abilities are associated with delays in successive ovipositions, which decrease the potential to attack hosts due to interference from conspecifics in the exploited patch.

For simulations where female parasitoids explored patches extremely efficiently, displaying low interference competition with conspecifics ($\beta = 0.01$), we observed a low coexistence probability (Fig. 2.6, circles). Similar results were obtained for females that were less responsive to variations in patch quality (*H/F*) and produced a high number of female offspring in poor-quality patches ($\gamma = 0.1$). Both cases evolved towards the overexploitation of hosts, which resulted in the extinction

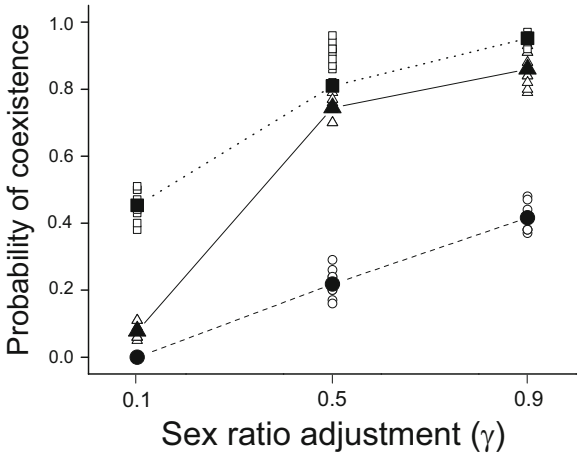

Fig. 2.6 Coexistence probabilities of host-parasitoid metapopulations as a function of the parasitoid sex ratio index (γ) for different values of the competitive interference parameter (β) after 5,000 time-steps ($\lambda = 1.5$; $\alpha = 0.15$). Open symbols represent the coexistence probability obtained from simulations with several combinations of host (μ_H) and parasitoid (μ_P) dispersal rates, with $0.1 \leq \mu_H \leq 1.0$ and $0.1 \leq \mu_P \leq 1.0$. *Full symbols* represent the average over five replicates of these simulations. The *circles* and *dashed lines*, *triangles* and *solid lines*, and *squares* and *dotted lines* represent the results for low ($\beta = 0.01$), medium ($\beta = 0.03$) and high ($\beta = 0.05$) parasitoid interference competition, respectively (Reprinted from Ecological Modelling: Reigada et al. (2012), Copyright (2012), with permission from Elsevier [3136490533560])

of the parasitoid population. Conversely, for parasitoid populations displaying some degree of demographic control, the probability of host-parasitoid coexistence was significantly higher (Fig. 2.6). In the rest of the section, we detail cases of medium and high levels of conspecific interference, as these are the most interesting situations where coexistence is possible.

Our results demonstrate that parasitoid populations where females are more responsive to patch quality have a higher probability of persistence. In these cases, this observation occurs because the number of female offspring is restricted when hosts are abundant in the patch. The fluctuations in population density also decreased when the sex ratio adjustment was high (Fig. 2.7).

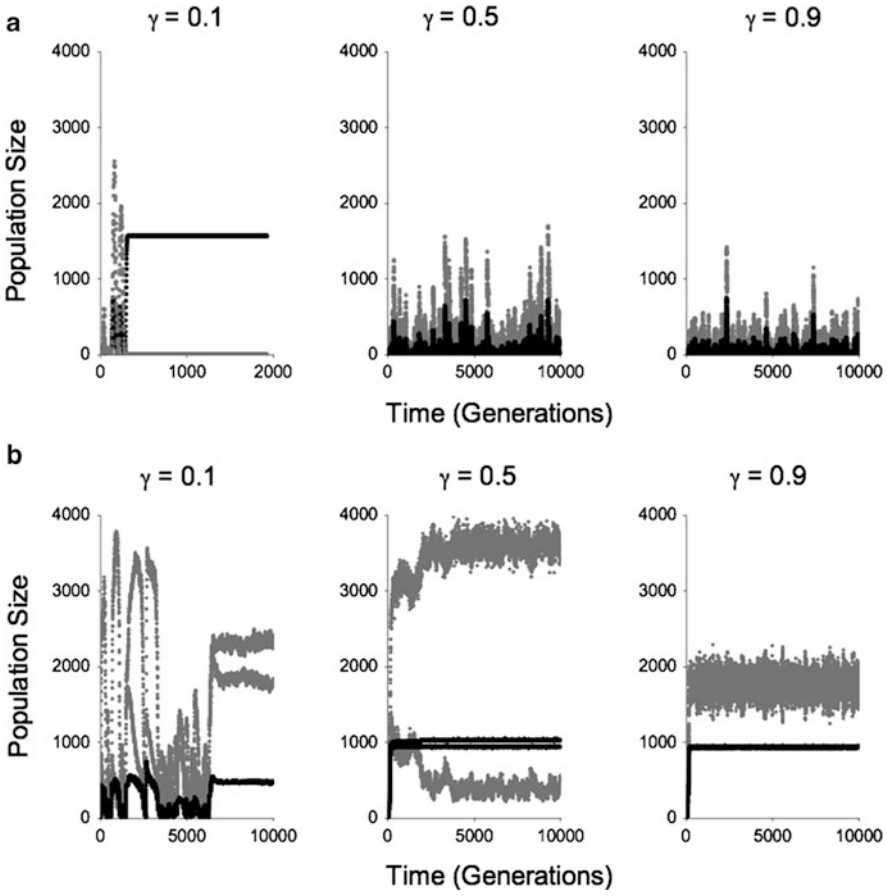

Fig. 2.7 Representative numerical simulations display the mean populations of hosts (*black*) and parasitoids (*gray*) over a grid of 20×20 patches as a function of time. In panel (**a**), $\beta = 0.03$ and in panel (**b**), $\beta = 0.05$. For both values, the degree of sex ratio adjustment varies from $\gamma = 0.1$ to $\gamma = 0.9$. The simulations were performed with $\lambda = 1.5$, $\alpha = 0.15$ and $\mu_H = \mu_F = 0.5$ (Reprinted from Ecological Modelling: Reigada et al. (2012), Copyright (2012), with permission from Elsevier [3136490533560])

Considering the effects of the female parasitoid foraging efficiency, we observed that parasitoids with a high degree of interference competition ($\beta = 0.05$, Fig. 2.7b) exhibited reduced oviposition rates in patches with a high density of parasitoids. This drastically decreased the oscillations in the parasitoid population. For medium levels of sex ratio adjustment ($\gamma = 0.5$), the host and parasitoid populations oscillated around two values in the abundance distribution. Conversely, parasitoid populations with intermediate interference competition ($\beta = 0.03$) always exhibited less stable oscillations, which reached extremely low population values (Fig. 2.7a). The combined results from the sex ratio adjustment and degree of interference competition suggest that stability in host-parasitoid populations occurs only when the population growth strongly correlates with patch conditions.

The different strategies of parasitoid foraging and reproductive behaviour have consequences for the spatial distribution of the populations in the landscape. Figure 2.8 presents snapshots of the patch occupancy of hosts and parasitoids for three instants of time separated by five steps of high degree of sex ratio adjustment ($\gamma = 0.9$) and two degrees of competitive interference, $\beta = 0.03$ and $\beta = 0.05$. For intermediate competitive interference ($\beta = 0.03$), the abundance distribution displays fluctuations for host and parasitoid species. This dynamical behaviour causes large peaks of high abundances in a patch that decreases to zero in a few generations and leaves the patch empty or nearly empty (Fig. 2.8a). This behaviour was observed for intermediary and high sex ratio adjustment values. For low values, ($\gamma = 0.1$), the parasitoids went extinct.

For a large degree of interference competition ($\beta = 0.05$) and intermediary and high sex ratio adjustment values, the behaviour changed drastically. The

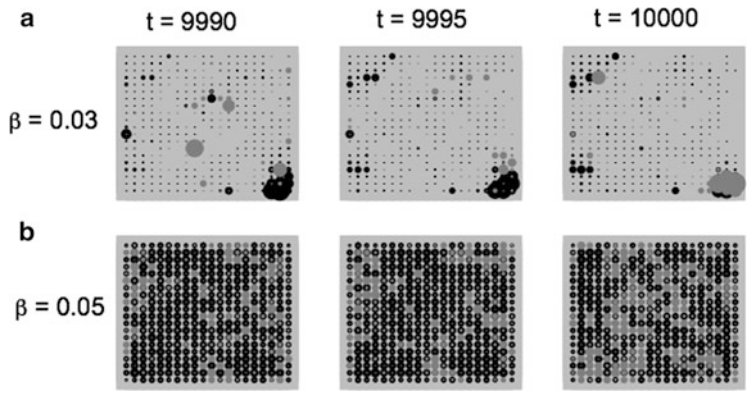

Fig. 2.8 Snapshots of host and parasitoid spatial occupancy for $t = 9{,}990$, 9,995 and 10,000. *Black* and *dark gray* symbols represent host and parasitoid abundance within each patch ($\lambda = 1.5$, $\alpha = 0.15$), respectively. The size of the *dots* is proportional to the population at the site. We compared the effects of different levels of competitive interference for $\gamma = 0.9$, $\mu_H = 0.2$ and $\mu_F = 0.8$. $\beta = 0.03$ in panel (**a**) and $\beta = 0.05$ in (**b**). (Reprinted with minor adaptations from Ecological Modelling: Reigada et al. (2012), Copyright (2012), with permission from Elsevier [3136490533560])

host population evolved to an approximately uniform spatio-temporal distribution, whereas the parasitoids still displayed fluctuations of density across the landscape. (Fig. 2.8b).

Our results suggest that the degree of interference competition can drastically change the spatio-temporal patterns of the populations from highly a variable pattern of densities to uniform as the interference competition increases. The degree of sex ratio adjustment also plays an extremely important role, as it contributes significantly to population persistence.

2.4.2.2 Dispersal Effects

In this section, we study the dynamics of extinction and patch colonisation for sets of parameters where coexistence was observed ($\beta = 0.03$ and $\beta = 0.05$ for interference competition and $\gamma = 0.5$ and $\gamma = 0.9$ for sex ratio adjustment). To characterise the dynamics of patch recolonisation, we defined the persistence time of extinction as the average time a patch remains empty or with population densities lower than 10 % of the average population per patch. We analysed the effects of demographic control (interference competition and sex ratio) for three combinations of species dispersal rates: (i) parasitoids are more dispersive than their hosts ($\mu_H = 0.2$, $\mu_F = 0.8$), (ii) parasitoids and hosts have the same dispersal rates ($\mu_H = \mu_F = 0.5$) and (iii) parasitoids are less dispersive than their hosts ($\mu_H = 0.8$, $\mu_F = 0.2$).

For intermediate degrees of interference competition ($\beta = 0.03$), patches with extinct or low-density populations remains so for relatively long periods of time before being recolonised (Fig. 2.9a, b). The recolonisation time decreased as the degree of competition increased to $\beta = 0.05$. The dispersal rates also influenced the recolonisation time, particularly for patches at the landscape boundaries. Generally, the lower the parasitoid dispersal rates, the longer the average time that boundary patches remained empty after extinction. The degree of sex ratio adjustment also affected the time of colonisation under fixed conditions of interference competition (compare Fig. 2.9a, b).

The recolonisation time was reduced to a single time-step for all values of sex ratio adjustment for $\beta = 0.05$, except for $\gamma = 0.1$. In this case (Fig. 2.9c), some of the local parasitoid populations remained extinct for long periods due to the clustering of hosts in a few patches, which limited the parasitoid occupation to these areas. The dispersal rates did not change the results for medium and high sex ratio adjustments.

2.4.3 Discussion

Parasitoid species can differ dramatically in their response to patch quality and also in their strategies to maximise the rate of progeny production (Bernstein and Driessen 1996; van Alphen et al. 2003; Wajnberg 2006; van Alphen and Bernstein 2008; Amat et al. 2009; Macke et al. 2011). These different reproductive

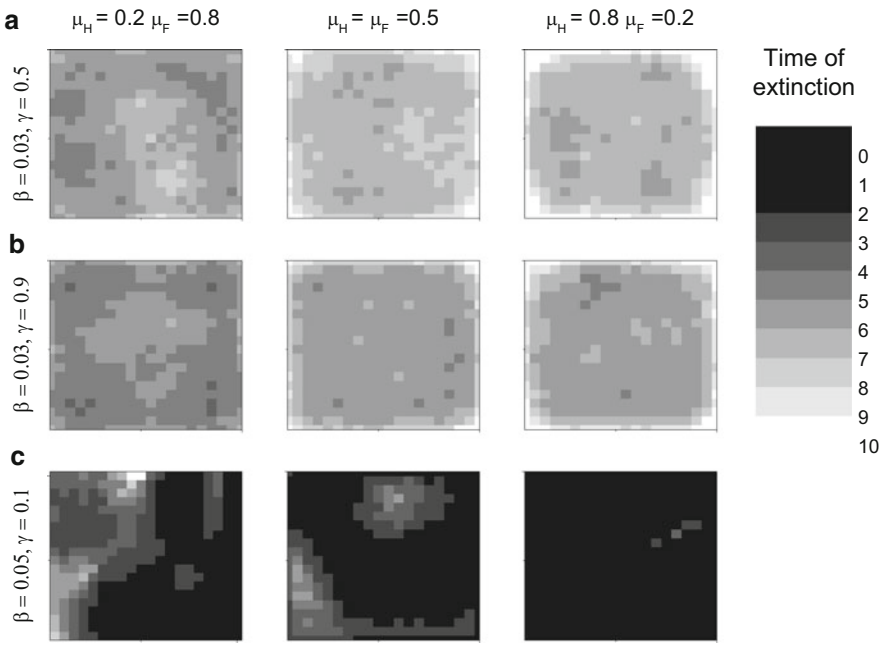

Fig. 2.9 The mean persistence time of extinction in parasitoid subpopulations for different values of parasitoid sex ratio adjustment (γ) after 8,000 time-steps (out of 10,000 time-steps) for $\lambda = 1.5$ and $\alpha = 0.15$. For each column, the persistence time is given for different host and parasitoid dispersal rate combinations: (**a**) $\beta = 0.03$, $\gamma = 0.5$; (**b**) $\beta = 0.03$, $\gamma = 0.9$; (**c**) $\beta = 0.05$, $\gamma = 0.1$. The *black* areas represent host subpopulations that were not extinct during the 2,000 time-steps analysed. The *white* areas represent host subpopulations that remained extinct and/or with low densities for at least 10 time-steps. The *gray colours* represent intermediate average persistence times at 1-time-step intervals (Reprinted from Ecological Modelling: Reigada et al. (2012), Copyright (2012), with permission from Elsevier [3136490533560])

and foraging adaptive behaviours have important consequences for the persistence and spatio-temporal distribution of both the parasitoids and theirs hosts. Here we used simulations to explore these features. The populations were characterised by different degrees of sex ratio control, competitive ability and dispersal rates.

Two key mechanisms that avoid the overexploitation of hosts are density-dependent interactions and spatially structured populations (Hassell et al. 1983; Bonsall et al. 2002). These features allow parasitoids to highly aggregate only in patches with a high host density so that small host populations can escape extinction (Sutherland 1983; Lozano et al. 1997; Hassell 2000; Briggs and Hoopes 2004). We demonstrated that foraging strategies that are regulated by patch quality can considerably affect the spatial and temporal distribution of individuals and may lead to self-regulating parasitoid populations. Our results also indicate that the effects sex ratio adjustment, interference competition and density-dependent dispersal in host-parasitoid systems are complex, and their effects are interrelated.

The parasitoids' ability to change the number and sex ratio of their offspring in response to changes in environmental properties is a widespread phenomenon in patchy landscapes that contributes significantly to the stability of host-parasitoid systems (Hassell et al. 1983). The number of female offspring depends on several factors, such as the local host density, the number of female and male parasitoids and the proportion of females to hosts (Hassell et al. 1983; Comins and Wellings 1985; Lozano et al. 1997; Meunier and Bernstein 2002; Reigada et al. 2012). The host-parasitoid equilibrium and spatial distribution depends on the specific mechanisms at work. In this section, we explore the dynamics dependence on the local ratio of hosts to female parasitoids, also known as the patch quality. In species that display this feature, the female parasitoids can access the density of conspecifics or their traces by encountering rates of parasitised hosts (Amat et al. 2009). We observed that high rates of encounter with parasitised hosts led to variations in parasitoid local demography due to the reduction of parasitoid reproductive success and changes in the sex ratio, which altered the parasitism rates.

Variation in the sex ratio of parasitoid populations significantly affected the female parasitoids. We observed coexistence for systems where parasitoid populations displayed a high degree of sex ratio control in response to fluctuations in the host population size (medium or high sex ratio degree). However, under high competition, medium or high adjustments to the sex ratio were relatively unimportant to the host-parasitoid dynamics.

Previous studies have already indicated that sex ratio adjustment by females has limited influence on host-parasitoid systems (Comins and Wellings 1985; Lozano et al. 1997; Meunier and Bernstein 2002; Reigada et al. 2012). The effects of controlling the sex ratio are usually associated with other biological factors, such as the host reproductive rate, parasitoid aggregation, parasitoid search efficiency and mutual interference competition (Lozano et al. 1997; Meunier and Bernstein 2002). Here we observed that sex ratio adjustment can be important when the degree of interference competition among parasitoids is low, thus increasing, in this case, the probability of coexistence; however, for higher levels of interference competition, its effects were suppressed. Conversely, the level of interference competition was always an important factor and constrained parasitoid effectiveness in reducing host populations and determined the overall species distribution in the landscape.

Intermediate degrees of interference competition generated fluctuations in the parasitoids subpopulations that led to highly variable patterns of density across the landscape in host and parasitoid population abundances. However, for high values of interference competition, the intrinsic demographic control of the parasitoid populations was higher, allowing hosts to spread to all patches in the metapopulation arena. In this case, the host population was uniformly distributed, although the parasitoids' distribution remained uneven across the arena.

High levels of interference competition and sex ratio adjustment in parasitoid populations reduced the production of dispersal individuals. In these cases, the ability to disperse has little effect, as the number of emigrants is constant and rarely reaches its maximum. High demographic control of parasitoid populations also reduced the fluctuations in host populations and increased the synchronisation

among patches. Consequently, host populations displayed a uniform distribution across the landscape, and colonisation/extinction events for parasitoid populations were not larger than a single time-step, reflecting the oscillations of the local populations instead of a dispersing species effect.

Previous models of foraging parasitoids have failed to include important co-evolutionary aspects of population dynamics in the interaction with the host species (Bonsall et al. 2002). Different foraging strategies are used during the exploitation of hosts in response to demographic fluctuations, thereby modifying the amount of time a female parasitoid stays in a patch (Hamilton 1967; Outreman et al. 2005; van Alphen and Bernstein 2008; Amat et al. 2009; Reigada et al. 2012). In natural systems, the landscape is fragmented into several patches, each with a different host density and different degrees of interference competition. Because the parasitoids cannot assess of the profitability of the entire set of patches, the female parasitoids must adopt the best possible local strategy to maximise the use of hosts before leaving the patch, as such a decision has high costs, such as exposure to predation or difficulty in finding another suitable patch.

Our results also indicate that the stabilising effects incurred from the tendency of parasitoids to aggregate in high-quality patches (Hassell 2000; Briggs and Hoopes 2004) need to be considered with caution, given that aggregation's association with changes in the sex ratio and mutual interference competition reduces the number of female offspring and the rate of parasitoid dispersal, thereby increasing the size and distribution of the host population in the landscape.

The stability of host-parasitoid systems depends on several complex interactions between intrinsic biological characteristics of the interacting species and cannot be attributed to a single mechanism (Lozano et al. 1997; Meunier and Bernstein 2002; Macke et al. 2011; Reigada et al. 2012; Reigada and de Aguiar 2012). In this study, we demonstrated that different behaviours and/or strategies adopted by female arrhenotokous parasitoids, as well as different patch quality requirements and patch uses, yield different population distributions. These observations indicate that the inclusion of life history traits of the host-parasitoid interaction can help understand the spatial and temporal distribution of these species. A natural direction for this research is to include the dynamics of co-evolution of these traits and to study the adaptation of the strategies to different environmental situations.

2.5 Remarks

Metapopulation models have highlighted the importance of patch size, patch quality and dispersal rates on metapopulation dynamics (Pulliam 1988; Hanski 1994; Hassell et al. 1991). Few studies, however, have considered the effects of foraging and reproductive behaviour on controlling the local patch demography (Hassell et al. 1983; Comins and Wellings 1985; Meunier and Bernstein 2002). In this chapter, we

outlined the importance of demographic control factors for the movement of species among patches and for understanding the extent to which the colonisation of new patches is facilitated or impeded by them.

We assumed that species are subject to density-dependent effects in two different periods of host-parasitoid interactions: pre and post-dispersal. During the pre-dispersal period, the number of dispersers and the number of residents that remained in each patch depended on the species "optimal decision" to explore or to leave the current patch, which is directly affected by the number of individuals in the patch. After dispersal, individuals arriving in a new patch are still influenced by the local densities, which define the host survival rate and the reproductive success of parasitoids. In addition to species behavioural aspects, we also demonstrated influences of patch spatio-temporal availability on species demography and dispersal. The results indicate that the different levels of demographic control that arise from species behaviours and ecological processes in response to changes in patch quality lead to different species spatial distributions and abundance in the landscape.

Parasitoid adjustments to patch quality (in terms of host availability) result from coevolutionary aspects of parasitoids and hosts species, on both ecological and evolutionary time scales. Although we did not include coevolutionary dynamics in host and parasitoid populations, future work should focus on elucidating how species traits evolve dynamically in a density-dependent interaction model and how they converge to an "optimum species response". This could help explain the different abundance and spatial occupancy patterns of real populations and also make inferences about their tolerance and persistence in the face of environmental changes.

In this study, we focused on the interference of one host species on the reproductive and foraging behaviour of parasitoids, although, in nature, more than one potential host species is commonly present for parasitoids. The presence of different host species exerts important effects on the parasitoid's decision to attack a specific host species. Normally, the host species attacked by a given parasitoid species can be classified by different suitability levels. According to different types of host cellular immune response to parasitoids, many hosts can debilitate or destroy immature parasitoids and survive to parasitism, which reduces the parasitoids' reproductive success (Heimpel et al. 2003). Therefore, the addition of a suboptimal prey in our host-parasitoid model can contribute to understanding how different host qualities, and the consequent asymmetry in parasitoid attack, change parasitoid foraging behaviour and offspring sex ratio and generate variations in species coexistence and distribution on the landscape.

Another interesting point to be explored in our model is the inclusion of a complex spatial structure in the landscape. In this study, the landscape where host and parasitoid species interact was represented by a regular square lattice. However, natural environments have become more and more fragmented because of deforestation, farming, urbanisation and climate change (Hagen et al. 2012). Different species are affected by fragmentation in different ways that depend strongly on their ability

to move between fragments, i.e., on their dispersal characteristics (Tscharntke 2000; Tscharntke et al. 2003; Cronin and Reeve 2005). In this context, few host-parasitoid spatial models have incorporated realistic heterogeneous dispersal strategies or embedded a complex structured landscape to host-parasitoid dynamics (Cronin and Reeve 2005). The model developed in Sect. 2.2 allows for the description of extremely general landscapes with any number of patches connected in arbitrary ways through the adjacency matrix.

The use of network-based models (or graph theoretical models) is an easy way to insert more complexity to landscape structure, defining spatial arrangement of patches and different probability of connection among them (Urban and Keitt 2001). Nodes in a spatially explicit landscape network represent the individual habitat patches, and the links between the nodes represent the possibility of individual flux among them (Urban and Keitt 2001; Cronin and Reeve 2005; Bodin and Saura 2010).

Considering the graphs approach in the landscape outline, modifications in the adjacency matrix presented in this model can easily allow for the insertion of different patterns in dispersal movement of individuals between patches. All of the dispersion equations were also written for generic landscape connectivities in a way that allowed the study of host-parasitoid dynamics for different network structures to be straightforward. In this way, this model can be easily modified to understand the effects of species behaviour and reproductive strategies in more complex landscapes, to make predictions for different connectivity patterns (or reach abilities on the landscape) and to assess the quantities of organisms that flow throughout the landscape in a more realistic overview.

References

Amat I, Desouhant E, Bernstein C (2009) Differential use of conspecific-derived information by sexual and asexual parasitic wasps exploiting partially depleted host patches. Behav Ecol Sociobiol 63:563–572

Arashiro E, Tome T (2007) Threshold of coexistence and critical behavior of a predator-prey cellular automaton. J Phys A 40:887–900

Bailey VA, Nicholson AJ, Williams EJ (1962) Interaction between hosts and parasites when some host individuals are more difficult to find than others. J Theor Biol 3:1–18

Bernstein C, Driessen G (1996) Patch-marking and optimal search patterns in the parasitoid Venturia canescens. J Anim Ecol 65:211–219

Bodin O, Saura S (2010) Ranking individual habitat patches as connectivity providers: integrating network analysis and patch removal experiments. Ecol Model 221:2393–2405

Bonsall MB, French DR, Hassell MP (2002) Metapopulation structures affect persistence of predator-prey interactions. J Anim Ecol 71:1075–1084

Briggs CJ, Hoopes MF (2004) Stabilizing effects in spatial parasitoid-host and predator models: a review. Theor Popul Biol 65:299–315

Charnov EL (1976) Optimal foraging: the marginal value theorem. Theor Popul Biol 9:126–136

Charnov EL (1982) The theory of sex allocation. Princeton University Press, Princeton

Chesson PL, Murdoch WW (1986) Aggregation of risk: relationships among host-parasitoid models. Am Nat 127:696–715

Comins HN, Wellings PW (1985) Density-related parasitoid sex-ratio: influence on host-parasitoid dynamics. J Anim Ecol 54(2):583–594
Cronin JT, Reeve JD (2005) Host-parasitoid spatial ecology: a plea for a landscape-level synthesis. Proc R Soc B 272:2225–2235
Diekmann O, Metz JA, Sabelis MW (1988) Mathematical models of predator/prey/plant interactions in a patch environment. Exp Appl Acarol 5:319–342
Edelstein-Keshet L (2005) Mathematical models in biology. Siam, Philadelphia
Fauvergue X, Boll R, Rochat J et al (2006) Habitat assessment by parasitoids: consequences for population distribution. Behav Ecol 17:522–531
Fretwell SD, Lucas HL (1970) On territorial behavior and other factors influencing habitat distribution in birds. Acta Biotheor 19:16–36
Gilpin M, Hanski I (1991) Metapopulation dynamics: empirical and theoretical investigations. Academic, London
Godfray HCJ (1994) Parasitoids behavioural and evolutionary ecology. Princeton University Press, Princeton
Godfray CJ, Shimada M (1999) Parasitoid as model organisms for ecologists. Res Popul Ecol 41:3–10
Godfray HCJ, Werren JH (1996) Recent developments in sex ratio studies. Trends Ecol Evol 11:59–63
Grillenberger BK, Zande LVZ, Bijlsma R et al (2009) Reproductive strategies under multiparasitism in natural populations of the parasitoid wasp *Nasonia* (Hymenoptera). J Evol Biol 22:460–470
Hagen M, Kissling WD, Rasmussen C et al (2012) Biodiversity, species interactions and ecological networks in a fragmented world. Adv Ecol Res 46:89–210
Hamilton WD (1967) Extraordinary sex ratios. Science 156:477–488
Hanski I (1994) A practical model of metapopulation dynamics. J Anim Ecol 63:151–162
Hanski I (1999) Metapopulation ecology. Oxford University Press, Oxford
Hanski I, Gilpin ME (1997) Metapopulation biology ecology, genetics and evolution. Academic, London
Hassell MP (1978) The dynamics of arthropod predator-prey systems. Princeton University Press, Princeton
Hassell MP (2000) Host-parasitoid population dynamics. J Anim Ecol 69:543–566
Hassell MP, May RM (1973) Stability in insect host–parasite models. J Anim Ecol 42:693–736
Hassell MP, May RM (1974) Aggregation of predators and insect parasites and its effect on stability. J Anim Ecol 43:567–594
Hassell MP, Waage JK, May RM (1983) Variable parasitoid sex ratios and their effect on host-parasitoid dynamics. J Anim Ecol 52(3):889–904
Hassell MP, Comins HN, May RM (1991) Spatial structure and chaos in insect population dynamics. Nature 353:255–258
Hawkins BA (1992) Parasitoid-host food webs and donor control. Oikos 65:159–162
Heimpel GE, Neuhauser C, Hoogendoorns M (2003) Effects of parasitoid fecundity and host resistance on indirect interaction among hosts sharing a parasitoid. Ecol Lett 6:556–566
Jongejans E, Sharpies O, Shea K (2008) Dispersal, demography and spatial population models for conservation and control management. Perspect Plant Ecol Evol Syst 9:317–325
Kerr B, Neuhauser C, Bohannan BJM, Dean AM (2006) Local migration promotes competitive restraint in a host–pathogen 'tragedy of the commons'. Nature 442:75–78
Lande R (1993) Risks of population extinction from demographic and environmental stochasticity and random catastrophes. Am Nat 911:927
Legendre S, Clobert J, Moller AP et al (1999) Demographic stochasticity and social mating system in the process of extinction of small populations: the case of passerines introduced to New Zealand. Am Nat 153:449–463
Levins R (1969) Some demographic and genetic con- sequences of environmental heterogeneity for biological control. Bull Entomol Res 15:237–240

Levins R (1970) Extinction. Some mathematical problems in biology. American Mathematical Society, Providence

Lozano C, Kidd NAC, Jervis MA et al (1997) Effects of parasitoid spatial heterogeneity, sex ratio and mutual interference on the interaction between the olive bark beetle Phloeotribus scarahaeoides (Col., Scolytidae) and the pteromalid parasitoid Cheiropachus quadrum (Hym., Pteromalidae). J Appl Entomol 121:521–528

Macke E, Magalhães S, Bach F et al (2011) Experimental evolution of reduced sex ratio adjustment under local mate competition. Science 334:1127–1129

Meunier J, Bernstein C (2002) The influence of local mate competition on host-parasitoid dynamics. Ecol Model 152:77–88

Murdoch WW, Oaten A (1975) Predation and population stability. Adv Ecol Res 9:1–131

Murray JD (1993) Mathematical biology. Springer, Berlin

Nicholson AJ, Bailey VA (1935) The balance of animal populations. Part 1. Proc Zool Soc London 3:551–598

Outreman Y, Ralec AL, Wajnberg E et al (2005) Effects of within- and among-patch experiences on the patch-leaving decision rules in an insect parasitoid. Behav Ecol Sociobiol 58:208–217

Pacala SW, Hassell MP (1991) The persistence of host-parasitoid associations in patchy environments II. Evaluation of field data. Am Nat 138:584–605

Price PW (1991) The plant vigor hypothesis and herbivore attack. Oikos 62:244–251

Pulliam HR (1988) Source, sinks and population regulation. Am Nat 132:165–661

Rauch E, Bar-Yam Y (2006) Long-range interactions and evolutionary stability in a predator–prey system. Phys Rev E 73:020903

Reigada C, de Aguiar MAA (2012) Host-parasitoid persistence over variable spatio-temporally susceptible habitats: bottom-up effects of ephemeral resources. Oikos 121:1665–1679

Reigada C, Araujo BLS, de Aguiar MAM (2012) Patch exploitation strategies of parasitoids: the role of sex ratio and forager's interference in structuring metapopulations. Ecol Model 230:11–21

Saether BE, Engen S, Islam A et al (1998) Environmental stochasticity and extinction risk in a population of a small songbird, the great tit. Am Nat 151:441–450

Santolamazza-Carbone S, Rivera AC (2003) Superparasitism and sex ratio adjustment in a wasp parasitoid: results at variance with local mate competition? Oecologia 136:366–373

Shuker DM, Sykes EM, Browning LE et al (2006) Male influence on sex allocation in the parasitoid wasp Nasonia vitripennis. Behav Ecol Sociobiol 59:829–835

Stacey B, Gross A, Bar-Yam Y (2012) Beyond the mean field in host-pathogen spatial ecology, arXiv:1110.3845v2 [nlin.CG]

Sutherland WJ (1983) Aggregation and the ideal free distribution. J Anim Ecol 52:821–828

Tscharntke T (2000) Parasitoid populations in agricultural landscapes. In: Hochberg ME, Ives AR (eds) Parasitoid population biology. Princeton University Press, Princeton

Tscharntke JJM, Bernstein C, Driessen G (2003) Information acquisition and time allocation in insect parasitoids. Trends Ecol Evol 18:81–87

Tscharntke T, Klein AM, Krues A et al (2005) Landscape perspectives on agricultural intensification and biodiversity- ecosystem service management. Ecol Lett 8:857–874

Urban D, Keitt T (2001) Landscape connectivity: a graph-theoretic perspective. Ecology 82:1205–1218

van Alphen JJM, Bernstein C (2008) Information acquisition, information processing, and patch time allocations. In: Wajnberg E, Bernstein C, van Alphen JJM (eds) Behavioural ecology of insects parasitoids: from theoretical approaches to field applications. Blackwell Publishing, Hong Kong, pp 172–192

van Alphen JJM, Bernstein C, Driessen G (2003) Information acquisition and time allocation in insect parasitoids. Trends Ecol Evol 18:81–87

Wajnberg E (2006) Time allocation strategies in insect parasitoids: from ultimate predictions to proximate behavioural mechanisms. Behav Ecol Sociobiol 60:589–611

Chapter 3
Abiotic Effects on Population Dynamics of Mosquitoes and Their Influence on Dengue Transmission

Hyun Mo Yang, José Luiz Boldrini, Artur Cesar Fassoni, Karla Katerine Barboza de Lima, Luiz Fernando Souza Freitas, Miller Ceron Gomez, Valmir Roberto Andrade, and André Ricardo Ribas Freitas

Abstract Dengue incidence is dependent on abiotic factors that directly affect the population dynamics of mosquitoes with serious implications for dengue transmission. By using estimated entomological parameters dependent on temperature, and including the dependency of these parameters on rainfall, the seasonally varying population size of the mosquito *Aedes aegypti* is evaluated using a mathematical model. The anthropophilic and peridomestic female *A. aegypti* bite humans for blood to mature fertilised eggs, during which the dengue virus can spread between mosquitoes and humans. As an example of applied entomology, mosquito and human populations are coupled to assess dengue virus transmission. Seasonal patterns of mosquito populations influence dengue epidemics, illustrating the importance of temperature and rainfall in designing control mechanisms.

Keywords Abiotic effects • Mosquitoes • Population dynamics • *Aedes aegypti* • Dengue • Environmental factors • Dengue epidemiology • Autonomous model • Subpopulations • Equilibrium

H.M. Yang (✉) • J.L. Boldrini • A.C. Fassoni • K.K.B. de Lima • L.F.S. Freitas
Departments in University of Campinas, Universidade Estadual de Campinas (UNICAMP), Rua Sérgio Buarque de Holanda, 651 – Cidade Universitária "Zeferino Vaz" – Distr. Barão Geraldo, Campinas, São Paulo, Brazil
e-mail: hyunyang@ime.unicamp.br

M.C. Gomez
Departamento de Matemática, Universidad de Nariño (UDENAR), Ciudad Universitaria Torobajo – Clle 18 Cr 50, San Juan de Pasto, Colombia

V.R. Andrade
Superintendência de Controle de Endemias (SUCEN), R. São Carlos, 546 – Vl. Industrial, Campinas, São Paulo, Brazil

A.R.R. Freitas
Coordenadoria de Vigilância Sanitária (COVISA), Avenida Anchieta, 200 – 11 andar – Paço Municipal, Campinas, São Paulo, Brazil

C.P. Ferreira, W.A.C. Godoy (eds.), *Ecological Modelling Applied to Entomology*, Entomology in Focus 1, DOI 10.1007/978-3-319-06877-0_3

3.1 Introduction

Although a vaccine is not available, the mechanisms for controlling dengue transmission rely on the control of its vector, the mosquito *Aedes aegypti*. This fact underscores the importance of understanding the dynamics of mosquito populations under abiotic influences, such as temperature and rainfall.

The *A. aegypti* life cycle comprises an aquatic phase (egg, larva and pupa stages) followed by an adult form. Female mosquitoes mate after emerging from the pupa stage and fertilise all of the eggs. Female mosquitoes feed on human blood to mature the fertilised eggs, which are laid in suitable recipients (breeding sites) from time to time (gonadotrophic cycle, a period of approximately 3 days). The eggs hatch into larvae, which encompass four instars, when they come in contact with water. Larvae can die during this stage or complete the cycle and become pupae. Pupae, in turn, can die (low probability) or emerge as adult mosquitoes. In this last stage, however, the mosquitoes are strictly considered to be at the stage of mortality and will die.

A. aegypti population dynamics aim to mimic its population size by using demographic parameters. Therefore, if the transition rates from larva to pupa and pupa to adult mosquito, the mortality rates in each stage (larva, pupa and adult), and the oviposition rates are known, then the population size can be estimated. These entomological parameters, however, vary with temperature and potentially with rainfall. Additionally, the number of breeding sites, which could be viewed as the carrying capacity in ecological terms, is an abiotic factor that determines the size of the mosquito population. These breeding sites, in fact, depend strongly on the rainfall.

With respect to the temperature influences on mosquito populations, entomological parameters, such as transition and mortality rates in the aquatic phase, the mortality rate of adult mosquitoes and oviposition rates, were obtained experimentally under a controlled temperature (Yang et al. 2009a, b, 2011). Briefly, temperature-controlled experiments were designed to assess the effect of temperature on the development, survival of immature (aquatic) forms and on the survival and oviposition of adult mosquitoes. In each experiment, a fixed number of larvae or mosquitoes were set in a germination chamber with a controlled temperature (the device did not allow for a controlled humidity). The *A. aegypti* strain used in the experiments was obtained from natural populations of the City of Marília ($-22°12'50''$ latitude and $49°56'45''$ longitude), which is northwest of São Paulo State, Brazil. A one day period was divided into "day" (light turned on) and "night" (light turned off) according to the photoperiod that occurs in the City of Marília. At low temperatures, we set the dark period to be slightly longer than the light period to mimic the winter season and vice versa at high temperatures. Inside the germination chamber, two temperatures were fixed to correspond to the light and dark periods. The weighted (with respect to periods of time when the light was turned on or off) mean temperature was taken to be the temperature of the experiment.

However, to verify if the programmed temperature was achieved during each experiment, a thermohygrograph was settled inside the chamber. Temperature and

humidity data were then recorded on week-period paper. The weekly data were then transcribed and used to calculate the weighted average temperature, which was taken as the actual temperature inside the germination chamber instead of the programed one.

There is a paucity of knowledge about the measurement of the effects of rainfall in mosquito population. We retrieved and reproduced some previously observed results. Vezzani et al. (2004) identified the highest adult *A. aegypti* density with accumulated rainfalls above 150 mm, and Micieli and Campos (2003) observed a close correlation between the highest peak of the *A. aegypti* population with high rainfall, and the population decreased for the months with less rainfall. Baruah and Dutta (2012) observed an extremely dense *A. aegypti* population with an annual average rainfall of 2,758 mm, and the highest density was observed in the post-monsoon season. Conversely, the larval population was not peak in these conditions as expected, as the heavy rain washed away most of the containers. Notwithstanding, immature *A. aegypti* stages resisted the rain flooding better than *Cx. pipiens*. This difference was most dramatic during the pupal stage (Koenraadt and Harrington 2008). An experiment performed by Dickerson et al. (2012) with *Anopheles* mosquitoes revealed that they can fly in the rain.

Other authors (Moore et al. 1978; Toma et al. 1982) have indicated that *Aedes* abundance is mainly regulated by temperature rather than precipitation. However, rainfall may be the only determining factor for *Aedes* proliferation where temperature is always above the marginal level. Baruah and Dutta (2012) found that rain fall, when it is too heavy and continuous, may also be a regulating factor for *A. aegypti* proliferation, where a significant reduction of adults and washing away of immature stages was observed. However, heavy rainfall prepares the habitat for *Aedes* proliferation when the temperature is highly suitable for mosquito proliferation.

In this work, we aim to assess the effects of temperature and rainfall on the mosquito population. The mosquito population variation is important to study, as this species is the dengue virus vector. *A. aegypti* is an anthropophilic and peridomestic insect (adapted to the modern life style of humans). Moreover, because their bites occur during the day, the chance of dengue virus transmission is enhanced. The interaction between humans and mosquitoes may result in sustained dengue virus transmission.

Another intention of this work is to assess the influence of rain fall on dengue transmission. To achieve this goal, we developed a deterministic model that considers entomological parameters and allows them to depend on temperature and rainfall if necessary.

The first part of this chapter (Sect. 3.2) addressed the variation of mosquito populations with temperature and rainfall or precipitation. A system of equations was developed based on the life cycle of the mosquito *A. aegypti*, where the parameters of the model rely on the entomological parameters depending on temperature and rainfall. In this section, our objective is to assess the mosquito population size based on the model parameters when they are: (1) constant, (2) temperature-dependent, or (3) both temperature- and precipitation-dependent.

The second part of this chapter (Sect. 3.3) addresses the transmission of dengue virus due to the interaction between human and mosquito populations. Considering the entomological parameters dependent on temperature and precipitation, dengue propagation is assessed by mathematical modelling. We discuss the results of the mosquito modelling and dengue transmission in Sect. 3.4, and the conclusions are presented in Sect. 3.5.

3.2 Mosquito Population Dynamics

Entomological parameters governing the dengue vector, the mosquito *Aedes aegypti*, are dependent on temperature and precipitation. A model considering these entomological parameters was developed to assess the population size of *A. aegypti*. The dependency on the model parameters with temperature and rainfall was developed based on a non-autonomous model. Given that the entomological parameters are constant, by considering average values, an autonomous model was studied in detail.

3.2.1 Model Formulation

Aedes aegypti population dynamics considers only female mosquitoes by assuming that all of them mate as soon as they emerge. Female mosquitoes lay eggs in suitable recipients (breeding sites). We assume that a fraction f of these eggs will become females and a fraction q will hatch to the larva stage. Eggs hatch to larvae without constraint (Regis et al. 2008); however, larvae are constrained to carrying capacity due to, for instance, limited resources and competition among them. The intrinsic oviposition rate and the carrying capacity (breeding sites) are designed by, respectively, $\varnothing_m$ and C. The per-capita egg production is $fq\varnothing_m(1-L/C)$, where L represents the number of larvae, and that multiplied by M, the number of adult female mosquitoes, obtains the total viable eggs that can yield females. The larvae die at a per-capita mortality rate μ_l or become pupae at the per-capita transition rate σ_l. The pupae, which are represented by P, die at a per-capita rate μ_p or emerge as adult mosquitoes at a per-capita rate σ_p. Finally, the females die at a per-capita mortality rate μ_m. All entomological parameters are dependent on temperature and were obtained experimentally in controlled temperature experiments (Yang et al. 2009a, b, 2011).

Notably, the egg stage was not considered in the previous description of mosquito population dynamics due to the difficulty in obtaining the entomological parameters at this stage. Additionally, the inverse of per-capita mortality and transition rates are the average survival time and the period of time spent in each stage, respectively. For example, μ_p^{-1} is the average survival time in the pupa stage, and σ_p^{-1} is the mean time spent in the pupa stage before emerging as an adult mosquito.

The model parameters are dependent on a variety of factors. Among them, we considered the temperature and precipitation and assessed how these factors are encompassed in the model's parameters.

From a series of daily recorded maximum (T_{max}) and minimum (T_{min}) temperatures (CEPAGRI/UNICAMP 2012), we interpolated any temperature T at time t as

$$T(t) = T_{min}(j) + [T_{max}(j) - T_{min}(j)]\, sin\left(\pi t'\right)$$

where the index j, which is the integer part of time t, refers to the *j-th* calendar day, and t' is the fractional part of time t, that is, $0 \leq t' < 1$. Notably, $t' = 0$ and $t' = 1$ correspond to midnight, whereas $t' = 0.5$ corresponds to midday.

The amount of rain precipitation (W) influences the carrying capacity and the mortality rates in the aquatic phase and the capacity of eggs being hatched. During heavy rain periods, larvae and pupae can be flushed, thereby cleansing breeding sites of aquatic forms (Madi et al. 2012). We call this physically induced mortality, and we do not consider this type of mortality among adult mosquitoes (Dickerson et al. 2012).

From a series of daily recorded precipitation (Instituto de Açucar e Álcool 2012), we defined the simplest physical additional mortality as

$$\mu_*^a = G_* \left[W(j) - V_c\right] \theta \left[W(j) - V_c\right],$$

where $*$ stands for l and p, the larva and pupa stages, *W(j)* is the rain precipitation at day j (the *j-th* calendar day), V_c is the critical rain volume sufficiently high to originate the overflow and unsuitability of breeding sites, and $\theta\ (x)$ is the Heaviside function, that where $\theta\ (x) = 1$ if $x \geq 0$ and is otherwise $\theta(x) = 0$. The parameter G_* is defined in terms of another parameter g_* as $G_* = \mu_* g_*$. Then, we have the total mortality rates for aquatic phases:

$$\begin{cases} \mu_l^s = \mu_l \left\{1 + g_l \left[W(j) - V_c\right] \theta \left[W(j) - V_c\right]\right\} \\ \mu_p^s = \mu_p \left\{1 + g_p \left[W(j) - V_c\right] \theta \left[W(j) - V_c\right]\right\}, \end{cases}$$

where μ_l and μ_p are temperature-dependent mortality rates, and g_l and g_p measure how the precipitation affects the additional physical mortality rates.

The daily recorded maximum (T_{max}) and minimum (T_{min}) temperatures and rain precipitation (W) are fixed along the entire day of observation. However, the temperature is allowed to vary along the day, which accounts for the inter-daily variability of the entomological parameters.

The fraction of eggs that are hatching (q) and the carrying capacity (C) are assumed to depend only on precipitation. We assume that the rain that has fallen in the past few days also influences both parameters.

During the dry seasons, the number of breeding sites is dramatically reduced. We assume that the amount of rainfall always increases the breeding sites, even in the

case of heavy rainfall. Hence, for carrying capacity, we describe the influence of rainfall in its number as

$$C = DC_i \left\{1 - c_0 e^{-c_1[W(j)+W_M]}\right\},$$

where D represents the magnitude of breeding sites found in a city, C_i is the rain-independent variation in breeding sites but can depend on time due to demographic changes in human population, $1 - c_0$, with $c_0 < 1$, is the minimum fraction of carrying capacity in the complete absence of rain (maybe due to vessels that store water), and c_1 is the change of breeding sites due to rain (the higher c_1, the higher the influence of rain on increasing breeding sites). The term W_M represents the rainfall of past days defined by

$$W_M = \sum_{k=1}^{j-1} \frac{W(j-k)}{\{w_1 \times [T_{max}(j-k) + T_{min}(j-k)]\}^k},$$

where $W(j-k)$ is the rainfall in *j-k-th* days before, w_1 is the residual effect of past rainfall (the higher w_1, the lower the contribution of past rain due to evaporation). If $w_1 = 1/2$, then the evaporation is a function of the daily mean temperature. Heavy and continuous rainfall may be a regulating factor for *A. aegypti* proliferation, as immature forms might have been washed away and thus significantly reduced the adult production. However, heavy rainfall prepares the habitat for *A. aegypti* proliferation in the post rainy season (Baruah and Dutta 2012).

For the fraction of eggs that hatch into larvae, we follow similar argumentation given for the carrying capacity. Because the relative humidity is almost 100 % when there is abundant rain, we assume that

$$q = 1 - q_0 e^{-q_1[W(j)+W_M]},$$

where $1-q_0$ is the capacity of eggs hatching even without rainfall, and q_1 is the rate of hatching due to humidity (the higher q_1, the higher the influence of humidity on hatching). Notably, $q = 1$ when $W \to \infty$.

We now want to consider control efforts, such as insecticide application and the removal of breeding sites. Breeding sites can be removed in two ways: (1) removal of breeding sites targeting houses surrounding case notification and (2) preventive removal to avoid dengue transmission. The total size of inhabitations in Campinas City Esteva and Vargas (2003) is approximately $n_T = 350{,}000$. We assume that the number of houses surveyed for breeding sites, and for further removal, is proportional to decreases in the carrying capacity, represented by

$$C = DC_i \left\{1 - c_0 e^{-c_1[W(j)+W_M]}\right\} \left(1 - \alpha_b \frac{n_b}{n_T} - \alpha_a \frac{n_a}{n_T}\right),$$

where n_b and n_a are the numbers of houses surveyed surrounding dengue cases; as preventive visits, and α_b and α_a correspond to the efficacy. Because the preventive visit is a random event, whereas the dengue-targeting house visitation is case-search event, we assumed that $\alpha_b > \alpha_a$.

Spraying insecticide aims to kill adult mosquitoes, which is represented by

$$\mu_m^s = \mu_m \left(1 + \alpha_s \frac{n_i}{n_T}\right),$$

where n_i is the number of houses where insecticide was sprayed surrounding dengue cases, and α_s is the insecticide efficacy.

Based on the above description of the *A. aegypti* life cycle and the parameter definitions, the dynamics of mosquito populations is described by

$$\begin{cases} \dfrac{dl}{dt} = fq\varnothing_m m \left(1 - \dfrac{l}{C}\right) - \left(\sigma_l + \mu_l^s\right) l \\ \dfrac{dp}{dt} = \sigma_l l - \left(\sigma_p + \mu_p^s\right) p \\ \dfrac{dm}{dt} = \sigma_p p - \mu_m^s m, \end{cases} \tag{3.1}$$

where the ratios are $l = L/D$, $p = P/D$ and $m = M/D$. The model parameters are

$$\begin{cases} q = 1 - q_0 e^{-q_1[W(j)+W_M]} \\ C = C_i \left\{1 - c_0 e^{-c_1[W(j)+W_M]}\right\} \left(1 - \alpha_b \dfrac{n_b}{n_T} - \alpha_a \dfrac{n_a}{n_T}\right) \\ \mu_l^s = \mu_l \left\{1 + g_l \left[W(j) - V_c\right] \theta \left[W(j) - V_c\right]\right\} \\ \mu_p^s = \mu_p \left\{1 + g_p \left[W(j) - V_c\right] \theta \left[W(j) - V_c\right]\right\} \\ \mu_m^s = \mu_m \left(1 + \alpha_s \dfrac{n_i}{n_T}\right), \end{cases} \tag{3.2}$$

where $\varnothing_m$, μ_m, σ_l and σ_p depend only on temperature; μ_l and μ_p depend on both temperature and precipitation; q and C depend only on precipitation; and f is the constant fraction of eggs that yield females.

The dynamical trajectories of the system of equations, Eq. (3.1), are obtained numerically considering the initial conditions, at $t = 0$, given by

$$\left(l(0) = 0, p(0) = 0, m(0) = m_0\right),$$

where $m_0 = 1/\left(D\overline{m}\right)$ and $\overline{m}$ is the equilibrium value (see Eq. (3.3) below). These initial conditions supplied to the dynamical system correspond to the introduction

of one mosquito in a community free of mosquitoes in a specified calendar time, which was set as $t = 0$.

Although the model is non-autonomous, that is, Eq. (3.1) depends explicitly on time t, we present an analysis of an autonomous model. This particular study assumes that all model parameters given by Eq. (3.2) are constant (for example, at a given temperature and constant precipitation).

3.2.2 *Analysis of an Autonomous Model*

The analysis of autonomous dynamics provides ideas for the expected local time behaviour of the general model in terms of medium values of the parameters. In this situation, Eq. (3.1) presents steady states, which are designed as the equilibrium point $(\overline{l}, \overline{p}, \overline{m})$. There are two possibilities:

1. Absence (extinction) of mosquito populations, called a trivial equilibrium, expressed as $Z_0 = (0,0,0)$.
2. Infestation of (colonisation by) mosquito populations, called a non-trivial equilibrium, expressed as $Z_1 = (\overline{l}, \overline{p}, \overline{m})$, where

$$\begin{cases} \overline{l} = C\left(1 - \dfrac{1}{Q_c}\right) \\ \overline{p} = \dfrac{\sigma_l}{\sigma_p + \mu_p^s} C\left(1 - \dfrac{1}{Q_c}\right) \\ \overline{m} = \dfrac{\sigma_p}{\mu_m^s} \dfrac{\sigma_l}{\sigma_p + \mu_p^s} C\left(1 - \dfrac{1}{Q_c}\right), \end{cases} \tag{3.3}$$

with Q_c, represented by

$$Q_c = \frac{\varnothing_m}{\mu_m^s} fq \frac{\sigma_l}{\sigma_l + \mu_l^s} \frac{\sigma_p}{\sigma_p + \mu_p^s}, \tag{3.4}$$

is the offspring number.

Z_1 is globally stable for $Q_c > 1$ Anderson and May (1991), whereas for $Q_c < 1$, Z_0 is globally stable. Therefore, $Q_c = 1$ is the bifurcation value. If we define

$$\varnothing_m^{th} = \frac{\mu_m^s}{fq} \frac{\sigma_l + \mu_l^s}{\sigma_l} \frac{\sigma_p + \mu_p^s}{\sigma_p},$$

which is the threshold of $\varnothing_m$ because the bifurcation occurs at $\varnothing_m = \varnothing_m^{th}$, for $\varnothing_m > \varnothing_m^{th}$, the non-trivial equilibrium appears. Notably, Z_1 is biologically feasible (positive numbers) if $Q_c > 1$.

The above results unequivocally demonstrate the dynamical trajectories of the autonomous system of equations, Eq. (3.1), with constant parameters. Disregarding the initial conditions supplied to the dynamical system due to the global stability results, all of the dynamical trajectories attain: (1) an equilibrium free of mosquitoes, Z_0 (if $Q_c < 1$); or (2) infestation by mosquito populations Z_I (if $Q_c > 1$). The offspring number Q_c therefore plays an important role in the dynamics, and it deserves more discussion.

First, if none of the controlling mechanisms for the mosquito population are considered, then the basic offspring number Q_0 is

$$Q_0 = \frac{\varnothing_m}{\mu_m} fq \frac{\sigma_l}{\sigma_l + \mu_l} \frac{\sigma_p}{\sigma_p + \mu_p}, \tag{3.5}$$

where μ_l, μ_p and μ_m are temperature-dependent natural mortality rates. Let us interpret the basic offspring number Q_0 biologically. A female mosquito, during its entire lifespan $(1/\mu_m)$, lays on average $\varnothing_m/\mu_m$ eggs; a fraction f of these eggs emerge as females, and a fraction q of these female eggs hatch into larvae. These larvae must survive the larval stage and transform to pupae, which occurs with a probability of $\sigma_l/(\sigma_l + \mu_l)$. These pupae must emerge as adult female mosquitoes with a probability of $\sigma_p/(\sigma_p + \mu_p)$. Hence, Q_0 is the average number of viable female mosquitoes (daughters) that one female generates during its entire lifespan. Therefore, the mosquito population does not go to extinction if $Q_0 > 1$ (one female mosquito generates more than one viable daughter).

Second, the controlling mechanisms decrease the basic number of offspring. The relationship between Q_c and Q_0 is

$$Q_c = Q_0 \frac{\sigma_l + \mu_l}{\sigma_l + \mu_l^s} \frac{\sigma_p + \mu_p}{\sigma_p + \mu_p^s} \frac{\mu_m}{\mu_m^s},$$

where $\mu_l < \mu_l^s$, $\mu_p < \mu_p^s$ and $\mu_m < \mu_m^s$ according to Eq. (3.2). The control mechanisms decrease the basic number of offspring and can result in the elimination of mosquito populations by decreasing it below unity ($Q_c < 1$).

3.2.3 *Analysis of a Non-autonomous Model*

The non-autonomous system of equations, given by Eq. (3.1), must be dealt with numerically. The dynamical trajectories of this system do not achieve any limiting values asymptotically. For this reason, the notion of the offspring number does not make sense.

However, we can introduce the effective offspring number Q_{ef} in the context of non-autonomous modelling from ideas borrowed from autonomous modelling: the time-independent model parameters of the offspring number Q_c are allowed to vary, originating the time varying effective offspring number Q_{ef}.

3.3 Dengue Transmission

The *A. aegypti* population, its dynamics described by Eq. (3.1), is linked to the human population to assess dengue propagation. The dependency of model parameters with temperature and rainfall results in a non-autonomous model. Considering that the entomological parameters are constant, by using average values, an autonomous model can be studied in detail.

3.3.1 Model Formulation

Dengue is caused by an arbovirus, and the infection in mosquitoes extremely weakens their innate immune response. However, among humans, this infection induces a strong and everlasting immune response (against one serotype). Dengue virus spreads among humans in a suitable environment to *A. aegypti* mosquitoes.

When dengue virus circulates in interacting mosquito and human populations, the female mosquito populations must be subdivided into three classes: susceptible (M_1), exposed (M_2) and infectious (M_3). Susceptible mosquitoes are infected according to, for example, a mass action law Lindsay and Birley (1996), where the per-capita incidence rate is generically referred to as B_m, and they enter an exposed class. The rate of transfer from exposed to infectious classes is represented by γ_m, where γ_m^{-1} is the extrinsic incubation period. Then, they spend the entire life time in the infectious class due to the assumption of absence of immune response. The total population size is $M = M_1 + M_2 + M_3$. The larval and pupal stages are described by the first two equations of Eq. (3.1). Hence, the dynamics of the dengue virus propagation among mosquitoes is

$$\begin{cases} \dfrac{dL}{dt} = fq\varnothing_m \left(1 - \dfrac{L}{C}\right) M - \left(\sigma_l + \mu_l^s\right) L \\ \dfrac{dP}{dt} = \sigma_l L - \left(\sigma_p + \mu_p^s\right) P \\ \dfrac{dM_1}{dt} = \sigma_p P - \left(B_m + \mu_m^s\right) M_1 \\ \dfrac{dM_2}{dt} = B_m M_1 - \left(\gamma_m + \mu_m^d\right) M_2 \\ \dfrac{dM_3}{dt} = \gamma_m M_2 - \mu_m^d M_3. \end{cases} \tag{3.6}$$

The human population is subdivided into four classes according to the natural history of the dengue infection: susceptible (S), exposed (E), infectious (I) and immune or recovered (R). Susceptible humans are infected according to, for example, a mass action law, where the per-capita incidence rate is generically

referred to as B_h, and they enter an exposed class. These exposed individuals are transferred to the infectious class at a per-capita rate γ_h, where γ_h^{-1} is the intrinsic incubation period. Infectious individuals are transferred to the immune or recovered class at a per-capita rate σ_h, where σ_h^{-1} is the period of time necessary to mount an immune response (or the period of time at which symptoms are apparent). The total human population size is $N = S + E + I + R$, and all classes of individuals are under the same natural mortality rate μ_h. Neither maternally derived antibodies nor the loss of an immune response is considered. Another assumption is the absence of additional mortality, as we are categorising infection by just one serotype. The dynamics describing dengue infection among humans are represented by

$$\begin{cases} \dfrac{dS}{dt} = \varnothing_h N - (B_h + \mu_h)\, S \\ \dfrac{dE}{dt} = B_h S - (\gamma_h + \mu_h)\, E \\ \dfrac{dI}{dt} = \gamma_h E - (\sigma_h + \mu_h)\, I, \end{cases} \tag{3.7}$$

where the decoupled immune class is represented by $R = N - S - E - I$. The total population is calculated by

$$\frac{dN}{dt} = (\varnothing_h - \mu_h)\, N, \tag{3.8}$$

where $\varnothing_h$ is the per-capita natality rate. For simplicity, we do not consider migratory movement.

Dengue virus transmission depends on mosquito biting and on the probability of ingestion (human to mosquito) or inoculation (mosquito to human) of a sufficient amount of virus to result in an infection. The rate at which one mosquito bites a human is directly proportional to the average biting rate of mosquitoes (intrinsic mosquito behaviour) and inversely proportional to the number of humans (one specific person has the chance of being bitten by one mosquito is reduced in a large population). Female mosquitoes bite humans at regular time intervals (gonadotrophic cycle) to mature the fertilised eggs during mating. We assume that the biting rate is proportional to the eggs laid by mosquitoes $\varnothing_m$, which increases with temperature. Considering the biting rate that is proportional to oviposition, the per-capita infection rates B_m and B_h can be written as

$$\begin{cases} B_m = \beta_m \varnothing_m \frac{I}{N} \\ B_h = \beta_h \varnothing_m \dfrac{M_3}{N}, \end{cases}$$

where β_m and β_h are the transmission rates (or coefficient of transmission) from mosquito bites. The terms β_h and β_m represent the biting rate and the probability (asymmetric) of dengue transmission, respectively.

Conversely, the per-capita incidence rates B_m and B_h can be understood as the infection propagation due to the contact between human and mosquito populations (mass action law). With respect to the biting rate, in lower temperatures, few eggs are laid by mosquitoes, but the variance is extremely high (Yang et al. 2009a), and thus, it must be taken into consideration through modelling. By considering both assumptions, the per-capita infection rates B_m and B_h can be written as

$$\begin{cases} B_m = \beta_m \sqrt{\varnothing_m} I \\ B_h = \beta_h \sqrt{\varnothing_m} M_3, \end{cases}$$

where β_m and β_h are the transmission rates (with different units compared with the previous definition) from mosquito bitings.

The previous two descriptions of per-capita incidence rates can be combined in two cases: (1) infection due to contact between populations with linear dependency with oviposition rate and (2) infection due to the biting probability with a square root dependency with oviposition. Hence, B_m and B_h can be written as

$$\begin{cases} B_m^{jk} = \beta_m \rho^j \delta_m^k i \\ B_h^{jk} = \beta_h \rho^j \delta_h^k m_3, \end{cases}$$

where ρ^j, δ_m^k and δ_h^k, with $(j,k) = 1,2$, are

$$\begin{cases} \rho^1 = \varnothing_m \\ \rho^2 = \sqrt{\varnothing_m}, \end{cases} \tag{3.9}$$

and

$$\begin{cases} \delta_m^1 = 1 \quad and \quad \delta_h^1 = \frac{D}{N} \\ \delta_m^2 = N \quad and \quad \delta_h^2 = D. \end{cases} \tag{3.10}$$

Notably, D is constant (magnitude of breeding sites given by the amount at time $t = 0$), and N is the size of the human population given by Eq. (3.8). Therefore, we have four subtly different models according to the combination $(j = 1, k = 1)$, $(j = 2, k = 1)$, $(j = 1, k = 2)$ and $(j = 2, k = 2)$. In the next section, these four models will be written explicitly. Remember that the sub-indices m and h refer to the mosquito and human populations, respectively.

The extrinsic incubation rate γ_m depends on temperature (Lindsay and Birley 1996) which is represented by

$$\gamma_m = \frac{\gamma_s}{T - T_m} = \frac{120}{T - 16},$$

where T is the ambient temperature (in degrees Celsius), γ_s is the thermic sum (in $^{\circ}C \times day$), and T_m is the threshold temperature below which the dengue virus cannot multiply.

A vaccine against dengue infection is not yet available. For this reason, all controlling mechanisms have targeted the mosquito population. The model incorporates two control methods: the spray of insecticide and the removal of breeding sites.

Insecticide spraying is used to kill infectious mosquitoes. With this purpose, the insecticide is applied in all houses surrounding suspected or confirmed dengue cases. This is the reason why the formulas presented in the following section is restricted to susceptible mosquitoes, whereas exposed and infectious mosquitoes are under the mortality rate given by

$$\mu_m^d = \mu_m \left(1 + \alpha_d \frac{n_i}{n_T}\right),$$

where α_d is the insecticide efficacy with $\alpha_d > \alpha_s$.

The human population fractions are represented as $s = S/N$, $e = E/N$, $i = I/N$ and $r = R/N$ with $s + e + i + r = 1$. Then, Eq. (3.7) can be rewritten using the relationship with, for example, susceptible humans,

$$\frac{1}{N}\frac{dS}{dt} = \frac{ds}{dt} + (\varnothing_h - \mu_h)\, s,$$

using Eq. (3.8), and the corresponding relationship with other compartments. With respect to mosquito populations, we previously defined the ratios $l = L/D$, $p = P/D$, $m_1 = M_1/D$, $m_2 = M_2/D$ and $m_3 = M_3/D$.

The dynamics of dengue virus transmission among mosquitoes, in terms of ratios of subpopulations, is described by

$$\begin{cases} \dfrac{dl}{dt} = fq\varnothing_m \left(1 - \dfrac{l}{C}\right) m - \left(\sigma_l + \mu_l^s\right) l \\ \dfrac{dp}{dt} = \sigma_l l - \left(\sigma_p + \mu_p^s\right) p \\ \dfrac{dm_1}{dt} = \sigma_p p - \left(\beta_m \rho^j \delta_m^k i + \mu_m^s\right) m_1 \\ \dfrac{dm_2}{dt} = \beta_m \rho^j \delta_m^k i m_1 - \left(\gamma_m + \mu_m^d\right) m_2 \\ \dfrac{dm_3}{dt} = \gamma_m m_2 - \mu_m^d m_3, \end{cases} \tag{3.11}$$

and among humans, in terms of subpopulation fractions, dengue propagation is described by

$$\begin{cases} \dfrac{ds}{dt} = \varnothing_h - \left(\beta_h \rho^j \delta_h^k m_3 + \varnothing_h\right) s \\ \dfrac{de}{dt} = \beta_h \rho^j \delta_h^k m_3 s - \left(\gamma_h + \varnothing_h\right) e \\ \dfrac{di}{dt} = \gamma_h e - \left(\sigma_h + \varnothing_h\right) i, \end{cases} \tag{3.12}$$

where the fraction of decoupled immune persons is $r = 1 - s - e - i$, and ρ^j, δ_m^k and δ_h^k, with $(j,k) = 1,2$, and the four submodels are represented by Eqs. (3.9) and (3.10).

The model parameters are

$$\begin{cases} q = 1 - q_0 e^{-q_1 [W(j) + W_M]} \\ C = C_i \left\{1 - c_0 e^{-c_1 [W(j) + W_M]}\right\} \left(1 - \alpha_b \frac{n_b}{n_T} - \alpha_a \frac{n_a}{n_T}\right) \\ \mu_l^s = \mu_l \left\{1 + g_l \left[W(j) - V_c\right] \theta \left[W(j) - V_c\right]\right\} \\ \mu_p^s = \mu_p \left\{1 + g_p \left[W(j) - V_c\right] \theta \left[W(j) - V_c\right]\right\} \\ \mu_m^s = \mu_m \left(1 + \alpha_s \frac{n_i}{n_T}\right) \\ \mu_m^d = \mu_m \left(1 + \alpha_d \frac{n_i}{n_T}\right). \end{cases} \tag{3.13}$$

This set of parameters differs from those given by Eq. (3.2) by the inclusion of last term, which was added to discriminate between susceptible and infected mosquitoes. The parameters with respect to human population are not dependent on temperature or precipitation.

The dynamical trajectories of the system of equations, Eqs. (3.11 and 3.12), are obtained numerically considering the initial conditions, at $t = 0$, given by

$$\begin{aligned} &\big(l(0) = \overline{l}, p(0) = \overline{p}, m_1(0) = \overline{m}, m_2(0) = 0, \\ &m_3(0) = 0, s(0) = 1 - i_0, e(0) = 0, i(0) = i_0\big), \end{aligned}$$

where $i_0 = 1/\overline{N}$. The equilibrium values $\overline{l}$, $\overline{p}$ and $\overline{m}$ are given by Eq. (3.3), and $\overline{N}$ is the constant size of the human population. These initial conditions supplied to the dynamical systems correspond to the introduction of one infectious person in a completely susceptible population in a specified calendar time, which was set as $t = 0$.

As we did in the previous section for mosquito populations, we present an analysis of an autonomous model. This study assumes that all model parameters given by Eq. (3.13) are constant (for example, at a given temperature and constant precipitation).

3.3.2 Analysis of an Autonomous Model

When mortality and natality rates are equal, that is when $\varnothing_h = \mu_h$, then the human population does not change with time ($dN/dt = 0$ in Eq. (3.8)), and the total size of the human population is constant, designated by $\overline{N}$. When we assume that all model parameters are constant (at a given temperature and constant precipitation), we get an autonomous model. In this situation, the autonomous systems of equations, Eqs. (3.11) and (3.12), have constant parameters and present steady states that are designated as the equilibrium point ($\overline{l}$, $\overline{p}$, $\overline{m}_1$, $\overline{m}_2$, $\overline{m}_3$, $\overline{s}$, $\overline{e}$, $\overline{i}$). There are three possibilities, assuming that $\mu_m^s = \mu_m^d$:

1. A human population without mosquitoes, U_0. This equilibrium corresponds to the absence of mosquitoes and all humans are susceptible, or,

$$U_0 = \left(\overline{l} = 0, \overline{p} = 0, \overline{m}_1 = 0, \overline{m}_2 = 0, \overline{m}_3 = 0, \overline{s} = 1, \overline{e} = 0, \overline{i} = 0\right).$$

2. An interacting human and mosquito population without dengue transmission, U_1. This equilibrium dictates that all humans and mosquitoes are susceptible, or,

$$U_1 = \left(\overline{l}, \overline{p}, \overline{m}_1 = \overline{m}, \overline{m}_2 = 0, \overline{m}_3 = 0, \overline{s} = 1, \overline{e} = 0, \overline{i} = 0\right),$$

   where $\overline{l}$, $\overline{p}$ and $\overline{m}$ are given by Eq. (3.3).
3. A dengue virus circulating between human and mosquito populations, U_2. In this equilibrium, the steady state values are

$$U_2 = \left(\overline{l}, \overline{p}, \overline{m}_1, \overline{m}_2, \overline{m}_3, \overline{s}, \overline{e}, \overline{i}\right),$$

   where the coordinates, depending on the fraction of infectious i, are

$$\begin{cases} \overline{l} = C\left(1 - \dfrac{1}{Q_c}\right) \\ \overline{p} = \dfrac{\sigma_l}{\sigma_p + \mu_p^s} C\left(1 - \dfrac{1}{Q_c}\right) \\ \overline{m}_1 = \dfrac{\sigma_p}{\beta_m \rho^j \delta_m^k \overline{i} + \mu_m^s} \dfrac{\sigma_l}{\sigma_p + \mu_p^s} C\left(1 - \dfrac{1}{Q_c}\right) \\ \overline{m}_2 = \dfrac{\beta_m \rho^j \delta_m^k \overline{i}}{\gamma_m + \mu_m^s} \dfrac{\sigma_p}{\beta_m \rho^j \delta_m^k \overline{i} + \mu_m^s} \dfrac{\sigma_l}{\sigma_p + \mu_p^s} C\left(1 - \dfrac{1}{Q_c}\right) \\ \overline{m}_3 = \dfrac{\gamma_m}{\mu_m^s} \dfrac{\beta_m \rho^j \delta_m^k \overline{i}}{\gamma_m + \mu_m^s} \dfrac{\sigma_p}{\beta_m \rho^j \delta_m^k \overline{i} + \mu_m^s} \dfrac{\sigma_l}{\sigma_p + \mu_p^s} C\left(1 - \dfrac{1}{Q_c}\right) \\ \overline{s} = 1 - \dfrac{\sigma_h + \varnothing_h}{\gamma_h} \dfrac{\gamma_h + \varnothing_h}{\varnothing_h} \overline{i} \\ \overline{e} = \dfrac{\sigma_h + \varnothing_h}{\gamma_h} \overline{i}, \end{cases} \tag{3.14a}$$

and $\bar{i}$ is given by

$$\bar{i} = \frac{R_c - 1}{\frac{\beta_m \rho^j \delta_m^k}{\mu_m^s} + \frac{(\sigma_h + \varnothing_h)(\gamma_h + \varnothing_h)}{\varnothing_h \gamma_h} R_c}, \tag{3.14b}$$

where the reproduction number R_c is represented by

$$R_c = \frac{\gamma_h \gamma_m \beta_m \rho^j \delta_m^k \beta_h \rho^j \delta_h^k}{\mu_m^s \left(\gamma_m + \mu_m^s\right) (\sigma_h + \varnothing_h) (\gamma_h + \varnothing_h)} \overline{m}, \tag{3.15}$$

where Q_c is calculated from Eq. (3.4), and $\overline{m}$, the sum of the ratios of subclasses of mosquitoes, $\overline{m} = \overline{m}_1 + \overline{m}_2 + \overline{m}_3$, is also obtained from Eq. (3.3). This equilibrium point is biologically feasible if $R_c > 1$ and assuming that $Q_c > 1$. Equation (3.14b) is generated from the fifth equation in Eq. (3.14a) with another equation for $\overline{m}_3$ represented by

$$\overline{m}_3 = \frac{(\sigma_h + \varnothing_h) (\gamma_h + \varnothing_h) \varnothing_h \bar{i}}{\left[\gamma_h \varnothing_h - (\sigma_h + \varnothing_h) (\gamma_h + \varnothing_h) \bar{i}\right] \beta_h \rho^j \delta_h^k}.$$

Notably, the maximum fraction of infectious humans $\bar{i}_M$ is obtained when R_c is extremely high ($R_c \to \infty$) and yields

$$\bar{i}_M = \frac{\gamma_h \varnothing_h}{(\sigma_h + \varnothing_h) (\gamma_h + \varnothing_h)},$$

which is an asymptote. Another important relationship from combining $\overline{m}$, $\overline{m}_1$ and $\bar{s}$ is

$$\bar{s} \frac{\overline{m}_1}{\overline{m}} = \frac{1}{R_c}.$$

With respect to the equilibrium points, we can establish that (Esteva and Vargas 2003): (1) if $Q_c < 1$, then U_0 is globally stable; (2) if $Q_c > 1$ and $R_c < 1$, then U_1 is globally stable; and (3) if $Q_c > 1$ and $R_c > 1$, then U_2 is globally stable. Consequently, the dynamical trajectories of the autonomous system of equations, Eqs. (3.11 and 3.12), are determined unequivocally. Disregarding the initial conditions supplied to the dynamical system, all of the dynamical trajectories attain: (1) U_0 (if $Q_c < 1$); (2) U_2 (if $Q_c > 1$ and $R_c > 1$); (3) or U_1 (if $Q_c > 1$ and $R_c < 1$). The reproduction number R_c therefore plays an important role in the dynamics of dengue transmission and thus deserves more discussion.

First, if none of the controlling mechanisms in mosquito populations are considered, then the basic reproduction number R_0 is

$$R_0 = \frac{\beta_h \rho^j \delta_h^k}{\mu_m} \frac{\gamma_h}{\gamma_h + \varnothing_h} \frac{\beta_m \rho^j \delta_m^k}{\sigma_h + \varnothing_h} \frac{\gamma_m}{\gamma_m + \mu_m} \overline{m}_0, \tag{3.16}$$

where $\overline{m}_0$ is given by Eq. (3.3) without control, or

$$\overline{m}_0 = \frac{\sigma_p}{\mu_m}\frac{\sigma_l}{\sigma_p+\mu_p}C_0\left(1-\frac{1}{Q_0}\right), \tag{3.17}$$

where the basic offspring number Q_0 is given by Eq. (3.5). The carrying capacity C_0 is obtained from C leading to the controlling parameters $\alpha_b = 0$ and $\alpha_a = 0$.

We explicitly write the basic reproduction number for submodels according to Eqs. (3.9 and 3.10) for $j = 1,2$ as:

$$R_0 = \begin{cases} \dfrac{\rho^j\beta_h\frac{D\overline{m}}{\overline{N}}}{\mu_m}\dfrac{\gamma_h}{\gamma_h+\varnothing_h}\dfrac{\rho^j\beta_m}{\sigma_h+\varnothing_h}\dfrac{\gamma_m}{\gamma_m+\mu_m}, & for\ k=1 \\ \dfrac{\rho^j\beta_h D\overline{m}}{\mu_m}\dfrac{\gamma_h}{\gamma_h+\varnothing_h}\dfrac{\rho^j\beta_m\overline{N}}{\sigma_h+\varnothing_h}\dfrac{\gamma_m}{\gamma_m+\mu_m}, & for\ k=2, \end{cases}$$

where $\rho^1 = \varnothing_m$ and $\rho^2 = \sqrt{\varnothing_m}$. Given that $\overline{M} = D\overline{m}$, we have, for $k = 1$:

$$R_0 = \frac{\rho^j\beta_h}{\mu_m}\frac{\gamma_h}{\gamma_h+\varnothing_h}\frac{\rho^j\beta_m}{\sigma_h+\varnothing_h}\frac{\gamma_m}{\gamma_m+\mu_m}\frac{\overline{M}}{\overline{N}}, \tag{3.18}$$

and for k = 2,

$$R_0 = \frac{\rho^j\tilde{\beta}_h}{\mu_m}\frac{\gamma_h}{\gamma_h+\varnothing_h}\frac{\rho^j\tilde{\beta}_m}{\sigma_h+\varnothing_h}\frac{\gamma_m}{\gamma_m+\mu_m}, \tag{3.19}$$

where $\tilde{\beta}_h = \beta_h\overline{N}$ and $\tilde{\beta}_m = \beta_m\overline{M}$. The basic reproduction number differs according to the model's assumption of dengue virus transmission. The basic reproduction number is linked to the introduction of one case in completely susceptible populations, and we assume that one infectious mosquito is introduced (the introduction of one infectious human follows a similar interpretation).

We interpret the basic reproduction number given by Eq. (3.18), the case $k = 1$, which is written as

$$R_0 = \left(\frac{\frac{\rho^j\beta_h}{\overline{N}}}{\mu_m}\overline{N}\right)\frac{\gamma_h}{\gamma_h+\varnothing_h}\left(\frac{\frac{\rho^j\beta_m}{\overline{N}}}{\sigma_h+\varnothing_h}\overline{M}\right)\frac{\gamma_m}{\gamma_m+\mu_m}.$$

The first term represents the mean number of humans in a completely susceptible population ($\overline{N}$) that become infected due to the mean number of bites given by an infectious mosquito during its lifespan ($\rho^j\beta_h/\left(\overline{N}\mu_m\right)$). The term $\gamma_h/(\gamma_h+\varnothing_h)$ is the probability that an infected human survives the exposed period and enters the infectious class. The third term is the mean number of mosquitoes in a completely susceptible population ($\overline{M}$) that become infected due to the average number of bites given by susceptible mosquitoes on an infectious human during his/her

lifespan $(\rho^j \beta_m / \left(\overline{N}\,(\sigma_h + \varnothing_h)\right))$. The term $\gamma_m/(\gamma_m + \mu_m)$ is the probability that an infectious mosquito survives the exposed period and enters the infectious class. Hence, R_0 is the mean number of secondary infectious mosquitoes produced by one infectious mosquito introduced in completely susceptible populations of humans and mosquitoes.

Dengue epidemics can be established in a community if one female mosquito generates more than one daughter, and an infectious mosquito can produce more than one secondary infectious mosquito. The severity of a dengue epidemic can be assessed by estimating R_c and Q_c: the higher both values, the more severe the epidemic.

The basic reproduction number calculated from Eq. (3.19), $k = 2$, follows a similar interpretation. Instead of infection probabilities, in this case, we use the effective contact rates. Only in the equilibrium state are the per-capita contact rates (β_h and β_m) and total contact rates ($\tilde{\beta}_h$ and $\tilde{\beta}_m$) interchangeable through $\tilde{\beta}_h = \beta_h \overline{N}$ and $\tilde{\beta}_m = \beta_m \overline{M}$.

Second, the controlling mechanisms decrease the basic reproduction number R_0. The relationship between R_c and R_0, Eqs. (3.15) and (3.16), is

$$R_c = R_0 \frac{\mu_m}{\mu_m^s} \frac{\gamma_m + \mu_m}{\gamma_m + \mu_m^s} \frac{\overline{m}}{\overline{m}_0},$$

with $\mu_m < \mu_m^s$ and $\overline{m} < \overline{m}_0$, where $\overline{m}$ and $\overline{m}_0$ are calculated from Eq. (3.3) and Eq. (3.17), respectively. The control mechanisms decrease the basic reproduction number and can result in the elimination of dengue transmission by decreasing it below unity ($R_c < 1$).

The time varying effective reproduction number, R_{ef}, is defined as

$$R_{ef} = R_c s \frac{m_1}{m}, \tag{3.20}$$

where the time varying fractions of susceptible humans and mosquitoes are, respectively, s and m_1/m, with $m = m_1 + m_2 + m_3$. This definition reproduces the previously obtained relationship existing among $\overline{m}$, $\overline{m}_1$ and $\overline{s}$. The effective reproduction number has two bounding results.

First, at $t = 0$, we assume that one case is introduced (one human, for example) in a completely susceptible human and mosquito populations. Hence, $s = (N-1)/N \approx 1$, $m_1/m = 1$ and $R_{ef} = R_c$. If controlling mechanisms are not considered ($R_c = R_0$), then in the beginning of an epidemic,

$$R_{ef} = R_0.$$

As time goes on, s and m_1/m decrease, and thus, R_{ef}, given by Eq. (3.20), also decreases.

Second, as $t \to \infty$, the asymptotic equilibrium values are reached when one infectious case produces exactly one secondary case. Hence, R_{ef} must obey

$$R_{ef} = R_c \overline{s} \frac{\overline{m}_1}{\overline{m}} = 1,$$

from which, if controlling mechanisms are not considered ($R_c = R_0$), we have the asymptotic relationship

$$\overline{s} \frac{\overline{m}_1}{\overline{m}} = \frac{1}{R_0},$$

where the inverse of the basic reproduction number is the product of the fractions of susceptible populations. To better explain this formula, the modelling of directly transmitted infections (such as rubella, measles, etc.) relies on the following formula:

$$\overline{s} = \frac{1}{R_0},$$

where $\overline{s}$ is the fraction (in the steady state) of susceptible humans (Anderson and May 1991; Yang 1999a, b).

3.3.3 *Study of the Non-autonomous Modelling*

The non-autonomous system of equations, given by Eqs. (3.11) and (3.12), must be dealt with numerically. The dynamical trajectories of this system do not achieve any limiting values asymptotically. For this reason the notion of reproduction number does not make sense.

However, we can define the effective reproduction number R_{ef} in the context of non-autonomous modelling from ideas borrowed from autonomous modelling: the time-independent model parameters of the reproduction number R_c are allowed to vary, originating the effective reproduction number R_{ef}.

The effective reproduction number regarded in the non-autonomous system, Eqs. (3.11 and 3.12), is provided by Eq. (3.20), but now the model parameters depend on time. Because two populations interact, we define the contributions of the human and mosquito populations, R^h_{ef} and R^m_{ef}, in the overall effective reproduction ratio R_{ef} at each time t as

$$\begin{cases} R^h_{ef} = \dfrac{\rho^j \beta_h}{\mu^s_m} \dfrac{\gamma_h}{\gamma_h + \varnothing_h} \dfrac{D}{N} s \\ R^m_{ef} = \dfrac{\rho^j \beta_m}{\sigma_h + \varnothing_h} \dfrac{\gamma_m}{\gamma_m + \mu^s_m} \overline{m} \dfrac{m_1}{m} = \dfrac{\rho^j \beta_m}{\sigma_h + \varnothing_h} \dfrac{\gamma_m}{\gamma_m + \mu^s_m} m_1, \end{cases}$$

for the model labeled $k = 1$, and for $k = 2$,

$$\begin{cases} R_{ef}^{h} = \dfrac{\rho^{j}\beta_h}{\mu_m^s}\dfrac{\gamma_h}{\gamma_h + \varnothing_h}Ds \\ R_{ef}^{m} = \dfrac{\rho^{j}\beta_m}{\sigma_h + \varnothing_h}\dfrac{\gamma_m}{\gamma_m + \mu_m^s}\overline{m}N\dfrac{m_1}{m} = \dfrac{\rho^{j}\beta_m}{\sigma_h + \varnothing_h}\dfrac{\gamma_m}{\gamma_m + \mu_m^s}Nm_1, \end{cases}$$

for $j = 1,2$, and N is the varying size of a human population (D is constant). Therefore, R_{ef} is given by

$$R_{ef} = R_{ef}^{h}R_{ef}^{m}, \tag{3.21}$$

which varies with time.

The effective reproduction ratio R_{ef} provides the risk of a dengue outbreak. Up to just before an epidemic, $R_{ef} = R_c$, or, in the absence of controlling efforts, $R_{ef} = R_0$. The severity of the first epidemic peak is given by the basic reproduction number R_0. After an epidemic peak, R_{ef} increases to trigger the next dengue outbreak.

3.4 Results

We first present model parameters and temperature and precipitation data used in the numerical simulations.

Table 3.1 summarises the model parameters. The values presented in Table 3.1 are the mean values with respect to mosquito population parameters, whereas for the human population, they are considered independent of temperature and precipitation; the value $\varnothing_{\mathrm{h}}$ was chosen to describe the varying population of Campinas City from 1991 (847,595) to 2010 (1,080,999) Esteva and Vargas (2003). The values given in Table 3.1 are used to numerically simulate the autonomous system of equations.

The entomological parameters $\varnothing_m$, μ_l, μ_p, μ_m, σ_l and σ_p of *A. aegypti* depend strongly on temperature. Table 3.2 illustrates the estimated entomological parameters from controlled temperature experiments (Yang et al. 2009a, b, 2011). An *n-th* degree polynomial $P_n(T) = b_0 + b_1T + \cdots + b_nT^n$, where b_i is represented by $days^{-1} \times (^{\circ}C)^{-i}$, was used to fit experimental data.

In addition to temperature, rainfall influences the entomological parameters μ_l, μ_p, q, and the carrying capacity C. Table 3.3 summarises the precipitation-dependent parameters and their values.

The control of dengue transmission relies on the reduction of mosquito populations by spraying insecticides and by removing breeding sites. In general, insecticides are applied in the areas surrounding houses where cases of active transmission of the dengue virus were specified. Concomitantly, the breeding sites

Table 3.1 Summary of model's parameters and respective mean values

Symbol	Meaning	Unit	Value
f	Fraction of eggs originating female mosquitoes	–	0.5
q	Fraction of eggs hatching to larva stage	–	0.5
C	Carrying capacity (breeding sites)	–	0.8
$\varnothing_m$	Intrinsic oviposition rate per female mosquito	1/day	4.0479
μ_l	Per-capita mortality rate of larva	1/day	6.28×10^{-2}
μ_p	Per-capita mortality rate of pupa	1/day	5.73×10^{-2}
μ_m	Per-capita mortality rate of female mosquito	1/day	3.73×10^{-2}
σ_l	Per-capita transition rate from larva to pupa	1/day	1.184×10^{-1}
σ_p	Per-capita transition rate from pupa to female mosquito	1/day	3.706×10^{-1}
γ_m	Per-capita extrinsic incubation rate	1/day	6.6×10^{-2}
μ_h	Per-capita mortality rate of human	1/day	3.8052×10^{-5}
$\varnothing_h$	Per-capita natality rate of human	1/day	7.3100×10^{-5}
γ_h	Per-capita intrinsic incubation rate	1/day	0.1428
σ_h	Per-capita recovery rate of human	1/day	0.1428
β_m	Transmission rate from human to female mosquito	1/day	3.0×10^{-1}
β_h	Transmission rate from female mosquito to human	1/day	6.0×10^{-2}

are removed. The removing of breeding sites also occurs during seasons preceding dengue epidemics to prevent dengue outbreaks. Table 3.4 summarises mosquito controlling parameters and their values.

Figure 3.1 presents the number of houses that were sprayed with insecticides and where the breeding sites were removed since 2000 in the City of Campinas.[1]

The daily maximum and minimum temperatures CEPAGRI/UNICAMP (2012) and precipitation Instituto de Açúcar e Álcool (2012) from January 1, 1991 to December 31, 2011 in the City of Campinas, São Paulo State, Brazil are used to numerically simulate the previously described dynamics systems. Figure 3.2 illustrates these data, assigning to January 1, 1991 as the 1st day 1st in the time axis, and so on. A restricted interval of time, from days 1,000 to 1,400 that correspond to September 26, 1993 to October 31, 1994, is also presented.

Results with respect to mosquito populations and dengue transmission models are presented. Three cases are used in the analyses of both mosquito populations and dengue transmission models with respect to dependency of the parameters on temperature and precipitation: (1) constant (the annual temperature and precipitation mean is used), (2) temperature-dependent, and (3) dependent on both temperature and precipitation.

[1] Data provided by Sucen (Superintendência de Controle de Endemias).

Table 3.2 Entomological parameters of female mosquito and aquatic phase estimated using an *n-th* degree polynomial, with unit of b_i being $days^{-1} \times (^\circ C)^{-i}$ and standard deviations are not shown

	b_0	b_1	b_2	b_3	b_4	b_5	b_6	b_7	b_8
$\varnothing_m$	-5.3999	1.800160	-2.12×10^{-1}	1.02×10^{-2}	-1.51×10^{-4}	–	–	–	–
μ_l	2.31532	-4.19×10^{-1}	2.73×10^{-2}	-7.53×10^{-4}	7.50×10^{-6}	–	–	–	–
μ_p	4.25×10^{-1}	-3.25×10^{-2}	7.06×10^{-4}	4.39×10^{-7}	–	–	–	–	–
μ_m	8.69×10^{-1}	-1.59×10^{-1}	1.12×10^{-2}	-3.41×10^{-4}	3.81×10^{-6}	–	–	–	–
σ_l	-1.84270	8.29×10^{-1}	-1.46×10^{-1}	1.31×10^{-2}	-6.46×10^{-4}	1.79×10^{-5}	-2.62×10^{-7}	1.5×10^{-9}	–
σ_p	21.9021	-10.31110	20.50830	-2.24×10^{-1}	1.47×10^{-2}	-5.89×10^{-4}	1.41×10^{-5}	-2.0×10^{-7}	1.0×10^{-9}

Table 3.3 Summary of model's parameters depending on precipitation and respective values

Symbol	Meaning	Unit	Value
w_1	Residual effect of past rain	1/°C	0.5
C_i	Rain independent variation in breeding sites	–	1
c_0	Minimum carrying capacity in the absence of rain	–	5.0×10^{-1}
c_1	Capacity of creation of breeding sites due to rain	1/mm	5.0×10^{-2}
q_0	Capacity of eggs hatching even without rain fall	–	7.0×10^{-1}
q_1	Rate of hatching due to humidity	1/mm	5.0×10^{-2}
g_l	Additional physical mortality among larvae	1/mm	1.0×10^{-4}
g_p	Additional physical mortality among pupae	1/mm	1.0×10^{-4}
V_c	Critical rain volume to overflow	1/mm	$5.0 \times 10^{+1}$

Table 3.4 Summary of controlling parameters

Symbol	Meaning	Unit	Value
α_a	Efficacy of preventive removing of breeding sites	–	2
α_b	Efficacy of targeted removing of breeding sites	–	8
α_s	Efficacy of insecticide application on susceptibles	–	2
α_d	Efficacy of insecticide application on infectious	–	13

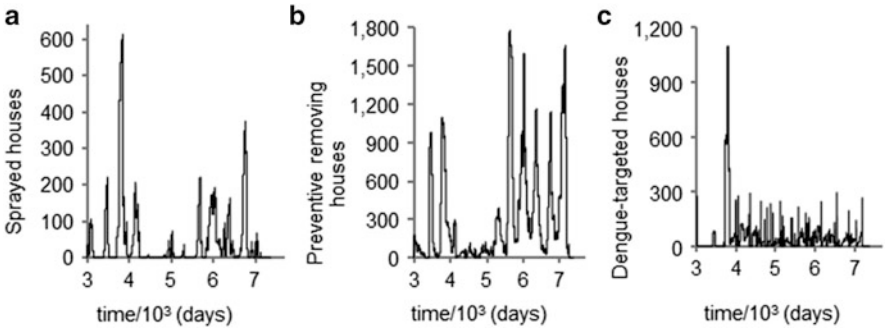

Fig. 3.1 Number of houses visited to spray insecticides (**a**), and removing of breeding sites as preventive (**b**) and dengue-targeted (**c**)

3.4.1 Mosquito Population

Equation (3.1), with model parameters defined by Eq. (3.2), is treated numerically. Initially, we present the time-independent model, assuming that the entomological parameters are constant values that average 1 year of variation. Temperature dependency is then considered, and finally precipitation is included.

Numerical results in this section are shown considering the entire time interval given in Fig. 3.2 and also in a restricted time interval to highlight some details.

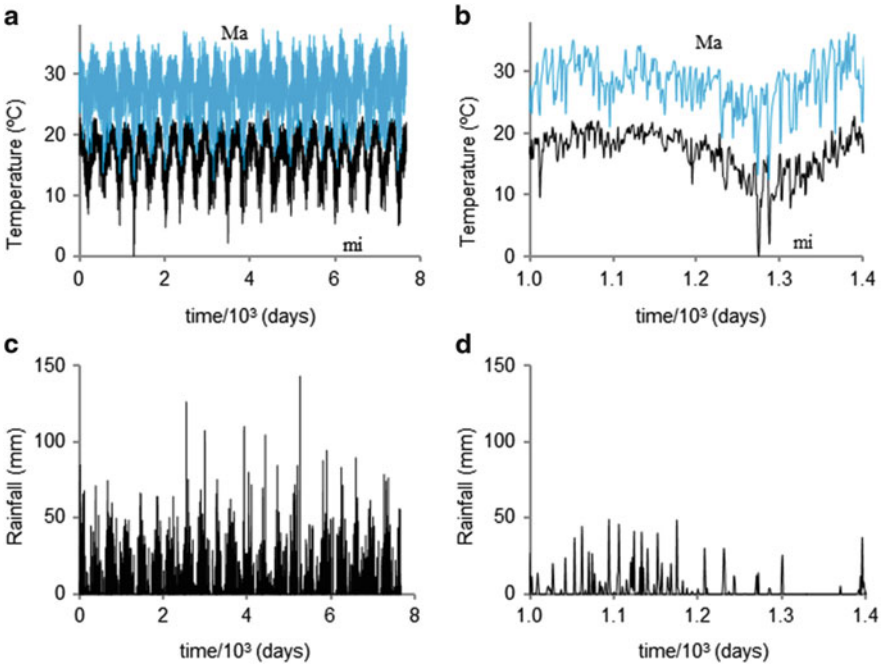

Fig. 3.2 Daily maximum and minimum temperatures (**a, b**), and precipitation (**c, d**) registered since 1991 in the City of Campinas, São Paulo State, Brazil

3.4.1.1 Constant Entomological Parameters

The fixed-value parameters used for assessing the mosquito population are presented in Table 3.1. The basic offspring number is $Q_0 = 15.369$, which was obtained from Eq. (3.5). If we change the values of parameters f and q to 0.1, the new basic offspring number becomes $Q_0 = 0.615$.

Figure 3.3 illustrates the dynamical trajectories of the mosquito population for $Q_0 > 1$ and $Q_0 < 1$. Figure 3.3b was obtained using values from Table 3.1, except $f = q = 0.1$. Figure 3.3 illustrates the classical population model when all parameters are constant: the change in behaviour occurs when the basic offspring number $Q_0 = 1$. When the average number of offspring is lower than 1, the mosquito population goes to extinction, and conversely the population is sustained if $Q_0 > 1$, and as this number increases, the population size reaches its maximum value given by the carrying capacity.

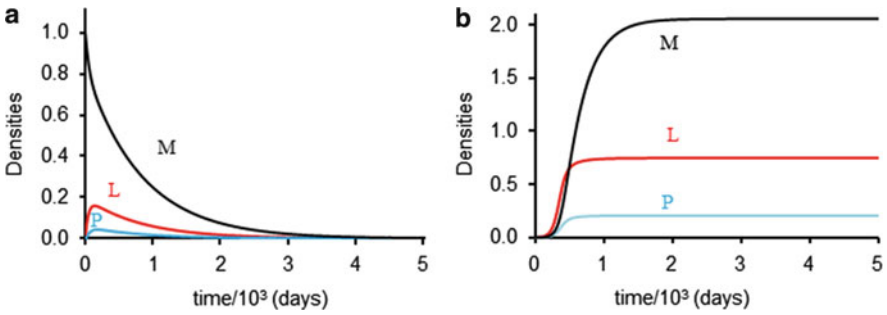

Fig. 3.3 Autonomous model – Densities of larvae (L), pupae (P) and female mosquitos (M) for $Q_0 < 1$ (**a**), and $Q_0 > 1$ (**b**)

3.4.1.2 Temperature-Dependent Entomological Parameters

Instead of constant entomological parameters, these parameters are allowed to vary with temperature. The temperature that is used in the modelling corresponds to the temperature of Campinas City (Fig. 3.2). Here we show the dependency of entomological parameters $\varnothing_m$, μ_m, σ_l and σ_p with varying temperatures as illustrated in Fig. 3.2. These parameters are assumed to be independent of precipitation. Other entomological parameters, μ_l and μ_p, are presented as follows, as both depend on precipitation.

The effective offspring number Q_{ef}, from Eq. (3.4), which changes Q_c by Q_{ef}, varies along time due to the temperature varying entomological parameters. This parameter provides an idea of the mean number of offspring at each time.

Figure 3.4 illustrates the temperature-dependent $\varnothing_m$ and μ_m (Yang et al. 2009a, b, 2011). Both parameters were fitted using a *4-th* order polynomial (Table 3.2). Figs. on the left encompass the entire time period, from January 1, 1991 to December 31, 2011, and the Figs. on the right illustrate the restricted time interval from September 26, 1993 to October 31, 1994.

Figure 3.5 shows the temperature-dependent σ_l and σ_p (Yang et al. 2009a, b, 2011). Both parameters were fitted using *7-th* and *8-th* order polynomials, respectively (Table 3.2). We present the entire (left Figs.) and restricted (right Figs.) time intervals.

Figure 3.6 presents the dynamical trajectories of the mosquito populations when parameters are allowed to depend on temperature. The fixed model parameters are those given in Table 3.1, and the varying entomological parameters are calculated using fitted polynomials given in Table 3.2. Figure 3.6 also demonstrates the effective offspring number Q_{ef}. We present the entire (left Figs.) and restricted (right Figs.) time intervals.

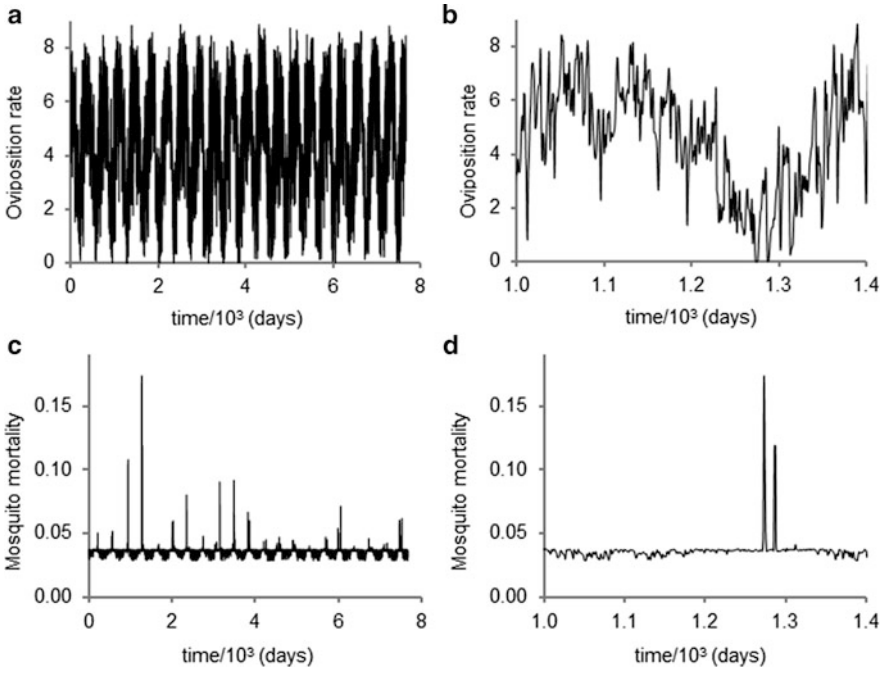

Fig. 3.4 Temperature dependent $\varnothing_m$ (**a**, **b**) and μ_m (**c**, **d**)

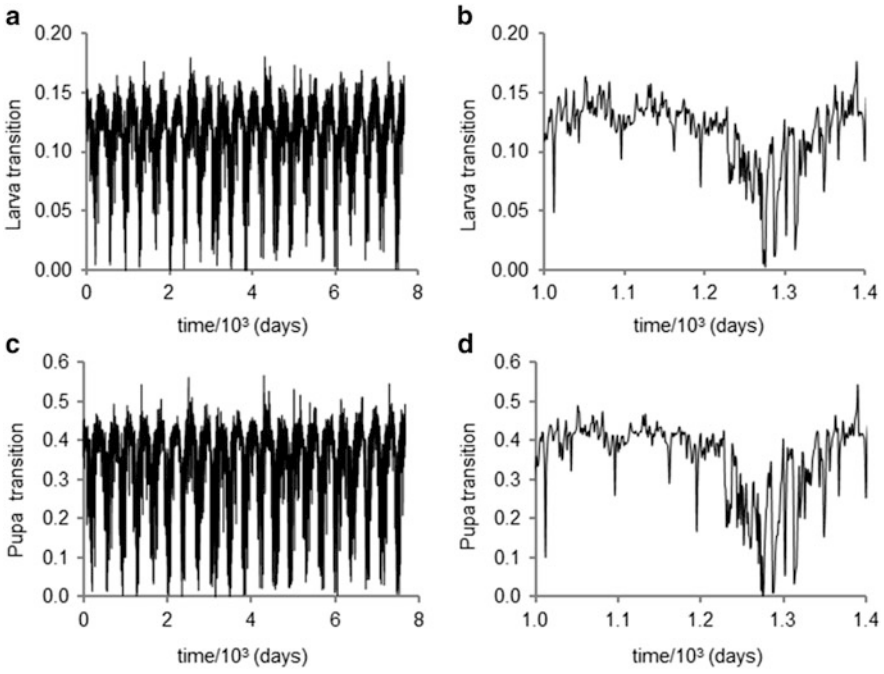

Fig. 3.5 Temperature dependent σ_l (**a**, **b**) and σ_p (**c**, **d**)

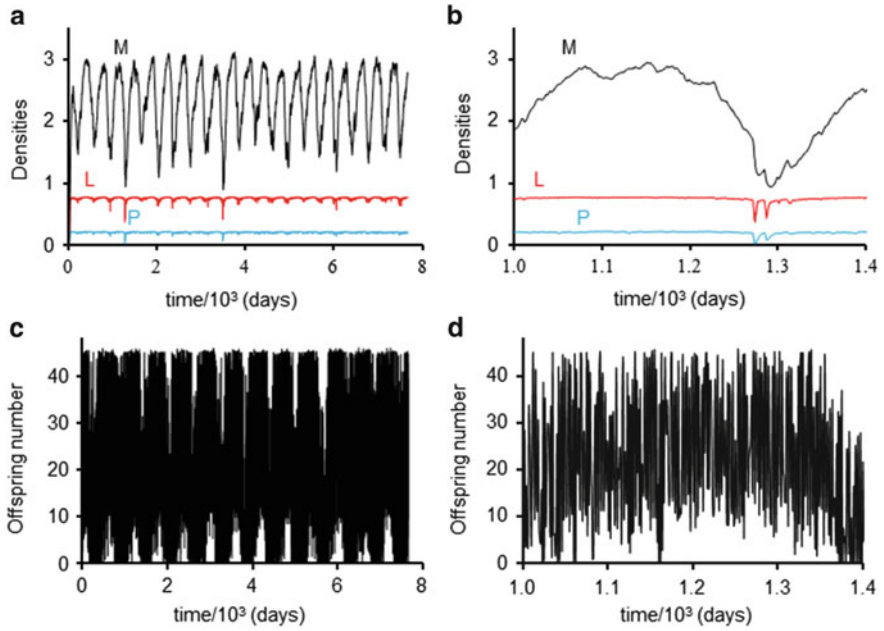

Fig. 3.6 Temperature dependency – Density of larvae (L), pupae (P) and female mosquitos (M) (**a**, **b**), and effective offspring number Q_{ef} (**c**, **d**)

Despite the intense intra- and inter-day fluctuations in the effective offspring number Q_{ef}, we observe damped amplitudes in the aquatic and adult stages, where the within-day oscillations are quite smooth in the adult mosquitoes. Therefore, the major mosquito population fluctuations occur seasonally.

3.4.1.3 Temperature- and Precipitation-Dependent Entomological Parameters

As we have already underscored, precipitation influences the parameters μ_l, μ_p, q and C. The additional contributions of precipitation on temperature-dependent μ_l and μ_p are given by the difference

$$\begin{cases} \mu_l^s - \mu_l = g_l\,[W(j) - V_c]\,\theta\,[W(j) - V_c] \\ \mu_p^s - \mu_p = g_p\,[W(j) - V_c]\,\theta\,[W(j) - V_c]\,, \end{cases}$$

from Eq. (3.2). The parameters q and C were assumed to be dependent only on precipitation.

Figure 3.7 presents the temperature-dependent μ_l and μ_p (Yang et al. 2009a, b, 2011) and the additional contribution by precipitation. The additional contribution with respect to μ_l was multiplied by factor *80* and translated upward by summing

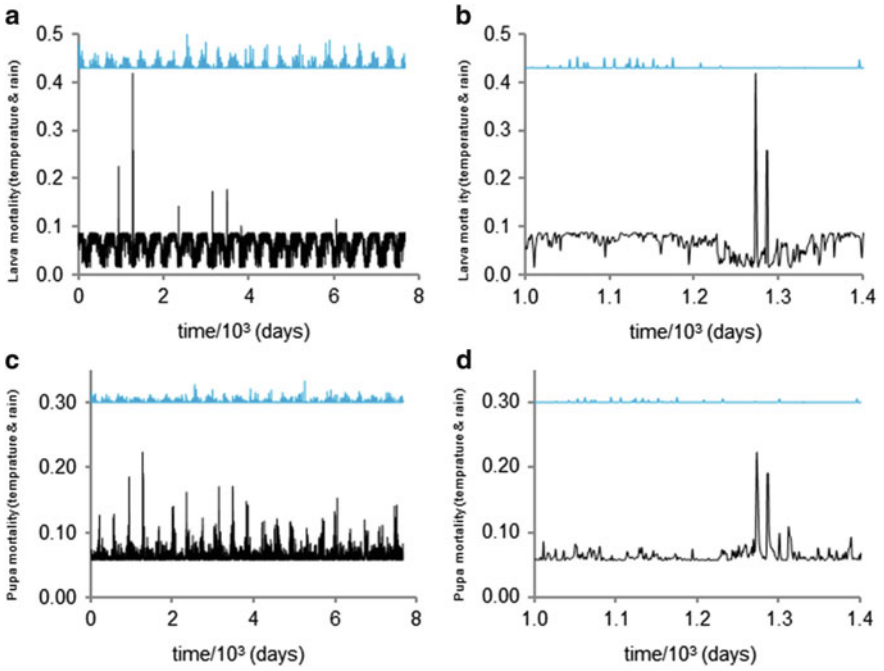

Fig. 3.7 Temperature dependent μ_l (**a**, **b**) and μ_p (**c**, **d**), and corresponding rainfall contributions

0.43 to fit it on the same scale of temperature-dependent μ_l. To the parameter μ_p, the multiplying factor was *35*, and the summing constant was *0.3*. We present the entire (left Figs.) and restricted (right Figs,) time intervals.

Figure 3.8 shows the precipitation-dependent q and C. We present the entire (left Figs.) and restricted (right Figs.) time intervals.

Figure 3.9 shows the dynamical trajectories of the mosquito populations when parameters are allowed to depend both on temperature and precipitation. The fixed model parameters are from Table 3.1. The varying entomological parameters are calculated using fitted polynomials from Table 3.2, and the precipitation parameters are provided in Table 3.3. Figure 3.9 presents the effective offspring number Q_{ef}, which varies along time due to the temperature and precipitation varying entomological parameters. We present the entire (left Figs.) and restricted (right Figs.) time intervals.

By comparing Figs. 3.6 and 3.9, we observe that the inclusion of rain in the parameters of the model yielded more concentrated fluctuations at a higher level of infestation. Specially, the effective offspring number sharply contrasts to that when rain is introduced in the parameters. The 'regular' oscillations exhibited a much more irregular pattern when rain was included.

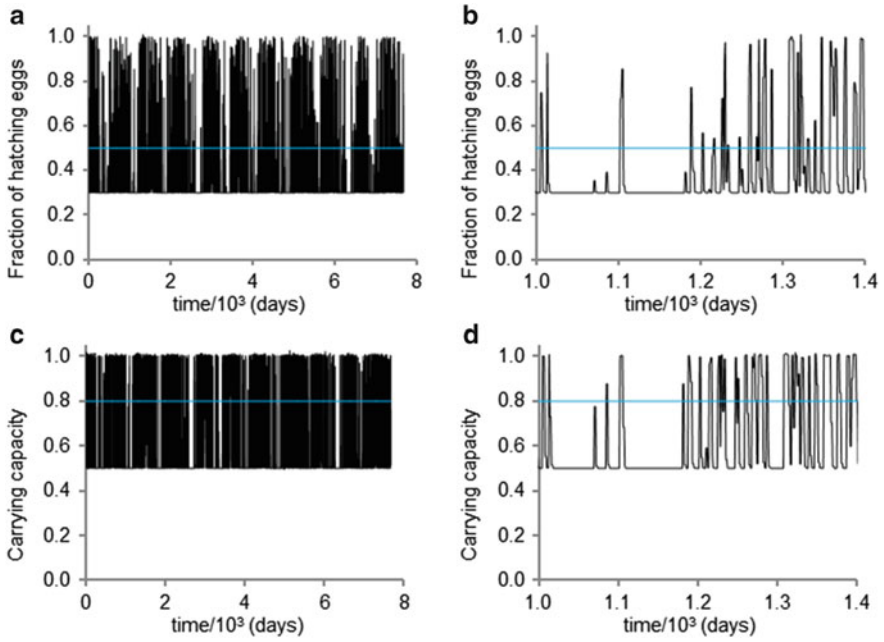

Fig. 3.8 Rainfall dependent q (**a**, **b**) and C (**c**, **d**)

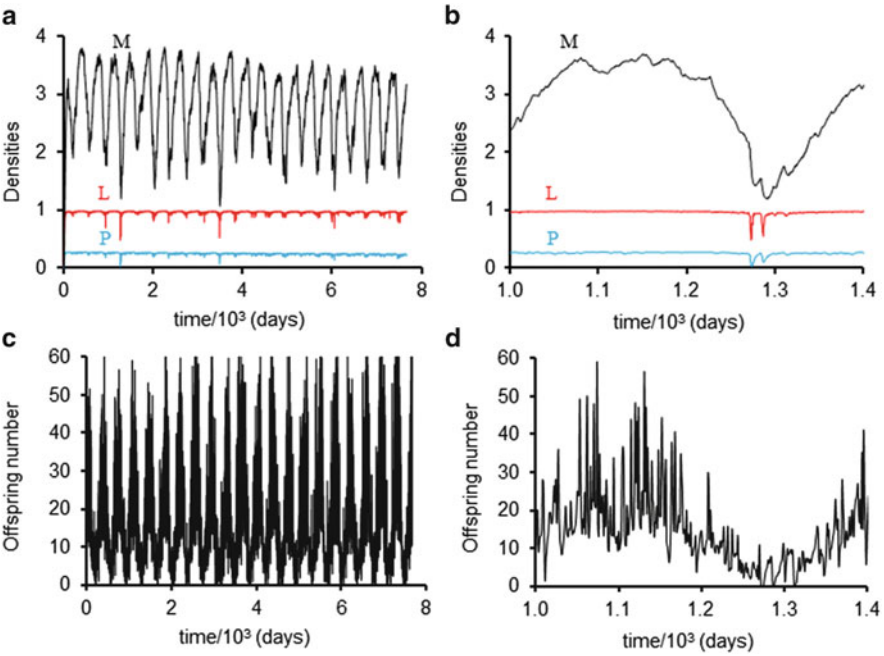

Fig. 3.9 Temperature and precipitation dependency – Densities of larvae (L), pupae (P) and female mosquitos (M) (**a**, **b**); and the effective offspring number Q_{ef} (**c**, **d**)

3.4.2 Dengue Transmission

Equations (3.11) and (3.12), with model parameters defined by Eq. (3.13), are treated numerically. Initially we present the time-independent model with the assumption that the entomological parameters are constant values that are averaged over 1 year of variation. Temperature dependency is then dealt with, and finally, precipitation is included.

The initial conditions supplied to the dynamical system correspond to the case where the mosquito and human populations co-exist without dengue. At t = 1,826 (or at calendar time January 1, 1996), one case of dengue among humans is introduced.

With respect to the mosquito population, curves of larvae and pupae are not shown because they are the same as those obtained in the preceding section. Notably, the sum of the three classes of mosquitoes m_1, m_2 and m_3 is calculated from the total mosquito density m provided in the preceding section.

3.4.2.1 Constant Entomological Parameters

Using fixed values of the parameters in Table 3.1, dengue transmission is assessed. The basic reproduction number is $R_0 = 12.022$ calculated using Eq. (3.19). If we change the value of parameters β_m and β_h to $\beta_m = 2.0 \times 10^{-1}$ and $\beta_h = 5.4 \times 10^{-2}$, the new basic reproduction number is $R_0 = 0.721$.

Figure 3.10 illustrates the model labeled 4, that is, $k = 2$ and $j = 2$. Figure 3.10 illustrates the classical population model when all parameters are constant: the change in behaviour occurs when the basic reproduction number $R_0 = 1$. When the mean number of secondary infectious mosquitoes is lower than 1, the dengue transmission goes to extinction, and conversely the infection is sustained if $R_0 > 1$. As this number increases, the fraction of infectious individuals reaches its maximum value given by $\bar{i}_M$.

3.4.2.2 Temperature and Precipitation-Dependent Entomological Parameters

Four types of models are analysed according to Eqs. (3.9) and (3.10). Therefore, the non-autonomous dengue transmission model is separated based on the type of the model and not according to temperature and precipitation, as we did in the analysis of the mosquito population. Only equations for susceptible populations of mosquitos and humans are written from Eqs. (3.11) and (3.12).

Using fixed parameter values with respect to humans given in Table 3.1, in Table 3.2 for temperature-dependent entomological parameters, in Table 3.3 for precipitation-dependent parameters, and in Table 3.4 for controlling efforts, dengue transmission is assessed. In each model, only β_m and β_h are changed.

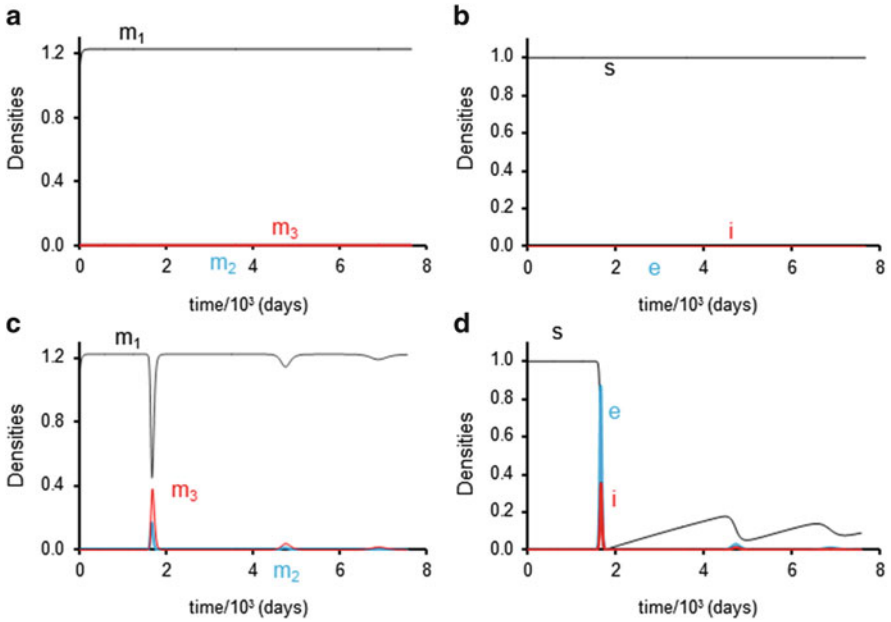

Fig. 3.10 Autonomous model – Densities of susceptible (m_1), exposed (m_2) and infectious (m_3) mosquitos; and fractions of susceptible (s), exposed (e) and infectious (i) humans, for $R_0 < 1$ (**a**, **b**); and $R_0 > 1$ (**c**, **d**)

The effective reproduction number R_{ef} varies along time due to the varying temperature and precipitation entomological parameters. This parameter provides an idea of the average number of secondary infectious cases at each time. The higher this value is, the more severe the epidemic.

The exposed and infectious classes of mosquitoes and humans are much lower than the susceptible classes. For this reason, those classes were multiplied by suitable factors so they could fit the same scale of susceptible classes.

Model 1: $j = 1$ and $k = 2$

The first model addresses the mass action law and biting rate that are dependent linearly on the oviposition rate. In this case, the equations for susceptible populations are

$$\begin{cases} \dfrac{dm_1}{dt} = \sigma_p p - \left(\beta_m \varnothing_m N i + \mu_m^s\right) m_1 \\ \dfrac{ds}{dt} = \varnothing_h - \left(\beta_h \varnothing_m D m_3 + \varnothing_h\right) s, \end{cases}$$

and, using the partial effective reproduction numbers due to human and mosquito populations

$$\begin{cases} R_{ef}^{h} = \dfrac{\gamma_h \varnothing_m \beta_h}{\mu_m^s \left(\gamma_h + \varnothing_h\right)} Ds \\ R_{ef}^{m} = \dfrac{\gamma_m \varnothing_m \beta_m}{\left(\sigma_h + \varnothing_h\right)\left(\gamma_m + \mu_m^s\right)} N m_1, \end{cases}$$

the overall effective reproduction number R_{ef} is

$$R_{ef} = \frac{\gamma_h \gamma_m \beta_m \beta_h \varnothing_m^2}{\mu_m^s \left(\gamma_m + \mu_m^s\right)\left(\sigma_h + \varnothing_h\right)\left(\gamma_h + \varnothing_h\right)} NDsm_1.$$

According to the effects of abiotic factors, two cases are presented.

The dynamical trajectories of dengue transmission were obtained using $\beta_h = 4 \times 10^{-7}$ and $\beta_m = 1 \times 10^{-9}$. The numerical results are shown in Figs. 3.11 and 3.12. In both Figs., the infectious mosquitoes m_3, the exposed e and infectious i humans must be divided by factors of 3, 35 and 20, respectively. The partial effective

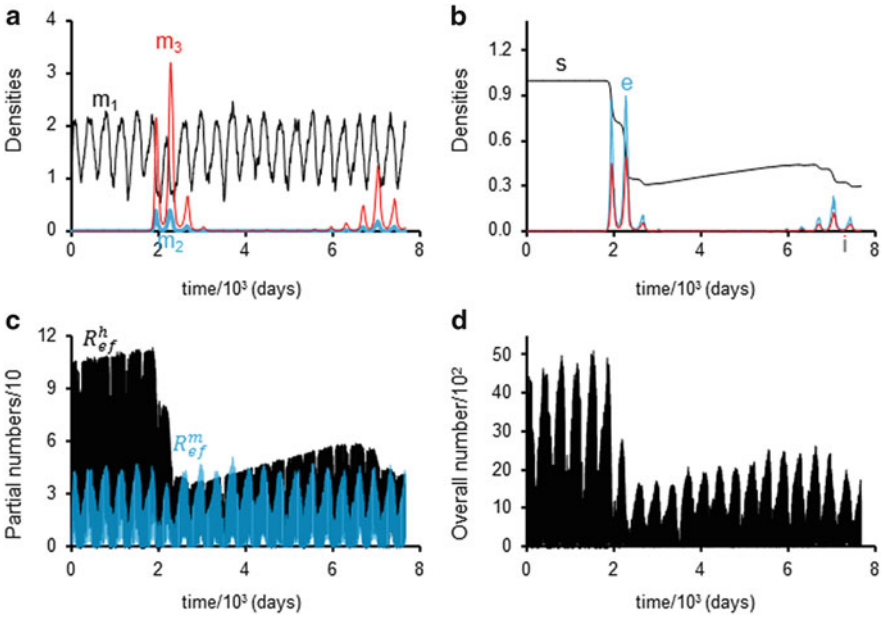

Fig. 3.11 Model 1 (temperature) – Densities of susceptible (m_1), exposed (m_2) and infectious (m_3) mosquitos (**a**); fractions of susceptible (s), exposed (e) and infectious (i) humans (**b**); partial effective reproduction numbers (**c**); and the overall effective reproduction number (**d**)

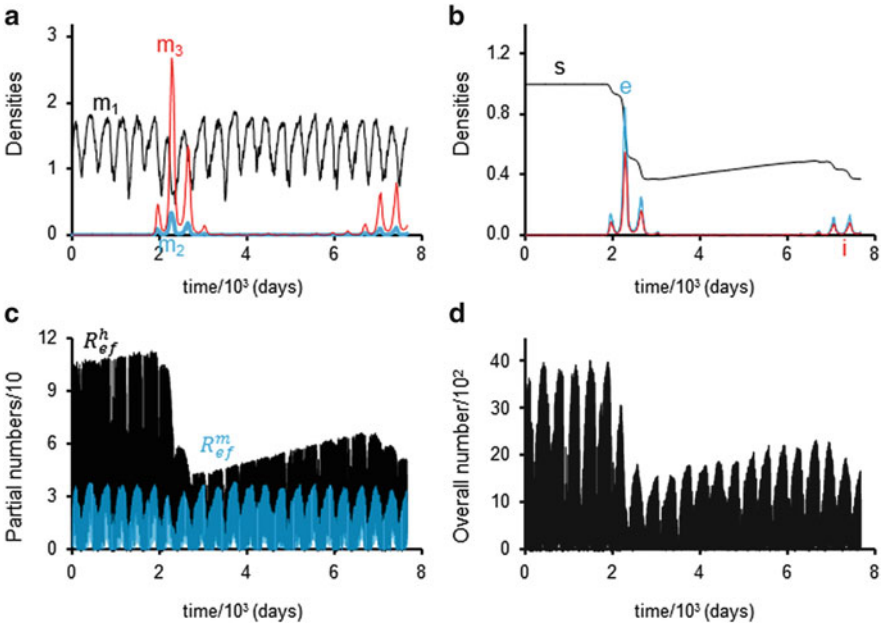

Fig. 3.12 Model 1 (temperature and precipitation) – Densities of susceptible (m_1), exposed (m_2) and infectious (m_3) mosquitos (**a**); fractions of susceptible (s), exposed (e) and infectious (i) humans (**b**); partial effective reproduction numbers (**c**); and the overall effective reproduction number (**d**)

reproduction numbers R^h_{ef} and R^m_{ef} as well as the overall reproduction number R_{ef}, must be multiplied by factors of 10 as well as 100, respectively.

Figure 3.11 shows temperature-dependent modelling that yields a relatively moderate epidemic. The fraction of susceptible humans decreases up to 0.3 with two major epidemics. The risk factor (effective reproduction number) before the outbreak of dengue transmission is approximately 5,000.

Figure 3.12 shows temperature and precipitation-depending modelling that yields a milder epidemic than the previous case. The fraction of susceptible humans decreases up to 0.4 with only one major epidemic peak. The risk factor before the outbreak of dengue transmission is approximately 4,000. The second wave of epidemics is delayed in comparison with Fig. 3.11, and the difference between partial effective numbers R^h_{ef} and R^m_{ef} are higher.

From Figs. 3.11 and 3.12, we observe that the amount of susceptible mosquitoes changes little and results in a practically unchanged partial R^m_{ef}. Conversely, the number of susceptible humans decreases reasonably and leads to an abrupt decrease in the partial R^h_{ef}. Rain decreases the risk factor (R_{ef} diminishes) for dengue transmission, and thus, the epidemic becomes milder.

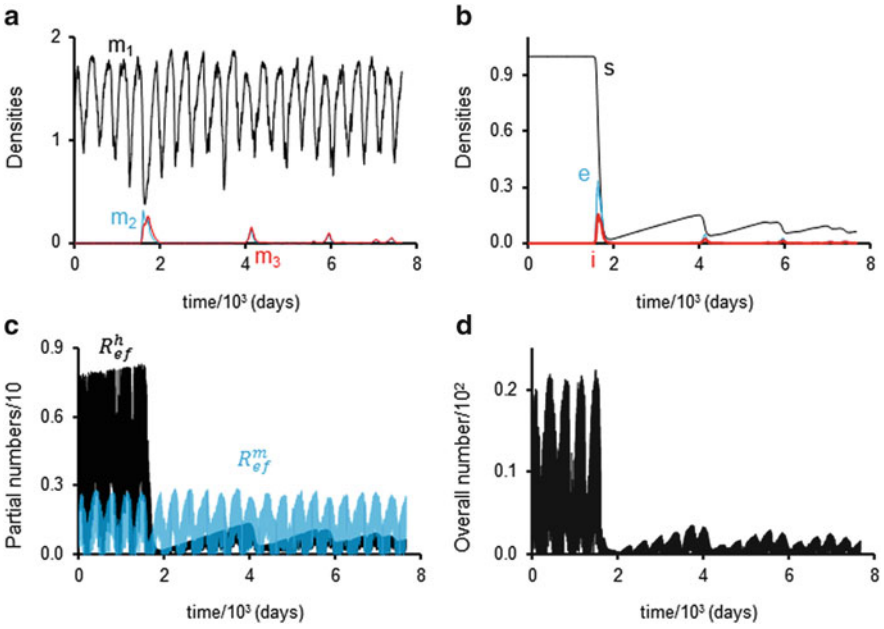

Fig. 3.13 Model 2 (temperature) – Densities of susceptible (m_1), exposed (m_2) and infectious (m_3) mosquitos (**a**); fractions of susceptible (s), exposed (e) and infectious (i) humans (**b**); partial effective reproduction numbers (**c**); and the overall effective reproduction number (**d**)

Model 2: $j = 2$ and $k = 2$

The second model addresses the mass action law and biting rate that are dependent on the square root of the oviposition rate. In this case, the equations for susceptible populations are

$$\begin{cases} \dfrac{dm_1}{dt} = \sigma_p p - \left(\beta_m \sqrt{\varnothing_m} N i + \mu_m^s\right) m_1 \\ \dfrac{ds}{dt} = \varnothing_h - \left(\beta_h \sqrt{\varnothing_m} D m_3 + \varnothing_h\right) s \end{cases}$$

and the overall effective reproduction number R_{ef} is

$$R_{ef} = \frac{\gamma_h \gamma_m \beta_m \beta_h \varnothing_m}{\mu_m^s \left(\gamma_m + \mu_m^s\right)(\sigma_h + \varnothing_h)(\gamma_h + \varnothing_h)} N D s m_1.$$

According to the effects of abiotic factors, two cases are presented.

The dynamicaltrajectories of dengue transmission were obtained using $\beta_h = 1.9 \times 10^{-9}$ and $\beta_m = 7.09 \times 10^{-6}$. The numerical results are shown in Figs. 3.13 and 3.14. In both Figs., the infectious mosquitoes m_3, the exposed e

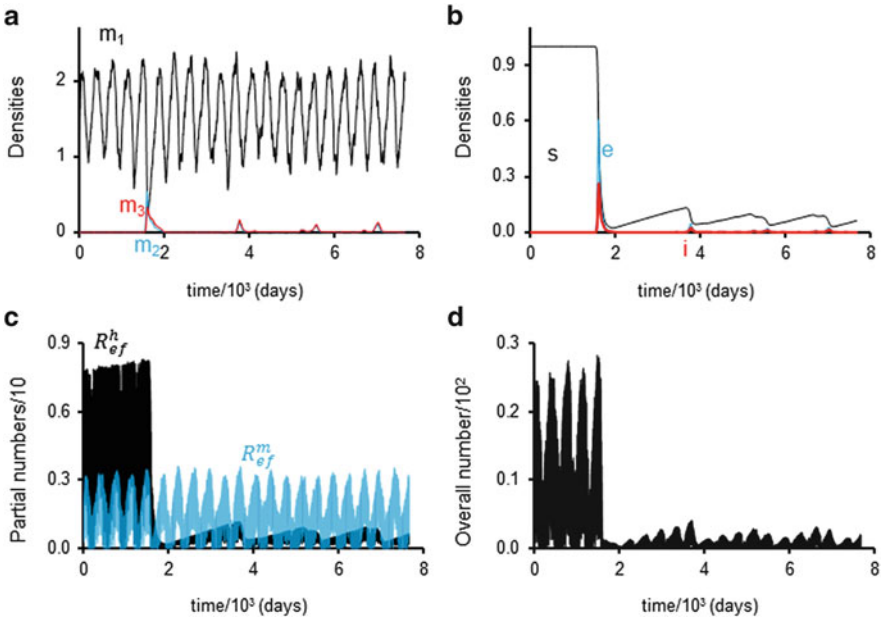

Fig. 3.14 Model 2 (temperature and precipitation) – Densities of susceptible (m_1), exposed (m_2) and infectious (m_3) mosquitos (**a**); fractions of susceptible (s), exposed (e) and infectious (i) humans (**b**); partial effective reproduction numbers (**c**); and the overall effective reproduction number (**d**)

and infectious i humans must be divided by factors 0.5, 6 and 3, respectively. The partial effective reproductions numbers R^h_{ef} and R^m_{ef}, and the overall reproduction number R_{ef}, must be multiplied by factors 10 and 100, respectively.

Figure 3.13 shows temperature-dependent modelling that yields a severe epidemic. The fraction of susceptible humans decreases up to 0.01 with successive epidemic peaks that elapse by 5.5 years. The risk factor before the outbreak of dengue transmission is approximately 200.

Figure 3.14 shows temperature and precipitation-depending modelling that yields a more severe epidemic than that of the previous case. The results are more similar than those of the temperature dependent model, but the risk factor is approximately 250, which is higher than in the previous case.

Comparing Figs. 3.13 and 3.14, when the biting rate is proportional to the square root of the oviposition rate, the epidemic is more severe. Additionally, this model presents an effective reproduction number that is ten times lower than the previous model, which depends linearly on the oviposition rate, as expected (see Fig. 3.4 for $\varnothing_m$).

Model 3: $j = 1$ and $k = 1$

The third model addresses infection being proportional to the probability of biting given by an infectious mosquito and the biting rate that is dependent linearly on the oviposition rate. In this case, the equations for susceptible populations are

$$\begin{cases} \dfrac{dm_1}{dt} = \sigma_p p - \left(\beta_m \varnothing_m i + \mu_m^s\right) m_1 \\ \dfrac{ds}{dt} = \varnothing_h - \left(\beta_h \varnothing_m \frac{D}{N} m_3 + \varnothing_h\right) s, \end{cases}$$

and using the partial effective reproduction numbers due to human and mosquito populations

$$\begin{cases} R_{ef}^h = \dfrac{\gamma_h \varnothing_m \beta_h}{\mu_m^s \left(\gamma_h + \varnothing_h\right)} \dfrac{D}{N} s \\ R_{ef}^m = \dfrac{\gamma_m \varnothing_m \beta_m}{\left(\sigma_h + \varnothing_h\right)\left(\gamma_m + \mu_m^s\right)} m_1, \end{cases}$$

the overall effective reproduction number from Eq. (3.21), $R_{ef} = R_{ef}^h R_{ef}^m$, is

$$R_{ef} = \frac{\gamma_h \gamma_m \beta_m \beta_h \varnothing_m^2}{\mu_m^s \left(\gamma_m + \mu_m^s\right)\left(\sigma_h + \varnothing_h\right)\left(\gamma_h + \varnothing_h\right)} \frac{D}{N} s m_1.$$

According to the effects of abiotic factors, two cases are presented.

The dynamical trajectories of dengue transmission were obtained using $\beta_h = 5.5 \times 10^{-2}$ and $\beta_m = 2.6 \times 10^{-2}$. The numerical results are shown in Figs. 3.15 and 3.16. In both Figs., the exposed m_2 and infectious m_3 mosquitoes, the exposed e and infectious i humans must be divided by factors 7, 5, 8 and 7, respectively.

Figure 3.15 shows temperature-dependent modelling that yields a severe epidemic. The fraction of susceptible humans decreases up to 0.01 with successive epidemic peaks elapsed by 8 years. The risk factor before the outbreak of dengue transmission is approximately 30.

Figure 3.16 shows temperature and precipitation-depending modelling that yields a less severe epidemic. The fraction of susceptible humans decreases up to 0.01 with successive epidemic peaks elapsed by 11 years. The risk factor before the outbreak of dengue transmission is approximately 23.

From Figs. 3.15 and 3.16, rain decreased the risk factor (R_{ef} diminishes) for dengue transmission, and thus, the epidemic became milder. The results are more similar than those observed in model 1.

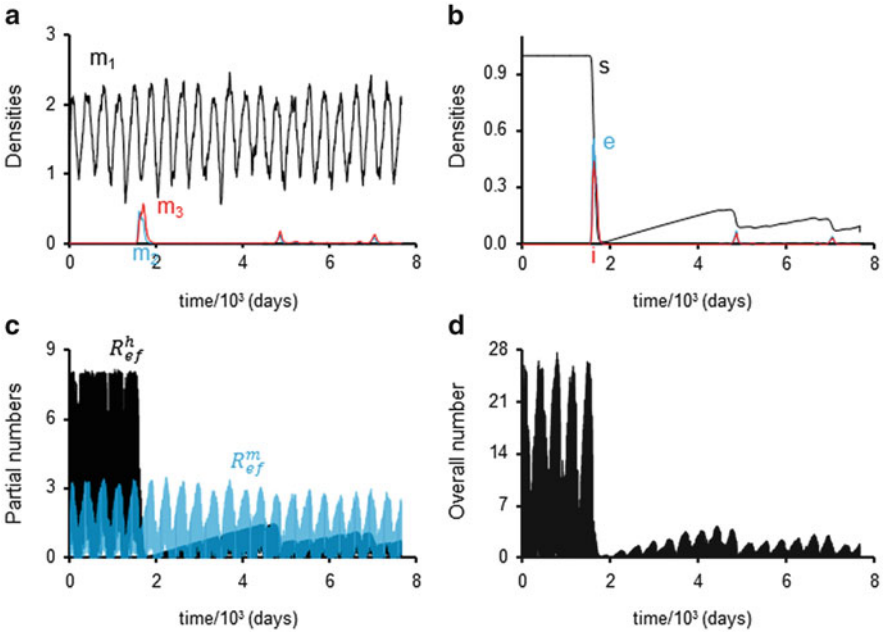

Fig. 3.15 Model 3 (temperature) – Densities of susceptible (m_1), exposed (m_2) and infectious (m_3) mosquitos (**a**); fractions of susceptible (s), exposed (e) and infectious (i) humans (**b**); partial effective reproduction numbers (**c**); and the overall effective reproduction number (**d**)

Model 4: $j = 2$ and $k = 1$

The fourth model simulates an infection that is proportional to the probability of biting by an infectious mosquito and the biting rate that is dependent on the square root of the oviposition rate. In this case, the equations for susceptible populations are

$$\begin{cases} \dfrac{dm_1}{dt} = \sigma_p p - \left(\beta_m \sqrt{\varnothing_m} i + \mu_m^s\right) m_1 \\ \frac{ds}{dt} = \varnothing_h - \left(\beta_h \sqrt{\varnothing_m} \frac{D}{N} m_3 + \varnothing_h\right) s \end{cases},$$

and the overall effective reproduction number R_{ef} is

$$R_{ef} = \frac{\gamma_h \gamma_m \beta_m \beta_h \varnothing_m}{\mu_m^s \left(\gamma_m + \mu_m^s\right)\left(\sigma_h + \varnothing_h\right)\left(\gamma_h + \varnothing_h\right)} \frac{D}{N} s m_1.$$

According to the effects of abiotic factors, two cases are presented.

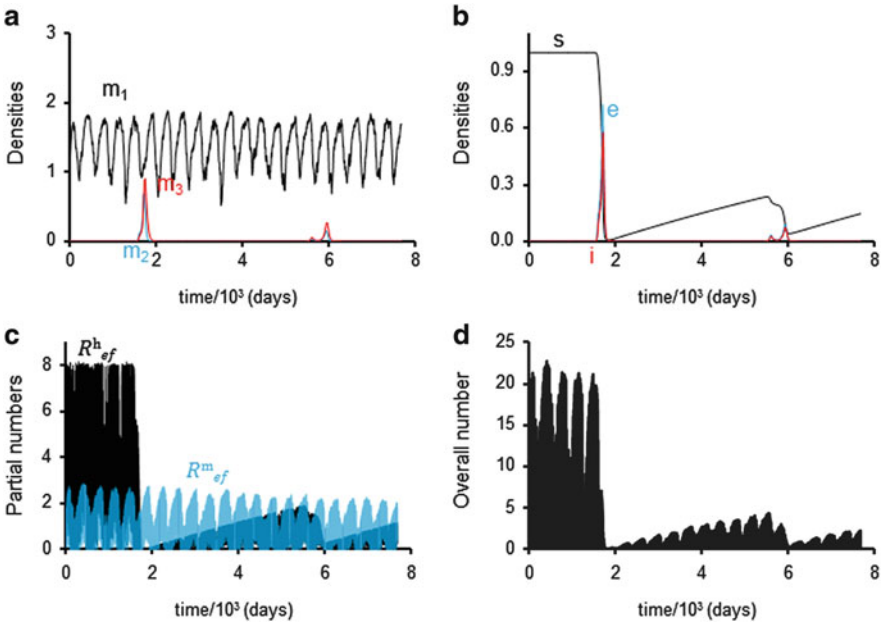

Fig. 3.16 Model 3 (temperature and precipitation) – Densities of susceptible (m_1), exposed (m_2) and infectious (m_3) mosquitos (**a**); fractions of susceptible (s), exposed (e) and infectious (i) humans (**b**); partial effective reproduction numbers (**c**); and the overall effective reproduction number (**d**)

The dynamical trajectories of dengue transmission were obtained using $\beta_h = 2.2 \times 10^{-2}$ and $\beta_m = 5.0 \times 10^{-2}$. The numerical results are shown in Figs. 3.17 and 3.18. In both Figs., the exposed m_2 and infectious mosquitoes m_3, the exposed e and infectious i humans must be divided by factors 200, 200, 60 and 120, respectively.

Figure 3.17 shows temperature-dependent modelling that yields an extremely mild epidemic. The fraction of susceptible humans decreases up to 0.95, and the epidemic incidence elapsed by 5.5 years after the introduction of one case. The risk factor before the outbreak of dengue transmission is approximately 1.8.

Figure 3.18 shows temperature and precipitation-depending modelling that yields a mild epidemic. The fraction of susceptible humans decreases up to 0.6, and the epidemic incidence elapsed by less than 1 year after the introduction of one case. The risk factor before the outbreak of dengue transmission is approximately 2.3.

From Figs. 3.17 and 3.18, rain increased the risk factor (R_{ef} diminishes) for dengue transmission, and thus, the epidemic became more severe. This model presents an effective reproduction number that is ten times lower than that of the previous model. The results are more similar than those observed in model 2.

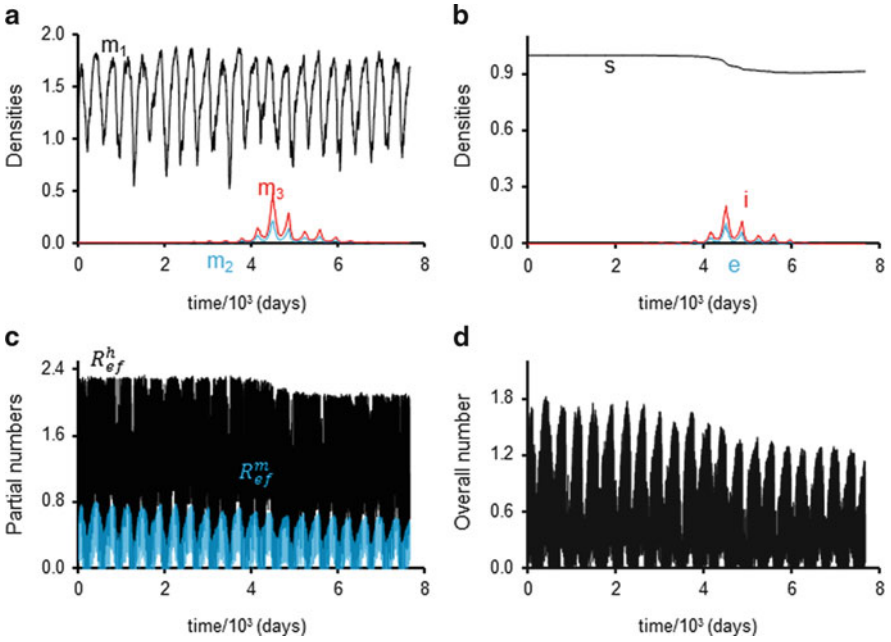

Fig. 3.17 Model 4 (temperature) – Densities of susceptible (m_1), exposed (m_2) and infectious (m_3) mosquitos (**a**); fractions of susceptible (s), exposed (e) and infectious (i) humans (**b**); partial effective reproduction numbers (**c**); and the overall effective reproduction number (**d**)

3.5 Conclusions

Based on entomological parameters, a mathematical model was developed to assess the mosquito population size. The consideration of temperature-dependent parameters resulted in seasonally fluctuating mosquito populations compared to the autonomous model. The additional consideration of precipitation dramatically changed the size of the mosquito populations.

By incorporating the temperature- and precipitation-independent dynamics of a human population to previous mosquito population dynamics, we assessed dengue transmission. Two different models of transmission were analysed: one structured the dengue transmission based on a mass action law, and another assumption considered dengue infection as a probabilistic event. To these two transmissions, we added two types of dengue biting rates: one assumed a linear dependency with the oviposition rate, where the second assumption considered the square root of the oviposition rate.

The inclusion of temperature in the model parameters resulted in oscillatory epidemics, with a period of longer than 1 year, despite the intense daily fluctuations

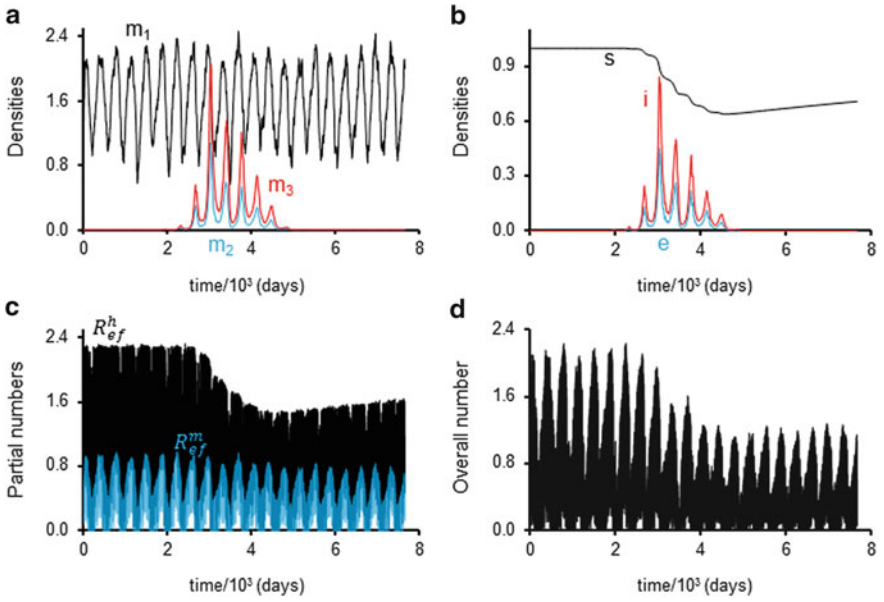

Fig. 3.18 Model 4 (temperature and precipitation) – Densities of susceptible (m_1), exposed (m_2) and infectious (m_3) mosquitos (**a**); fractions of susceptible (s), exposed (e) and infectious (i) humans (**b**); partial effective reproduction numbers (**c**); and the overall effective reproduction number (**d**)

in mosquito populations. This behaviour is due to the larger human parameters as compared with the mosquito parameters. The additional inclusion of rainfall changed dramatically the dengue outbreaks.

The mass action law considers the per-capita transmission rate, which was the reason that extremely low values for the transmission factors β_h and β_m were used. In the case of a probabilistic event, these factors were interpreted in the steady state as population transmission factors.

In this work, the precipitation that was included in the modelling as playing minor effects. Notwithstanding, dynamical behaviors was changed in some order of degree. In a future work, the effects of rain in the dynamics will be enhanced to obtain very different behaviors.

Acknowledgments We thank financial support from FAPESP (Projeto Temático, grant 2009/15098-0) and CNPq (Edital Universal, grant 477034/2011-0).

References

Anderson RM, May RM (1991) Infectious diseases of humans: dynamics and control. Oxford University Press, Oxford/New York/Tokyo, 757p

Baruah S, Dutta P (2012) Seasonal pattern of abundance of Aedes albopictus in urban and industrial areas of Dibrugarh District Assam. Asian J Exp Biol Sci 3:559

CEPAGRI/UNICAMP (2012) Centro de Pesquisa Meteorológicas e Climáticas Aplicadas à Agricultura. http://www.cpa.unicamp.br/. Accessed 2 December 2012

Dickerson AK, Shankles PG, Madhavan NM, Hu DL (2012) Mosquitoes survive raindrop collisions by virtue of their low mass. Proc Natl Acad Sci 109:9822

Esteva L, Vargas C (2003) Coexistence of different serotypes of dengue virus. J Math Biol 46:31

Instituto de Açúcar e Álcool (2012) Centro integrado de informações agrometeorológicas. http://ciiagro.iac.sp.gov.br/. Accessed 2 December 2012

Koenraadt CJM, Harrington LC (2008) Flushing effects of rain on container-inhabiting mosquitoes *Aedes aegypti* and Culex pipiens (Diptera: Culicidae). J Med Entomol 45:28

Lindsay SW, Birley MH (1996) Review: climate change and malaria transmission. Ann Trop Med Parasitol 90:573

Madi M, Ahmad E, Kulaimi NAM, Ali WM, Ismail S, Lim LH (2012) Climatic influences on Aedes mosquito larvae population. Malays J Sci 31:30

Micieli MV, Campos RE (2003) Oviposition activity and seasonal pattern of population of *Aedes* (stegomya) *aegypti* (L) (Diptera: Culicidae) in subtropical Argentina. Mem Inst Oswaldo Cruz 98:659

Moore CG, Cline BL, Ruiz-Tiben E, Lee D, Romney-Joseph H, Rivera-Correa E (1978) *Aedes aegypti* in Puerto Rico: environmental determinants of larva abundance and relation to dengue virus transmission. Am J Trop Med Hyg 27:1225

Regis L, Monteiro AM, Melo-Santos MAV et al (2008) Developing new approaches for detecting and preventing *Aedes aegypti* population outbreaks: basis for surveillance, alert and control system. Mem Inst Oswaldo Cruz 103:50

Toma TS, Sakamoto S, Miyagi I (1982) The seasonal appearance of *Aedes aegypti* in Okinawajina, the Ryukyu archipelago, Japan. Jpn Mosq News 42:179

Vezzani D, Velazquez SM, Schweigmann N (2004) Seasonal pattern of abundance of *Aedes aegypti* (Diptera: Culicidae) in Buenos Aires City, Argentina. Mem Inst Oswaldo Cruz 99:351

Yang HM (1999a) Directly transmitted infections modeling considering age-structured contact rate. Math Comput Model 29:39

Yang HM (1999b) Directly transmitted infections modeling considering age-structured contact rate – epidemiological analysis. Math Comput Model 29:11

Yang HM, Macoris MLG, Galvani KC, Andrighetti MTM, Wanderley DMV (2009a) Assessing the effects of temperature on the population of *Aedes aegypti*, vector of dengue. Epidemiol Infect 137:1188

Yang HM, Macoris MLG, Galvani KC, Andrighetti MTM, Wanderley DMV (2009b) Assessing the effects of temperature on dengue transmission. Epidemiol Infect 137:1179

Yang HM, Macoris MLG, Galvani KC, Andrighetti MTM (2011) Follow up estimation of *Aedes aegypti* entomological parameters and mathematical modellings. BioSystems 103:360

Chapter 4
Modelling the Implications of Temperature on the Life Cycle of *Aedes aegypti* Mosquitoes

Marcelo Margon Rossi, Lêuda Ólivêr, and Eduardo Massad

Abstract Dengue is an infectious disease that is transmitted by the *Aedes aegypti* mosquito. Each stage of the life cycle is influenced by climate variation. The transmission of the dengue virus can be related to increased mosquito survival due to rain and temperature conditions that are optimal for the mosquito's maturation. The aim of this paper is to propose a mathematical model to study how temperature influences each stage of the mosquito's life cycle dynamics by representing transitions and death rates as an explicit function of temperature. The model is thus able to show the influence of temperature on dengue transmission. It can also be used as an operational tool due to its simplicity regarding data requirements and computational effort. The model demonstrates that an expected increase in global temperature will influence the mosquito's life cycle and, consequently, increase the incidence of dengue cases in areas that were previously free from the disease.

Keywords Dengue • Climate change • *Aedes aegypti* • Mathematical modelling • Public health

4.1 Introduction

The influence of climatic conditions on human diseases, such as dengue, yellow fever and other viral disorders that are transmitted by arthropods, is particularly worrying due to the recently observed drastic changes in climate. As a result of these changes, arthropod-borne diseases will increase their geographical ranges

M.M. Rossi (✉) • L. Ólivêr
LIM01 – HCFMUSP, School of Medicine, University of São Paulo, São Paulo, SP, Brazil
e-mail: mrossi@dim.fm.usp.br

E. Massad
LIM01 – HCFMUSP, School of Medicine, University of São Paulo, São Paulo, SP, Brazil

Department of Infectious and Tropical Diseases, London School of Hygiene and Tropical Medicine, London, UK
e-mail: edmassad@dim.fm.usp.br

C.P. Ferreira, W.A.C. Godoy (eds.), *Ecological Modelling Applied to Entomology*, Entomology in Focus 1, DOI 10.1007/978-3-319-06877-0_4

and spread the burden of these diseases (Guha-Sapir and Schimmer 2005; Hales et al. 2002; Simmons et al. 2012). According to epidemiological studies (Campbell-Lendrum et al. 2003; Choi et al. 2005; Gadelha and Toda 1985), diseases that are currently endemic to tropical regions could be directly affected by changes in temperature or, indirectly, by rainfall patterns. The parasites that cause these diseases proliferate and develop in mosquito vectors, whose life cycle is influenced by air temperature, rainfall and relative humidity. Dengue virus is a flavivirus transmitted by mosquitoes that belong to the *Aedes* genus. The *Aedes aegypti* mosquito is the principal vector for dengue, and its prevalence worldwide has spread dengue infection in almost all countries from tropical and subtropical areas (Burattini et al. 2008; Coelho et al. 2008; Hopp and Foley 2001; Massad and Forattini 1998; Seligman 2008; Simmons et al. 2012). An investigation into how climatic variations influence the vector's life cycle would help understand which factor or factors influence the appearance of new cases of the vector-borne infection.

Studies that model the mosquito life cycle and climate change have focused mainly on changes in temperature. These studies have evaluated patterns of mosquito evolution in environments where the seasonal variation effect is more influential rather than focusing on geographic regions that are far from the tropics (Tan et al. 2008). Rainfall (Padmanabha et al. 2011) was investigated to evaluate biological parameters that can be influenced by changes in the water regime (Monteiro et al. 2007). In addition, rainfall intensity has an important influence on the rate of vector-host contact (Bicout and Sabatier 2004) and can sharply increase the rate of virus transmission. The effects of seasonality on the biological and population parameters of *Aedes albopictus* were studied by Alto and Juliano (2001), who observed that alterations in both temperature and precipitation regimes were extremely important to mosquito growth and geographical spreading.

Massad and Forattini (1998) modelled the temperature-dependence of physiological parameters of *Anopheles* mosquitoes, including the effects of temperature on all stages of the mosquitoes' growth. That study was based on the strong correlation between malaria cases and environmental variables, including rainfall assessments, elevated temperatures and geographical characteristics such as altitude and wind. Some mathematical expressions were elaborated to show how these factors influence the dynamics of *Anopheles* mosquitoes. In *Aedes aegypti* mosquito life cycle modelling studies, most of the relationships between physiological parameters and temperature were fitted by polynomials (Costa et al. 2008; Maidana and Yang 2007; Yang et al. 2007, 2009a, b).

In the present study, we propose a mathematical model that assesses the relationship between temperature variation and different mosquito life cycle stages to evaluate the effect of temperature on the dynamics of mosquito populations. We elaborate this model to study how climatic variations (or climate change) could influence the *A. aegypti* life cycle and help to predict how the *A. aegypti* population can spread to locations in which increased temperatures are expected. The entomological data associated with the *Aedes* life cycle was collected from Yang et al. (2009a, b), Löwenberg-Neto and Navarro-Silva (2004) and (Calado and

Navarro-Silva 2002) to estimate the population size of mosquitoes, larvae, pupae and eggs. This approach aims to evaluate the impact of temperature on each stage of the mosquito life cycle at different places from Brazil and to demonstrate the model applicability in other places of the world.

4.2 Theory from Mathematical Model

We first developed a set of equations describing the aquatic phases and the air stage of mosquito development. The influence of the average daily temperature is represented as a climate variable. In theory, the size of a population can be estimated if each key parameter that governs its development is known. In the case of mosquito dynamics, these parameters represent the transition rates between each stage, which depend on temperature. The dynamics of the *A. aegypti* life cycle are represented by the following system:

$$\begin{aligned}
\frac{dE}{dt} &= op\left(T_{air}\right) pic\left(1-\frac{E}{K_e}\right) A-\mu_e\left(T_{air}\right) E-h\left(T_{air}\right) E \\
\frac{dL}{dt} &= \frac{1}{E+K'+\dfrac{L^2}{K_i}} h\left(T_{air}\right) E-\mu_l\left(T_{air}\right) L-pt\left(T_{air}\right) L \\
\frac{dP}{dt} &= pt\left(T_{air}\right) L-\mu_p\left(T_{air}\right) P-ptA\left(T_{air}\right) P \\
\frac{dA}{dt} &= ptA\left(T_{air}\right)-\mu_a\left(T_{air}\right) A
\end{aligned} \tag{4.1}$$

where E, L, P and A represent the egg, larval, pupal and adult mosquito populations, respectively. The others parameters are *pic*, as the number of bites per day of a human being; K_e, the carrying capacity relative to the egg-laying sites; K', the saturation constant growth rate of eggs when larvae are present in same environment and K_i, a constant that represents the inhibitory effect of larvae super-population on larval development. The other parameters in the equation are *op* (oviposition rate) and μe, μ_l, μp and μa, which represent the death rate of egg, larval, pupal and adult populations, respectively, and are all functions of the daily average air temperature (T_{air}). The hatching rate is given by h, and *pt* and *ptA* represent the fraction of larvae that become pupae and the fraction of these pupae that develop into adult mosquitoes, respectively. The first term in the second equation of model (4.1) contains a "yield" term, $\frac{1}{E+K'+L^2/K_i}$, that denotes the competitive influence of larvae on the hatching rate, egg population and the development of the super-population of the larvae. All parameters and values are listed in Table 4.1.

A mathematical model, which correlates the effect of latitude, longitude and altitude on temperature in any location, was used to demonstrate the seasonal variations (Antonini et al. 2009). A time series of mean air temperatures from 1990

Table 4.1 Values of model parameters related to the environmental temperatures of Santos city

Parameter	Parameter meaning	Value
β_0	Mean temperature value	23
β_1	Implication of latitude	−0.008
β_2	Implication of longitude	−0.032
β_3	Implication of altitude	−0.036
a_1	First harmonic of Fourier sine series	25
a_2	Second harmonic of Fourier sine series	−0.35
b_1	First harmonic of Fourier cosine series	0.97
b_2	Second harmonic of Fourier cosine series	0.017
ω	Phase oscillations of Fourier series	0.017

to 2009 were obtained from NCEP[1] data to the Santos city (São Paulo, Brazil) as an example of applicability of the model (4.1).

The data were fitted to the following equation:

$$T_{air} = \beta_0 + \beta_1 Lat + \beta_2 Long + \beta_3 Alt + \sum_{n=0}^{N} (a_n \cos(n\omega t) + b_n \sin(n\omega t)), \tag{4.2}$$

where β_0 represents the average daily temperature in the period studied; β_i ($i = 2$, 3, 4) incorporates the geographic coordinates; *an* and *bn* represent the amplitude of seasonal variation, respectively; and n and ω represent the number of terms and the phase of the Fourier series, respectively.

4.2.1 Calculation of the Temperature-Dependent Parameters

4.2.1.1 Oviposition and Egg Death Rates

To initiate the *A. aegypti* mosquito life cycle, female adults must oviposit in a suitable environment. This phenomenon can be described by the following equation:

$$op(T_{air}) = \alpha_0 \left(1 - e^{\alpha_1 (T_{air} - T_{\max})}\right) (T_{air} - T_{\min})^{\alpha_2}. \tag{4.3}$$

The rate of oviposition *op* (Eq. 4.3) is similar to the Brière nonlinear model (Brière et al. 1999; Loetti et al. 2007) and illustrates the effect of temperature on the variation in the number of eggs. Oviposition is slow at low temperatures and increases exponentially as the temperatures increase. This process is controlled by

[1]Provided by NOAA/OAR/ESRL PSD, Boulder, Colorado USA http://www.cdc.noaa.gov/

Table 4.2 Values of temperature-dependent parameters of the *A. aegypti* mosquito life cycle

Parameter	Biological meaning	Value
α_0	Maximum oviposition rate	0.0011
α_1	Temperature influence factor on oviposition	0.0101
α_2	Exponent of attenuation of eggs' metabolism	3.445
δ_1	Death rate at low temperature	0.0731
δ_2	Influence factor of temperature	0.0595
ζ	Hatching rate	0.00764
μ_{lo}	Temperature-independent death rate factor of larval stage	0.0143
μ_{po}	Temperature-independent death rate factor of pupae	0.0143
π_l	Temperature-dependent death rate factor of larval stages	4.03×10^{-6}
π_p	Temperature-dependent death rate factor of pupae	4.03×10^{-6}
υ	Transition rate from larval stage to pupal stage	0.00129
η_1	Temperature-independent transition rate parameter	1.1324
η_2	Pupal and adult mosquito populations relation parameter	1.2728
η_3	Temperature factor on transition rate	0.19
ϕ_1	Mean value of adult mosquito survival	0.053
ϕ_2	Survival rate	0.081
ϕ_3	Temperature direct effect parameter	6.375×10^{-4}

an exponential term associated with the maximum temperature (indicating a maximum oviposition value) and a power-law term derived from the difference between the estimated temperature calculated in Eq. 4.2 and the minimum values observed in the region under study. The parameters α_0, α_1 and α_2, which represent the maximum oviposition rate, influence of climate and attenuation of the physiological processes, are affected by increased temperature, respectively (α_1 and α_2 are constants). T_{min} and T_{max} are the minimum and maximum ambient temperatures that support the life of the mosquito. T_{air} is calculated from Eq. 4.2. All of the parameters are listed in Table 4.2.

Some eggs develop to the next larval stage, and some die. The egg death rate can be represented by

$$\mu_e\left(T_{air}\right) = \delta_1 e^{\delta_2 T_{air}}, \tag{4.4}$$

where δ_1 and δ_2 represent the death rate at low temperature and the influence of temperature, respectively (Table 4.2).

This expression is extremely similar to the concept of "generation time" found in cellular development (Bermingham 2003) and mosquito ecology (Christopher 1960). Seasonality is another important factor in the death rates of eggs because eggs depend on suitable temperatures for embryonic development and hatching. In the winter, when temperatures are low, eggs are not particularly susceptible to lethal effects from the weather conditions, depending on the time of exposure.

4.2.1.2 Hatching Rate

The number of eggs that hatch per unit of time as a function of temperature, $h(T_{\text{air}})$, can be represented by

$$h\left(T_{air}\right) = \zeta\left(T_{air} + 273\right) \frac{\exp\left(40.55 - \dfrac{13094.10}{T_{air} + 273}\right)}{1 + \exp\left(92.501 - \dfrac{28169.2}{T_{air} + 273}\right)}. \tag{4.5}$$

Equation 4.5 is composed of a linear term related to the temperature increase and a logistic-like term related to enzymatic mechanisms. Parameter ζ is a constant. The numeric values in this equation are related to the enthalpy and entropy of metabolic reactions according to Tan et al. (2008) and Schoolfield et al. (1981). The enthalpy value is in *cal/K*, where *K* is the temperature in Kelvin.

Equation 4.5 demonstrates that if the hatching rate is positive, the larval population increases. Larval mosquitoes and eggs then compete for space in the same place where rain-water is collected or stored (Gama et al. 2005; Serpa et al. 2008). Larvae inhibit egg proliferation by decreasing the hatching rate either by outcompeting the eggs for high-density resources or by consuming the eggs as a nutrient source (Padmanabha et al. 2011). The saturation expression that appears in the first term of the larval population balance is "Andrews inhibitory kinetics"-like (Andrews 1968), akin to the functional forms used in biochemical reactions. This form was chosen because the larval mosquitoes compete for survival when they share the same environment, which is analogous to two enzymes competing for a substrate. The enzyme that has the higher affinity and better access to the substrate has the better chance of producing the final product, even if the other enzyme is present. The intra-specific competition between larvae and eggs is thus represented by an inhibitory effect of the larval density-dependent stress on the egg population.

4.2.1.3 Death Rates of Larval and Pupal Populations

Larval mosquito populations either pupate or die. The effect of temperature on the death rate of larval mosquitoes is not extremely pronounced, although it can be influenced by the food supply (Beserra et al. 2009; Ndiaye et al. 2006) conforming Eq. 4.6. In this work, we constructed a general representation from all larval *instars* while not losing the model's purpose. The larval death rate (Massad and Wilder-Smith 2009) can be written as:

$$\mu_l\left(T_{air}\right) = \mu_{l_0} \exp\left(0.00189 {T_{air}}^2\right). \tag{4.6}$$

According to this relationship, for each one degree Celsius increase, the μ_1 parameter increases by approximately 4 % in a low temperature and to 13 % in a high temperature season. The death rate grows slowly at low and medium

temperatures but can rapidly increase at higher temperatures (Fig. 4.5). Because the survival temperatures are equal to larvae and pupae under similar ambient conditions (Gadelha and Toda 1985), we used the same mathematical expression for the pupal death rate:

$$\mu_p\left(T_{air}\right) = \mu_{p0} \exp\left(0.00189 {T_{air}}^2\right). \tag{4.7}$$

4.2.1.4 Pupation Rate, from the Larval to the Pupal Stage

After some days in the fourth *instar*, the larvae enter the pupal stage, and this rate is influenced by biological and metabolic mechanisms that are temperature-dependent (Christopher 1960; Gomes et al. 1995; Rinne 2009). We represent these processes by the following equation:

$$pt\left(T_{air}\right) = \upsilon\left(T_{air} + 273\right) \exp\left(25.21 - \frac{7,514.34}{T_{air} + 273}\right). \tag{4.8}$$

Equation 4.8 represents the enthalpy of the metabolic processes used by the mosquito in the pupation process and shows how temperature regulates this process. High values support a faster transition between the larval and pupal stages. Again, the values in the exponential terms are relative to the velocities of enzymatic mechanisms and correspond to enthalpy processes. As in Eq. 4.5, υ is a constant linked to the dynamics of the metabolic and enzymatic processes.

4.2.1.5 Emergence Rate to Adults and the Adult Death Rate

Pupae consume oxygen but no other nutrients. The transition rate of the pupal population to the winged stage (Poletti et al. 2011) is represented by

$$ptA\left(T_{air}\right) = 0.21 \exp\left(-0.5\left(\frac{T_{air} - \eta_1}{\eta_2}\right)^2\right) - \eta_3. \tag{4.9}$$

An increase in the ambient temperature of the surrounding air near where the pupae grow improves the efficiency of the mosquito metabolism and outcomes in over-maturation of the pupae. Equation 4.9 reveals that the pupation process is Gaussian relative to weather variations, which is demonstrated by the daily temperature oscillations that range between the maximum and minimum values. In this equation, η_1 represents the mean daily air temperature value, η_2 is a dispersion parameter that correlates with values from the same daily range and η_3 is a constant.

Mosquitoes die at a death rate that is temperature-dependent,

$$\mu_a\left(T_{air}\right) = \phi_1 \exp\left(-\phi_2 (T_{air} - 23)^2\right) + \phi_3 (T_{air} - 23)^2. \tag{4.10}$$

Table 4.3 Evaluation of goodness of fit from the temperature-dependent parameters

Parameter	r^2	d	RMSD	p
op	0.9127	0.980	1.0427	$<10^{-5}$
h	0.7764	0.960	0.0131	$<10^{-4}$
μ_e	0.9307	0.992	0.0370	$<10^{-5}$
$\mu_{p/}\mu_l$	0.8178	0.504	0.1251	<0.005
ptA	0.8971	0.978	0.0188	$<10^{-6}$
pt	0.8886	0.981	0.0158	0.001
μ_a	0.7464	0.925	0.0115	$<10^{-4}$

This process is similar to a Weibull reliability function (Rinne 2009). This equation is composed of two terms, a Weibull's reliability-like probability (Rinne 2009) and a potential well-like model, which is similar to some mathematical representations used in particle physics (Dybiec and Gudowska-Nowak 2007; Coon et al. 1966). In this equation, ϕ_1 and ϕ_3 are constant parameters, and ϕ_2 is similar to the scale parameter of the Weibull distribution (Rinne 2009).

We were able to elaborate these mathematical relations based on entomological data found in (Yang et al. 2009a; Löwenberg-Neto and Navarro-Silva 2004; Calado and Navarro-Silva 2002).

4.2.1.6 Correlation Measures and Model Fitness

When the data and estimated equation values are related by regression, some information about precision and accuracy may be attained, indicating the consistency of estimated values together with the data. To evaluate the goodness of fit, a regression analysis was applied in a correlation matrix (determined by R^2, Spearman's p, Willmott's index of agreement d, RMSD) on all of the temperature relations to determine the precision (of dependence level between data and models estimative) and accuracy (Katok and Hasselblatt 1995; Turell et al. 1985; Krause et al. 2005; Willmott et al. 1985; Willmott 1982). The adult death rate exhibited a larger dispersion ($R^2 = 0.7464$) than the egg death rate ($R^2 = 0.9307$), and the Willmott's d-index ranged from 0.504 to 0.992 for the same variables. All of the other indexes are shown in Table 4.3. All equations were fitted using the "nls" package from R Statistical software with a Gauss-Newton algorithm.

4.3 Results and Discussion

4.3.1 Temperature-Dependent Transition Parameters

To simulate the stages of the *A. aegypti* mosquito life cycle, we used the Santos city (23.95S, 46.33O and altitude of 20 m) location parameters to represent the

Table 4.4 Geographic coordinates from the cities in which dengue cases were registered in Brazil in 1990–2009

	CITY	STATE	LAT	LONG	ALT
RB	RIO BRANCO	AC	9.58 S	67.48 W	153 m
MO	MACEIO	AL	9.40 S	35.43 W	7 m
MP	MACAPA	AP	0.02 N	51.03 W	14 m
MU	MANAUS	AM	3.08 S	60.01 W	92 m
SR	SALVADOR	BA	12.59 S	38.31 W	8.3 m
FO	FORTALEZA	CE	3.43 S	38.30 W	21 m
VI	VITORIA	ES	20.19 S	40.21 W	12 m
GO	GOIÂNIA	GO	16.40 S	49.16 W	749 m
SL	SÃO LUIS	MA	2.31 S	44.16 W	4 m
CO	CORUMBÁ	MS	19.01 S	57.39 W	118 m
BH	BELO HORIZONTE	MG	19.92 S	43.94 W	820 m
BE	BELÉM	PA	1.27 S	48.29 W	10 m
JP	JOÃO PESSOA	PB	7.07 S	34.52 W	40 m
LO	LONDRINA	PR	23.31 S	51.16 W	610 m
RE	RECIFE	PE	8.03 S	34.54 W	4 m
THE	TERESINA	PI	5.05 S	42.49 W	72 m
NA	NATAL	RN	5.47 S	35.13 W	30 m
RJ	RIO DE JANEIRO	RJ	22.54 S	43.15 W	20 m
BV	BOA VISTA	RR	2.49 N	60.40 W	85 m
SP	SÃO PAULO	SP	23.33 S	46.38 W	792 m
AR	ARACAJU	SE	10.54 S	37.04 W	4 m

temperature's seasonal dynamics. Other cities in Brazil in which dengue cases have been registered may be found in Tables 4.4 and 4.5.

Figure 4.1 shows the fit of the temperature-dependent hatching profile to Eq. 4.3. According to this figure, egg hatching occurs at a low rate at low temperatures and increases with increasing temperature. After reaching a maximum value, egg hatching drops quickly to zero when the temperature is near 40 °C. The exponential term of Eq. 4.3 demonstrates that this rate is a Poisson process with mean $1/\alpha_1$, which is regulated by another term (a potential term). The maximum rate is in the same range of the optimal temperature for biochemical and enzymatic mechanisms and nutrient uptake. The dynamics of egg death are influenced by temperature variation; egg death rates show an exponential increase with increasing temperature increments (Fig. 4.2).

The carrying capacity regulates the fraction of hatched and dead eggs, which leads to a steady state plateau that is also temperature-dependent. Mature eggs develop to the larval stage depending on the salinity and larval density present in the specific place. The larval super-population imparts a "regulator mechanism" on adult mosquito size (Gama et al. 2005) when some resource-limited habitats are present, and larvae inhibit egg maturation due to intra-specific competition (Livdahl and Edgerly 1987; Serpa et al. 2008).

Table 4.5 Parameter values from Eq. 4.2 relative to each city mentioned in Table 4.4. All parameters were obtained by temporal series evaluation in 1990–2009

	β_0	β_1	β_2	β_3	a_1	a_2	a_3	b_1	b_2	b_3	ω
RB	25.8	−0.00001	−0.01	−0.02	0.5	−0.01	0	−0.8	−0.002	−0.25	0.01885
MO	26.2	−0.008	−0.0032	−0.03644	0.8	0.05	−0.01	1	−0.21	−0.003	0.01713
MP	26.5	−0.0008	−0.0032	−0.009	−0.5	−0.5	0.1	−0.9	−0.001	−0.001	0.01497
MU	27.1	−0.0003	−0.0032	−0.036	−0.55	0.2	0.09	0.02	0.02	−0.02	0.0104
SR	26.3	−0.005	−0.01	−0.03644	0.95	−0.05	0	1.2	0	0	0.01721
FO	28.6	−0.01	−0.0032	−0.0372	0.001	0.001	0.001	0.45	0.001	0.001	0.0172
VI	25.7	−0.005	−0.05	−0.03644	1.5	−0.4	0	1.2	0.005	0.005	0.017
GO	26	−0.0007	−0.018	−0.05	1.4	−1.1	0.22	−0.6	0.4	0.5	0.01807
SL	27	−1	−0.3	0.101	0.8	−0.0001	−0.005	−1.2	−0.5	−0.001	0.01955
CO	26.3	−0.001	−0.001	−0.03	1.8	−0.5	0.3	−1.6	0.8	−0.001	0.0159
BH	22	−0.001	−0.032	−0.02	1.4	−0.95	0	0.002	0.05	0.35	0.0186
BE	25.7	−0.5	−0.1	0.1	0.5	−0.1	−0.1	−1.3	−0.9	−0.2	0.01893
JP	25.3	−0.0008	−0.001	−0.02	0.69	−0.2	0.01	0.5	−0.15	0.15	0.017
LO	22.6	−0.0008	−0.0032	−0.009	2.75	−0.99	−0.2	−0.2	0.12	0	0.0172
RE	25.1	−0.1	0.01	−0.01	1	−0.035	−0.001	0.6	0.001	0.001	0.0172
THE	27.5	−0.008	−0.032	−0.01	−0.9	−0.5	0.35	−1.8	0.6	0.1	0.0154
NA	23	0.101	0.001	0.001	0.2	0.001	0.001	0.95	−0.1	−0.01	0.0193
RJ	22.8	0.01	−0.032	−0.03644	2	−0.35	0	0.97	0.1	0	0.0164
BV	25.9	−0.01	−0.1	−0.013644	0.25	0	0.01	0.02	−0.01	−0.005	0.0164
SP	21.8	−0.00002	−0.00032	−0.04	2.4	−0.8	0.001	0.1	0.1	0	0.0172
AR	25.5	−0.002	−0.032	−0.036	1.9	−0.2	−0.001	1	0.1	0.1	0.0169

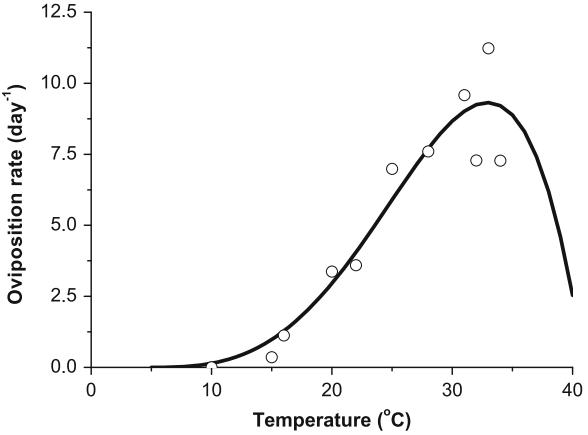

Fig. 4.1 Temperature-dependent oviposition rate. The temperature stress on the oviposition rate of female *A. aegypti* may be seen at one acceleration stage (15–20 °C) and an interval of maximum acceleration may occur with a temperature elevation up to 30 °C (temperate climate). Above 35 °C, the rate declines due to the deleterious effects from the elevated temperature. The *points* represent experimental values, and the *solid line* represents Eq. 4.3 ($R^2 = 0.9127$; Willmott's $d = 0.980$; $p < 10^{-5}$)

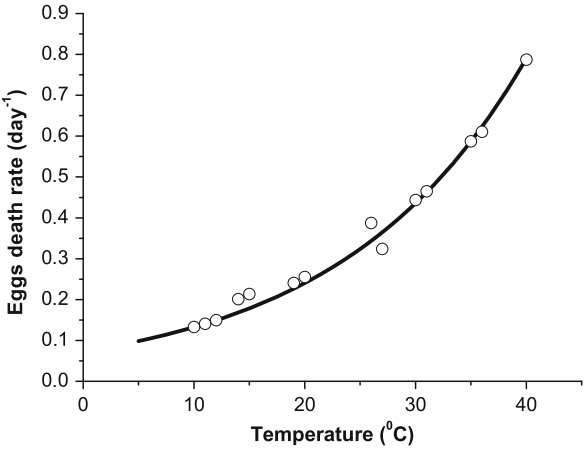

Fig. 4.2 Temperature-dependent egg death rate. Estimation of the temperature influence on the death of eggs in an environment where larval density-dependent level inhibition is not observed and intra-repellent action is proportional to the container size. The *solid line* represents Eq. 4.4 ($R^2 = 0.9307$; Willmott's $d = 0.992$; $p < 10^{-5}$)

Interestingly, the equilibrium value of the pupal population is influenced not by the larval or egg stages but by the adult mosquitoes. This equilibrium is reached when the temperature of the interface between the water and the air controls the dynamical trade-off between each population. These factors lead to the formation of new adult male and female mosquitoes because the number of pupae that die is smaller than the number that emerges into the adult form. The larval population increases as the eggs spread and hatch, in contrast to the adult mosquito population. Larval growth dynamics are influenced by temperature on the water-air interface, the food supply, larval density and salinity (Beserra et al. 2009; Esteva and Yang 2006; Ndiaye et al. 2006), and the eclosion rate peaks near 30 °C (Fig. 4.3).

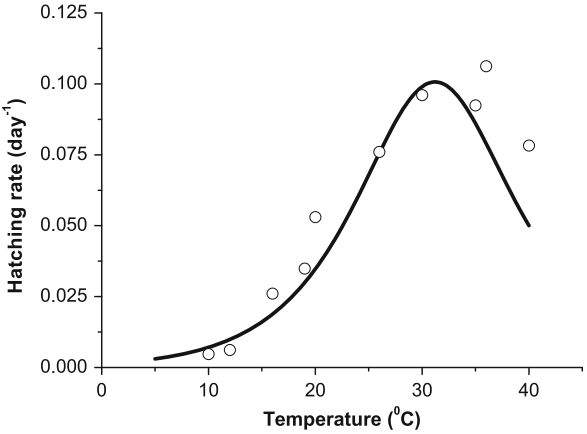

Fig. 4.3 Temperature-dependent egg hatching rate. Profile from temperature effects on the hatch rate of the *A. aegypti* mosquito. The maximum influence of environmental temperature on egg eclosion occurs between 20 and 30 °C. If the temperature increases, the mosquito metabolism optimises by spending little time in each stage. The rate declines at temperatures warmer than 30 °C most likely due to the deleterious effects of the temperature on the mosquito's metabolism. The *points* represent experimental values, and the *solid line* represents Eq. 4.5 ($R^2 = 0.7764$; Willmott's $d = 0.960$; $p < 10^{-4}$)

After the eggs hatch, the larvae feed on organic matter in the water, such as algae. Most of the larval stage is spent at the water's surface and comprises four stages (*instars*). Three are short compared to the fourth *instar*, which encompasses several days. Temperature directly affects the enthalpy and entropy values from Eq. 4.5, and food supply affects the ζ parameter. Because larval anabolic and catabolic processes have different dependencies on temperature, various modification responses in the regulation of the population density are observed (Ndiaye et al. 2006). In optimal feeding conditions, the temperature-dependent larvae formation profile is presented in Fig. 4.4. The larval death rate is not only *instar*- and temperature- dependent (Christopher 1960) but also density-dependent due to the resource competition (Ndiaye et al. 2006) that larvae undergo to survive before entering the pupal stage (Fig. 4.5).

The pupation process is attenuated by a lack of food required to maintain the basal level of energy and, even if there is a suitable temperature for a high pupation rate, resource-limited habitats may delay the transitions of the immature stages. The pupation process (Fig. 4.6) exhibits a Gaussian-like relationship with temperature, which differs from Massad and Forattini (1998), which relates the adult mosquitoes successful "jump" from pupa to the winged stage. However, both mathematical expressions relate the successful emergence rate from pupae to winged adult mosquitoes; the expression from Eq. 4.9 shows that the environmental temperature must oscillate occasionally, and the average value near T_{air} through the η_1 and η_2 parameters, to a best emergence rate.

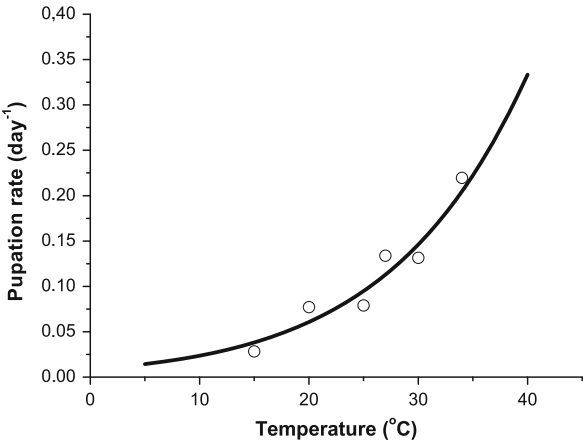

Fig. 4.4 Temperature-dependent pupation rate. The effects of temperature on the transition from the larval stages (*instar* 1–4) to the pupal stage. A temperature elevation supports substrate uptake and a larval density increase, which has a potential direct impact on pupal death (due to high larval density), even with a smaller adult body size and an abundance of female adult mosquitoes in the population. The *points* represent experimental values, and the *solid line* represents Eq. 4.8 ($R^2 = 0.8886$; Willmott's $d = 0.981$; $p = 0.001$)

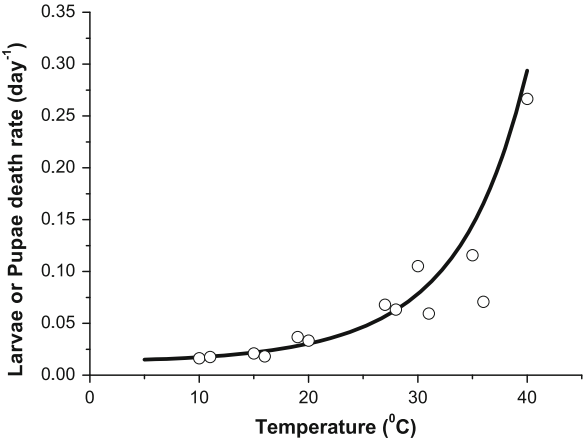

Fig. 4.5 Temperature-dependent larval and pupal death rates. The effects of temperature on larval and pupal population deaths. At elevated temperatures, the immature form dies more rapidly at temperatures warmer than 25 °C, and the larvae that are smaller than the viable ones that pupate eventually die. This shows the resistance of the larval population to climate change variations (the same occurs to pupae). The *points* represent experimental values, and the *solid line* represents Eqs. 4.6 and 4.7 ($R^2 = 0.8178$; Willmott's $d = 0.504$; $p < 0.005$)

The adult death rate formulation has two expressions: one similar to a Weibull reliability function, which represents the frequency of survival of mosquitoes at each temperature, and one similar to a "potential well" profile, which represents a possible stability of those frequencies. The survival of these mosquitoes displays

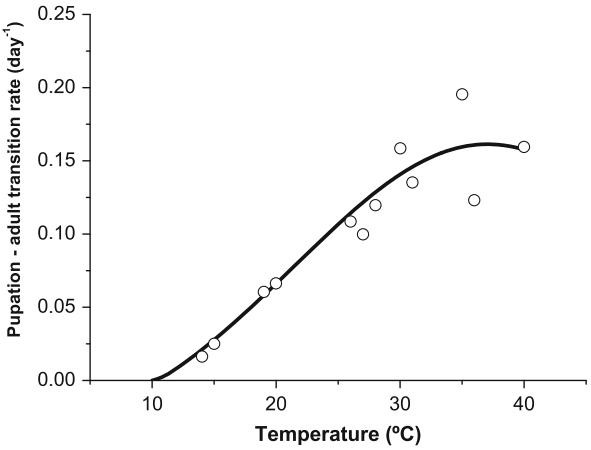

Fig. 4.6 Temperature-dependent emergence rate. Estimated relationship from the temperature effects on the transition from the aquatic to aerial phase of *A. aegypti* mosquitoes. Pupae derive oxygen from the air, and the gradient between ambient and water temperatures drives this consumption, reducing the water-air transition period at elevated temperatures exponentially. The *points* represent experimental values, and the *solid line* represents Eq. 4.9 ($R^2 = 0.8971$; Willmott's $d = 0.978$; $p < 10^{-6}$)

a classic "bathtube curve", indicating at low temperature (or winter) that "failures" decrease with small temperature elevations. At medium or intermediary temperature ranges, these "failures" are constants and minimal, and the mosquitoes have a productive life. At high temperatures (for example, in the summer), a "wear-out" phenomenon is observed possibly due to the low tolerance from *Aedes* to elevated temperatures.

The lowest death rate for adult mosquitoes occurs between 18 and 28 °C, and the death rate increases rapidly at temperatures that are below or above that range. Therefore, the optimum temperature range for mosquito survival is between 20 and 28 °C (Fig. 4.7). The values of each parameter from Eq. 4.2 are presented in Table 4.1. The values relative to each parameter are shown in Table 4.2.

4.3.2 Equilibrium Analysis

The model's equations reveal that equilibrium values can be observed for all subpopulations. According to the dynamical model (4.1), some equilibria depend on the larval densities and are observed when the mosquitoes complete their life cycle and survive. The mathematical structures that represent these states are shown in Eqs. 4.11, 4.12 and 4.13. The notation of rates has been simplified to enhance understanding of the Jacobian matrix.

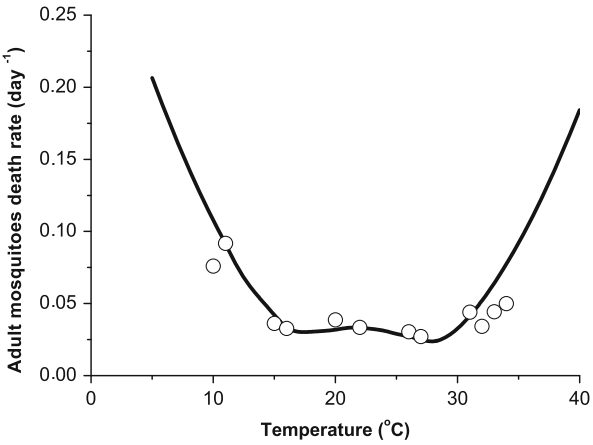

Fig. 4.7 Temperature-dependent adult mosquito death rate. The effects of temperature on the death rate of the adult female mosquito *A. aegypti*. A temperature range from 15 to 28 °C exhibits a smaller death rate (and a bigger survival rate). At higher temperatures, an increased death rate is observed most likely due to a maximum temperature tolerance. The *points* represent experimental values, and the *solid line* represents Eq. 4.10 ($R^2 = 0.7464$; Willmott's $d = 0.925$; $p < 10^{-4}$)

With '*ss*' denoting the steady-state, the equilibrium states are

$$E_{ss}\left(T_{air}\right) = \frac{op.pic.K_e.A_{ss}\left(T_{air}\right)}{op.pic.K_e.A_{ss}\left(T_{air}\right) + K_e\left(\mu_e + h\right)}, \tag{4.11}$$

$$P_{ss}\left(T_{air}\right) = \frac{\mu_a}{ptA} A_{ss}\left(T_{air}\right), \tag{4.12}$$

and

$$A_{ss}\left(T_{air}\right) = \sqrt{1 + 4\left(\frac{op.pic}{K_e\left(\mu_e + h\right)}\right)^2 K_i\left(\Phi K_e^2\left(\mu_e + h\right) + K'\left(\frac{K_e\left(\mu_e + h\right)}{op.pic} - 1\right)\right)}, \tag{4.13}$$

where

$$\Phi = \left(\frac{ptA}{\mu_a}\right)^2 \left(\frac{pt}{\mu_p + ptA}\right)^2 \left(\frac{h}{\mu_l + pt} - 1\right). \tag{4.14}$$

Considering the larval population from the second equation of model (4.1), when larvae and eggs coexist in the same location, multiple equilibria are possible. However, we consider only three, which are described separately below.

Case 1 Due to the application of larvicide, the larval numbers are diminished, and the remaining larvae compete for survival by searching for food in large-volume vessels or sites. The equilibrium is denoted by

$$L_{ss}(T_{air})_1 = \frac{h}{\mu_l + pt}\frac{E}{E + K'}. \tag{4.15}$$

Egg populations that hatch under favourable climatic conditions control this equilibrium, saturation of the egg-laying site (where both eggs and larvae coexist) and optimal feeding conditions for larval growth.

Case 2 Assuming that both populations densely coexist at the same site, these dynamics could lead to another equilibrium. In this case, the intra-specific competition between larvae and eggs by space regulates the larval super-population at a density-dependent level, which is represented by

$$L_{ss}(T_{air})_2 = \sqrt[3]{\frac{h}{\mu_l + pt} K_i E_{ss}(T_{air})}. \tag{4.16}$$

Case 3 A third possible equilibrium occurs when control strategies are applied to control both larval and egg abundances. Eventually, and under favourable climatic conditions, the larval and egg populations can grow without limitation from density-dependent interactions. The size of the larval population will be directly proportional to the number of eggs that are present. The steady state in this scenario is thus

$$L_{ss}(T_{air})_3 = \frac{h}{\mu_l + pt} E_{ss}(T_{air}). \tag{4.17}$$

Once eggs mature, they hatch at a rate that is influenced by the environmental conditions. Temperature affects several enzymatic and metabolic processes in the mosquito (Eq. 4.14), and temperature variations increase eggs' developmental requirements. The hatching rate peaks near 30 °C (Fig. 4.3). Some of the eggs do not hatch and actually die as the temperature increases (Fig. 4.2), showing an exponential profile.

The mathematical expressions used to characterise the temperature dependence of the life cycle of the *A. aegypti* has phenomenological and biological bases, exhibiting representations such as Boltzmann-Arrhenius function-like from biochemical kinetics. In environments subject to seasonal variation in temperature, the mosquito population dynamics respond to this variation as shown in Fig. 4.12a, b.

4.3.2.1 Equilibrium with Only Adult Mosquitoes

According to (Silver 2008), when some information about the size of the emergent adult population is present, the probability that viable eggs persist to adulthood can

be estimated. Cuéllar (1969) stressed the parameter's importance for predicting the potential size of mosquito populations. Consider the equilibrium $S1 = (0;0;0;A^*)$, where females mosquitoes feed on human blood during their life cycle to survive in a region that has no dengue cases and where the mosquito population does not have the dengue virus.

The characteristic polynomial, $p(\lambda)$, from the first equilibrium ($S1$) occurs where adult mosquitoes are present, and the other populations (eggs, larva and pupa) are equal to zero. The resulting polynomial is

$$a_4\lambda^4 + a_3\lambda^3 + a_2\lambda^2 + a_1\lambda + a_0, \tag{4.18}$$

where the *ai* parameters have the following forms:

$$\begin{aligned}
a_4 &= 1 \\
a_3 &= \left(\frac{op.picA^*}{K_e} + \mu_e + h\right) + \mu_l + pt + ptA + \mu_a \\
a_2 &= 2\left(\left(\mu_p + ptA\right)\mu_a + \left(\frac{op.picA^*}{K_e}\right)(\mu_l + pt)\,\mu_a + (\mu_l + pt)\,(\mu_a + ptA)\right) \\
a_1 &= \left(\frac{op.picA^*}{K_e}\right)\left(\left(\mu_p + ptA\right)\mu_a + \left(\mu_l + pt\right)\left(\mu_a + ptA\right)\right) \\
&\quad + (\mu_l + pt)\left(\mu_p + ptA\right)\mu_a \\
a_0 &= \left(\frac{op.picA^*}{K_e} + \mu_e + h\right)(\mu_l + pt)\left(\mu_p + ptA\right)\mu_a
\end{aligned} \tag{4.19}$$

The Routh-Hurwitz condition for stability is $a_1a_2 - a_0a_3 > a_1$ and

$$G_{0,\text{adults}} = \frac{op.pic}{K_e\,(\mu_e + h)}A_0 \tag{4.20}$$

where $G_{0,\text{adults}}$ is the *basic offspring number* (Fankhauser and Tol 1997) that describes how many new mosquitoes can be born to an active A_0 female population.

Lemma 1 The equilibrium with only adult mosquitoes, given by Eq. 4.20, is locally-asymptotically stable if $G_{0,\text{adults}} < 1$ and is unstable if $G_{0,\text{adults}} > 1$.

4.3.2.2 Equilibrium with Only Eggs

Another possible steady state occurs when only eggs, and no mosquitoes, are present in the environment (e.g., under some type of mosquito control). In this case, $S_2{}^* = (E^*; 0; 0; 0)$. The characteristic polynomial, $p(\lambda)$, has the structure and values

$$\lambda\left\{a_3\lambda^3 + a_2\lambda^2 + a\lambda\right\} + a_0 \tag{4.21}$$

where the parameters *ai* are

$$
\begin{aligned}
a_3 &= 1 \\
a_2 &= \mu_a + \mu_p + ptA + \mu_l + pt \\
a_1 &= \left(\mu_p + ptA\right)\mu_a + \left(\mu_l + pt\right)\mu_a + \left(\mu_l + pt\right)\left(\mu_p + ptA\right) \\
a_0 &= \left(\mu_l + pt\right)\left(\mu_p + ptA\right) - \frac{h}{E^*}\left(\frac{E^*}{E^* + K'} - 1\right) ptA.pt.op.pic.\left(1 - \frac{E^*}{K_e}\right)
\end{aligned}
\tag{4.22}
$$

The Ruth-Hurwitz stability criterion has the condition $a_1 a_2 - a_0 a_3 > a_1$.

Thus, the model is stable under the assumption that there are only eggs in the environment, and the *basic offspring number* is

$$
G_{0,\text{eggs}} = \Theta \frac{2hK_e}{K_e\left(2 + h\right) + 2h} \tag{4.23}
$$

where

$$
\Theta = \frac{ptA}{\mu_p + ptA}\frac{pt}{\mu_l + pt}\frac{op.pic}{\mu_a}. \tag{4.24}
$$

Lemma 2 The equilibrium given by Eq. 4.23 is locally-asymptotically stable if $G_{0,\text{eggs}} < 1$ and unstable if $G_{0,\text{eggs}} > 1$.

4.3.3 Analysis of Local and Global Stability

To identify the local stability of the positive equilibrium from model (4.1), a Jacobian matrix was calculated at the population equilibrium. The equilibrium value of the larval population is composed of terms that show the inhibition by substrate uptake. The equilibrium value also includes the relationship between the hatching rate, the larval mosquito death rate and the velocity with which the larvae transform into pupae. Larval-induced inhibition in egg uptake appears in two terms: one term is related to the equilibrium and the other is related to the half-maximum velocity of nutrient uptake.

The adult mosquito can reach a temperature-dependent equilibrium, which is derived from all of the transition parameters. Egg populations possess an equilibrium state that is only affected by the temperature-dependent hatching rate. This phenomenon can explain why active eggs have been observed after months in conditions without water.

The Jacobian matrix J^* of model (4.1) evaluated at the equilibrium is

$$J^* = \begin{bmatrix} -\frac{op.pic}{K_e}A^* - (\mu_e + h) & 0 & 0 & op.pic.\left(1 - \frac{E^*}{K_e}\right) \\ -\frac{(E^*)^2 h}{\left(E^* + K' + \frac{(L^*)^2}{K_i}\right)^3} & -\frac{h\frac{2L^*}{K_i}E^*}{\left(E^* + K' + \frac{(L^*)^2}{K_i}\right)} & 0 & 0 \\ 0 & pt & -\left(\mu_p + ptA\right) & 0 \\ 0 & 0 & ptA & -\mu_a \end{bmatrix} \tag{4.25}$$

When the positive equilibrium $S^* = (E^*;\ L^*;\ P^*;\ A^*)$ (shown in Eq. 4.11) is locally-asymptotically stable, it is interesting to analyse the global asymptotic stability. Methods for this type of analysis have been published, and they include Lyapunov functions (Lakshmikantham et al. 1991), the Poincaré-Bendixon theorem (Chicone 1999; Lakshmikantham et al. 1991) and the Bendixon criterion of Li and Muldowney (1993). According to these methods, it is sufficient to show what is known as the second compound equation,

$$\frac{dM}{dt} = \frac{\partial F^{[2]}}{\partial X}\left(X\left(t; X_0\right)\right) M(t) \tag{4.26}$$

with respect to a solution $\mathbf{X}(t;\mathbf{X_0})$ is asymptotically stable (Sun and Loreau 2009). Equation 4.26 shows that model (4.1) is also asymptotically stable. If the equations that represent the stages of the mosquito life cycle have a periodic solution, the orbit Γ of which is contained in the *int* Ω cone, then, in accordance with the criterion given by Muldowney (1990) to determine the asymptotic stability of the periodic orbit of a general autonomous system, it is sufficient to prove that the linear non-autonomous system from Eq. 4.26 is asymptotically stable.

When the second additive compound matrix methodology is applied, the calculation can be a bit complex, and the outcome matrix $J^{[2]}$ has the form

$$J^{[2]} = \begin{bmatrix} -(a+\lambda) & 0 & 0 & -f\left(E_{ss}\right) & 0 & 0 \\ pt & -(b+\lambda) & 0 & 0 & 0 & -f\left(E_{ss}\right) \\ 0 & ptA & -(c+\lambda) & 0 & 0 & 0 \\ 0 & -f_1\left(E_{ss}, L_{ss}\right) & 0 & -(d+\lambda) & 0 & 0 \\ 0 & 0 & -f_1\left(E_{ss}, L_{ss}\right) & ptA & -(m+\lambda) & 0 \\ 0 & 0 & 0 & 0 & pt & -(\omega+\lambda) \end{bmatrix} \tag{4.27}$$

where, if the trace of $J^{[2]} < 0$ and the determinant of $J^{[2]} > 0$, then

$$a = \mathrm{f}\left(\mathrm{A_{ss}}\right) + \mathrm{g}\left(\mathrm{E_{ss}}, \mathrm{L_{ss}}\right) \tag{4.28}$$

$$c = \mathrm{f}\left(\mathrm{A_{ss}}\right) + \mu_a \tag{4.29}$$

$$m = \mathrm{g}\left(\mathrm{E_{ss}}, \mathrm{L_{ss}}\right) + \mu_a \tag{4.30}$$

$$b = \mathrm{f}\left(\mathrm{A_{ss}}\right) + \left(\mu_p + ptA\right) \tag{4.31}$$

$$d = \mathrm{g}\left(\mathrm{E_{ss}}, \mathrm{L_{ss}}\right) + \left(\mu_p + ptA\right) \tag{4.32}$$

$$\omega = \left(\mu_p + ptA\right) + \mu_a \tag{4.33}$$

where the functionals are $f\left(E_{ss}\right) = op.pic\left(1 - \frac{E_{ss}}{K_e}\right)$, $f\left(A_{ss}\right) = \frac{op.pic}{K_e} A_{ss} + \left(\mu_e + h\right)$, $-f_1(E_{ss}, L_{ss}) = J_{21}^{[2]}$ and $-g(E_{ss}, L_{ss}) = J_{22}^{[2]}$.

By analysing the $J^{[2]}$ (Eq. 4.27), we can verify that model (4.1) is stable under the conditions with adult mosquito, egg, larval and pupal populations at the location being studied. The Ruth-Hurwitz criterion can be used to verify whether the dynamical system is stable. The characteristic polynomial of matrix $J^{[2]}$ has the form

$$T_6\lambda^6 + T_5\lambda^5 + T_4\lambda^4 + T_3\lambda^3 + T_2\lambda^2 + T_1\lambda + T_0 \tag{4.34}$$

where

$$T_6 = 1 \tag{4.35}$$

$$T_5 = d + m + \omega + a + b + c \tag{4.36}$$

$$T_4 = (dm + d\omega + m\omega) + (ab + bc + ac) + (a + b + c)(d + m + \omega) \tag{4.37}$$

$$T_3 = abc + dm\omega\,(a + b + c)(dm + d\omega + m\omega) + (ab + bc + ac)(d + m + \omega) \tag{4.38}$$

$$T_2 = abc\,(d + m + \omega) + dm\omega\,(a + b + c) + (ab + bc + ac)(dm + d\omega + m\omega) \tag{4.39}$$

$$T_1 = (dm + d\omega + m\omega)\,abc + dm\omega\,(ab + bc + ac) \tag{4.40}$$

$$T_0 = abcdm\omega \tag{4.41}$$

Lemma 3 The model (4.1) has a unique positive equilibrium if and only if $T_0 > 1$.

The solution to this system implies that we must have two conditions associated with the complete mosquito life cycle satisfied for the dynamical system to be stable. These conditions are $T_1T_2 > T_3$ and $T_1T_4 > T_5$. By analysing the T_i parameters and the parameter vector $\theta = (a;\ b;\ c;\ d;\ m;\ \omega)$, it is clear that even with the climatic variation, the conditions will be obeyed.

4.3.4 Adult Mosquito Population

When Eqs. 4.20 and 4.23 and the temperature-dependent population expansion of an adult mosquito shown in Eq. 4.13 are considered, the maximum development of the mosquito population occurs near 28 °C. This temperature could be considered as an optimum value for the *A. aegypti* colonisation and for widespread distribution. Interestingly, these mathematical equations correlate with a mosquito infestation, possibly from eggs or from adult mosquitoes, and either in alterations in the climate variables or the environmental conditions, unlike what was previously observed by Yang et al. (2009b) and Esteva and Yang (2006). In Fig. 4.9, the effect of temperature on the mosquito population is estimated from Eq. 4.13 and illustrates that temperatures near 30 °C are optimal for mosquito development.

In temperatures ranging from 25 to 30 °C, all transition rates increased, resulting in a larger adult mosquito population. After the optimum temperature is reached, adult mosquito tolerance to survive at the maximum temperature can be observed in Figs. 4.7 and 4.9, and higher values may lead to an elevated death rate and a decrease in the mosquito population (Christopher 1960).

4.3.5 Colonisation Risk

We observe that the colonisation risk from adult mosquitoes increased (Fig. 4.8a, and Eq. 4.20) in a temperate environment with temperatures ranging into the limits evaluated in model (4.1) and decreasing after the optimal value when the temperature increased. Likewise, when only eggs are present in the environment (Fig. 4.8b; Eq. 4.24) with temperatures ranging between 25 and 35 °C, the risk

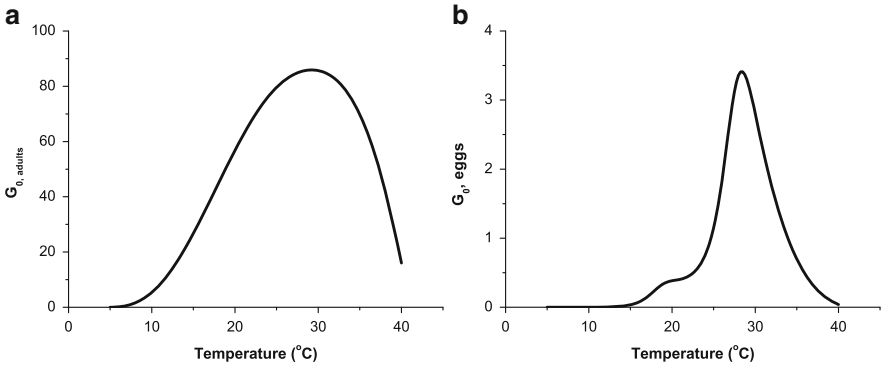

Fig. 4.8 Profile of the basic offspring numbers. (**a**) $G_{0,adults}$ (Eq. 4.20); (**b**) $G_{0,eggs}$ (Eq. 4.23). These equations demonstrate that elevations in temperature contribute to an increase in the mosquito population in an environment that initially contains only adult mosquitoes or only eggs. $G_{0,adults}$ calculations were performed assuming $A_0 = 8{,}000{,}000$ female mosquitoes

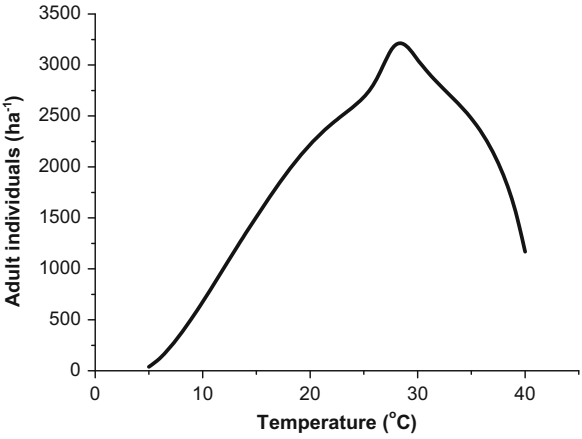

Fig. 4.9 Amount of temperature-dependent adult mosquitoes, A_{ss}, estimated by Eq. 4.13. Considering the temperature variation in the entomological parameters modeled by Eqs. 4.3, 4.4, 4.5, 4.6, 4.7, 4.8, 4.9 and 4.10, the maximum adult mosquito population may occur near 30 °C

profile shows a simple peak at 28 °C and values ten-fold less than those observed for adult mosquitoes. This approach is useful for predicting the emergence of *A. aegypti* mosquitoes into geographic areas where significant increases in temperature are possible, e.g., in southern Europe (Fig. 4.9).

In the temperature range of 19 to 28 °C, we might expect an increased risk of dengue outbreaks because at these temperatures, we observed the lowest death rate of adult mosquitoes. Higher adult mosquito populations will lead to an increased contact rate between infected mosquitoes and humans. In addition, within this temperature range, we observed the highest amount of eggs oviposited and subsequently hatched into larval-stage mosquitoes, further contributing to the risk of infection.

Above 25 °C, the death rate of the larval and pupal stages is extremely pronounced due to environmental factors and the metabolic processes of mosquitoes (Figs. 4.10 and 4.11). Interestingly, the death rate of larval and pupal populations remained low at a low temperature range possibly because they become sluggish to prevent energy depletion and the elevated potential metabolic costs. This pattern could be due to a temperature variation in the aquatic environment because air and water have different temperature gradients, which occur at the same time. Above 30 °C, egg viability suffers, and hatching rates could decline because of the influence of the larval super-population or desiccation in rearing sites, among other factors. The transition rate from the pupal to the adult form plateaus near 30 °C, and this fact may be associated with the "jump" from the aquatic to the air environment that occurs when temperature range variations only influence the metabolism of adult mosquitoes. This temperature range is more favourable for breeding, and seasonality can drive the *Aedes aegypti* population (Fig. 4.12a, b).

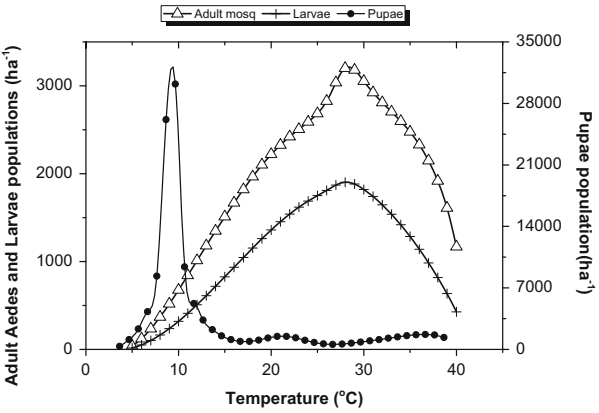

Fig. 4.10 Estimated temperature-dependent amount of adult mosquitoes, A_{ss}, and pupal and larval levels, P_{ss} and L_{ss}. Relationship of adult mosquitoes, pupal and larval concentrations, estimated by the steady state from Eqs. 4.12, 4.13 and 4.16, and the temperature variation. Interestingly, the estimations show that adult and larval populations peak at 30 °C to, and at 10 °C, pupae peak most likely due to "sluggish" individuals that survive at low temperatures

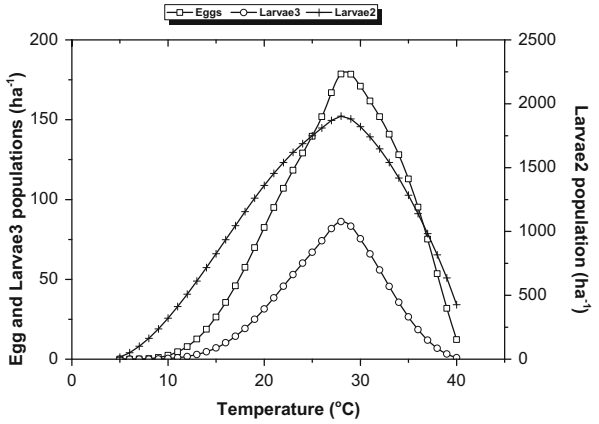

Fig. 4.11 Estimated egg and larval populations at steady state. All of these profiles were obtained by a simulation of the model 1 for a period of 365 days, considering Santos city and the temperature profile found in this city. Larvae2 (Eq. 4.16) considers the larval super-population on the same site as the eggs, and Larvae3 (Eq. 4.17) shows that the larval population is proportional to the egg steady state population. The initial simulation values are Eggs, $E_0 = 8{,}200$; Larvae, $L_0 = 8{,}000$

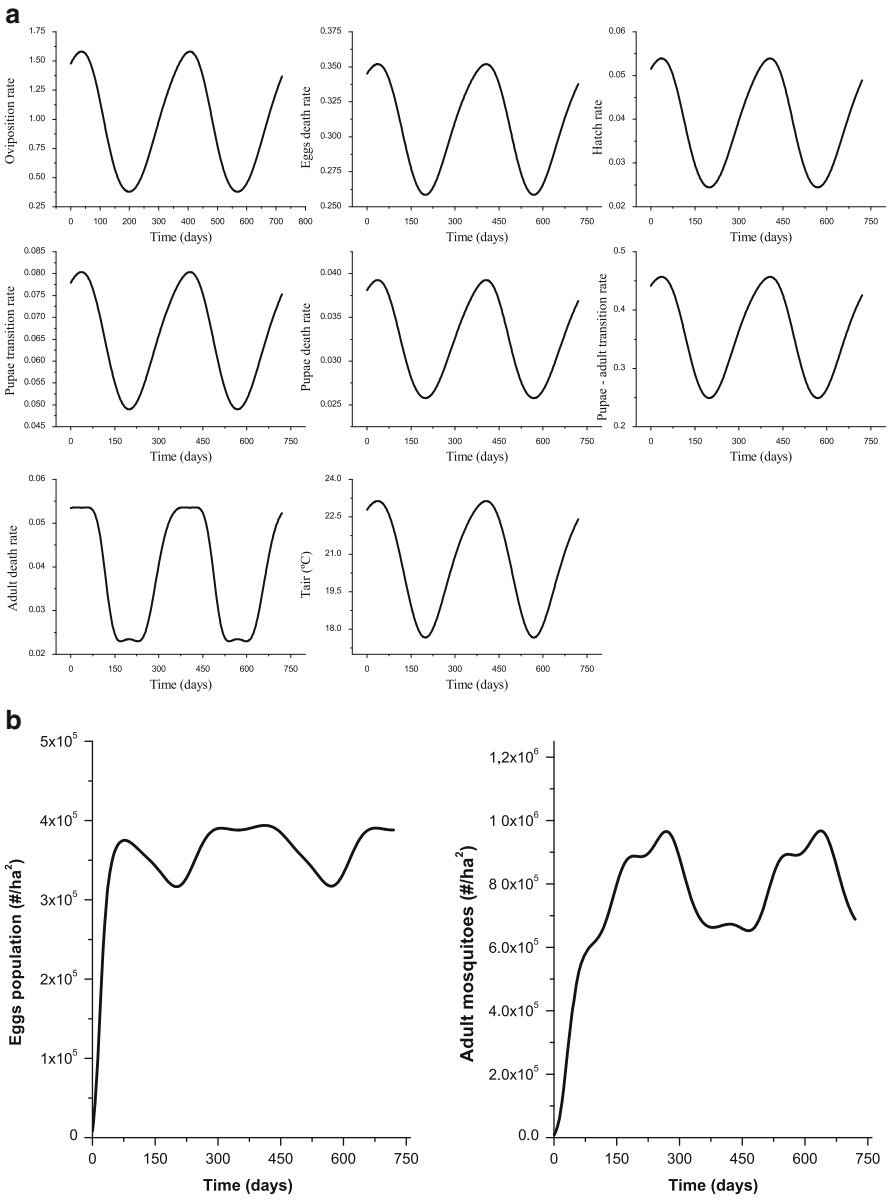

Fig. 4.12 Seasonality affects the mosquito's life cycle parameters and the *Aedes* population. (**a**) Temporal variation of each parameter cited in Sect. 4.2, considering the temperature profile of Santos city; (**b**) Influence of the daily average temperature variation on egg and adult populations from *Aedes aegypti* mosquitoes. These profiles were calculated according to Sect. 4.2.1

4.4 Conclusions

In developing this model, the main consideration was that each of the equations be as simple as possible while still retaining the essential features of the *A. aegypti* life cycle. With this objective in mind, some aspects have been simplified, such as the larval stages of the growth phase. The mathematical expressions in the model illustrate the behaviour of temperature-dependent parameters, such as death rates and transition rates, among different life cycle stages of the *A. aegypti* mosquito. The model dynamics capture extremely well the seasonality of the mosquito's life cycle and forecasting possibilities, once it used the temperature data (applied directly on "entomological" equations) or estimated by T_{air}.

Even though the model does not consider the temperature-dependent adult mosquito size explicitly, this aspect is assumed by the "yield" term of the larval population. A limited-food habitat or climatic unfavourable conditions may impact on larval size and the adult *A. aegypti* population, resulting in fluctuations on mosquito's life-cycle dynamics and in whole final population. The vectorial capacity or competence of the mosquito requires a higher temperature to guarantee that the dengue virus has a better proliferation rate.

Thus, all of these aspects favour the intense dengue virus transmission and a high number of dengue cases on a geographical location with a high colonisation risk.

Acknowledgements This work was supported by a grant from LIM01-HCFMUSP, CNPq and FAPESP. M. R. thanks the CNPq and L. O. thanks FAPESP for fellowship awards.

References

Alto BW, Juliano SA (2001) Precipitation and temperature effects on populations of *Aedes albopictus*: implications for range expansion. J Med Entomol 38:646–656

Andrews JF (1968) A mathematical model for the continuous culture of microorganism utilizing inhibitory substance. Biotechnol Bioeng 10:707–723

Antonini JCA, Silva EM, de Oliveira LFC et al (2009) Modelo matemático para estimativa da temperatura média diária do ar no Estado de Goiás. Pesq Agropec Bras Brasilia 44:331–338

Bermingham JR (2003) On exponential growth and mathematical purity: a reply to Bartlett. Popul Environ 25:71–73

Beserra EB, Freitas EM, Souza JT et al (2009) Ciclo de vida de *Aedes* (*Stegomyi*a) *aegypti* (Diptera, Culicidae) em águas com diferentes características. Iheringia 99:281–285

Bicout DJ, Sabatier P (2004) Mapping Rift Valley fever vectors and prevalence using rainfall variations. Vector Borne Zoonotic Dis 4:33–42

Brière JF, Pracros P, le Roux AY, Pierre JS (1999) A novel rate model of temperature dependent development for arthropods. Environ Entomol 28:22–29

Burattini MN, Chen M, Chow A et al (2008) Modeling the control strategies against dengue in Singapore. Epidemiol Infect 136:309–319

Calado DC, Navarro-Silva MA (2002) Avaliação da influência da temperatura sobre o desenvolvimento de *Aedes albopictus*. Rev Saude Publica 36:173–179

Campbell-Lendrum D, Pruss-Ustun A, Corvalan C (2003) How much disease could climate change cause? In: McMichael A, Campbell-Leundrum D, Corvalan C et al (eds) Climate change and human health: risks and responses. WHO/WMO/UNEP, Geneva, p 133

Chicone C (1999) Ordinary differential equations with applications, vol 34, Texts in applied mathematics. Springer, New York

Choi GY, Choi JN, Kwon HJ (2005) The impact of high apparent temperature on the increase of summertime disease-related mortality in Seoul: 1991-2000. J Prev Med Public Health 38:283–290

Christopher SR (1960) *Aedes aegypti* (L.): the yellow fever mosquito. Cambridge University Press, London, 739 pp

Coelho GE, Burattini MN, Teixeira MG et al (2008) Dynamics of the 2006/2007 dengue outbreak in Brazil. Mem Inst Oswaldo Cruz 103:535–539

Coon JB, Naugle NW, McKenzie RD (1966) The investigation of double minimum potentials in molecules. J Mol Spectrosc 20:107–129

Costa FS, da Silva JJ, de Souza CM et al (2008) Dinâmica populacional de *Aedes aegypts* em área urbana de alta incidência de Dengue. Rev Soc Bras Med Trop 41:309–312

Cuéllar CB (1969) A theoretical model of *Anopheles gambiae* population under challenge with eggs giving rise to sterile males. Bull World Health Org 40:205–212

Dybiec B, Gudowska-Nowak E (2007) Quantifying noise induced effects in the generic double-well potential. Acta Phys Pol B 38:1759–1774

Esteva L, Yang HM (2006) Control of dengue vector by sterile insect technique considering logistic recruitment. TEMA – Tendências em Matemática Aplicada e Computacional 7:259–268

Fankhauser S, Tol RSJ (1997) The social cost of climate changes: the IPCC second assessment report and beyond. Mitig Adapt Strateg Glob Chang 1:385–403

Gadelha DP, Toda AT (1985) Biologia e comportamento do *Aedes aegypti*. Revista Brasileira de Malariologia e Doenças Tropicais 37:29–36

Gama RA, Alves KC, Martins RF et al (2005) Efeito da densidade larval no tamanho de adultos de *Aedes aegypti* criados em condições de laboratório. Rev Soc Bras Med Trop 43:64–66

Gomes ACG, Gotlieb SLD, Marques CCA, de Paula MB, Marques GRAM (1995) Duration of larval and pupal development stages of *Aedes albopictus* in natural and artificial containers. Revista Saúde Pública 29:15–19

Guha-Sapir D, Schimmer B (2005) Dengue fever: new paradigms for a changing epidemiology. Emerg Themes Epidemiol 2:1–10

Hales S, de Wet N, Maindonald J et al (2002) Potential effect of population and climate changes on global distribution of dengue fever: an empirical model. Lancet 360:830–834

Hopp MJ, Foley JA (2001) Global-scale relationships between climate and the dengue fever vector, *Aedes aegypti*. Clim Changes 48:441–463

Katok A, Hasselblatt B (1995) Introduction to the modern theory of dynamical systems (Encyclopaedia of mathematics and its applications). Cambridge University Press, Cambridge. ISBN 0521341876

Krause P, Boyle DP, Bäse F (2005) Comparison of different efficiency criteria for hydrological model assessment. Adv Geosci 5:89–97

Lakshmikantham V, Matrosov VM, Sivasudarm S (1991) Vector Lyapunov functions and stability analysis of nonlinear systems, Mathematics and its applications. Kluwer, Dordrecht/Boston

Li MY, Muldowney J (1993) On Bendixson's criterion. J Differ Equ 106:27–39

Livdahl TP, Edgerly JS (1987) Egg hatching inhibition: field evidence for population regulation in a treehole mosquito. Ecol Entomol 12:395–399

Loetti MV, Burroni NE, Schweigmann N et al (2007) Effect of different thermal conditions on the pre-imaginal biology of *Culex apicinus* (Philipp, 1865). J Vector Ecol 32:06–111

Löwenberg-Neto P, Navarro-Silva MA (2004) Development, longevity, gonothrophic cycle and oviposition of *Aedes albopictus* Skuse under cyclic temperature. Neotrop Entomol 33:29–33

Maidana NA, Yang HM (2007) A spatial model to describe the dengue propagation. Tendências em Matemática Aplicada e Computacional 8:83–93

Massad E, Forattini OP (1998) Modeling the temperature sensitivity of some physiological parameters of epidemiological significance. Ecosyst Health 4:19–129
Massad E, Wilder-Smith A (2009) Risk estimates of dengue in travelers to dengue endemic areas using mathematical models. J Travel Med 16:191–193
Monteiro LCC, de Souza JRB, Albuquerque CMR (2007) Eclosion rate, development and survivorship of *Aedes albopictus* (Skuse) (Diptera: Culicidae) under different water temperatures. Neotrop Entomol 36:966–971
Muldowney JS (1990) Compound matrices and ordinary differential equations. Rocky Mt J Math 20:857–872
Ndiaye PI, Bicout DJ, Mondet B, Sabatier P (2006) Rainfall triggered dynamics of *Aedes* mosquito aggressiveness. J Theor Biol 243:222–229
Padmanabha H, Lord CC, Lounibos LP (2011) Interactive effects of temperature and instar on starvation resistance in *Aedes aegypti* (L.) larvae. Med Vet Entomol 25:445–453
Poletti P, Messeri G, Ajelli M, Vallorani R, Rizzo C et al (2011) Transmission potential of Chikungunya virus and control measures: the case of Italy. PLoS One 6(5):e18860. doi:10.1371/journal.pone.0018860
Rinne H (2009) The Weibull distribution: a handbook. Chapman and Hall/CRC, Boca Raton
Schoolfield RM, Sharpe PJH, Magnuson CE (1981) Non-linear regression of biological temperature-dependent rate models based on absolute reaction rate theory. J Theor Biol 88:719–731
Seligman SJ (2008) Constancy and diversity in the flavivirus fusion peptide. Virol J 5:27
Serpa LLN, Kakitani I, Voltolini JC (2008) Competição entre larvas de *Aedes aegypti* e *Aedes albopictus* em laboratório. Rev Soc Bras Med Trop 41:479–484
Silver JB (2008) Mosquito ecology: field sampling methods, 3rd edn. Springer, Dordrecht, 1477 pp
Simmons CP, Farrar JJ, Chan NV, Wills B (2012) Dengue: current concepts. N Engl J Med 366:1423–1432
Sun C, Loreau M (2009) Dynamics of a three-species food chain model with adaptive traits. Chaos Solitons Fractals 41:2812–2819
Tan KB, Koh HL, Ismail AI Md et al (2008) Modeling mosquito population with temperature effects. In: International Conference on Environmental Research Technology- ICERT. The Environmental Division of the School of Industrial Technology, University Sains Malaysia, Penang, p 536
Turell M, Rossi C, Bailey C (1985) Effect of extrinsic incubation temperature on the ability of *Aedes taeniorhynchus* and Culex pipiens to transmit Rift Valley fever virus. Am J Trop Med Hyg 34:1211–1218
Willmott CJ (1982) Some comments on the evaluation of model performance. Bull Am Meteorol Soc 63:1309–1313
Willmott CJ, Ackleson SG, Davis RE et al (1985) Statistic for the evaluation and comparison of models. J Geophys Res 90:8995–9005
Yang HM, Macoris MLG, Galvani KC et al (2007) Dinâmica da Transmissão da dengue com dados entomológicos temperatura-dependentes. Tendências em Matemática Aplicada e Computacional 8:159–168
Yang HM, Macoris MLG, Galvani KC et al (2009a) Assessing the effects of temperature on the population of *Aedes aegypti*, the vector of dengue. Epidemiol Infect 137:1188–1202
Yang HM, Macoris MLG, Galvani KC et al (2009b) Assessing the effects of temperature on dengue transmission. Epidemiol Infect 137:1179–1187

Chapter 5
Predictive Modelling of Insect Metacommunities in Biomonitoring of Aquatic Networks

Tadeu Siqueira, Lucas Danilo Durães, and Fabio de Oliveira Roque

Abstract Aquatic insects are used extensively in freshwater bioassessment because they are good indicators of human impact. The most successful bioassessment initiatives have focused mainly on comparing insect communities from potential impacted sites to those predicted by empirical correlative models that occur in pristine sites. The theoretical scope that underpins the use of these models is derived from a deterministic view of ecology, particularly based on niche theory – i.e., predicting taxa occurrence from environmental conditions. In recent years, however, the development of new concepts (e.g., the metacommunity concept), use of new techniques (e.g., artificial neural networks) and availability of better datasets (e.g., geographic information system layers) could change this scenario. In this chapter, we explore the use of metacommunity models, the geometry of riverine networks and organism dispersal conceptually with a simulation exercise to discuss the challenges of modelling metacommunities in biomonitoring aquatic networks.

Keywords Bioassessment • Dispersal • Macroinvertebrates • RIVPACS

T. Siqueira (✉)
Departamento de Ecologia, Instituto de Biociências, UNESP – Univ Estadual Paulista, Rio Claro, Brazil
e-mail: tsiqueira@rc.unesp.br

L.D. Durães
Departamento de Biologia Geral, Universidade Estadual de Montes Claros, Montes Claros, MG, Brazil
e-mail: lucasdanilo@gmail.com

F.O. Roque
Centro de Ciências Biológicas e da Saúde, Universidade Federal de Mato Grosso do Sul, Campo Grande, MS, Brazil
e-mail: roque.eco@gmail.com

C.P. Ferreira, W.A.C. Godoy (eds.), *Ecological Modelling Applied to Entomology*, Entomology in Focus 1, DOI 10.1007/978-3-319-06877-0_5

5.1 Introduction

Freshwater habitats, the biodiversity they support and the services they supply are directly threatened by human activities through land cover change, water pollution, construction of dams, overexploitation and invasion by exotic species (Dudgeon et al. 2006). Even worse, global climate change is predicted to exacerbate some of these threats (Hamilton et al. 2010), placing headwater streams, rivers and lakes among the most endangered ecosystems in the world. This raises serious concerns about the status of aquatic biodiversity, especially considering that the diversity of many groups (e.g., microbes and insects), as well as the ecosystem goods and freshwater supply services (e.g., water consumption, fishing, and climate regulation) are not even known. Researchers must, therefore, develop efficient ways to measure, monitor and share information on freshwater biodiversity and water quality to achieve good management and conservation practices. As noted by Friberg et al. (2011), although it is not a scientific discipline in itself, biomonitoring needs to be supported by strong science to guarantee its credibility so that wrong costly decisions are avoided. Herein, we show and discuss the statistical modelling approach used in most biomonitoring programs around the world (i.e., community-based predictive modelling; Wright 1995, 2000) and explore the potential of the concepts of metacommunity models, which are illustrated using a simulation exercise with hopes of helping to advance the field of research.

5.1.1 The Use of Aquatic Insects in Biomonitoring

Aquatic insects, together with other macroinvertebrates, have been extensively used in modern bioassessment programs in North America, Europe and Australia (Rosenberg and Resh 1993; Bonada et al. 2006). Although the use of biological information in freshwater ecology to access human impact had begun in the late nineteenth century, there has been a dissemination of studies using ecological and statistical theory to discuss good biomonitoring practices just in the past 25 years (Bonada et al. 2006; Dolédec and Statzner 2010; Friberg et al. 2011). This was accompanied by the implementation of biomonitoring programs by some governmental agencies, such as the UK Environment Agency and the US Environmental Protection Agency, and by its use in marine and terrestrial systems.

Two main different analytical approaches have emerged from this feedback exchange between researchers and managers, which promoted further development of the field and implementation by agencies around the world, e.g., the EU Water Framework Directive uses both. The first approach, called the multimetric index approach (Karr and Chu 1999; Karr 1999), is based on the idea of using several metrics that represent major aspects of composition and function of biological communities that change with increased human impact, e.g., number of species (or genera), taxonomic and trophic composition, and abundance. Metrics are rated

to what would be expected at a preserved site and combined into an index of biological integrity. A discussion of this approach is beyond the scope of the present article. For those interested in details about its rationale and use, we recommend the publications by Karr and Chu (1999), Karr (1999), Norris and Hawkins (2000), and Bonada et al. (2006). The second approach, called predictive modelling (Wright 1995, 2000), is one of our focuses here and will be detailed in the next section.

5.1.2 Predictive Models in Freshwater Biomonitoring

The use of predictive models for freshwater bioassessment started with the development of the River In Vertebrate Prediction And Classification System (RIVPACS) by the Institute of Freshwater Ecology, UK, in 1977 (Wright 2000). The initial objectives were two-fold: i-develop a biological classification of near pristine river sites in Great Britain, based on macroinvertebrates; ii-evaluate whether macroinvertebrate communities could be predicted by using water variables. The success and further improvement of the RIVPACS approach (Hawkins et al. 2000) stimulated the development of similar predictive modelling tools in other countries. The most common approaches are the AUStralian RIVer Assessment Scheme (AUSRIVAS) and BEnthic Assessment of SedimenT (BEAST). Although these may differ greatly among each other, more recently, they have been referred to as RIVPACS-type models, i.e., multivariate predictive models that use macroinvertebrates to support the detection and interpretation of anthropogenic impacts on aquatic communities of streams and rivers. Hereafter, we emphasise the original RIVPACS, as our simulations are closest to it.

Composed of several sequential steps, in general, RIVPACS-type models evaluate the deviation of a given site from the expected biological condition if that site was in a minimally disturbed reference condition. The expected taxonomic composition is then compared with the one observed by sampling the site. Discrepancies between the two taxonomic compositions indicate the degree of impact. The sequential steps usually include (for a more detailed description of the steps, see Wright et al. 2000; Hawkins 2006; Hawkins et al. 2010): (1) *a posteriori* biological classification of reference sites based on biological information that is derived from some type of classification analysis (different dissimilarity measures and clustering algorithms are available); (2) establishment of environmental variables that best discriminate the biological classification of reference sites; (3) prediction of taxonomic composition and richness for new sites; (4) calibration and predictions for null models; (5) calculation of indices that evaluate discrepancies between the predicted and the observed. Usually, the predictive modelling step is performed with general linear models – from multivariate discriminant function analysis to logistic regressions. Predictive models based upon Artificial Intelligence, such as Artificial Neural Networks or Bayesian Belief Networks, have also been proposed (Feio and Poquet 2011). Among the indices calculated in step (5), the O/E ratio of observed to expected taxon richness is one of the most used. The O/E ratio is used to compare

observed and expected assemblages, and a value different from 1.0 indicates that the community at a site is not in reference condition. More recent studies, however, have also used a measure of compositional dissimilarity (based on the Bray-Curtis index) that complements O/E and summarises the taxon-specific disparities between observed and expected assemblages directly (Van Sickle 2008).

The theoretical scope that underpins the use of these models is derived from a deterministic view of ecology, particularly based on niche theory, i.e., predicting taxa occurrence from environmental conditions. In recent years, however, the development of new concepts (e.g., the metacommunity concept), use of new techniques (e.g., graph theory, spatial modelling) and availability of better datasets (e.g., geographic information system layers) could change this scenario. Hereafter, we explore the use of metacommunity models (Leibold et al. 2004) that can account for non-random spatially distributed anthropogenic impacts, the geometry of riverine networks and organism dispersal to discuss the challenges of modelling metacommunities in biomonitoring aquatic networks.

5.1.3 Biomonitoring in the Context of the Metacommunity Theory

For freshwater biomonitoring research, it is crucial to be able to make reliable predictions about community changes in a system. In this context, ecologists have increasingly begun recognising the insights provided by viewing freshwater systems from the perspective of multiple communities connected by dispersing organisms, i.e., from a metacommunity perspective (Leibold et al. 2004). Metacommunity theory is still under development (Scheiner and Willig 2008; Winegardner et al. 2012), with debates being fuelled, at a first moment, over its conceptual paradigms and, more recently, over the support from empirical evidence (Logue et al. 2011). Metacommunity theory has advanced our understanding of how spatial dynamics and local interactions shape biodiversity patterns by changing the longstanding deterministic assumption of community ecology. This assumption states that variation in a local community structure is simply determined by the responses of different species to environmental gradients, which is also the cornerstone of all freshwater bioassessment schemes. Ecologists now recognise that communities are organised at multiple scales and that non-deterministic processes such as dispersal within the river network also act as drivers of diversity patterns.

In their seminal paper, Leibold et al. (2004) organised the metacommunity framework and proposed four characterisations or views of metacommunities by using theoretical models developed previously: species sorting (Chase and Leibold 2003), patch dynamics (Tilman 1994), mass effects (Amarasekare and Nisbet 2001) and the neutral model (Hubbell 2001). In short, these views of metacommunities mainly differ in the assumption of whether patches are similar or heterogeneous in respect of abiotic and biotic conditions and whether the amount of organism

dispersal among patches is limited, moderate or intense (Holyoak et al. 2005). Metacommunity models can be viewed as a continuum of the main drivers of community structure and dynamics. At one extreme of this gradient, sufficient dispersal of organisms results in species at sites well suited to their environmental preferences along environmental gradients (i.e., species sorting). The neutral model, at the other extreme of the continuum, describes a metacommunity that is structured by dispersal limitation, speciation and ecological drift and not by ecological differences between species (Hubbell 2001). Winegardner et al. (2012) recently proposed that the other two models – patch dynamics and mass effects – can actually be considered as special cases of the species sorting model. In patch dynamics, the interacting species differ from each other by specialising their abilities as either good competitors or good colonisers within a uniform environment. Within a heterogeneous environment, strong priority effects caused by differential dispersal abilities can lead to different community dynamics. In the mass effects framework, intensive and constant dispersal from a source habitat provide a constant supply of individuals to a sink habitat so that species exist at habitats outside of their environmental range (Mouquet and Loreau 2003).

Notably, metacommunity models should not be seen as four discrete views but rather as the simultaneous interaction between dispersal and environmental processes in metacommunities (Leibold and McPeek 2006; Logue et al. 2011; Winegardner et al. 2012). Thus, although integrating metacommunity ideas into the scope of freshwater biomonitoring is not a simple task, it is fair to suggest that biomonitoring approaches should recognise the importance of dispersal and the level of connectivity among patches as an important driver structuring local communities. In this sense, Siqueira et al. (2012a) proposed the selection of biodiversity surrogates and indicators of environmental conditions with the explicit integration of environmental and spatial variables into the selection approach. Heino (2013) went further and provided a more complete conceptual framework for bioassessment in a metacommunity. None of these articles, however, explicitly considered the role of the dendritic nature of the riverine network into their analyses or conceptual models; and that is crucial, as demonstrated by recent studies that have highlighted how riverine topology and organismal dispersal among habitat patches can determine community structure (Campbell Grant et al. 2007; Auerbach and Poff 2011; Brown et al. 2011).

5.1.4 Metacommunities in Hydrographic Networks

The spatial structure of ecosystems has long been recognised as a key component in structuring ecological patterns. The role of spatial networks in generating and maintaining biodiversity patterns has recently received increasing attention from scientists and conservationists (Campbell Grant et al. 2007). Part of this interest is due to the implications of this issue for understanding the forces that shape riverine metacommunities (Heino et al. 2003, 2012; Ackerly 2004; Roque et al. 2010;

Auerbach and Poff 2011; Siqueira et al. 2012b) and for the monitoring, management and conservation of network systems (Economo 2011; Siqueira et al. 2012a).

Historically, the longitudinal dimension of aquatic systems has received more attention than the vertical or lateral ones. Part of this interest is due to the ideas of the "River Continuum Concept" that emphasises the predictable longitudinal shift in biological communities caused by physical gradients and energy inputs from the headwaters to the mouth (Vannote et al. 1980). The lateral dimension of large rivers have also influenced our knowledge about the biodiversity organisation in aquatic systems by placing major emphasis on the predictable pulsing of river discharge and exchange processes of matter and organisms across river floodplain gradients (Junk et al. 1989). Such a linear (longitudinal and lateral) view has been the dominant paradigm in studies of aquatic insects during the 1980s and 1990s. Recently, our view about the process that shapes biodiversity distribution is moving beyond linear conceptual models of aquatic ecosystems to consider the role that the spatial structure of river networks might play in determining diversity patterns. This view has rapidly impacted our knowledge of aquatic insect biodiversity. For example, consider the review by Clarke et al. (2008) as a landmark about the role of dendritic networks on the distribution of aquatic macroinvertebrates, including insects. Since this review, there has been an exponential increase in the number of publications about the distribution of biodiversity in aquatic dendritic networks.

Despite advances in understanding the role of dendritic systems in biodiversity distribution, the spatial configuration of riverine networks *per se* as a major factor influencing the results of bioassessment and biomonitoring has been highlighted only in the last few years (Heino 2013). We argue that not only environmental heterogeneity but also spatial configuration are crucial for RIVPACS-type models.

5.2 Simulating Insect Metacommunities in Networks Under Punctual Anthropogenic Impacts

We simulated riverine metacommunities in a hypothetical aquatic network to understand how the spatial position of the anthropogenic impact and the connectivity among patches can affect the species richness and composition of local communities under different metacommunity scenarios and consequently the result of RIVPACS-type models. Below, we provide a brief overview of the model construction. For further details and codes, please contact the authors. The model was prepared using the R software (R Development Core Team 2012). Steps 1–5 describe how we simulated the aquatic networks. As with any model, these five steps simplify the processes assembling natural metacommunities. For example, our simulation used the same probability of survival for all species. This is likely not the case for real metacommunities. However, we do not have empirical evidence from stream metacommunities to use here. Thus, additional investigation is needed to evaluate how changing parameters may influence the outcome of our analyses. Steps 6–8

describe the standardised procedures for building and applying RIVPACS-type models. For calculating RIVPACS metrics, we used the scripts for building and applying predictive models (available from http://www.epa.gov/wed/pages/models/rivpacs/rivpacs.htm).

1. We first developed riverine networks that resembled realistic hierarchical structuring of habitat patches in stream networks using nodes (habitat patches) and edges. The dendritic network in the model was represented as a graph consisting of a set of vertices connected by lines. Each vertex of a given graph corresponded to a discrete patch that could be colonised by species of the regional species pool. Thus, our network aimed to simulate a small hydrographic basin. Communities in the networks have already been represented by graphs, and this procedure is an approximation of many real systems (Auerbach and Poff 2011).
2. For simplicity, all simulated metacommunities were composed of 20 species because the number of species within the species pool can greatly affect the structure of metacommunities (McPeek and Brown 2000). We started the simulation with two individuals per species per patch. Each individual gives birth to ten new individuals at each reproductive event. These individuals have a 70 % probability of surviving. The survivors are subject to a process of environmental filtering and stochastic events that can cause local extinction (see step 4). For simplicity, we assumed Zero-Sum dynamics with a limit of 6,000 individuals regionally and a maximum of ten individuals per species per patch.
3. Species disperse throughout the simulated network with the probability of reaching a given patch dependent on the dispersal capacity and distance between patches. We began by assuming that all nodes were initially occupied by an equal number of species and used a dispersal kernel correspondent to a Brownian motion (Lutscher et al. 2005) to represent the movement of insects throughout each metacommunity:

$$P_{ij} = \frac{1}{\pi\left(1 + \alpha \times d_{ij}^2\right)}$$

   where P_{ij} is the probability of individuals present in patch j colonising patch i as a function of the distance between patches i and j (d_{ij}). The coefficient α reflects the dispersal capacity of the species, which determines the slope of the curve. The lower the value of α, the greater the dispersal capacity.
4. The environment of each patch was represented by two abiotic variables (x_1 and x_2), in which one of them (x_2) was related to anthropogenic impacts (e.g., dissolved oxygen concentration). x_1 is analogous to the predictors unaffected by human influence used in RIVPACS models (e.g., stream width). x_2 assumed a subtle variation (0.01) in patches free from anthropogenic impacts. In these simulations, we modelled stochastic local extinction as a factor regulating local species. We based our model on the premise that anthropogenic impacts enhance the probability of local extinction. Thus, each species had an environmental

tolerance interval, defined as the range of environmental conditions that is capable of maintaining a population. The probability of colonisation as a function of environment was calculated following Tilman (2004) and Gravel et al. (2006):

$$P_{si}\,(x_i) = \exp\left(\frac{-(x_i - \mu_s)^2}{2\sigma_s^2}\right)$$

where $P_{si}\,(x_i)$ is the probability that species s will colonise patch i as a function of x_i, the value of the environmental variable in patch i, and μ represents the optimal value of the environmental variable for species s. The parameter σ describes the tolerance of species s for that variable. The greater the σ value for a given species, the greater the width of the niche for that species. The μ values of each species are environmental values of randomly chosen patches in the network.

5. The following factors determine the number of immature individuals that become adults: probability of the immature to die (0.7), which does not depend on the species identity; stochastic events that are able to remove a number of individuals, which occur at a probability 0.1 at each time step and have a probability of 0.95 for removing the surviving individuals (Fig. 5.1).

   The steps described above were run for two scenarios considering the degree of dispersal among local communities: i- metacommunities with moderate rates of dispersal (MD); and ii- metacommunities with high rates of dispersal (HD) (Fig. 5.2). In both scenarios, most species respond to the environmental gradient, i.e., 70 % of the species (sensitive) with a niche breadth varying from 0.2 to 0.25 in relation to environmental variables x_1 and x_2 and 30 % of the species (tolerant) with a niche breadth varying from 2 to 5 (Fig. 5.3).

   Applying the RIVPACS model

6. To analyse how the spatial position of the anthropogenic impact and the connectivity among patches affect the results of the RIVPACS-type models,

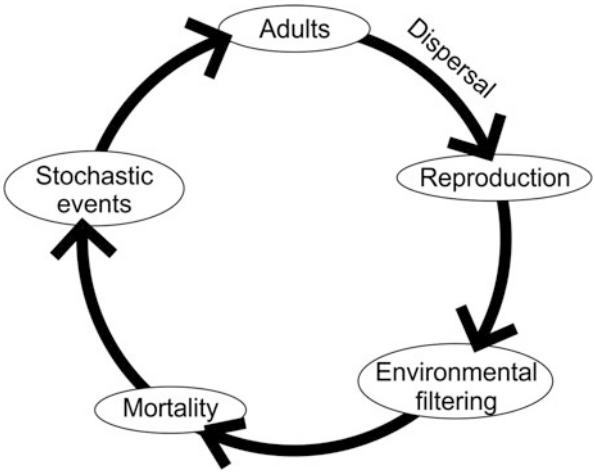

Fig. 5.1 Schematic representation of the simulation

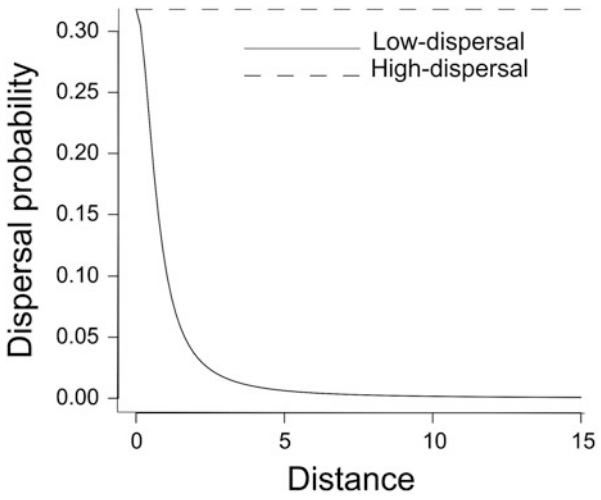

Fig. 5.2 Dispersal probability as a function of distance for species with low or high dispersal capacities. A distance of 15 is equal to the largest distance between network patches

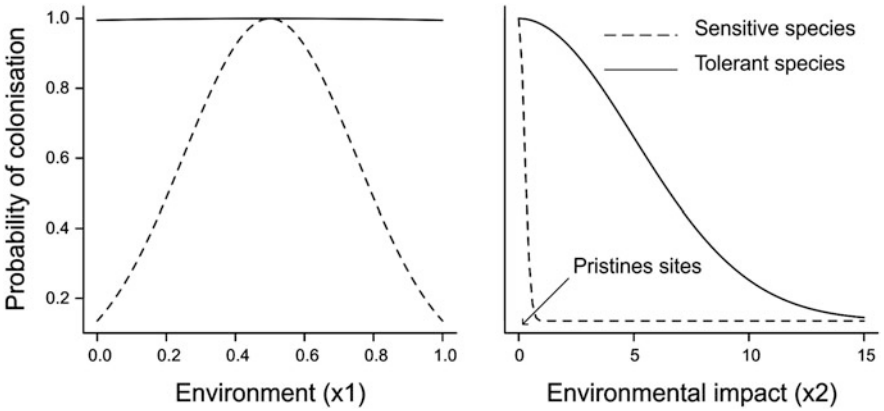

Fig. 5.3 Probability of colonisation as a function of environmental x_1 and x_2

we simulated an anthropogenic impact by altering the value of x_2 for a given patch (test patch, hereafter, Fig. 5.3). The difference between the altered value and the original value defines the level of the impact. We simulated both a strong ($x_2 = 15$) and an intermediate ($x_2 = 7$) level of impact. This procedure was applied in three test patches within the network (Fig. 5.4): one more isolated (patch Z), one more connected (patch X) and another with intermediate connectivity (patch Y). In these patches, the variable x_1 has the same value. Through this step, we generated the observed values of species richness and composition for comparison with RIVPACS predictions.

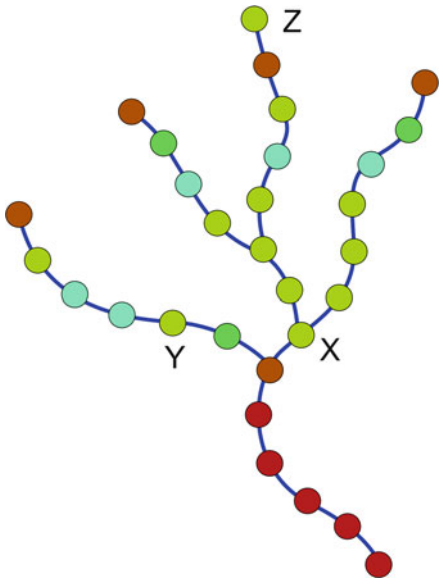

Fig. 5.4 Representation of the riverine network. *Colours* in patches illustrate the differences in environmental conditions. Test patches chosen for RIVPACS analysis (different levels of connectivity) are identified as Z, Y, X. In these patches, the variable x_1 has the same value

7. We simulated 100 networks with the same original spatial configuration and environmental heterogeneity. Following the standardised steps for building and applying RIVPACS-type models (http://www.epa.gov/wed/pages/models/rivpacs/rivpacs.htm), these networks were used to cluster patches, define the reference condition and predict communities by using discriminant function analysis. In our predictive model, the expected species composition for sites free from anthropogenic impact is given by the set of patches of the reference networks that have the same value of x_1. The probability of occurrence (pc) for each taxon was estimated for each patch as the ratio of the number of simulations in which the taxon occurred by the total number of simulated networks. As the predetermined probability threshold (pt) used to select subsets of taxa for the O/E index calculations can influence the output, only taxa that are predicted to occur with a probability >0.5 were included in the calculations.
8. Finally, we calculated the O/E ratio of observed to expected species richness and the compositional dissimilarity (based on Bray-Curtis index), which indicates discrepancies between the two assemblages as a result of ecosystem stress or impairment (Van Sickle 2008). We compared the O/E ratio and dissimilarity values among patches with different levels of connectivity. Considering only the impact, which was the same in these patches, there should be no significant difference in these metrics among these patches. If the spatial configuration of the network matters, conversely, then there should be a significant difference in these metrics among the more isolated (patch Z), more connected (patch X) and the patch with intermediate connectivity.

5.3 Results

We observed that in the scenario where the environmental impact in the test patches was strong (high x_2 values), both the O/E index and the compositional dissimilarity responded strongly to the impact regardless of the spatial position of the test patch (Fig. 5.5). In other words, in that scenario, the RIVPACS model performed well regardless of the level of patch connectivity.

However, we also observed that under intermediate impact levels, the performance of the RIVAPCS model was affected by the spatial position of the test patch. Our results indicate that in a scenario of moderate dispersal rates, the difference between the observed and expected values (for both the O/E index and Bray-Curtis dissimilarity) is stronger in less connected patches (Fig. 5.5). In this scenario, patch Z, located in the headwaters of the network, had the lowest O/E values (mean = 0.113, SE = 0.005), which were approximately 42 % smaller than the mean O/E value of patch X (the most connected) and 37 % smaller the patch with an intermediate level of connectivity (patch Y) ($F = 16.904$, $P < 0.001$). We observed extremely similar results for the Bray-Curtis composition dissimilarity index. The less connected patch Z had the highest dissimilarity values

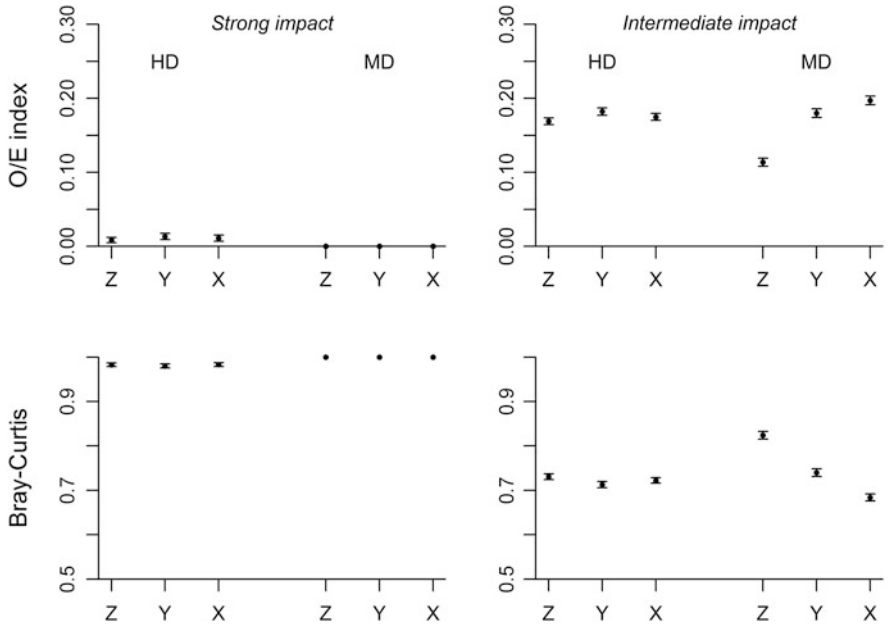

Fig. 5.5 Mean values (±SE) of the O/E ratio and Bray-Curtis index in each of our simulated scenarios. HD and MD refer to high and moderate dispersal, respectively. *Z* more isolated patch, *Y* patch with intermediate connectivity, *X* more connected patch

(mean = 0.824, SE = 0.008), followed by patch Y (mean = 0.74, SE = 0.008) and patch X (mean = 0.683, SE = 0.007) ($F = 17.133$, $P < 0.001$).

This, however, was not the case for networks under intermediate impact levels and higher dispersal rates (Fig. 5.5). In that scenario, there was no significant difference between the different test patches. This indicates that a type of mass effect may lead to the homogenisation of the biota, where populations in impacted patches are maintained by source non-impacted patches.

5.4 Implications for Biomonitoring

The results of our simulations suggest three important properties of impacts in insect metacommunities in dendritic networks that are relevant to biomonitoring: (i) context dependency regarding the strength of the environmental impact; (ii) the spatial position of the impact within the network; and (iii) the degree of dispersal among local communities. The performance of RIVPACS-type models can be severely affected depending on the combination of these factors. In cases where the environmental impact was too strong, it overwhelmed the importance of the two other factors – the spatial configuration of the network and the degree of dispersal. This happened because only those species with extremely broad tolerance (i.e., wide niche breadth in our simulations) were able to maintain populations in impacted test patches, independent of their position within the network. In that case, according to our simulations, the model correctly classified all three test patches as not in the reference condition. RIVPACS-type models are known to have a high potential to discriminate overall strong human impact (Wright 2000). High enrichment by organic pollution is a good example of a strong impact that results in a high performance of predictive models based on aquatic insects. The response of insect communities to this type of impact is extremely predictable (Bonada et al. 2006). In that case, pollution works as a strong environmental filter on a local scale and results in a local community with few tolerant organisms (e.g., chironomids). The challenge, however, is to perform well in detecting subtle and different types of human impact, and this is where our results have something to add.

Under intermediate levels of impact, the spatial position of the test patch within the network and the degree of dispersal among patches can make a big difference in the RIVPACS model results. The first consideration in this situation of moderate impact is whether the degree of dispersal among local communities is high or moderate. First, our results suggest that in metacommunities with high dispersal rates (i.e., dominated by species with good dispersal abilities), the spatial position of the test patch within the network does not affect the performance of RIVPACS models. We found that all three test patches, with varying levels of connectivity, were classified with same level of impact – as we expected – because at high dispersal rates, even the less connected sites can receive new colonisers. This would guarantee that species reach suitable habitat patches according to their environmental tolerances. Because all test patches had the same level of impact, they

ended up with extremely similar O/E index and Bray-Curtis dissimilarity values. This high dispersal scenario, however, should not be the rule in natural stream networks, especially in headwater streams. Empirical evidence from genetic data, including aquatic insects, is mixed. For example, whereas a hydropsychid caddisfly with an adult flight stage exhibits frequent dispersal between adjacent catchments (Baker et al. 2003), both larval and adult dispersal of the non-biting freshwater midge *Echinocladius martini* is largely limited to within a stream channel (Krosch et al. 2011). Thus, our moderate dispersal scenario seems to better reflect real-world scenarios.

In metacommunities with moderate dispersal rates and under moderate impact, the level of connectivity of the test patch influences our ability to identify the level of the impact. We found that the least connected test patch (a headwater site) had O/E and Bray-Curtis values that indicated stronger levels of impact (Fig. 5.4). This is not correct, as we simulated the same level of impact in all three test patches. There are two not mutually exclusive explanations for this result. The least connected patch did not receive all of the species that could tolerate the new environmental condition. In that case, species sorting with limiting dispersal (sensu Winegardner et al. 2012) could attribute to this mismatch between the observed and predicted communities in comparison with the other two more connected patches. This is a likely explanation because more isolated patches always have fewer species that could potentially occur as a function of the environment. Another possibility is that the least connected patch was classified as it should be, and the two more connected patches underestimated the level of impact. In that case, species sorting with high dispersal (sensu Winegardner et al. 2012) would be the reason for this mismatch between the observed and predicted communities. That is, the more connected patches would have species that do not tolerate the impacted condition but their populations are maintained by a constant supply from neighbouring non-impacted sites. We cannot indicate which of these explanations is more plausible at the moment. However, it is important to say that the O/E and Bray-Curtis values can only be compared within each simulated scenario. We cannot compare the least connected patch from this scenario with patches from the moderate impact-high dispersal scenario because the predicted communities were generated under different model assumptions. We are able to note, however, that under the same moderate impact level, RIVPACS models can perform differently in sites with varying levels of connectivity.

The spatial configuration of ecosystems can affect community-environment analysis in the context of biomonitoring schemes in two main ways. First, when both species and the environment are spatially structured, statistical tests may overestimate the importance of environmental factors and thus generate false community-environment association (Legendre 1993). Second, mass effects (i.e., the presence of species in environmentally suboptimal sites due to intense dispersal from environmentally suitable sites) may obscure the effects of a stressor, as dispersal from a source neighbouring site (e.g., an unaltered site) allows persistence at a sink site (e.g., an impacted site). Thus, we potentially have to address a spatial structure that is inherent to natural and human-induced environmental

gradients and a spatial structure caused by spatially contagious processes, such as dispersal. This has important implications for the construction of predictive models and interpretation of anthropogenic impacts in biomonitoring, as predictive modelling is mainly based on the idea of species sorting dynamics. For example, during the model building phase, a false community-environment association would result in wrongly predicted communities. In the phase of comparing observed communities with predicted ones, in addition to the previous problem, one could find an observed community that appears to be similar to the reference condition when it is actually impacted but with populations that are maintained by source-sink dynamics (i.e., species sorting with high dispersal, Winegardner et al. 2012). Although some RIVPACS-type models account for spatial location by using latitude and longitude as predictors – potentially accounting for the problem of false community-environment association – this is only a coarse approximation for dispersal processes. In this sense, we have two main suggestions for incorporation by RIVPACS-type models. First, we reinforce the use of spatial variables together with environmental variables as predictors during the phase of model building. Several recent studies have addressed this issue in community ecology, biogeography and macroecology (e.g., Borcard et al. 1992, 2004; Borcard and Legendre 2002; Diniz-Filho and Bini 2005; Dray et al. 2006; Bini et al. 2009; Peres-Neto and Legendre 2010). By doing this, one could at least obtain community-environment associations that are free from spatial correlation. Second, we suggest that network measures of habitat connectivity that identify particular barriers contributing to fragmentation of riverine networks should be considered when selecting test sites.

As in any study involving simulations, our model makes several simplifications regarding natural river networks and insect metacommunity dynamics. Although there are an increasing number of studies on stream insects, there is still a paucity of information about their basic biology (e.g., dispersal abilities, survival rates) that would be used in our model. For example, we assumed that survival rates were constant across patches and the same for all species. This neutral assumption is unlikely to hold for species-rich insect metacommunities, such as those in tropical areas. In addition to this lack of information on basic biology, we also simplified our models regarding the spatial structure of the hydrographic basin. For example, we simulated only three connectivity levels that did not strongly differ among the test patches (Fig. 5.3). Although our network was too simplistic in this sense, we suspect that in real-world scenarios, where sites can differ more in the level of connectivity, the influence of the network configuration in the performance of predictive models can become even stronger. Many RIVPACS modelling exercises comprise multiple drainage basins. In these cases, we cannot measure connectivity levels based on watercourse distances among sites as we did here. In such cases, the way spatial configuration of ecosystems affects community-environment analysis in the context of biomonitoring may be different. For example, across drainage basins, dispersal limitation (instead of mass affects) would cause spatial structures and most likely affect the outcome of RIVPACS models in a different way. In cases where dispersal

limitation is important, RIVPACS models may not detect the anthropogenic impact because not all potential species are present at reference sites. Alternatively, if one is examining the effects of a restoration of impacted stream, RIVPACS models may fail to detect the recovery if species cannot reach that newly suitable site due to dispersal limitation.

Finally, another major aspect that was not addressed in our simulations – and that also deserves further investigation – was the way the results could change across different temporal scales. First we must consider that the role of dispersal limitation and environmental filtering in structuring metacommunities may change in short time scales. For example, Fernandes et al. (2014) analysed a seasonal floodplain in the Pantanal and demonstrated that the fish-metacommunity structure was more strongly affected by spatial connectivity at the beginning of the flood season, whereas the environment was only important at the end when habitat patches were more connected. Conversely, Nabout et al. (2009) did not observe a significant signal of environmental or spatial control in structuring phytoplankton metacommunities across different periods of a flood season. Thus, seasonal changes in both environmental conditions and spatial connectivity may have some effects on the results of RIVPACS models if metacommunity patterns are affected by these changes. Second, we must consider that extinction may change the number of species in a metacommunity in both short and long time scales. For example, Halley and Iwasa (2011) demonstrated that, in a neutral scenario, habitat loss might cause an immediate loss of species richness that is followed by a gradual process of extinction – some populations drift to low numbers and then disappear. Unless there is immigration or speciation, the eventual state of the community after habitat loss is dominated by a single species (Halley and Iwasa 2011). Our model assumes a fixed number of species within the metacommunity but that dispersal occurs as a function of distance. Thus, the consequences of species loss could also affect the performance of RIVPACS models, especially in situations where fragmentation reduces the probability of dispersal.

In summary, we have known for a long time that (i) streams are not linear but are rather dendritic systems, (ii) aquatic insects are complex organisms that interact with the landscape at multiple scales using multiple dispersal routes, both aquatic and terrestrial, and (iii) many species respond to environmental changes in a predictable way. However, we have only recently begun to integrate these ideas. As demonstrated here, the framework of metacommunities applied to dendritic systems can improve our understanding of patterns in nature and consequently improve our ability to construct predictive models based on aquatic insects to be used for biodiversity conservation and biomonitoring.

Acknowledgments We thank Professor Wesley Godoy for inviting us to contribute to this book and an anonymous reviewer for providing helpful comments on an earlier version of this manuscript. FOR is supported by a productivity grant from the Brazilian National Council for Scientific and Technological Development (CNPq, #303293/2009-8).

References

Ackerly DD (2004) Adaptation, niche conservatism, and convergence: comparative studies of leaf evolution in the California chaparral. Am Nat 163:654–671

Amarasekare P, Nisbet RM (2001) Spatial heterogeneity, source-sink dynamics, and the local coexistence of competing species. Am Nat 158:572–584

Auerbach DA, Poff NL (2011) Spatiotemporal controls of simulated metacommunity dynamics in dendritic networks. J N Am Benthol Soc 30:235–251

Baker AM, Williams SA, Hughes JM (2003) Patterns of spatial genetic structuring in a hydropsychid caddisfly (Cheumatopsyche sp. AV1) from southeastern Australia. Mol Ecol 12:3313–3324

Bini LM, Diniz-Filho JAF, Rangel TFLVB et al (2009) Coefficient shifts in geographical ecology: an empirical evaluation of spatial and non-spatial regression. Ecography 32:193–204

Bonada N, Prat N, Resh VH et al (2006) Developments in aquatic insect biomonitoring: a comparative analysis of recent approaches. Annu Rev Entomol 51:495–523

Borcard D, Legendre P (2002) All-scale spatial analysis of ecological data by means of principal coordinates of neighbour matrices. Ecol Model 153:51–68

Borcard D, Legendre P, Drapeau P (1992) Partialling out the spatial component of ecological variation. Ecology 73:1045–1055

Borcard D, Legendre P, Avois-Jacquet C et al (2004) Dissecting the spatial structure of ecological data at multiple scales. Ecology 85:1826–1832

Brown BL, Swan CM, Auerbach DA et al (2011) Metacommunity theory as a multispecies, multi-scale framework for studying the influence of river network structure on riverine communities and ecosystems. J N Am Benthol Soc 30:310–327

Campbell Grant EH, Lowe WH, Fagan WF (2007) Living in the branches: population dynamics and ecological processes in dendritic networks. Ecol Lett 10:165–175

Chase JM, Leibold MA (2003) Ecological niches: linking classical and contemporary approaches. University of Chicago Press, Chicago

Clarke A, Mac Nally R, Bond N et al (2008) Macroinvertebrate diversity in headwater streams: a review. Freshw Biol 53:1707–1721

Diniz-Filho JAF, Bini LM (2005) Modelling geographical patterns in species richness using eigenvector-based spatial filters. Glob Ecol Biogeogr 14:177–185

Dolédec S, Statzner B (2010) Responses of freshwater biota to human disturbances: contribution of J-NABS to developments in ecological integrity assessments. J N Am Benthol Soc 29:286–311

Dray S, Legendre P, Peres-Neto PR (2006) Spatial modelling: a comprehensive framework for principal coordinate analysis of neighbour matrices (PCNM). Ecol Model 196:483–493

Dudgeon D, Arthington AH, Gessner MO et al (2006) Freshwater biodiversity: importance, threats, status and conservation challenges. Biol Rev 81:163–182

Economo EP (2011) Biodiversity conservation in metacommunity networks: linking pattern and persistence. Am Nat 177:E167–E180

Feio MJ, Poquet JM (2011) Predictive models for freshwater biological assessment: statistical approaches, biological elements and the Iberian Peninsula experience: a review. Int Rev Hydrobiol 96:321–346

Fernandes IM, Henriques-Silva R, Penha J et al (2014) Spatiotemporal dynamics in a seasonal metacommunity structure is predictable: the case of floodplain-fish communities. Ecography 37:464–475

Friberg N, Bonada N, Bradley DC et al (2011) Biomonitoring of human impacts in freshwater ecosystems: the good, the bad and the ugly. In: Woodward G (ed) Advances in ecological research: ecosystems in a human-modifed lanscape: a European perspective. Advances in ecological research. Academic, London/New York, pp 1–68

Gravel D, Canham CD, Beaudet M, Messier C (2006) Reconciling niche and neutrality: the continuum hypothesis. Ecol Lett 9:399–409

Halley JM, Iwasa Y (2011) Neutral theory as a predictor of avifaunal extinctions after habitat loss. Proc Natl Acad Sci 108:2316–2321
Hamilton AT, Barbour MT, Bierwagen BG (2010) Implications of global change for the maintenance of water quality and ecological integrity in the context of current water laws and environmental policies. Hydrobiologia 657:263–278
Hawkins CP (2006) Quantifying biological integrity by taxonomic completeness: its utility in regional and global assessments. Ecol Appl 16:1277–1294
Hawkins CP, Norris RH, Hogue JN, Feminella JW (2000) Development and evaluation of predictive models for measuring the biological integrity of streams. Ecol Appl 10:1456–1477
Hawkins CP, Cao Y, Roper B (2010) Method of predicting reference condition biota affects the performance and interpretation of ecological indices. Freshw Biol 55:1066–1085
Heino J (2013) The importance of metacommunity ecology for environmental assessment research in the freshwater realm. Biol Rev 88:166–178
Heino J, Muotka T, Paavola R (2003) Determinants of macroinvertebrate diversity in headwater streams: regional and local influences. J Anim Ecol 72:425–434
Heino J, Gronroos M, Soininen J et al (2012) Context dependency and metacommunity structuring in boreal headwater streams. Oikos 121:537–544
Holyoak M, Leibold MA, Holt RD (2005) Metacommunities: spatial dynamics and ecological communities. University of Chicago Press, Chicago
Hubbell SP (2001) The unified neutral theory of biodiversity and biogeography. Princeton University Press, Princeton
Junk WJ, Bayley PB, Sparks RE (1989) The flood pulse concept in river-floodplain systems. Can Spec Publ Fish Aquat Sci 106:110–127
Karr JR (1999) Defining and measuring river health. Freshw Biol 41:221–234
Karr JR, Chu EW (1999) Restoring life in running waters: better biological monitoring. Island Press, Washington, DC
Krosch MN, Baker AM, Mather PB, Cranston PS (2011) Spatial population genetic structure reveals strong natal site fidelity in Echinocladius martini (Diptera: Chironomidae) in northeast Queensland, Australia. Freshw Biol 56:1328–1341
Legendre P (1993) Spatial autocorrelation: trouble or new paradigm? Ecology 74:1659–1673
Leibold MA, McPeek MA (2006) Coexistence of the niche and neutral perspectives in community ecology. Ecology 87:1399–1410
Leibold MA, Holyoak M, Mouquet N et al (2004) The metacommunity concept: a framework for multi-scale community ecology. Ecol Lett 7:601–613
Logue JB, Mouquet N, Peter H et al (2011) Empirical approaches to metacommunities: a review and comparison with theory. Trends Ecol Evol 26:482–491
Lutscher F, Pachepsky E, Lewis MA (2005) The effect of dispersal patterns on stream populations. SIAM Appl Math 65:1305–1327
McPeek MA, Brown JM (2000) Building a regional species pool: diversification of the Enallagma damselflies in eastern North America. Ecology 81:904–920
Mouquet N, Loreau M (2003) Community patterns in source-sink metacommunities. Am Nat 162:544–557
Nabout JC, Siqueira T, Bini LM, Nogueira IS (2009) No evidence for environmental and spatial processes in structuring phytoplankton communities. Acta Oecol 35:720–726
Norris RH, Hawkins CP (2000) Monitoring river health. Hydrobiologia 435:5–17
Peres-Neto PR, Legendre P (2010) Estimating and controlling for spatial structure in the study of ecological communities. Glob Ecol Biogeogr 19:174–184
Roque FO, Siqueira T, Bini LM et al (2010) Untangling associations between chironomid taxa in Neotropical streams using local and landscape filters. Freshw Biol 55:847–865
Rosenberg DM, Resh VH (1993) Freshwater biomonitoring and benthic macroinvertebrates. Chapman & Hall, New York
Scheiner SM, Willig MR (2008) A general theory of ecology. Theor Ecol 1:21–28
Siqueira T, Bini LM, Roque FO et al (2012a) A metacommunity framework for enhancing the effectiveness of biological monitoring strategies. PLoS ONE 7:e43626

Siqueira T, Bini LM, Roque FO et al (2012b) Common and rare species respond to similar niche processes in macroinvertebrate metacommunities. Ecography 35:183–192
Tilman D (1994) Competition and biodiversity in spatially structured habitats. Ecology 75:2–16
Tilman D (2004) Niche tradeoffs, neutrality, and community structure: a stochastic theory of resource competition, invasion, and community assembly. Proc Natl Acad Sci 101: 10854–10861
Van Sickle J (2008) An index of compositional dissimilarity between observed and expected assemblages. J N Am Benthol Soc 27:227–235
Vannote RL, Minshall GW, Cummins KW et al (1980) The river continuum concept. Can J Fish Aquat Sci 37:130–137
Winegardner AK, Jones BK, Ng ISY et al (2012) The terminology of metacommunity ecology. Trends Ecol Evol 27:253–254
Wright JF (1995) Development and use of a system for predicting the macroinvertebrate fauna in flowing waters. Aust J Ecol 20:181–197
Wright JF (2000) An introduction to RIVPACS. Freshwater Biological Association, Ambleside
Wright JF, Sutcliffe DW, Furse MT (2000) Assessing the biological quality of fresh waters: RIVPACS and other techniques. Freshwater Biological Association, London

Chapter 6
Modeling Trophic Interactions in Insect Population Dynamics

Michel Iskin da Silveira Costa and Lucas Del Bianco Faria

Abstract The complexity of insect communities involves a large number of interacting species. Predators may often exploit a wide range of food sources, frequently acting as generalists, omnivores or intraguild predators. In addition to these kinds of interactions, natural communities also contain species with two types of reproductive strategy, known as semelparity and iteroparity. In this chapter, different mathematical models representing trophic interactions will be considered, assuming both types of life history, in the framework of insect population dynamics and biocontrol. The results show that among other factors the interaction strength of the species involved plays an important role in the determination of the food web dynamics.

Keywords Mathematical modeling • Reproductive strategy • Food web • Population dynamics

6.1 Introduction

Natural communities are extremely complex and often involve different biological levels (i.e., individuals, populations and species) interacting with one another. Ecological communities are usually composed of many food webs/chains with a myriad of potential interactions, which results in multiple channels of energy flow (Pianka 2000).

The importance of understanding the patterns that emerge from food web studies lies in the development of an explanatory theory to identify the underlying factors that determine community structure and ecosystem functioning. Given that the

M.I.S. Costa (✉)
Laboratório Nacional de Computação Científica, Av. Getúlio Vargas, 333 – Quitandinha, 25651-070 Petrópolis, Rio de Janeiro, Brazil
e-mail: michel@lncc.br

L.D.B. Faria
Departamento de Biologia, Universidade Federal de Lavras, 37200-000 Lavras, Minas Gerais, Brazil
e-mail: lfaria@dbi.ufla.br

C.P. Ferreira, W.A.C. Godoy (eds.), *Ecological Modelling Applied to Entomology*, Entomology in Focus 1, DOI 10.1007/978-3-319-06877-0_6

nature of population ecology is essentially quantitative, a formal mathematical approach can be used to model the dynamics of a population or of several species in order to provide biological patterns that explain community structure and ecosystem functioning (Roughgarden 1998).

Essentially, the modeling of population dynamics can take on two possible forms: a continuous or discrete time framework. The choice of structure is closely related to the characteristics of the life history of individual species.

The term "life history" summarizes the timing and magnitude of growth, reproduction and mortality of an individual organism. Reproduction is one of the most important individual traits to be considered, since it has a direct impact on the next generation of offspring. Two types of reproductive strategy, with respect to reproductive pattern, can be named: semelparity, when individuals reproduce only once in their lifetime; and iteroparity, in which individuals reproduce more than once (Morris 2009). Hence, depending on the patterns of reproduction, species can have generations that overlap (iteroparity) or not (semelparity). The intensity or the absence of generational overlapping can dictate, among other factors, the choice of the time interval of modeling the population dynamics. Usually, iteroparous species are modeled by continuous time models, while semelparous species are modeled by discrete time models.

In this chapter, a biocontrol model will be couched by means of a system of nonlinearly coupled differential equations (continuous time), and a stage-structured intraguild insect population dynamics will be described by a set of nonlinearly coupled difference equations (discrete time). In addition to the description of the dynamics, the models will be shown to provide insights into disturbances, in order to achieve the desired results from the biological standpoint.

6.2 Continuous Time Modeling of Food Web Dynamics

A continuous time model of food web dynamics should consist of a differential equation for each trophic level (or species) of the whole system. Each equation must include terms that reflect how each individual species evolves in the absence of others, as well as how its dynamics is affected by the presence of the other species.

The time evolution of the basal species can be described by the logistic equation:

$$\frac{dN_i}{dt} = r_i N_i \left(1 - \frac{N_i}{K_i}\right) \tag{6.1}$$

N_i is the abundance of species *i;* r_i and K_i are the *per capita* instantaneous growth rate and the carrying capacity of species *i*.

Functional responses (*sensu* Holling 1959) may represent the impact of a predator on its prey. Different kinds of functional response can be found in the literature (Turchin 2003); however, "classical" functional response types I, II and III will be considered here.

Functional response types I, II and III (Eqs. 6.2, 6.3 and 6.4, respectively) can be defined as follows:

$$FR_1 = a_{ij} N_j N_i \tag{6.2}$$

$$FR_2 = \frac{a_{ij} N_j}{1 + a_{ij} T_{hij} N_j} N_i \tag{6.3}$$

$$FR_3 = \frac{a_{ij} {N_j}^2}{1 + a_{ij} T_{hij} {N_j}^2} N_i \tag{6.4}$$

a_{ij} represents the attack coefficient of species i on species j; T_{hij} represents the handling time of species i on species j. When more than one prey species is available to a single predator, a multi-species functional response type 2 can have the following form (Hassell 1978; Case 2000):

$$FR_m = \frac{a_{ij} N_i}{1 + a_{ij} T_{hki} N_i + a_{ij} T_{hij} N_{kj}} N_k \tag{6.5}$$

The functional response is converted into predator offspring by means of the numerical response. Then, predators evolve as a balance between prey consumption and mortality, as follows (in the case of a functional response type II):

$$\frac{dN_i}{dt} = e_{ji} \frac{a_{ij} N_j}{1 + a_{ij} T_{hij} N_j} N_i - m_i N_i \tag{6.6}$$

e_{ji} represents the efficiency constant in converting consumed prey (N_j) into predator (N_i) offspring; m_i represents the *per capita* mortality rate of the predator.

As an example, a predator-prey model with logistic growth and functional response type II can be given by Rosenzweig and MacArthur (1963):

$$\begin{aligned} \frac{dN_j}{dt} &= r_j N_j \left(1 - \frac{N_j}{K_j}\right) - e_{ij} \frac{a_{ij} N_j}{1 + a_{ij} T_{hij} N_j} N_i \\ \frac{dN_i}{dt} &= e_{ji} \frac{a_{ij} N_j}{1 + a_{ij} T_{hij} N_j} N_i - m_i N_i \end{aligned} \tag{6.7}$$

where N_j represents the prey density and N_i the predator density.

Similarly, a general multi-trophic food web model with functional response type I can be stated as:

$$\frac{dN_i}{dt} = N_i \left(r_i + e_{ji} \sum_{j=1}^{n} a_{ij} N_j \right) \tag{6.8}$$

where $r_i > 0$ or $r_i < 0$ depending on the characteristics of the species, and $a_{ij} = 0$ when there is no interaction between species i and j.

6.3 Continuous Time Modeling in Biological Control and Integrated Pest Management

The mathematical structure presented in the previous section can be employed to model the dynamics of species involved in a biocontrol food web scenario. The trophic diagrams of Fig. 6.1 depict possible food webs describing a biocontrol setting.

In diagram I, a generalist predator (P_g) feeds upon two prey species: a pest prey (N_p) and an endemic prey (N_e), which gives rise to a shared predator food web. In diagram II, a specialist predator (P_s) feeding on pest prey (N_p) is included in diagram I, which, in turn, concomitantly gives rise to a shared predator and a shared prey food web.

Since the structures of food webs I and II both involve multispecies predation, one can resort to the multispecies functional response type 2 (Eq. 6.5) to model the trophic interaction dynamics of the related species. Therefore, the population dynamics of N_p, N_e, P_g and P_s of food webs I and II are respectively described by food web models (Eqs. 6.9 and 6.10):

$$\begin{aligned}
\frac{dN_p}{dt} &= r_p N_p \left(1 - \frac{N_p}{K_p}\right) - \frac{(1-p)\, a_{P_g N_P} N_p}{1 + (1-p)\, a_{P_g N_P} T_{hP_g N_P} N_p + p a_{P_g N_e} T_{hP_g N_e} N_e} P_g \\
\frac{dN_e}{dt} &= r_e N_e \left(1 - \frac{N_e}{K_e}\right) - \frac{p a_{P_g N_e} N_e}{1 + (1-p)\, a_{P_g N_p} T_{hP_g N_p} N_p + p a_{P_g N_e} T_{hP_g N_e} N_e} P_g
\end{aligned} \tag{6.9}$$

$$\begin{aligned}
\frac{dP_g}{dt} &= e_{N_P P_g} \left(\frac{(1-p)\, a_{P_g N_p} T_{hP_g N_p} N_p}{1 + (1-p)\, a_{P_g N_p} T_{hP_g N_p} N_p + p a_{P_g N_e} T_{hP_g N_e} N_e} \right) P_g \\
&\quad + e_{N_e P_g} \left(\frac{p a_{P_g N_e} N_e}{1 + (1-p)\, a_{P_g N_p} T_{hP_g N_p} N_p + p a_{P_g N_e} T_{hP_g N_e} N_e} \right) P_g - m_g P_g
\end{aligned}$$

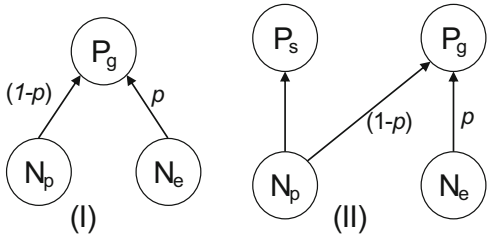

Fig. 6.1 Food web **I**: a generalist predator (P_g) feeds on two prey species (N_P and N_e) – a shared-predator food web (generalist food web). Food web **II**: a specialist predator (P_s) is added to food web I – a shared-predator and a shared-prey food web (specialist-generalist food web)

$$\begin{aligned}
\frac{dN_p}{dt} &= r_p N_p \left(1 - \frac{N_p}{K_p}\right) - \frac{a_{P_s N_P} N_p}{1 + a_{P_s N_P} T_{hP_s N_P} N_p} P_s \\
&\quad - \frac{(1-p)\, a_{P_g N_P} N_p}{1 + (1-p)\, a_{P_g N_P} T_{hP_g N_P} N_p + p a_{P_g N_e} T_{hP_g N_e} N_e} P_g \\
\frac{dN_e}{dt} &= r_e N_e \left(1 - \frac{N_e}{K_e}\right) - \frac{p a_{P_g N_e} N_e}{1 + (1-p)\, a_{P_g N_p} T_{hP_g N_p} N_p + p a_{P_g N_e} T_{hP_g N_e} N_e} P_g \\
\frac{dP_g}{dt} &= e_{N_P P_g} \left(\frac{(1-p)\, a_{P_g N_P} N_p}{1 + (1-p)\, a_{P_g N_P} T_{hP_g N_P} N_p + p a_g T_{hP_g N_e} N_e} \right) P_g \\
&\quad + e_{N_e P_g} \left(\frac{p a_{P_g N_e} N_e}{1 + (1-p)\, a_{P_g N_P} T_{hP_g N_P} N_p + p a_g T_{hP_g N_e} N_e} \right) P_g - m_g P_g \\
\frac{dP_s}{dt} &= e_{N_p P_s} \left(\frac{a_{P_s N_P} N_p}{1 + a_{P_s N_P} T_{hP_s N_P} N_p} \right) P_s - m_s P_s
\end{aligned} \tag{6.10}$$

r_p and K_p are the pest growth rate and its carrying capacity; r_e and K_e are the endemic growth rate and its carrying capacity; $e_{N_p P_g}$, $e_{N_e P_g}$, $e_{N_p P_s}$ are the efficiency conversion factors of the specific prey biomass into the corresponding predator offspring; $a_{P_s N_P}$ is the specialist predator attack coefficient on the endemic species; and $a_{P_g N_P}$ is the generalist predator attack coefficient on the pest species, while $a_{P_g N_e}$ is the generalist predator attack coefficient on the endemic species; $T_{hP_g N_p}$ and $T_{hP_g N_P}$ are the handling times of the generalist predator on the pest and endemic prey respectively; $T_{hP_s N_p}$ is the handling time of the specialist predator on the pest prey; m_s and m_g are the *per capita* mortality rate of the specialist and the generalist predator, respectively.

The analysis assumes that a trade-off exists between the specialist and the generalist such that the specialist has a higher attack rate on its prey, while the generalist has the ability, by definition, to feed on multiple prey items (Chang and Kareiva 1999). The precise trade-off is accomplished by the use of a prey preference parameter (p) for the generalist predator (Fig. 6.1). The parameter "p" can be thought of as the proportion of time spent foraging for the endemic prey, while $1-p$ is the proportion of time spent foraging on the pest. Note that the type 2 functional response is obtained when $p = 0$ and $p = 1.0$, and elsewhere a multi-species functional response is obtained. Thus, at the endpoints $p = 0$ and $p = 1.0$ the model simulates a generalist – playing the role of a specialist – feeding exclusively on the pest and the endemic prey, respectively.

Three conditions are considered to evaluate the theoretical efficiency of the models (Eqs. 6.9 and 6.10): (*i*) predator species must be able to control the pest prey species, leading to low levels of abundance or even local extinction; (*ii*) predator

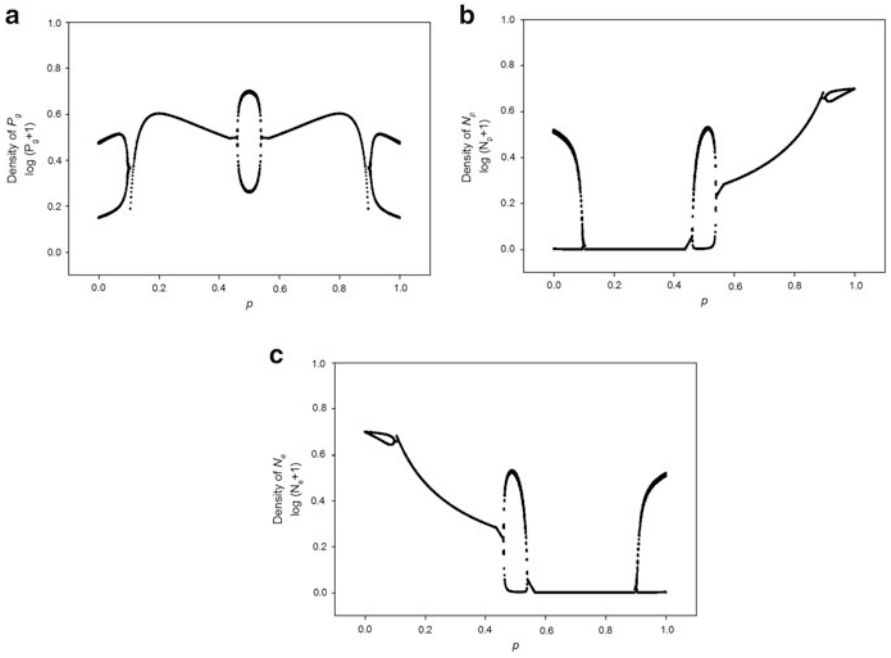

Fig. 6.2 Bifurcation analyses (i.e., local minima and maxima on the attractor) for a generalist food web (system I) over a range of values of the parameter p for the (**a**) Generalist predator (N_g), (**b**) Pest prey (N_p), and (**c**) Endemic prey (N_e). The parameters have been set so that the specialist on the pest prey gives oscillatory dynamics ($p = 0$), and were held constant at $r_p = r_e = 1.0$, $K_p = 4$, $K_e = 4$, $c = 0.3$, $h_g = 0.5$, $d_g = 0.1$, $a_g = 1.0$ (Reprinted from Faria and Costa 2009, License # 3157040097416, Elsevier)

species must not have a strong impact on endemic prey species, here assumed to be an endemic non-target species; (*iii*) the biocontrol food webs must persist through time without the need for addition of more individuals to the systems.

Figure 6.2a–c plots the local minimum and maximum of the trajectories of the model (Eq. 6.9) (the generalist food web of Fig. 6.1 – I) for a range in prey preference values ($0 < p < 1$). Two main features can be noted. First, as p increases, the food web becomes stable and the pest species is suppressed. Over the range of preference, where the generalist prefers the pest but still expends significant effort on the endemic, the pest is held in a stable equilibrium at low densities, and is even eliminated over some regions (Fig. 6.2b). Second, when the preference becomes skewed toward the endemic ($p > 0.50$), the food web becomes stable again, but with a preference range where the endemic species is locally extinct. In this range, the generalist predator reaches high densities because of its overconsumption of the endemic prey, which causes the suppression of the endemic prey population.

The long-term dynamic implications of using both a generalist and a specialist predator simultaneously are analyzed for the specialist-generalist food web

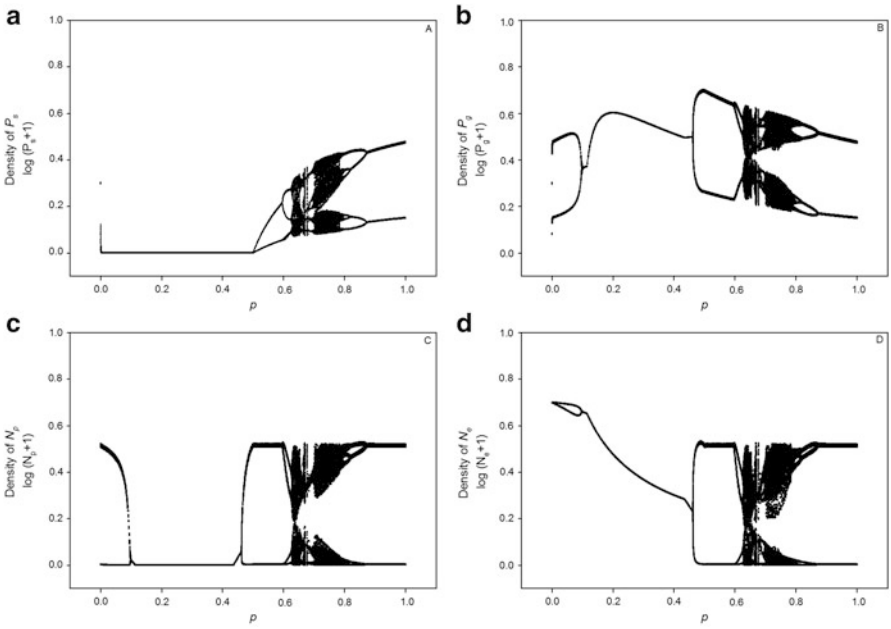

Fig. 6.3 Bifurcation analyses (i.e., local minima and maxima on the attractor) for system II (4-species model) over a range of values of the parameter p for the (**a**) Specialist predator (N_s), (**b**) Generalist predator (N_g), (**c**) Pest prey (N_p), and (**d**) Endemic prey (N_e). The parameters have been set so that the specialist on the pest prey gives oscillatory dynamics ($p = 0$), and were held constant at $r_p = r_e = 1.0$, $K_p = 4$, $K_e = 4$, $c = 0.3$, $h_s = h_g = 0.5$, $d_s = d_g = 0.1$, $a_s = a_g = 1.0$

(Fig. 6.1 – II) by means of a plot of the local minimum and maximum of the trajectories of the model (Eq. 6.10) for a range of prey preference values ($0 < p < 1$), as shown in Fig. 6.3a–d.

In the preference range where the generalist predator prefers the pest species, the dynamic results are similar to the generalist food web (Fig. 6.2) in that suppression of the pest occurs. In the preference range ($0 < p < 0.5$), the specialist predator is initially outcompeted by the generalist because of the indirect effects caused by predation on the endemic species. This kind of predation by the generalist increases its density level, which in turn, augments its predation pressure on the pest prey, leading this prey to reach levels that cannot sustain the specialist predator (i.e., the whole food web of Fig. 6.1-II is not biologically feasible over the long term).

However, the range in which the specialist is eliminated can be reduced by increasing the specialist species attack coefficient ($a_{P_s N_P}$) relative to the generalist species attack coefficients ($a_{P_g N_P}$ and $a_{P_g N_e}$). Persistence of the specialist predator is possible when the generalist prefers the endemic ($0.5 < p < 1$) and so decreases the strength of the indirect competition between the two prey species. Importantly, the inclusion of the specialist predator for $p > 0.50$ appears to limit the suppression

of the endemic population by means of sustained oscillations (Fig. 6.3c), while in its absence the endemic population is driven to extinction for $p > 0.50$ (Fig. 6.2c).

The development of the above two biocontrol food web models suggests that the generalist predator was able to control the pest species abundance (even causing its extinction) when the generalist's preference for the pest was superior to that for the endemic species. However, the model simulations also suggested that the endemic prey species is strongly impacted by the generalist predator. Further, the extent of this stable pest suppression depends on the attack coefficient of the generalist, so that a weak attack coefficient mutes the suppression potential of the generalist. Nonetheless, it is generally true that the presence of the generalist stabilizes the dynamics relative to the specialist case (i.e., $p = 0$ in Fig. 6.2). Two reasons for this stabilization can be suggested. First, the trade-off ensures that the generalist predator has a lower consumption rate than the specialist on the preferred prey. Secondly, the region of stabilization occurs where there exists a relatively strong interaction coupled with a weak interaction. This asymmetry in interaction strength has been shown to frequently enhance stability (Faria and Costa 2009; McCann et al. 1998; Post et al. 2000).

Since the biocontrol aim proposed here was to control the pest prey species without harming the endemic species, the results could be considered incomplete because it was necessary to include a specialist predator. The inclusion of the specialist predator clearly led to a wider range of stability, since the pest prey species was driven to low levels of abundance or even to local extinction, whereas the endemic prey species – i.e., non-target endemic species – was no longer extinct. These results are generally true and, as above, the relative stability is driven by the same mechanisms – the specialist-generalist trade-off dampens the strongest interaction relative to the specialist case, and the strong-weak asymmetry enhances the stability, as has been shown frequently in recent theoretical results (McCann et al. 1998; Faria et al. 2008).

Although the simulations of model (Holling 1959) suggest that the proposed specialist-generalist food web model is capable of simultaneously controlling pest-species density and avoiding endemic-species extinction, complex behavior dynamics – comprising (i) aperiodic behavior; (ii) two-point and (iii) four-point limit cycles ($p > 0.5$ – Fig. 6.3) – may ensue over some preference parameter (p) ranges, impeding to some extent the precise monitoring of species, and consequently thwarting proper management decisions.

Importantly, the specialist-generalist food web model (Fig. 6.1-II; Eq. 6.10) is amenable to other analyses in the context of pest management, such as, for instance, Integrated Pest Management.

Integrated Pest Management (Stern et al. 1959) is a pest-control strategy that uses an array of additive methods such as biological control and chemical control. This strategy purports to allow more efficient control of pest outbreaks, minimizing the direct and indirect effects caused by pesticide application. The modeling of IPM could be conveyed by means of the alteration of the *per capita* mortality rates of all components of the model, $m_s - \varepsilon_{Ps}$ and $m_g - \varepsilon_{Pg}$, for the specialist and the generalist

predator, respectively, where ε_{Ps} and ε_{Pg} are the per capita mortality coefficients inflicted upon the predator(s) by chemicals used in IPM; correspondingly, $(r_i - \varepsilon_{Ni})$ and $K_{Ni}\ (1 - \varepsilon_{Ni}/r_i)$ $[i = p,e]$ for the prey species. This framework was employed in the analysis of an IPM with a generalist and specialist predator subject to a threshold policy, in order to maintain pest prey species at a low level while preserving the endemic species (Costa and Faria 2010).

In a specialist-generalist food web model (Eq. 6.10) the result of this IPM formulated as a threshold management policy consisted of stabilization (i.e., species coexistence without pest outbreaks) of the related system. In other words, it was shown that with this strategy in the context of Integrated Pest Management, the dynamics of a specific food web can be strongly stabilized. In fact, given a proper combination of pesticide application intensity, generalist predator preference and specialist predator threshold density, a previously chosen specialist predator level was attained by means of a threshold policy applied to the pesticide application intensity. This stable behavior occurred despite the dynamic complexity of the food web model related to biocontrol only, and/or the direct and indirect effects caused by a combined regime of continuous pesticide application and biocontrol.

6.4 Discrete Time Modeling of Predation Between Immature Stages

Insect populations generally have life cycles with well-defined stage structures during their life spans. Given this demographic setting, a reasonable approach to mathematically describe insect population dynamics could consist of discrete time dynamic models. Several discrete time mathematical models have been proposed to describe unstructured as well as structured single-insect population dynamics (Cushing et al. 2003). Accordingly, interspecific predation among unstructured as well as structured insect populations has also given rise to some discrete time dynamic models (Crawley 1975; Prout and McChesney 1985; Wang and Gutierrez 1980) with the aim of establishing relatively general criteria for coexistence and stability in the systems studied. A common assumption of these models is that predation occurs between mature stages and/or between mature and immature stages. Since in these cases predation necessarily involves mature phases, the modeling effort focuses on functional and numerical responses in order to couple predator and prey dynamics.

However, predation among insect populations may occur only in immature phases, which, in turn, requires relations linking predation in immature life stages with survival and fecundity in mature stages. An example of this kind of trophic interaction is the behavior of the blowfly *Chrysomya albiceps* and its larval prey species. Initially, adult females of *C. albiceps* lay eggs in carcasses, which may also support other species of Calliphoridae. Larvae hatch and start to consume the food substrate, which is usually insufficient to support them, initiating a possible set of

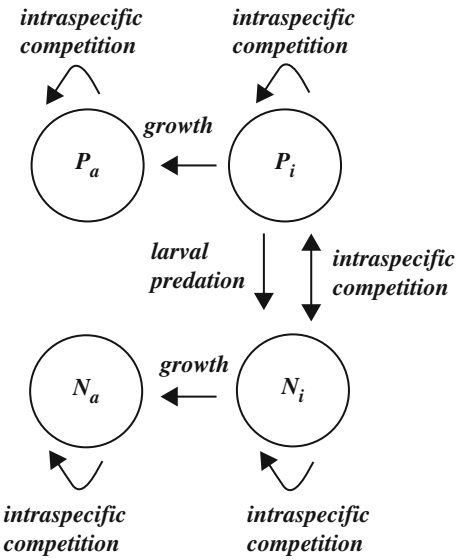

Fig. 6.4 *N* prey, *P* predator; subscripts: *l* young, *a* adult. The interspecific competition in the larval phase together with the larval predation characterizes an intraguild predation (Reprinted from Faria et al. 2011, Licence # 3157040097416, Elsevier)

intra- as well as interspecific competition processes. Consequently, in response to food scarcity, *C. albiceps* third-instar larvae begin to prey on other larvae species, i.e., an intraguild larval predation situation (Faria et al. 2007), which ceases when the third-instar predator larva reaches the pupal stage.

Figure 6.4 depicts schematically this set of stage-dependent interactions, where it is assumed that both prey (N) and predator (P) populations consist of two stages, larva (l) and adult (a), and that predation as well as interspecific competition will take place only during the larval phase (thus characterizing an intraguild predation), while intra-specific competition occurs in the adult as well as in the larval phase.

A possible model to describe the dynamics of the prey larvae (N_l) and the predator larvae (P_l) of the trophic scheme in Fig. 6.4 can be given by Faria et al. (2011):

$$\begin{aligned} N_l\,(t+1) &= N_l(t)e^{-aP_l(t)}e^{-\alpha P_l(t)}S_{\max\_prey}e^{-bN_l(t)}e^{-a'N_a(t)}E_{\max\_prey} \\ P_l\,(t+1) &= P_l(t)e^{-\gamma N_l(t)}S_{act}e^{-\beta P_l(t)}e^{-c'P_a(t)}E_{act} \end{aligned} \tag{6.11}$$

A central feature of model (6.11) consists of the terms E_{act}, the actual fecundity of an adult predator, and S_{act}, the actual survival of the larval predator, both functions of the functional response of the intraguild predator. These terms make the connection between predation in immature stages, and survival and fecundity in mature stages, and they are expressed as:

$$S_{act} = \begin{cases} S_{\max\_pred}Z^{\upsilon} & \text{if} \quad Z \leq 1 \\ S_{\max\_pred} & \text{if} \quad Z > 1 \end{cases}$$

and

$$E_{act} = \begin{cases} E_{\max\_pred} Z^{\upsilon} & \text{if} \quad Z \leq 1 \\ E_{\max\_pred} & \text{if} \quad Z > 1 \end{cases}$$

with Z, the fraction of the diet obtained by one predator, given by Crawley (1975):

$$Z = \frac{N_l(t)\left(1 - e^{[-aP_l(t)]}\right)}{P_l(t)A}$$

A is the amount of prey required for satiation of one predator, and a is the attack coefficient of P_l on N_l. The constant υ ($\upsilon > 0$) determines the shape of the continuous incremental survival and fecundity curves before they reach saturation.

In model (6.11), $P_l(t)e^{-\gamma N_l(t)} S_{act} e^{-\beta P_l(t)}$ is the adult predator population in generation t (resulting from P_l predator larvae at the beginning of generation t); β is the intraspecific competition coefficient among predator larvae; γ is the interspecific competition coefficient between predator and prey larvae; c' is the intraspecific competition coefficient among adult predators. $N_l(t)e^{-aP_l(t)}e^{-\alpha P_l(t)} S_{\max\_prey} e^{-bN_l(t)}$ is the adult prey population in generation t (resulting from N_l prey larvae at the beginning of generation t); a is the larval predation coefficient of predator larvae on prey larvae; α is the interspecific competition coefficient between predator and prey larvae; b is the intraspecific competition coefficient among prey larvae; a' is the intraspecific competition coefficient among the adult prey; S_{max_prey} and E_{max_pred} stand respectively for the density-independent maximum survival to mature stages and the fecundity of the prey.

Model (6.11) can help in the analysis of the influence that the intraguild predator attack rate (a) and its satiation (A) may exert on the success of its invasion into the community and species coexistence. To this end, a parametric space composed by attack rate vs. satiation rate is drawn in Fig. 6.5 for some values of υ. It suggests that the higher the intraguild predation satiation, the higher the attack rate must be in order to promote species coexistence (i.e., success of the intraguild predator invasion).

Given that in natural systems, predation during immature stages of the life cycles of the species involved can occur (e.g., intraguild predation frog larvae–Sours and Petranka 2007), and the plausibility of the dynamic results generated by (6.11), it seems worthwhile to improve the modeling of interactive populations that comprise this kind of predation. Furthermore, the proposed model is amenable to: *(i)* the incorporation of other predation and competition structures; *(ii)* an explicit dynamic equation for the resource; *(iii)* its modification for a continuous time setting.

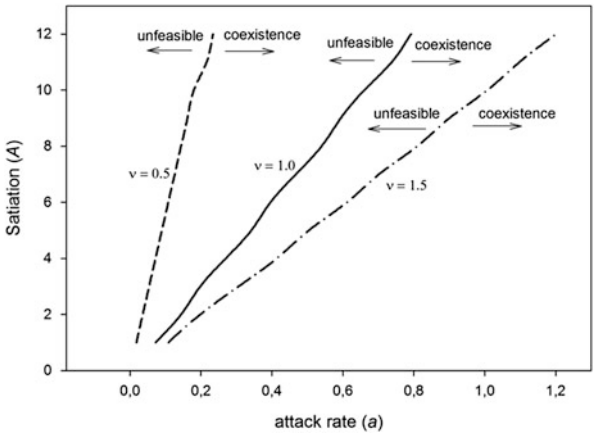

Fig. 6.5 Relationship between satiation term (A) and attack rate (a) for different values of ν. *Dashed line* ($\nu = 0.5$); *dash-dotted line* ($\nu = 1.5$); *solid line* ($\nu = 1$). For each value of ν the *arrow* on the *left side* indicates an unfeasible system (predator unable to invade) and the *arrow* on the *right* indicates coexistence of both species (predator successful invasion). Parameter values: $S_{max\_prey} = 0.6$; $S_{max\_predator} = 0.6$; $E_{max\_prey} = 20$; $E_{max\_predator} = 20$; $a' = 0.5$; $c' = 0.5$; $b = 0.1$; $\beta = 0.1$; $\alpha = 0.1$; $\gamma = 0.1$ (Reprinted from Faria et al. 2011, Licence # 3157040097416, Elsevier)

6.5 Final Considerations

A mathematical approach based on systems of nonlinear difference and differential equation is advanced, to model insect population dynamics in the contexts of biocontrol and species invasion.

In both cases, the models are strategic in nature; that is, they eschew precise descriptions of a specific biological system in favor of obtaining general principles that could be applied to a relatively large set of biological systems.

In the continuous case, a generalist and a specialist-generalist food web model were used to control outbursts of pest species. It was shown that to achieve this aim, the proposed generalist-specialist food web model was more appropriate in that it avoided low endemic pest-species population levels – a major requirement of pest biocontrol. More importantly, this performance was accomplished when a trade-off between generalist and specialist predator interaction strength ensured that a generalist predator species has a lower consumption rate than the specialist on the preferred prey. In addition, it was shown that the generalist-specialist food web model could be extended in order to model an Integrated Pest Management scenario.

In the discrete time case, a stage-structured food web population model purported to describe the invasion of an exotic species into an endemic food web. One main result concerns the dependence of the invasion success on the attack coefficient of the invasive species, where the higher the intraguild predation satiation, the higher the attack rate must be in order to promote species coexistence.

Theoretical modeling of population dynamics and interactions is of necessity a process of ecological abstraction, because of the myriad of factors pertaining to the biological systems involved. Accordingly, this process usually requires a relatively small set of selected interactions and related parameters in order to describe and predict patterns of abundance and species coexistence (or extinction) – a requirement that is fulfilled by empirical observation, experiments and biological theory. In the entomological context (as well as in other ecological contexts), although theoretically robust general predictions are very unlikely to come by, new trophic interaction models have been generating numerous assumptions and forecasts about insect population dynamics and their structural and functional communities.

In closing, it is worth mentioning that theoretical population ecology has been spurring investigations in many different areas (Kareiva 1989; Wang and Gutierrez 1980; Loreau 2010). Mathematical models applied to predict population dynamics and species trophic interaction patterns constitute a fundamental tool to gain a better understanding of, among other topics, the role of trophic interactions in the determination of species coexistence in natural communities (Kareiva 1989).

References

Case TJ (2000) An illustrated guide to theoretical ecology. Oxford University Press, Oxford

Chang GC, Kareiva P (1999) The case for indigenous generalist in biological control. In: Hawkins BA, Cornell HV (eds) Theoretical approaches to biological control. Cambridge University Press, Cambridge

Costa MIS, Faria LDB (2010) Integrated pest management: theoretical insights from a threshold policy. Neotrop Entomol 39:1–8

Crawley MJ (1975) The numerical responses of insect predators to changes in prey density. J Anim Ecol 44:877–892

Cushing J, Costantino RF, Dennis B, Desharnais RA, Henson SM (2003) Chaos in ecology: experimental nonlinear dynamics. Academic, Amsterdam

Faria LDB, Costa MIS (2009) The interplay between predator's prey preference and environmental heterogeneity in food web long-term stability. J Theor Biol 258:339–343

Faria LDB, Reigada C, Trinca LA, Godoy WAC (2007) Foraging behaviour by an intraguild predator blowfly, *Chrysomya albiceps* (Diptera: Calliphoridae). J Ethol 25:287–294

Faria DBF, Umbanhowar J, McCann KS (2008) The long-term and transient implications of multiple predators in biocontrol. Theor Ecol 1:45–53

Faria DBF, Costa MIS, Godoy WAC (2011) A model for intraguild predation dynamics between immature stages. Ecol Model 222:3295–3299

Hassell MP (1978) The dynamics of arthropod predator-prey systems. Princeton University Press, Princeton

Holling CS (1959) Some characteristics of simple types of predation and parasitism. Can Entomol 91:385–398

Kareiva P (1989) Renewing the dialogue between theory and experiments in population ecology. In: Roughgarden J, May R, Levin SA (eds) Perspectives in ecological theory. Princeton University Press, Princeton

Loreau M (2010) From populations to ecosystems: theoretical foundations for a new ecological synthesis. Princeton University Press, Princeton

McCann KS, Hastings A, Huxel GR (1998) Weak trophic interactions and balance of nature. Nature 395:794–798

Morris WF (2009) Life history. In: Levin S (ed) The Princeton guide to ecology. Princeton University Press, Princeton

Pianka ER (2000) Evolutionary ecology, 6th edn. Addison Wesley Education Publisher, San Francisco

Post DM, Conners ME, Goldberg DS (2000) Prey preference by a top predator and the stability of linked food chains. Ecology 81:8–14

Prout T, McChesney F (1985) Competition among immatures affects their fertility: population dynamics. Am Nat 126:521–558

Rosenzweig ML, MacArthur RH (1963) Graphical representation and stability conditions of predator-prey interactions. Am Nat 97:209–223

Roughgarden J (1998) Primer of ecological theory. Prentice Hall, Upper Saddle River

Sours GN, Petranka JW (2007) Intraguild predation and competition mediate stage-structured interactions between WoodFrog (Rana sylvatica) and upland chorus frog (Pseudacris feriarum). Copeia 1:131–139

Stern V, Smith R, Bosch VDR, Hagen KS (1959) The integrated control concept. Hilgardia 29:81–101

Turchin P (2003) Complex population dynamics: a theoretical/empirical synthesis. Princeton University Press, Princeton

Wang YH, Gutierrez AP (1980) An assessment of the use of stability analyses in population ecology. J Anim Ecol 49:435–452

Chapter 7
Coupled Map Lattice Model for Insects and Spreadable Substances

Luiz Alberto D. Rodrigues, Maria C. Varriale, Wesley A.C. Godoy, and Diomar C. Mistro

Abstract Understanding the spreading dynamics of insects and particles naturally or artificially associated with them, such as seeds, pollen, repellents or insecticides, is of paramount importance for pest management and conservation programs. Insects and chemical or natural products exhibit dispersal patterns that depend on the environment where they are and their respective sizes. In this chapter, we present a Coupled Map Lattice formalism to investigate the theoretical dynamics of the spread of insects and chemical substances sprayed over them. The models consider a habitat with abundant resources and therefore insects moving only in response to chemical concentrations. Diffusion and wind are the mechanisms used to spread chemical substances. Continuous and discrete models are used to describe the system on a macroscopic scale. The results are discussed taking into account rules for movement, escape behaviour and integrated pest management strategies.

Keywords Dispersal • Insect movement behaviour • Chemotaxis • Coupled map lattice • Continuum limit

---

Electronic supplementary material The online version of this chapter (doi:10.1007/978-3-319-06877-0_7) contains supplementary material, which is available to authorized users.

L.A.D. Rodrigues (✉) • D.C. Mistro
Departamento de Matemática, Universidade Federal de Santa Maria, Santa Maria, RS, Brasil
e-mail: ladiazrodrigues@gmail.com; dcmistro@gmail.com

M.C. Varriale
Instituto de Matemática, Universidade Federal do Rio Grande do Sul, Porto Alegre, RS, Brasil
e-mail: cris@mat.ufrgs.br

W.A.C. Godoy
Departamento de Entomologia e Acarologia, Escola Superior de Agricultura "Luiz de Queiroz", Universidade de São Paulo, Piracicaba, São Paulo, Brasil
e-mail: wacgodoy@usp.br

C.P. Ferreira, W.A.C. Godoy (eds.), *Ecological Modelling Applied to Entomology*, Entomology in Focus 1, DOI 10.1007/978-3-319-06877-0_7

7.1 Introduction

The dispersal of particles associated with insects, such as pollen, seeds, pheromones, repellents, or even insecticides, may depend on the insect population movement or on external stimuli such as the wind or climate changes (Esker et al. 2007; Snell 2014). Pollen dispersal in particular has been studied by coupled map lattice formalism with results showing that the principles of pollen spread are well described by the model, as occurs with diffusion models (Yamamura 2004). An interesting example of the coupled map lattices application in the analysis of particles associated with insects is the study performed by Beck et al. (2003), which aimed to evaluate the efficiency in controlling the spread scentless chamomile by using seed weevils *Omphalapion hookeri* and the gall midge *Rhopalomyia tripleurospermi*. In this study, the authors investigated interactions between scentless chamomile, a weed native to Europe considered to be a serious problem in Canadian agricultural systems and the predators (Beck et al. 2003). They studied the weed and the two insects mentioned above by employing a coupled map lattice model incorporating an age structure for the pest scentless chamomile and the two natural enemies. The model also included dispersal kernels for all species and a geographical information system. The coupled map lattice model illustrated the dispersal of scentless chamomile on a hypothetical landscape, providing a formalism that can be applied to other weed biocontrol systems in a spatial context.

In an elegant study, Liere et al. (2012) investigated trophic interactions involving a predatory ladybird, a beetle that depends on the patchy distribution of the mutualism between its prey, the green coffee scale, and the ant *Azteca instabilis*. A spatial model was proposed showing that the aggregated pattern of ant nests helps to guarantee the persistence of the beetles. In addition, the consumption of the scale insects by ladybirds induced a clumped distribution of the ants (Liere et al. 2012). The model has a stochastic component for the local and global migration of the beetle, taking into account the beetles' ability to sense ant pheromones and therefore including the pheromone transport.

Conventionally, problems emphasising biological diffusion are frequently studied or solved based on examples of animal movement (Benhamou 2014), diffusion of plants or seeds (Coulson et al. 2014) and spores (Ito 2013). However, there are situations in which spreading particles are not living organisms, despite being associated with them. For scenarios such as this, the complexity of the system requires a different approach to better describe its diffusion. Diffusion processes describe not only non-living particles but also living organisms. Natural or chemical repellents would be examples of spreadable particles that are most likely associated with insects and that should be investigated with respect to their pattern of spread.

Taking as an initial example the dispersal patterns of living organisms, we begin with animal movement. In the simplest scenario, looking only at the dispersal of an individual, it is not hard to recognise forces that influence the animal to leave a place and go to another one. This pattern would result in regular, easily comprehended movement (Okubo and Levin 2001). Nevertheless, with scenarios with more than

one individual, the animals' movement is most likely not identical (Okubo and Grünbaum 2001). In a similar vein, if it is thought that insects and particles are to some extent associated with each other and therefore could be governed by the same forces, the result of their dispersal would depend on the intensity and frequency of each force. This reasoning allowed us to draw conclusions about environmental variability (Okubo and Grünbaum 2001).

Natural or chemical particles may be present in environments containing insects and can also be used to repel them. In spite of the existence of several chemical products that repel insects, their efficiency has been questioned (Semmler et al. 2014), and currently, there is a growing interest in the use of natural products. There are essential oils in nature that can be used as alternative products to keep insects away from humans, animals or plants (Olivero-Verbel et al. 2013; Tabanca et al. 2013; Tong and Bloomquist 2013). There are real examples of oils decreasing the infestation of insect pests at a high percentage (Brendel 2013; Nikpay 2007). Citrus intercropped with guava may have a lower incidence of its main pest than isolated crops (Yang et al. 1998). The use of natural repellents has also been investigated in mosquitoes with promising results (Govindarajan and Sivakumar 2012). Although the literature emphasising repellents has been increasing in recent years, both the spreading dynamics of particles and insect movement in response to repellents have not be systematically investigated.

In this chapter, an approach to investigate the spread of insects and chemical substances sprayed over them is presented. We take into account insect chemotactic behaviour and the influence of environmental factors, such as the wind, in the spread of the chemical substance. The theoretical scheme is presented in detail using the Coupled Map Lattice theory employed by Rodrigues et al. (2013), who recently investigated the dynamics of insects influenced by chemicals. The particles depicted here are natural or artificial repellents or insecticides, which are supposed to move by diffusion and advection influenced by the wind (Ngueleu et al. 2013; Rodrigues et al. 2013), but the natural degradation of the particles has also been considered.

The distribution and persistence of insects in time and space are analysed, assuming that they are influenced by the behaviour of the insect and the chemical substance. To model the insect populations influenced by a chemical substance (pollutant, repellent or pesticide), different assumptions can be made about insect behaviour and sensory ability. It is known that insects have different sensory abilities; some of them exhibit sophisticated systems to measure chemical signals over a long distance, as occurs with some Lepidoptera insects (Oliver and Stein 2011), whereas others are unable to do this and only perceive signals when visiting a specific site, such as some blowfly species (Huntington and Higley 2010). We show two different models depending on the insect movement behaviour. The first model, Model I, considers insects with limited sensory ability, then the individuals can only sense chemicals at the site at which they are located. In Model II, insects have a better ability to detect chemical particles in their neighbourhood and are able to move to lowest chemical concentration.

Four sections were prepared as follows. In Sect. 7.2, we present the Coupled Map Lattice formalism for modelling population spatio-temporal dynamics. In Sect. 7.3, we propose and analyse a model for insects with local perception: the model formulation, simulations as well as the continuous limit for the rules proposed are presented. Section 7.3 brings the analyzes of a model for insects with quasi-local perception while in Sect. 7.4 we discuss the ecological implications of our results.

7.2 The Spatial Structure and the Movement Rules

Although space has been neglected by theoretical models applied to entomology in recent decades, currently its importance is well recognised in theoretical ecology. In previous models, only a mean density of species were used, and it was assumed that individuals are well distributed, implying that all predators are able to reach prey with the same probability. There are many justifications to including space in population biology models emphasising insects. Among them we note environmental heterogeneity, which causes the parameters and the population density to vary with geographical location, the heterogeneity of the initial distribution of the population, which may lead to spatial invasions and consequently to heterogeneous spatial distribution, different interacting species exhibiting distinct dispersal rates, which once again may cause heterogeneous patterns in space (Godoy and Costa 2005; Kot 2001), and, finally, the model predictions can be different when space is considered (Godoy and Costa 2005). The classical example is the host-parasitoid discrete model presented by Nicholson and Bailey (1935), which shows instability and extinction, except in its spatial counterpart proposed by Hassell et al. (1991) in which the persistence of both species is observed. The discrepancy between these models is mainly due to the explicit usage of space (Solé and Bascompte 2006).

Depending on the species life history and movement behaviour, different modelling approaches can be adopted. These features determine the type of the independent variables – continuous or discrete – and consequently the model framework.

When individuals present discrete generations (like many insect species that reproduce in a well-established period of time), time-discrete formalisms are better than continuous ones. Furthermore, if the space, at some appropriate scale of examination, has a markedly discrete feature such as, for example, citrus orchards, where each tree could be considered as a patch, a system characterised by crop can be described by the coupled map lattice (CML) formalism.

CML models are characterised by discrete space and time but encompass continuous state variables. Substance concentrations are examples of continuous state variables. The habitat is split into patches or sites representing real locations where the population is distributed. Coupled map lattices were first introduced by the Japanese physicist Kunihiko Kaneko (1986) with the purpose of investigating spatiotemporal chaos. The application to population ecology dates back to the early 1990s (Hassell et al. 1991; Solé and Valls 1991; Solé et al. 1992). Hassell et al. (1991) and Comins et al. (1992) extended Nicholson-Bailey's host-

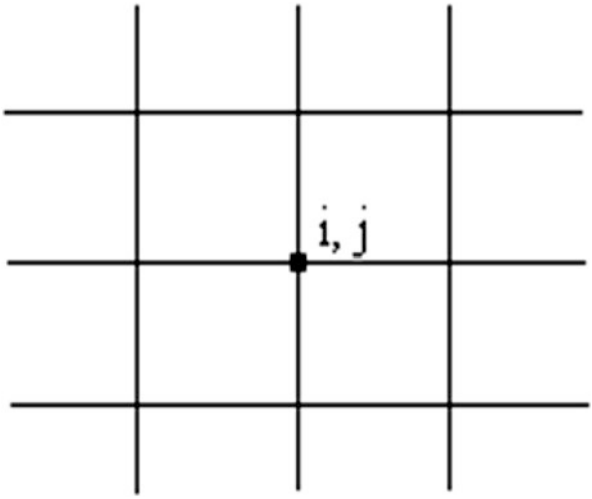

Fig. 7.1 Two dimensional lattice

parasitoid model to incorporate space by using a coupled map lattice with diffusion movement for both populations. Depending on the species diffusivities, they observed the following three types of self-organising spatial patterns: spiral waves, crystal lattices and spatial chaos. This formalism has been used to study host-parasitoid interactions, dispersal-driven instability, critical patch-size and invasion processes (de-Camino-Beck and Lewis 2009; Gao et al. 2007; Hassell et al. 1991; Méndez et al. 2010; Mistro et al. 2012; Reigada and Aguiar 2012; Rodrigues et al. 2012).

In a two-dimensional model of the dispersal problem, the total environment is assumed to be subdivided into local habitats, dubbed 'patches', that are arranged in a grid or lattice (Fig. 7.1).

In each point, at the centre of the patch and associated with integer coordinates (i, j), the population mean density over the patch is represented. The system is assumed to have discrete generations. Within each generation, there are two distinct phases, as follows:

1. *A between-patch dispersal phase*, in which a fraction of the individuals leaves its current patch for neighbouring patches according to some dispersal rule while some individuals remain in their original patch; and
2. *A within-patch interaction and reproduction/mortality phase*, that is, a sedentary reaction stage, in which all intra- and inter-species interactions occur (Rodrigues et al. 2011, 2012).

In this chapter, we will present state variables including insect population densities and chemical substance concentrations. The dispersal phase for both the insects and the substance occurs prior to the reaction stage; different types of dispersion movement such as diffusion, convection and taxis can be described in the former, while the latter includes substance decay and insect mortality due to the effects of the substance.

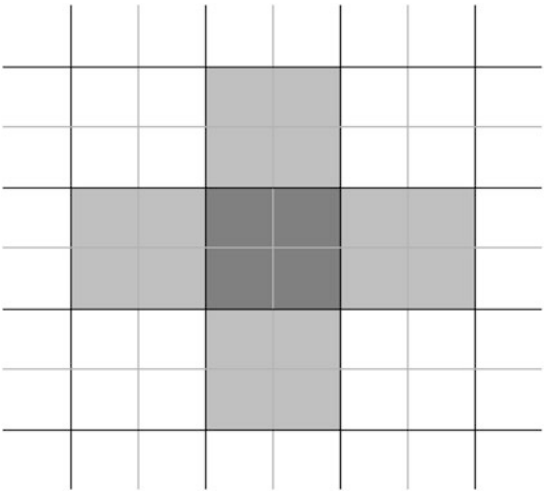

Fig. 7.2 The von Neumann neighborhood: the central patch i, j and its four neighbors

The dynamics occurring within each patch are connected to their neighbours in different ways. Each site can be coupled with neighbouring sites (partial) or with the entire lattice (global mixing). For partial couplings, the rules frequently used are related to their range; the von Neumann neighbourhood (Fig. 7.2) which will be used in this chapter, considers the four nearest neighbours while the Moore neighbourhood takes eight neighbours into account. It is also possible to define different neighborhood to take into account long-range movements.

Representing the output from (i, j) to site (r, s) of its neighbourhood by $S_{r,s}$ and the entries in (i, j) from the (r, s) neighbours by $E_{r,s}$, we can write, for any sort of dispersal reduced to the neighbouring patches, the following equation:

$$X'_{i,j} = X^t_{i,j} - \sum_{(r,s)\in V_{i,j}} S_{r,s} + \sum_{(r,s)\in V_{i,j}} E_{r,s}, \tag{7.1}$$

where $X^t_{i,j}$, $X'_{i,j}$ are the population densities of X species in generation t prior to dispersal and postdispersal, respectively, and $V_{i,j}$ is the neighbourhood considered. Figures 7.3 and 7.4 depict movement scheme given by (7.1).

The simplest movement rule considers that a constant fraction λ of individuals leaves each site and is evenly distributed among the neighbouring sites. The corresponding equation is given by

$$X'_{i,j} = (1-\mu)X^t_{i,j} + \frac{\mu}{4} \sum_{(r,s)\in V_{i,j}} X^t_{r,s}, \tag{7.2}$$

since

$$S_{r,s} = \frac{\mu}{4} X^t_{i,j}, \text{ for all } (r, s) \in V_{i,j}.$$

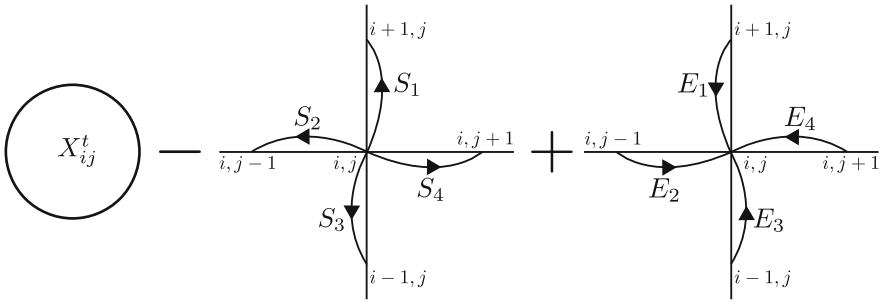

Fig. 7.3 The density of individuals in each patch after dispersal, correspond to their density prior dispersal minus the density of those who left the patch plus the density of those who migrate to the patch from the neighboring patches

Fig. 7.4 General movement scheme: during the dispersal stage, some individuals remain in the original patch while others migrate to the neighboring ones

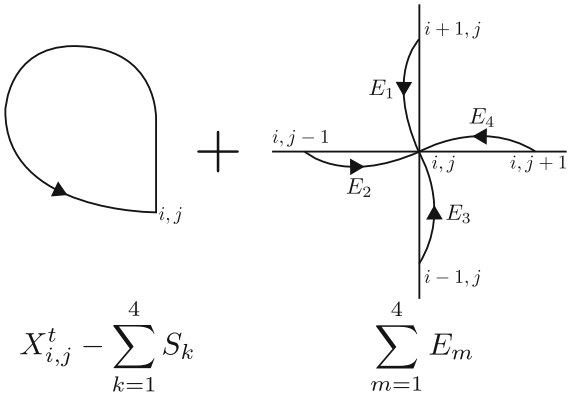

The diagram pictured in Fig. 7.5 illustrates the diffusion movement described by Eq. (7.2).

Other movements can be described using CML, such as convection and taxis movement, as will be illustrated in this chapter. In the former, a fraction of individuals is carried by the wind or a fluid in which the population is immersed. In the latter, the movement is driven by an external stimulus. Hence, the fraction of individuals leaving the patch may not be constant; depending on the individuals' movement behaviour, $S_{r,s}$ may depend on the local population density or even on the density of an external interacting population or stimulus. For example, the fraction of predators that leaves each patch may depend on the prey density.

For individuals in the patches located at the **boundary** of the habitat, it is necessary to define a particular movement rule that is called boundary condition (BC). Three main types of BCs usually considered are reflective, absorbing and periodic or cyclic (Comins et al. 1992; Solé and Bascompte 2006; White and White 2005):

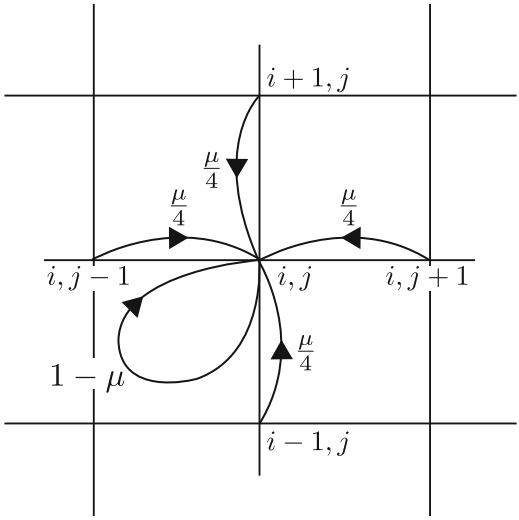

Fig. 7.5 Diffusive movement scheme

- In the reflective BC, individuals do not cross the border; individuals that would disperse out in other conditions remain in the edge patches, that is, they are sent back into the habitat. This type of BC is used when individuals are located in a very favourable area or when there are restrictions on their geographical dispersion.
- In the absorbing BC, individuals who move out of the domain are lost, which therefore imposes additional "mortality" on the system. In this type of BC, the individuals abandon a region that becomes unfavorable.
- In periodic or cyclic BC, each end of the lattice is linked to its opposite one as in a torus, so individuals moving north (east) of the first row (column) reappear at the last row (column), which is obviously unrealistic, but has the advantage that all patches are equivalent, with no edge effects.

For the second phase, the reaction stage, we represent the population density of site (i, j) at generation t by $X_{i,j}^t$, and write the following:

$$X_{i,j}^{t+1} = F(X_{i,j}^{'})$$

to account for the particular features of the map corresponding to the local dynamics. The interaction can include features such as the chemical's effects reducing the insect population, chemical degradation reducing its concentration, insect mortality and birth, etc. F can depend explicitly on the position reflecting spatial inhomogeneities. In spatial refuges, for example, hosts are protected in certain areas where the attack rate of the parasitoid is drastically reduced, which implies a spatial dependence of the corresponding parameter (Mistro et al. 2009). Shigesada et al. (1986, 1987) studied a continuous model where not only the vital rates but also the movement coefficient were affected by habitat heterogeneity.

Now we will analyze the macroscopic behavior resulting from the microscopic rule (7.2) proposed. We argue that for appropriate spatial and temporal scales, it is possible to approximate discrete models by continuum models expressed in terms of reaction diffusion equations. We aim at obtaining some insight about the macroscopic behavior from the schemes assumed and use the knowledge about continuous models to a better understand the results.

Indeed, a limit model is not the real model but only a continuum model which is amenable to partial differential equations techniques and approaches discrete counterparts as closely as the scales of the latter are set in the correct limit path. This approach allows us to avail ourselves of the continuum theoretical tools available for partial differential equations from one hand and from the other hand, as we will see, to take advantage of the handiness of the discrete model to simulate situations that could hardly be dealt with the continuous model.

In order to obtain a macroscopic model equivalent to the discrete simulation model (7.2), we consider that the individuals move on a two-dimensional lattice. At each time step τ, the individuals can move a distance δ either left or right, up or down, with probabilities given by $\frac{\lambda}{4}$, or they may stay at the same location with probability $1-\lambda$. Thus, we have the following difference equation for the population:

$$\begin{aligned} X(x,y,t+\tau) = (1-\lambda)X(x,y,t) \\ +\frac{\lambda}{4}X(x-\delta,y,t) + \frac{\lambda}{4}X(x+\delta,y,t) \\ +\frac{\lambda}{4}X(x,y-\delta,t) + \frac{\lambda}{4}X(x,y+\delta,t), \end{aligned} \tag{7.3}$$

where the first term represents the individuals that stay in the same location, and the other four terms represent the individuals that arrive from the nearest neighbouring sites.

Now, we suppose that, from a macroscopic point of view, we can interpolate the lattice values by a smooth function that satisfies the discrete equation (7.3). Then, we replace each term in (7.3) by its corresponding Taylor expansion in δ and τ, according to the following:

$$\begin{aligned} X(x,y,t+\tau) &= X(x,y,t) + \frac{\partial X}{\partial t}\tau + \frac{1}{2}\frac{\partial^2 X}{\partial t^2}\tau^2 + \cdots \\ X(x\pm\delta,y,t) &= X(x,y,t) \pm \frac{\partial X}{\partial x}\delta + \frac{1}{2}\frac{\partial^2 X}{\partial x^2}\delta^2 + \cdots \\ X(x,y\pm\delta,t) &= X(x,y,t) \pm \frac{\partial X}{\partial y}\delta + \frac{1}{2}\frac{\partial^2 X}{\partial y^2}\delta^2 + \cdots \end{aligned} \tag{7.4}$$

Substituting (7.4) in (7.3) and keeping terms up to $O(\delta^2)$, we obtain the expression:

$$\frac{\partial X}{\partial t} \approx -\frac{\partial^2 X}{\partial t^2}\tau + \frac{\lambda}{4}\frac{\partial^2 X}{\partial x^2}\frac{\delta^2}{\tau} + \frac{\lambda}{4}\frac{\partial^2 X}{\partial y^2}\frac{\delta^2}{\tau}. \tag{7.5}$$

Now, taking the limit $\tau \to 0$ and $\delta \to 0$ first term on the right disappears. Furthermore, defining

$$\lim_{\tau,\delta\to 0} \frac{\lambda\delta^2}{4\tau} = D,$$

the equation reduces to

$$\frac{\partial X}{\partial t} = D\nabla^2 X,$$

where $\nabla^2 = \frac{\partial^2}{\partial x^2} + \frac{\partial^2}{\partial y^2}$ is the Laplacian corresponding to the diffusion equation. Hence, hereafter we will refer to (7.2) as a discrete diffusive movement scheme.

The time interval τ and the distance unit δ are not "as small as we want", but they can actually be determined by the experimental procedures. Turchin (1989) presents a detailed explanation of how to obtain the resulting partial differential equation parameters through experiments.

Finally, we observe that a continuum approach is valid when the time of description of the phenomenon T is much greater than the duration of a step τ and when the spatial scale of description L is much greater than the step size δ (Lin and Segel 1988; Okubo and Levin 2001).

7.3 The Model for Insects That Only Have Local Perception Abilities

We assume a patchy environment such as citrus groves in a suitable spatial scale where each tree can be represented as the CML site and is occupied by insects. Assuming that the habitat is homogeneous and that the resources are abundant, the spatio-temporal dynamics were analysed considering chemicals released over the insects.

Here, the model describes the propensity of the insects for leaving their patch in response to the chemical concentration in the patch (Model I). The chemical substance is assumed to move by diffusion and advection due to wind.

The herbivore density in the site (i, j) at time t is described by $a^t_{i,j}$. Given that the system is intended to model biological individuals, as Keller and Segel (1971), we assume that there is a threshold value c_m of the chemical concentration below which neither insects are not able to perceive it nor the chemical is enough to kill the insects. Hence $c^t_{i,j}$ represents the difference between the observed concentration of the substance in (i, j) and the minimum value c_m at which individuals can sense it.

7.3.1 Model I Formulation

Now, we describe the movement stage, which comprises the substance and insect equations followed by the reaction stage.

7.3.1.1 Chemical Substance Spread

The substance disperses randomly by simple diffusion and also by advection due to the wind, which has been considered as a key factor for substances dispersal in the air. For the diffusive component of the motion, a constant fraction $0 \leq \lambda \leq 1$ of the chemical concentration is evenly distributed in the four nearest patches. We assume that the wind blows from the left to the right hand side of the dominium, so that, at each time step, a fraction $0 \leq \varepsilon \leq 1$ of the chemical concentration is carried by advection from patch (i, j) to the patch $(i, j+1)$. Note that λ and ε must satisfy $0 \leq \lambda + \varepsilon \leq 1$. Hence, the concentration of the chemical substance at site (i, j), after the movement stage of generation t, can be written as

$$c'_{i,j} = (1 - \lambda - \varepsilon)c^t_{i,j} + \sum_{(r,s)\in V_{(i,j)}} \frac{\lambda}{4} c^t_{r,s} + \varepsilon c^t_{i,j-1}, \tag{7.6}$$

where $c'_{i,j}$ represents the chemical density in (i, j) after the dispersal stage of time step t, and $V_{(i,j)} = \{(i-1, j), (i+1, j), (i, j-1), (i, j+1)\}$ is the Von Neumann neighbourhood of patch (i, j).

Equation (7.6) describes the substance permanence and arrival. The first term determines the chemical concentration remaining in patch (i, j) after dispersal, the second one gives the concentration that arrived at patch (i, j) by diffusion, and the third term describes the chemical concentration reaching the patch (i, j) via the wind (Fig. 7.6).

7.3.1.2 Insect Movement Stage

We assume that the habitat is full of resources so that the herbivores move (flee) only in response to the concentration of the chemical substance.

In this scenario, insects are able to detect chemicals only in the patch in which they are located. Hence, the population of insects in site (i, j) is repelled according to the chemical concentration in this patch. During the movement stage, a fraction of insects, proportional to the local concentration of the chemical, is uniformly distributed in the four neighbouring sites. Then, $c^t_{i,j} a^t_{i,j}$ is the density of individuals that leave site (i, j) at each time step. From a macroscopic point of view, this process will result in the net movement of individuals to areas of low concentration of the substance, as we will show in Sect. 7.3.3 (Fig. 7.7).

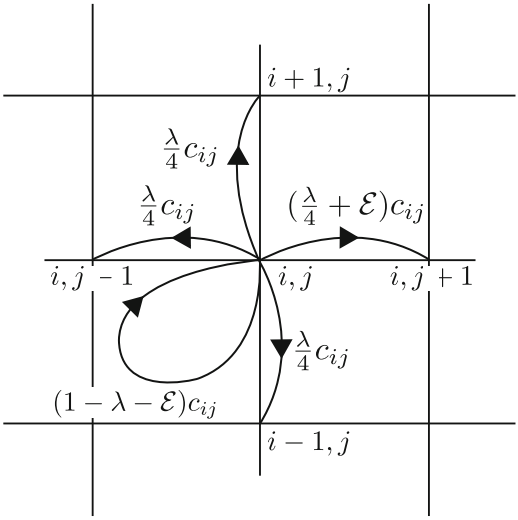

Fig. 7.6 Diffusive and convective movement scheme for the chemical

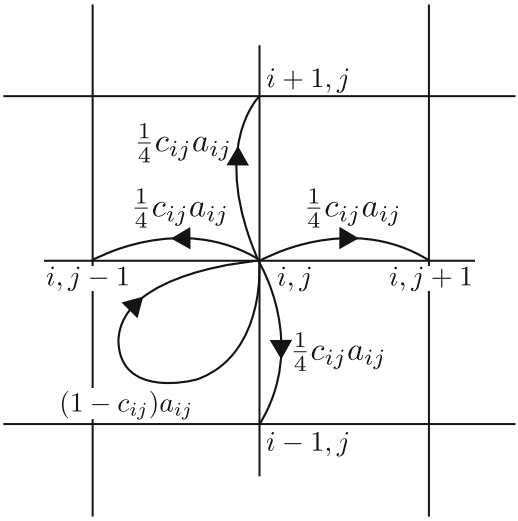

Fig. 7.7 Insects movement scheme

These assumptions lead to the following equation for the insect density in (i, j) after the movement stage at generation t:

$$a'_{i,j} = (1 - c^t_{i,j})a^t_{i,j} + \sum_{(r,s)\in V_{(i,j)}} \frac{1}{4} c^t_{r,s} a^t_{r,s}, \tag{7.7}$$

where $a'_{i,j}$ is the density of insects in (i, j) after dispersal.

The first term appearing in Eq. (7.7) describes the insects that stay in their original patch. The second one represents individuals migrating to patch (i, j) at generation t.

7.3.1.3 Reaction Stage

All the interactions take place at the reaction stage. The time scale of observation of the phenomenon was restricted to the time interval in which the chemical concentration can be sensed by the insects in the habitat. Since the time interval in which the chemical acts on the insects is short compared to their growth time scale, the insect population growth can be neglected. Hence, only insect mortality due to the action of the chemical and the natural degradation of the substance will be considered.

We consider that in each time step, a fraction of insects will be killed depending on the chemical concentration and efficiency. In the course of time, the chemical substance concentration will decay following an exponential function.

After the movement stage, the reaction, which is described by the following equations, takes place:

$$\begin{aligned} a_{i,j}^{t+1} &= a_{i,j}^{'} \exp\left(-\alpha c_{i,j}^{'}\right), \\ c_{i,j}^{t+1} &= \beta c_{i,j}^{'}, \end{aligned} \tag{7.8}$$

where $a_{i,j}^{'}$ and $c_{i,j}^{'}$ represent the insect and chemical densities after the movement stage of time step t. α estimates the lethal efficiency of the substance so that $1/\alpha$ represents the substance concentration that significantly decreases the insect population, at each time step. The case $\alpha = 0$ refers to a repellent. The natural degradation of the substance is described by β, $0 < \beta < 1$.

7.3.2 Simulations

The behavioural effects of individuals on the spatiotemporal dynamics of the population were studied by means of numerical simulations in a 50×50 square domain. These dimensions were chosen to obtain better visualisation of the substance effects.

We began with different initial distributions of insects and substance depending on the specific goal of the simulation. We assumed absorbing boundary conditions for the insects and the chemical because on one hand chemicals spread and leave the area of interest and, on the other hand, the insects can leave the area sprayed with the substance.

The results of the simulations are illustrated through: (i) density plots, which are snap shots of insects and chemical spatial distributions with dark (light) gray color describing high (low) densities according to each figure legend and, (ii) time series of the total density of both, insects and chemical, over the lattice. Hereafter, we present the results of the simulations developed for Model I.

The following two cases were taken into account: (1) the substance is a repellent ($\alpha = 0$) and (2) it is an insecticide ($\alpha > 0$). Equations (7.6)–(7.8) were applied to the insects and chemicals.

7.3.2.1 Repellent Chemical

Two different initial distributions of insects were assumed. In the first one, they are homogenously distributed in the habitat; in the second one, the insect distribution is heterogeneous.

Homogeneous Initial Distribution

In the first experiment, we assumed that the insects were initially homogeneously distributed over the habitat at a density of 0.5. The chemical substance was released in the center of the environment at time $t = 0$ according to

$$c^0_{i,j} = \exp\left[-\left((i-25)^2 + 0.5\,(j-25)^2\right)\right].$$

In order to better observe the repulsive effects of the substance, we assumed that the active component of the substance did not decay, which means, $\beta = 1$. The chemical diffusivity is fixed as $\lambda = 0.4$, and the wind intensity is $\varepsilon = 0.5$. These parameters were chosen to show significant qualitative behavior of the model, however they can be easily estimated in the experimental scenario.

In the upper panels of Fig. 7.8 the repellent distribution in time steps $t = 5$, $t = 20$ and $t = 50$ are shown. In the lower panels, the insect spatial distributions, at same time steps are also presented. The simulations indicate dispersion of the substance to the right as an effect of advection. The concentration of repellent diminishes in each site because of its diffusion into the neighbouring sites. The insect movement is a response to the repellent concentration. With the movement of the chemical particles, the insects leave high-concentration areas and go to areas of low concentrations of the substance. Behind the chemical, we observe the formation of a "furrow" in the insects' distribution that does not change anymore because the chemical concentration is not sufficient to promote any significant change (Fig. 7.8). The interpretation of this result can be described as follows. High concentrations of chemicals stimulate insect movement. However, after the repellent density diminishes to low levels, the insects cease movement. The distribution of the chemical and insects in line 25 (Fig. 7.9), corroborates these behavioural results.

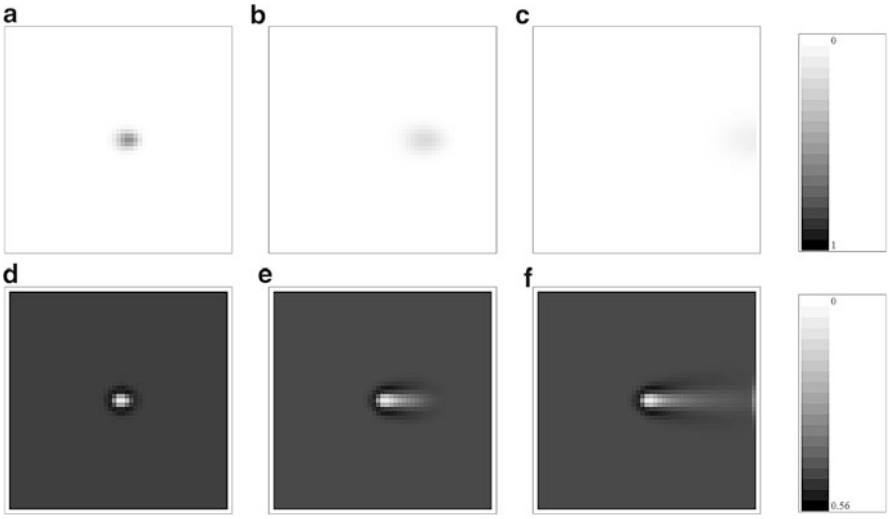

Fig. 7.8 Density plots of a repellent substance (*upper panels*) and insects (*lower panels*) at time steps: 5, 20 and 50. *Dark (light) grey colors* show highest (lowest) densities. The parameters used were $a = 0$, $\beta = 1.$, $\lambda = 0.4$ and $\varepsilon = 0.5$. Reprinted with minor adaptations from Ecological Complexity, Copyright (2013), with permission from Elsevier [3415301090462]

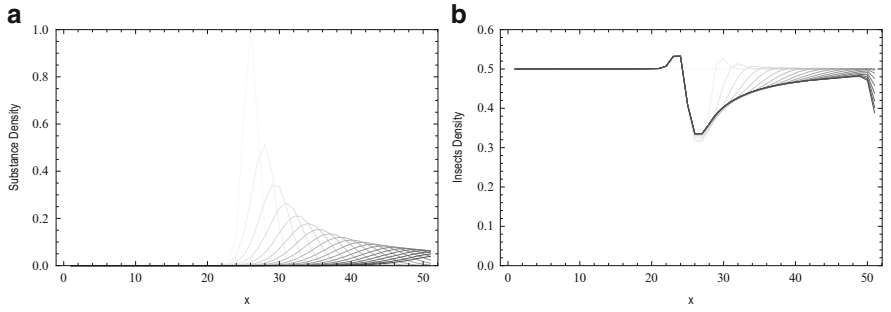

Fig. 7.9 Distribution at line 25 for: (**a**) chemical substance and (**b**) insects, at different time steps indicated by the *gray scale colors*. Initial time steps correspond to *light curves* while final time steps are represented by *dark curves*

To investigate the effect of the wind on the spread of the chemical, an initial concentration was released at some site (i_0, j_0) and the mean square distance of the chemical density, as a function of time, defined as

$$\sigma_t^2 = \frac{\sum_{i=1}\sum_{j=1} c_{i,j}^t \left((i-i_0)^2 + (j-j_0)^2\right)}{\sum_{i=1}\sum_{j=1} c_{i,j}^t},$$

was measured.

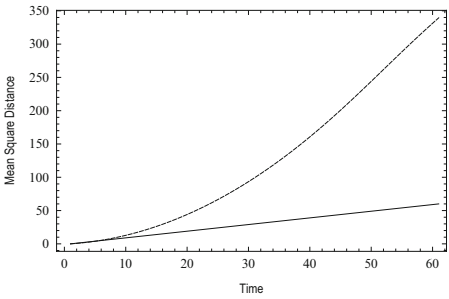

Fig. 7.10 Variation of the mean square distance with time comparing a diffusive process with wind (*dashed curve*) with a classic diffusive process without wind (*continuous curve*)

As expected, the wind exerts a significant influence on the dispersion process. Figure 7.10 shows different curves for the variation of the mean square distance with time; the dashed curve represents the influence of the wind ($\varepsilon = 0.4$) with moderate diffusion ($\lambda = 0.4$), while the continuous curve corresponds to absence of wind ($\varepsilon = 0$) and high diffusivity ($\lambda = 1$). In the latter, the dispersal of particles is due to diffusion. However, the wind produces a faster spread of the repellent compared to the diffusion process. The σ_t^2 curve is approximately proportional to t^2 when wind is present, which is typical of diffusion processes with drift, and it is approximately proportional to λt for the diffusion-only process (Codling et al. 2008).

Heterogeneous Initial Distribution

In this scenario the insects initially occupy 40 % of the patches at random at density of 0.5. It is important mention that the insect distribution used in this study is suitable for a discrete model but not for a continuous model, despite being reasonable in the natural population. Aiming to recognise the distribution of insects over a long time scale, the repellent is initially distributed at the left hand side of the dominium, following the equation below

$$c_{i,j}^0 = \exp\left[-\left((i-25)^2 + 0.5\,(j-5)^2\right)\right].$$

We assume that the active component of the chemical degrades gradually with time ($\beta = 0.99$), and the diffusivity of the repellent is given by $\lambda = 0.4$. The wind intensity is taken as $\varepsilon = 0.4$.

The upper panels in Fig. 7.11 illustrate the repellent distribution in time steps $t = 5$, $t = 50$ and $t = 100$. The lower panels show the spatial distribution of the insects at same time steps. In the presence of the chemical we now observe the formation of a "splotch" in the insects' distribution that, as previously shown, ceases to change (Fig. 7.11).

Fig. 7.11 Density plots of a repellent substance (*upper panels*) and insects (*lower panels*) at time steps: 5, 50 and 100. *Dark (light) grey colors* show highest (lowest) densities. The parameters used were $a = 0$, $\beta = 0.99$, $\lambda = 0.4$ and $\varepsilon = 0.45$. Reprinted with minor adaptations from Ecological Complexity, Copyright (2013), with permission from Elsevier [3415301090462]

7.3.2.2 Insecticides

For this case, we considered that the chemical is an insecticide with lethality parameter $\alpha = 1.1$ and low degradation factor $\beta = 0.99$. The wind intensity is $\varepsilon = 0.45$ and diffusivity $\lambda = 0.4$. Initially, the insects occupy 40 % of the patches at random at a density of 0.5. The chemical substance is released at the left hand side of the dominium according to

$$c^0_{i,j} = \exp\left[-\left((i-25)^2 + 0.5\,(j-5)^2\right)\right],$$

as previously assumed.

Figure 7.12 shows the spatial distribution of insects at time steps $t = 5$, $t = 50$ and $t = 100$. These simulations show that the insect density decays where the substance was spread. Figure 7.13a presents the insect density as a function of time in response to the chemical concentration for different wind intensities. The large dashed curve illustrates a weak wind ($\varepsilon = 0.2$); the small dashed curve describes a moderate wind ($\varepsilon = 0.45$); and the dotted curve depicts a strong wind ($\varepsilon = 0.6$) for $\lambda = 0.4$. The corresponding total concentration of the substance in the habitat is shown in Fig. 7.13b. The wind has a strong influence on the insecticide spread

Fig. 7.12 Density plots of insects at time steps: 5, 50 and 100 considering an insecticide. *Dark (light) grey colors* show highest (lowest) densities. The parameters are the same as before except $\alpha = 1.1$. Reprinted with minor adaptations from Ecological Complexity, Copyright (2013), with permission from Elsevier [3415301090462]

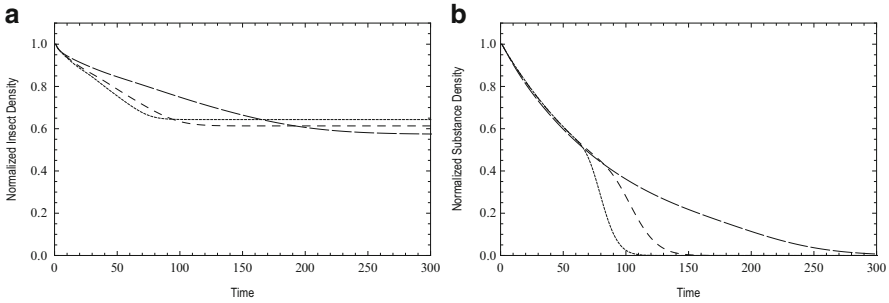

Fig. 7.13 (**a**) Normalized insect total population and (**b**) normalized total pesticide concentration over the habitat for $\lambda = 0.4$ and different wind intensity: $\varepsilon = 0.6$ (*dotted curve*), $\varepsilon = 0.45$ (*small dashed curve*) and $\varepsilon = 0.2$ (*large dashed curve*). Reprinted from Ecological Complexity, Copyright (2013), with permission from Elsevier [3415301090462]

as shown by the drastic change in the chemical curves. If the wind is weak the substance has a high residual power, and the insect population decreases slowly. However, the insect equilibrium density is the lowest (dotted curve in Fig. 7.13a). Strong wind dissipates the insecticide, resulting in the highest insect equilibrium (large dashed curve in Fig. 7.13b).

7.3.3 The Continuum Limit

In order to obtain a macroscopic model equivalent to the discrete simulation model I, we considered a random walk on a two dimensional lattice. The insect movement

depends on the "degree of repellence" of the chemical $c(x, y, t)$. At each time step τ, insects can move a distance δ down, up, left or right with probabilities given by $\frac{1}{4}c(x, y, t)$ or remain at the same location with probability $1 - c(x, y, t)$. The equation below describes the insects' density

$$\begin{aligned} n(x, y, t + \tau) = (1 - c(x, y, t))n(x, y, t) + \\ + \tfrac{1}{4}c(x - \delta, y, t)n(x - \delta, y, t) + \tfrac{1}{4}c(x + \delta, y, t)n(x + \delta, y, t) \\ + \tfrac{1}{4}c(x, y - \delta, t)n(x, y - \delta, t) + \tfrac{1}{4}c(x, y + \delta, t)n(x, y + \delta, t), \end{aligned} \tag{7.9}$$

The first term indicates individuals remaining at the same site. Insects arriving from the neighbouring locations are represented by the other four terms. The random walk model can be approximated by a continuous model for pertinent choices of δ and τ (Jeanson et al. 2003; Segel 1978; Turchin 1989). According to the implementation in Sect. 7.2, it is feasible to interpolate lattice values for insect and substance densities, replacing the differences by Taylor expansions up to a suitable order. Maintaining the corresponding terms, it is possible to write an equation for the insects' density as follows:

$$\begin{aligned} \frac{\partial a}{\partial t} \approx -\frac{1}{2}\frac{\partial^2 a}{\partial t^2}\tau + \frac{\delta^2}{4\tau}\left[c\frac{\partial^2 a}{\partial x^2} + a\frac{\partial^2 c}{\partial x^2} + 2\frac{\partial a}{\partial x}\frac{\partial c}{\partial x}\right] \\ + \frac{\delta^2}{4\tau}\left[c\frac{\partial^2 a}{\partial y^2} + a\frac{\partial^2 c}{\partial y^2} + 2\frac{\partial a}{\partial y}\frac{\partial c}{\partial y}\right]. \end{aligned} \tag{7.10}$$

By taking the limit $\tau \to 0$ and $\delta \to 0$, we obtain

$$\frac{\partial a}{\partial t} = \frac{D}{2}\nabla^2(ac)$$

or

$$\frac{\partial a}{\partial t} = \frac{D}{2}\nabla \cdot [c\nabla a + a\nabla c],$$

where $D = \frac{\delta^2}{2\tau}$, ∇^2 is the Laplacian and ∇ is the gradient operator.

A partial differential equation can also be obtained for the chemical spread by diffusion and advection. We substitute the proper Taylor series in scheme (7.6), divide both sides by τ and keep terms up to $O(\delta^2)$ to obtain

$$\frac{\partial c}{\partial t} \approx -\frac{1}{2}\frac{\partial^2 c}{\partial t^2}\tau + \frac{\lambda\delta^2}{4\tau}\left[\frac{\partial^2 c}{\partial x^2} + \frac{\partial^2 c}{\partial y^2}\right] - \frac{\varepsilon\delta}{\tau}\frac{\partial c}{\partial x} + \frac{\varepsilon\delta^2}{2\tau}\frac{\partial^2 c}{\partial x^2}. \tag{7.11}$$

Now, taking the limit $\tau, \delta, \varepsilon \to 0$, and defining

$$\lim_{\tau,\delta,\varepsilon\to 0} \frac{\varepsilon\delta}{\tau} = v,$$

we obtain

$$\frac{\partial c}{\partial t} = \nabla \cdot \left[\frac{\lambda}{2} D \nabla c - \mathbf{v}c\right],$$

where $|\mathbf{v}| = \frac{\varepsilon\delta}{\tau}$.

Hence, a reaction-diffusion system with equations qualitatively similar to discrete model I can be presented as follows:

$$\frac{\partial a}{\partial t} = \frac{D}{2}\nabla \cdot [c\nabla a + a\nabla c] - kac, \tag{7.12}$$

$$\frac{\partial c}{\partial t} = \nabla \cdot \left[\frac{\lambda}{2} D \nabla c - \mathbf{v}c\right] - rc. \tag{7.13}$$

The first term of the equation for insects, between brackets, describes a diffusive flow characterised by diffusivity proportional to the concentration $c(x, y, t)$. The second term indicates a flux in the opposite direction to the gradient of the chemical substance, that is, a negative taxis, although there is no bias in the discrete rule. In the chemical substance equation, the terms between brackets represent a classical diffusion and a convective flux with constant velocity $\mathbf{v}$, respectively. The reaction term kac (k constant) in the first equation represents the insect mortality due to chemical and rc, in the second equation, describes the exponential decay of the chemical concentration.

Equation (7.12) indicates that the insects flux does not depend on the wind. However, the chemical dispersal indirectly acts in the insects movement, in particular, the wind modify the insects spread by changing the chemical gradient and spatial concentration. Although the continuous model clarify the macroscopic behaviour of the system, it does not completely explain how the original parameters such as the wind intensity affects the insects spatio-temporal distribution and total population. Numerical simulations of the discrete model, presented in the previous section, elucidate these issues.

7.4 The Model for Quasi-local Perception Insects

7.4.1 Model II Formulation

For this case, it was assumed that insects may exhibit much more refined chemical recognition, including the ability to perceive substance concentration gradients in the neighbourhood in which they are exploring for resources. Thus, the insects can change their future location based on the presence of chemicals. This behaviour can be mathematically described by taking into account the fraction $l_{i,j}$ of insects leaving site (i, j) and going to another site (r, s), defined as

$$l_{i,j} = \begin{cases} \frac{1}{4}\left(1 - \frac{c^t_{r,s}}{m^t_{i,j}}\right), & \text{if } m^t_{i,j} \neq 0 \\ 0, & \text{if } m^t_{i,j} = 0 \end{cases} \tag{7.14}$$

where,

$$m_{i,j} = \sum_{(k,p)\in\overline{V}_{(i,j)}} c^t_{k,p}, \text{ and } \overline{V}_{(i,j)} = V_{(i,j)} \cup \{(i, j)\}.$$

The probability of moving to site (r, s), given by Eq. (7.14) reflects the propensity of going to locations with lower substance concentrations, i.e., the lower the concentration of the chemical at (r, s) compared to the concentration in the other sites of the neighbourhood, the greater is the probability of moving to this site. It is important to emphasize that since the habitat has plenty of resource and, by hypothesis, insects only move in response to the chemical, we defined $l_{i,j} = 0$ when $m^t_{i,j} = 0$. This hypothesis suggest insects remain in patch they are when the substance is below the threshold c_m in all the neighbourhood. We also point out that this movement scheme represents highly sensitive individuals: even for very low chemical density in the neighbourhood, insects can react with a high movement factor. The multiplying factor has a normalizing rule.

Looking at the probability that the insects move (7.14), their density at site (i, j) after the movement of generation t is given by

$$a'_{i,j} = a^t_{i,j} - \sum_{(r,s)\in V_{(i,j)}} \frac{a^t_{i,j}}{4}\left(1 - \frac{c^t_{r,s}}{m^t_{i,j}}\right) + \sum_{(r,s)\in V_{(i,j)}} \frac{a^t_{r,s}}{4}\left(1 - \frac{c^t_{i,j}}{m^t_{r,s}}\right). \tag{7.15}$$

The first summation in (7.15) accounts for the individuals who leave site (i, j) while the third term represents those individuals who migrate to site (i, j) from the neighbourhood.

7.4.2 Simulations

The following simulations are for insects that perceive the insecticide around them and make the decision to move away, looking for a place with a lower concentration of the substance, which is now lethal. The same initial conditions previously used in model I were employed with parameters $\alpha = 1.1$, $\beta = 0.99$, $\varepsilon = 0.2$ and $\lambda = 0.4$.

In Fig. 7.14 the spatial distribution of insects is presented at time steps $t = 5$, $t = 30$, $t = 50$ and $t = 100$. In this scenario, the insects vigorously respond to the presence of the insecticide, resulting in an approximately homogeneous spatial distribution (Fig. 7.14d). Note the substance concentration to the right side (Fig. 7.14a, b) is lower than c_m, justifying the permanence of the insects in the area.

The influence of sensory abilities on the spatial distribution and density of insects is shown (Figs. 7.15 and 7.16) using: local, quasi-local and no sensory ability (that is, $a'_{i,j} = a^t_{i,j}$). The scenarios observed are equivalent to models I, II and the indifference of insects with respect to the substance concentration. The parameters were taken as $\alpha = 1.1$, $\beta = 0.99$, $\varepsilon = 0.45$ and $\lambda = 0.2$ and insects are initially distributed inside a small region located at the center of the habitat as it can be when an alien species appear in a new habitat. The insecticide or repellent is applied at the centre of the occupied region, inducing insects to flee. After five time steps, the substance is reapplied according to

$$f^{5k}_{i,j} = \begin{cases} 1, & (i,j) = (i_0, j_0) \\ \beta c'_{i,j}, & (i,j) \neq (i_0, j_0) \end{cases}, k = 0, 1, 2, \ldots,$$

then the second equation in (7.8) is rewritten as

$$c^{t+1}_{i,j} = \begin{cases} \beta c'_{i,j}, & \text{for } t+1 \neq 5k,\ k = 1, 2, \ldots \\ f^{5k}_{i,j}, & \text{for } t+1 = 5k,\ k = 1, 2, \ldots \end{cases}.$$

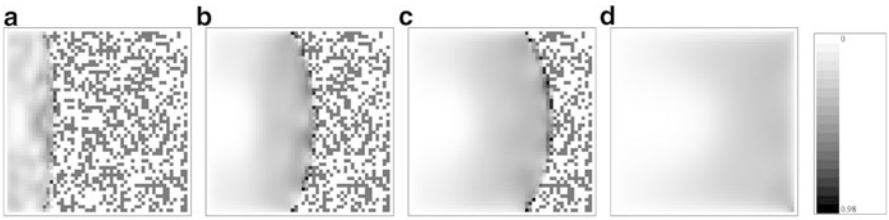

Fig. 7.14 Spatial distribution of insects for $\alpha = 1.1$, $\beta = 0.99$, $\varepsilon = 0.2$ and $\lambda = 0.4$ for time steps: $t = 5$, $t = 30$, $t = 50$ and $t = 100$. Reprinted with minor adaptations from Ecological Complexity, Copyright (2013), with permission from Elsevier [3415301090462]

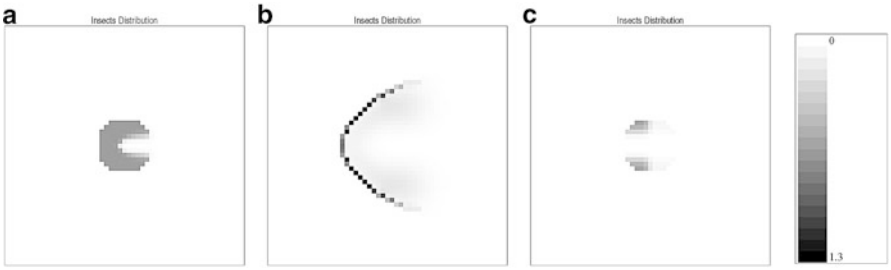

Fig. 7.15 Insects spatial distribution at generation $t = 40$, for different chemical perceptions: (**a**) local sensory ability, (**b**) quasi-local sensory ability and (**c**) no sensory ability. Reprinted with minor adaptations from Ecological Complexity, Copyright (2013), with permission from Elsevier [3415301090462]

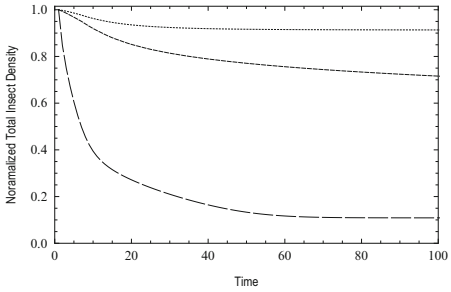

Fig. 7.16 Comparison of the normalized total population of insects. The *large dashed curve* indicates insects without sensory ability; *small dashed curve* represents insects with local sensory ability and the *dotted curve* illustrates insects with quasi-local sensory ability. Reprinted with minor adaptations from Ecological Complexity, Copyright (2013), with permission from Elsevier [3415301090462]

In Fig. 7.15 the distribution of insects is presented three different chemical perception, at time step $t = 40$. For insects perceiving chemicals only in the site where they are, movement to neighbouring sites takes place without regard to the chemical concentration of other places (Fig. 7.15a). When the insects discern the presence of harmful chemical around them, many more individuals try to leave these areas, migrating to places with a lower substance concentration (Fig. 7.15b). In contrast, the action of chemicals has more impact on immobile organisms (Fig. 7.15c).

Figure 7.16 shows the normalised total population of insects for the three different movement schemes. For the reaction and movement parameters considered, the asymptotic total insect density for quasi-local sensory ability (dotted curve) is greater than that for local sensory ability (small dashed curve). The population of insects that remain in their position (large dashed curve) suffer almost 80 % of loss in this period of time.

7.4.3 The Continuum Limit

Using similar reasoning as before, we define

$r(x, y, t)$, the individual fraction that migrates to the right-hand side
$l(x, y, t)$, the individual fraction that migrates to the left-hand side
$n(x, y, t)$, the individual fraction that migrates to the northern direction and,
$s(x, y, t)$, the individual fraction that migrates to the southern direction of site (x, y),

so that the individual density at site (x, y) after dispersal can be written as

$$\begin{aligned} a(x, y, t+\tau) = {} & r(x-\delta, y, t)a(x-\delta, y, t) + l(x+\delta, y, t)a(x+\delta, y, t) \\ & + s(x, y+\delta, t)a(x, y+\delta, t) + n(x, y-\delta, t)a(x, y-\delta, t) \\ & + [1 - r(x, y, t) - l(x, y, t) - s(x, y, t) - n(x, y, t)]\,. \end{aligned}$$

Substituting by Taylor series where necessary, and conveniently rearranging the terms, we obtain

$$\begin{aligned} \frac{\partial a}{\partial t} = {} & -\frac{\delta}{\tau}\frac{\partial}{\partial x}\left[(r(x, y, t) - l(x, y, t))\, a(x, y, t)\right] \\ & -\frac{\delta}{\tau}\frac{\partial}{\partial y}\left[(n(x, y, t) - s(x, y, t))\, a(x, y, t)\right] \\ & +\frac{\delta^2}{2\tau}\frac{\partial^2}{\partial x^2}\left[(r(x, y, t) + l(x, y, t))\, a(x, y, t)\right] \\ & +\frac{\delta^2}{2\tau}\frac{\partial^2}{\partial y^2}\left[(n(x, y, t) + s(x, y, t))\, a(x, y, t)\right]. \end{aligned} \tag{7.16}$$

We now suppose $c \neq 0$ and use (7.14) to calculate $r(x, y, t) \pm l(x, y, t)$ and $n(x, y, t) \pm s(x, y, t)$, which can be approximated by

$$\begin{aligned} r(x, y, t) + l(x, y, t) &= \frac{2}{5} + \frac{50c}{\triangle c\delta^2} - \frac{1}{20c}\frac{\partial^2 c}{\partial x^2}\delta^2 \\ r(x, y, t) + l(x, y, t) &= -\frac{1}{2}\frac{1}{5c}\frac{\partial c}{\partial x}\delta \\ n(x, y, t) + s(x, y, t) &= \frac{2}{5} + \frac{50c}{\triangle c\delta^2} - \frac{1}{20c}\frac{\partial^2 c}{\partial y^2}\delta^2 \\ n(x, y, t) - s(x, y, t) &= -\frac{1}{2}\frac{1}{5c}\frac{\partial c}{\partial y}\delta, \end{aligned} \tag{7.17}$$

which, substituted in (7.16), gives

$$\begin{aligned}\frac{\partial a}{\partial t} &= -\frac{\delta}{\tau}\frac{\partial}{\partial x}\left[-\frac{1}{2}\frac{1}{5c(x,y,t)}\frac{\partial c}{\partial x}a(x,y,t)\delta\right] \\ &\quad -\frac{\delta}{\tau}\frac{\partial}{\partial y}\left[-\frac{1}{2}\frac{1}{5c(x,y,t)}\frac{\partial c}{\partial y}a(x,y,t)\delta\right] \\ &\quad +\frac{\delta^2}{2\tau}\frac{\partial^2}{\partial x^2}\left\{\left[\frac{2}{5}+\left(\frac{\triangle c}{50c}-\frac{1}{20c}\frac{\partial^2 c}{\partial x^2}\right)\delta^2\right]a(x,y,t)\right\} \\ &\quad +\frac{\delta^2}{2\tau}\frac{\partial^2}{\partial y^2}\left\{\left[\frac{2}{5}+\left(\frac{50c}{\triangle c}-\frac{1}{20c}\frac{\partial^2 c}{\partial y^2}\right)\delta^2\right]a(x,y,t)\right\}\end{aligned} \tag{7.18}$$

or

$$\begin{aligned}\frac{\partial a}{\partial t} &= \frac{\delta^2}{10\tau}\frac{\partial}{\partial x}\left[\frac{\partial}{\partial x}\ln c(x,y,t)a(x,y,t)\right] \\ &\quad +\frac{\delta^2}{10\tau}\frac{\partial}{\partial y}\left[\frac{\partial}{\partial y}\ln c(x,y,t)a(x,y,t)\right] \\ &\quad +\frac{\delta^2}{5\tau}\frac{\partial^2}{\partial x^2}a(x,y,t)+\frac{\delta^2}{5\tau}\frac{\partial^2}{\partial y^2}a(x,y,t).\end{aligned} \tag{7.19}$$

Hence, Model II results in the following partial differential equation for the moving insects:

$$\begin{aligned}\frac{\partial a}{\partial t} &= D\nabla\cdot\left[\nabla a+\frac{\nabla c}{2c}a\right]-kac \\ &= D\triangle a+D\nabla\cdot\left[\frac{\nabla c}{2c}a\right]-kac,\end{aligned} \tag{7.20}$$

where $D=\frac{\delta^2}{5\tau}$.

The movement scheme in Model II corresponds to a rather different insect response to the chemical in the macroscopic scale. In this case, insect movement shows classical diffusion and chemotactic components. However, the diffusion coefficient is constant regardless the substance concentration. The chemotactic component of the flux, in this case, obeys the Weber-Fechner law, which states that the response to the chemical concentration is proportional to the relative gradient rather than to its absolute value (Keller and Segel 1971). The same type of relation has also been used for modelling the response of microorganisms to chemical signals in the seminal chemotaxis paper by Keller and Segel (1971).

It is important to mention that model II could be implemented in ideal scenarios in which the substance is smoothly distributed over the habitat and is never equal to zero in the area studied. Therefore, real field situations such as initial distribution

of the substance only in a small region of the dominium, can hardly be analyzed by the continuous model. These mathematical properties constitute another reason to undertake simulations directly from the discrete models proposed in the previous section. Nevertheless, the continuous model shed light upon the general tendencies of the postulates made in the discrete models.

7.5 Discussion and Final Remarks

In this chapter, a Coupled Map Lattice model was proposed to describe a hypothetical insect pest population being influenced by harmful chemical substances, taking into account the ability of the insect to flee and the environmental conditions. Two different rules for insect population movement with dependence on sensory ability were considered, local and quasi-local perception. A movement rule for chemical dispersal by wind and diffusion was also implemented. Continuous equations were designed to show the system on a macroscopic scale. With numerical simulations, spatial distribution of the movement rules above was investigated to describe the effects of dispersal in insect populations associated with repellents.

The models investigated here are consistent with advection, diffusion and taxis processes and were able to extract essential qualitative aspects from the mechanisms inherent to the spread dynamics. The discrete models proposed showed to be consistent with the mechanisms of advection, diffusion and taxis and captured the qualitative features expected for these processes. The model results confirm that the absence of insect flight from unfavorable areas has a highly significant impact on mortality due to insecticide application. This conclusion is narrowly associated with the perceptive ability of the insects' species. Additionally, species able to perceive harmful substances only locally are not capable of choosing a better destination and consequently exhibit much more susceptibility to the action of chemicals than insects with sensory abilities over a quasi-local range.

Despite the simplicity of the model, it has enough flexibility to investigate other strategies of integrated pest management (IPM) and to include influence on natural enemies (Fogel et al. 2013) or new ranges of individuals' perceptions (Haynes 1988). These aspects are of paramount importance for pest management scenarios, mainly for scenarios that take into account strategies for substance applications (Hassanali et al. 2008). The approach proposed here may also be useful for different particles associated with insects such as pollen, seeds and pheromones, as presented in the introduction of this chapter (Esker et al. 2007; Snell 2014).

The study presented in this chapter is an attempt to show the essential mathematical tools used in a Brazilian research program in progress by researchers at the Universidade Federal de Santa Maria and the Universidade Federal do Rio Grande do Sul who are focused on the combination of population theory, experimentation and evidence from the literature, aiming to support new strategies for IPM (Mistro et al. 2009, 2012; Rodrigues et al. 2011, 2012, 2013).

Acknowledgements DCM and LADR have been supported by FAPERGS, grants number 12/2199-1 and 12/2133-4, respectively. The authors thank Nicolas Z. Coelho for the technical assistance with Figs. 7.3–7.7.

References

Beck TC, McClay A, Lewis M (2003) Spatially explicit models for weed-biocontrol agent interactions: scentless chamomile as a case study. In: Proceedings of the XI international symposium on biological control of weeds, Canberra

Benhamou S (2014) Of scales and stationarity in animal movements. Ecol Lett 17:261–272

Brendel E (2013) The effect of linseed oil on rose scale *Aulacaspis rosae* (Bouch,) (Hemiptera: Diaspididae) in Greenhouse grown rose crops as an alternative pest management strategy. Gesunde Pflanzen 65:73–77

Codling EA, Plank MJ, Benhamou S (2008) Random walk models in biology. J R Soc Interface 5:813–834

Comins HN, Hassell MP, May RM (1992) The spatial dynamics of host-parasitoid systems. J An Ecol 61:735–748

Coulson C, Spooner PG, Lunt ID, Watson SJ (2014) From the matrix to roadsides and beyond: the role of isolated paddock trees as dispersal points for invasion. Divers Distrib 20:137–148

de-Camino-Beck T, Lewis MA (2009) Invasion with stage-structured coupled map lattices: Application to the spread of scentless chamomile. Ecol Model 220:3394–3403

Esker PD, Sparks AH, Antony G, Bates M, Dall'Acqua W, Frank EE, Huebel L, Segovia V, Garrett KA (2007) Ecology and epidemiology in R: modeling dispersal gradients. Plant Health Instructor. doi:10.1094/PHI-A-2007-1226-03. https://www.apsnet.org/edcenter/advanced/topics/EcologyAndEpidemiologyInR/ModelingDispersalGradients/Pages/default.aspx

Fogel MN, Schneider MI, Desneux N, González B, Ronco AE (2013) Impact of the neonicotinoid acetamiprid on immature stages of the predator *Eriopis connexa* (Coleoptera: Coccinellidae). Ecotoxicology 22:1063–1071

Gao M, Li WL, Li ZZ, Dai HW, Liu HT (2007) Spatial synchrony in host-parasitoid populations. Ecol Model 204:29–39

Godoy WAC, Costa MIS (2005) Dynamics of extinction in coupled populations of the flour beetle *Tribolium castaneum*. Revista Brasileira de Biologia 65:271–280 (corrigir no Texto que está 2006, o correto é 2005)

Govindarajan M, Sivakumar R (2012) Adulticidal and repellent properties of indigenous plant extracts against *Culex quinquefasciatus* and *Aedes aegypti* (Diptera: Culicidae). Parasitol Res 110:1607–1620

Hassanali A, Herren H, Khan ZR, Pickett JA, Woodcock CM (2008) Integrated pest management: the push-pull approach for controlling insect pests and weeds of cereals, and its potential for other agricultural systems including animal husbandry. Philos Trans R Soc B 363:611–621

Hassell MP, Comins HN, May RM (1991) Spatial structure and chaos in insect population dynamics. Nature 353:255–258

Haynes KF (1988) Sublethal effects of neurotoxic insecticides on insect behaviour. Ann Rev Entomol 33:149–168

Huntington TE, Higley LG (2010) Decomposed flesh as a vitellogenic protein source for the forensically important *Lucilia sericata* (Diptera: Calliphoridae). J Med Entomol 47:482–486

Ito K (2013) Integrated numerical simulation with fungal spore deposition and subsequent fungal growth on bathroom wall surface. Indoor Built Environ 22:881–896

Jeanson R, Blanco S, Fournier R, Deneubourg J-L, Fourcassié V, Theraulaz G (2003) A model of animal movements in a bounded space. J Theor Biol 225:443–451

Keller EF, Segel LA (1971) Travelling bands of chemotactic bacteria: a theoretical analysis. J Theor Biol 30:235–248

Kot M (2001) Elements of mathematical ecology. Cambridge University Press, Cambridge
Kaneko K (1986) Turbulence in coupled map lattices. Phys D 18:475–476
Liere H, Jackson D, Vandermeer J (2012) Ecological complexity in a coffee agroecosystem: spatial heterogeneity, population persistence and biological control. PLoS One 7:e45508
Lin CC, Segel LA (1988) Mathematical applied to deterministic problems in the natural sciences. SIAM, Philadelphia
Méndez V, Llopis I, Campos D, Horsthemke W (2010) Extinction and chaotic patterns in map lattices under hostile conditions. Bull Math Biol 72:432–443
Mistro DC, Rodrigues LAD, Varriale MC (2009) The role of spatial refuges in coupled map lattice model for host-parasitoid systems. Bull Math Biol 71:1934–1953
Mistro DC, Rodrigues LAD, Petrovskii S (2012) Spatiotemporal complexity of biological invasion in a space- and time-discrete predator-prey system with the strong Allee effect. Ecol Complex 9:16–32
Ngueleu SK, Grathwohl P, Cirpka AO (2013) Effect of natural particles on the transport of lindane in saturated porous media: laboratory experiments and model-based analysis. J Contam Hydrol 149:13–26
Nicholson AJ, Bailey VA (1935) The balance of animal population. Part I. Proc Zool Soc Lond 3:551–598
Nikpay A (2007) Insecticidal efficacy of three vegetable oils as post-harvest grain protectants of stored wheat against *Rhyzopertha dominica* (F.) (Coleoptera : Bostrychidae). Insect Sci 14: 145–150
Okubo A, Grünbaum D (2001) Mathematical treatment of biological diffusion. In: Okubo A, Levin SA (eds) Diffusion and ecological problems: Modern Perspectives. Springer, New York
Okubo A, Levin SA (2001) Diffusion and ecological problems. Modern perspectives, 2nd edn. Springer, New York
Oliver JC, Stein LR (2011) Evolution of influence: signalling in a lycaenid-ant interaction. Evol Ecol 25:1205–1216
Olivero-Verbel J, Tirado-Ballestas I, Caballero-Gallardo K et al (2013) Essential oils applied to the food act as repellents toward *Tribolium castaneum*. J Stored Prod Res 55:145–147
Reigada C, Aguiar MAM (2012) Host-parasitoid persistence over variable spatio-temporally susceptible habitats: bottom-up effects of ephemeral resources. Oikos 121:1665–1679
Rodrigues LAD, Mistro DC, Petrovskii S (2011) Pattern formation, long-term transients, and the Turing-Hopf bifurcation in a space- and time-discrete predator-prey system. Bull Math Biol 73:1812–1840
Rodrigues LAD, Mistro DC, Petrovskii S (2012) Pattern formation in a space- and time-discrete predator-prey system with strong Allee effect. Theor Ecol 5:341–362
Rodrigues LAD, Varriale MC, Godoy WAC, Mistro DC (2013) Spatiotemporal dynamics of an insect population in response to chemical substances. Ecol Complex 16:51–58
Segel LA (1978) Mathematical models for cellular behavior. In: Levin SA (ed) Studies in mathematical biology, vol 15 Mathematical Association of America, Washington, pp 156–190
Semmler M, Abdel-Ghaffar F, Schmidt J et al (2014) Evaluation of biological and chemical insect repellents and their potential adverse effects. Parasitol Res 113:185–188
Shigesada N, Kawasaki K, Teramoto E (1986) Traveling periodic waves in heterogeneous environments. Theor Popul Biol 30:143–160
Shigesada N, Kawasaki K, Teramoto E (1987) The speed of traveling frontal waves in heterogeneous environments. In: Teramoto E, Yamaguti M (eds) Mathematical topics in population biology, morphogenesis and neurosciences. Lecture notes in biomathematics, vol 71. Springer, Berlin, pp 88–97
Snell RS (2014) Simulating long-distance seed dispersal in a dynamic vegetation model. Global Ecol Biogeogr 23:89–98
Solé RV, Bascompte J (2006) Self-organizing in complex ecosystems. Princeton University Press, Princeton/Oxford
Solé RV, Valls J (1991) Order and chaos in a 2D-Lotka-Volterra coupled map lattice. Phys Lett A 153:330–336

Solé RV, Bascompte J, Valls J (1992) Nonequilibrium dynamics in lattice ecosystems: chaotic stability and dissipative structures. Chaos 2:387–395

Tabanca N, Wang M, Avonto C, Chittiboyina AG, Parcher JF, Carrol JF, Kramer M, Khan IA (2013) Bioactivity-guided investigation of geranium essential oils as natural tick repellents. J Agric Food Chem 61:4101–4107

Tong F, Bloomquist JF (2013) Plant essential oils affect the toxicities of carbaryl and permethrin against *Aedes aegypti* (Diptera: Culicidae). J Med Entomol 50:826–832

Turchin P (1989) Beyond simple diffusion: models of not-so-simple movement of animals and cells. Comments Theor Biol 1(2):65–83

White SM, White KAJ (2005) Relating coupled map lattices to integro-difference equations: dispersal-driven instabilities in coupled map lattices. J Theor Biol 235:463–475

Yamamura K (2004) Dispersal distance of corn pollen under fluctuating diffusion coefficient. Popul Ecol 46:87–101

Yang Y, Wilson LT, Makela ME, Marchetti MA (1998) Accuracy of numerical methods for solving the advection-diffusion equation as applied to spore and insect dispersal. Ecol Model 109:1–24

Chapter 8
Computational Methods for Accurate Evaluation of Pest Insect Population Size

Natalia Petrovskaya and Nina Embleton

Abstract Ecological monitoring aims to provide estimates of pest insect abundance, where the information obtained as a result of monitoring is then used for making decisions about means of control. In our paper we discuss the basic mathematics behind evaluating the pest insect abundance when a trapping procedure is used to collect information about pest insect species in an agricultural field. It will be shown that a standard approach based on calculating the arithmetic average of local densities is often not the most efficient method of pest population size evaluation and more accurate alternatives, known as methods of numerical integration, can be applied in the problem. A mathematical background for methods of numerical integration on regular grids of traps will be provided and examples of their implementation in ecological problems will be demonstrated. We then focus our attention on the issue of pest abundance evaluation accuracy when data available in the problem are sparse and consider the extreme case when the uncertainty of evaluation is so big, that an estimate becomes a random value. We complete our discussion with the consideration of irregular grids of traps where numerical integration techniques can also be applied.

Keywords Ecological monitoring • Numerical integration • Pest control • Coarse grid

8.1 Introduction

Pests are a sustained and significant problem in the production of food across the globe. The term ‘pest’ can be used to describe any organism which is deemed to cause harm to mankind in some manner; in crop production this label is given to those which damage or destroy potential produce to an unacceptable extent. In many

N. Petrovskaya (✉) • N. Embleton
School of Mathematics, University of Birmingham, Birmingham B15 2TT, UK
e-mail: n.b.petrovskaya@bham.ac.uk; embleton@for.mat.bham.ac.uk

C.P. Ferreira, W.A.C. Godoy (eds.), *Ecological Modelling Applied to Entomology*,
Entomology in Focus 1, DOI 10.1007/978-3-319-06877-0_8

ecologically important cases the definition above implies that an agglomeration of organisms is considered: for example, while one or two occasional insects do not make any significant harm to the crop in an agricultural field, the damage to the crop can become dramatic if the number of insects exceeds a certain threshold. Hence, in many ecological situations the definition of the term pest also requires the definition of the *pest abundance* or the *pest density distribution* in the spatial domain under consideration.

Crops are vulnerable to attack from pests both during the growing process and after they have been harvested. When pests of crops prior to harvest are considered, the focus is often predominantly on arthropods, plant pathogens and weeds (e.g. Louws et al. 2010; Ruberson 1999). Estimates of the annual worldwide loss due to pests at this stage in the production process lie between 35 and 42 % (Oerke 2006; Pimentel 1997). In particular, the pre-harvest loss of 14–15 % of the world's crops has been attributed to insect pests (Pimentel 2009; Pimentel and Pimentel 2008). Further losses are incurred after the crops have been harvested. This can be due to infestation of stored crops by pests such as insects, rodents, birds, as well as micro-organisms which cause damage both quantitative and qualitative in nature (Gwinner et al. 1996). Such losses have been estimated to range from 10 to 25 % (Pimentel and Pimentel 2008).

8.1.1 Basic Principles of Integrated Pest Management

Pest management has the obvious goal of preventing or minimising the damage pests cause to crops and various approaches have been used to achieve this goal. Measures of so-called 'preventative pest management' can be put into practise; the idea being to try to stop the pest population from becoming a problem in the first place. Age-old examples of such a tactics are crop rotation and intercropping. In a crop rotation, instead of an agricultural field consistently being used to grow the same crop, different crops which critically host different pests, are grown sequentially. Intercropping is the planting of different crops within the same field at the same time. Variety can also be introduced by planting several genotypes of the same crop species within a field. Introducing heterogeneity in such ways, either spatially, temporally, or genotypically, can destabilise the life cycle of a pest and has been documented to help to control pest populations (Liebman and Dyck 1993; Shoffner and Tooker 2013). A pest's preference for a certain plant can be exploited to the farmer's advantage using a technique called trap cropping. Here, crops are interspersed with plants that are more attractive to the pest and thus act as sacrificial decoys. This diversionary ploy can be sufficient to protect the crop in itself, otherwise, it reduces the area of the field to be subjected to further management tactics should they be needed since the pests are then located in some field sub-domain (Hokkanen 1991). Another precautionary measure is to grow crops which have been cultivated to be resistant to pest attack. Grafting has been used for centuries to manage certain pathogens and it has also been deemed to be useful in

the control of arthropod pests and weeds (Louws et al. 2010). A more scientifically advanced means of pest resistant plant cultivation is genetic modification. This is a relatively recent initiative of which the risks are not yet fully understood, however, its potential to become the dominant pest management strategy has certainly been recognised and consequently it has become the focus of much research (e.g. Bates et al. 2005; Christou et al. 2006; Gatehouse et al. 2011; Smigocki et al. 2013).

Another way of managing pests is to implement a control action, that is, to employ a means of killing the pest organisms. The most widely used control action is the application of pesticides. It has been estimated that around 3×10^9 kg are used across the globe per year (Pimentel 2009). Biological control actions, e.g. releasing a natural enemy of the targeted pest into the agroecosystem, provide an alternative to the use of chemicals. However, the indiscriminate use of control actions or using them as a preventative measure can have serious negative consequences. For instance, the regular use of pesticides often leads to the pest becoming resistant making future management a more difficult task (Alyokhin et al. 2008). Another unwanted side effect can be that the pesticide has lethal or sub-lethal effects on natural enemies (Sohrabi et al. 2013) which can cause a resurgence in the pest population or a secondary pest to emerge.

Recognition that precautionary tactics are rarely sufficient to manage pests alone and that relying entirely on control action is not a durable approach led to the emergence of the concept of *integrated pest management* (IPM) (Kogan 1998). IPM is the incorporation of several different tactics which work cooperatively together to protect crops from pest attack in a more sustainable way. It consists of the three phases. Firstly, preventative measures of pest management are put into place. Subsequently, the pest abundance is monitored. The decision of whether or not to implement a control action is then made by comparing the abundance of pests against some threshold level, i.e. the limit at which intervening becomes worth the effort or expense. Such threshold values can be decided upon by taking a variety of factors into consideration. The most often used are economic thresholds (Stern et al. 1959) as usually the overriding concern is that the pest management programme is financially viable (e.g. see Higley and Pedigo 1996). The basic principle of IPM is therefore that a control action is only used if and when it is necessary. Thus monitoring is key to the decision process and is considered an essential part of any integrated pest control and management programme (Burn et al. 1987; Metcalf and Luckmann 1982).

8.1.2 Monitoring Methodologies in IPM

A correct choice of a monitoring methodology is very important for the success of an IPM programme. Since different pest types have different behaviours, the monitoring methodologies in IPM programmes vary accordingly. We thus limit our scope to the consideration of insect pests; henceforth in the text the generic term ‘pest’ is used synonymously with ‘insect pest’ unless otherwise stated. The

procedure also depends on the environment to be monitored. In our paper we consider pest management of crops prior to harvest, where we take the spatial scale of the monitoring procedure to be that of an agricultural field. A complete census in this case is hardly practical or indeed possible, therefore the population abundance must instead be estimated. The data to form such an estimate is collected by sampling the pest population for which there exists a multitude of techniques (Ausden 1996; Blackshaw 1983; Hutchins 1994; Mayor and Davies 1976; Southwood and Henderson 2000).

A direct, in-situ count can be made of the number of pests in a sample unit e.g. a plant or a unit area of habitat. For the more inconspicuous species, the counting process can be made easier by dislodging the pests from the plant using a practise known as 'knockdown'. In some instances a sample of the habitat itself may be carefully removed and taken to a laboratory where the count can then be made.

Once the data has been collected the arithmetic mean number of pests M per sample unit is calculated as follows:

$$M = \frac{1}{K} \sum_{k=1}^{K} f_k, \tag{8.1}$$

where f_k are the individual sample counts, and K is the number of sample counts taken (Davis 1994). From the mean number of pests per unit area, an estimate of the number of pests in the entire agricultural field is obtained by multiplying by the area of the field (Snedecor and Cochran 1980). A mean number of pests per plant can be converted to the mean per unit area by multiplying by the mean number of plants in such an area. Such an estimate of pest abundance is considered an 'absolute' estimate since the sample counts directly reflect the number of pests in the sample unit.

Alternatively samples can be taken via netting. For example, a net can be swung into the crops for a prescribed time or number of sweeps. The number of pest insects caught inside is then counted (e.g. see Pedigo and Rice 2009; Southwood and Henderson 2000). Netting is often used to sample insects on large agricultural fields, because it is quicker and more cost effective than inspection of individual plants.

Another widely used sampling technique is trapping. Traps are installed in the field, exposed for a certain amount of time (e.g. for a week), after which the traps are emptied and the pests counted. The position of the traps can be arbitrary; some ecologists opt for random grids of traps or choose appropriate sampling patterns (Alexander et al. 2005; Mayor and Davies 1976), but in many cases they are placed at the nodes of a rectangular grid (Ferguson et al. 2000; Holland et al. 1999). The traps can either be active, whereby an attractant is used to draw the pests into the traps e.g. bait or a pheromone, or they can be passive where capture relies on the activity of the pest species. The trap counts provide information about the pest population density at the position of the traps (Byers et al. 1989; Raworth and Choi 2001) and the sample mean density can then be calculated by scaling (8.1)

with relation to the area of the agricultural field, where f_k are now the pest densities at the sample locations.

The above techniques yield a relative estimate of the mean pest density rather than an absolute estimate. The counts are not a direct measure of pest abundance but are relative to the efficiency of the netting or trapping technique and the conditions at the time of sampling. Therefore only relative estimates which have been obtained via the same sampling technique and in the same conditions can be compared. It is possible to convert an estimate that is relative to an absolute estimate using regression analysis (Browde et al. 1992) or through calibration using experimental data (Evans et al. 1983). Steps to achieve this via mathematical modelling have also been made (Petrovskii et al. 2012).

An estimate of the population abundance can also be achieved using mark-release-recapture methods. Initial sampling is performed and the catch is counted and marked in some way (Hagler and Jackson 2001). The marked population is then released back into the agroecosystem and another round of sampling is conducted. An estimate of the population size can then be formulated using the condition that the proportion of marked insects in the field is equal to the proportion of marked insects found in the second sample. That is, the following can be rearranged to solve for I

$$\frac{I_M}{I} = \frac{I_{\tilde{M}}}{\tilde{I}}, \tag{8.2}$$

where I_M is the total number of marked insects, I is the number of insects in the entire population, $\tilde{I}$ is the number of insects caught in the second sample and $I_{\tilde{M}}$ is the number of those which are marked. This method works well in scientific studies but can hardly be afforded in nation-wide monitoring programmes as it requires considerable additional effort (such as insect marking and recapture).

8.1.3 The Problem of Accurate Estimation of Pest Abundance

Once an estimate of the pest population size or the mean pest density in an agricultural field has been acquired, a decision is made by comparing it to some threshold value(s). Let us consider the simplest case where a single threshold value is used. If the estimate falls below the threshold the decision is to take no action, whereas if it exceeds the threshold the decision is to intervene and implement a control action (e.g. see Binns et al. 2000, Chapter 1). Such action can, for instance, be the application of pesticides (Ester and van Rozen 2005; Stern 1973). Clearly the accuracy of the estimate is important in ensuring the correct decision is made, with the accuracy becoming particularly vital when it is close to the threshold value. An underestimate could mean action is not taken when it is needed leading to the loss of crops. Even with the use of pesticides the value of crops lost in the field to

pests has been estimated to be $2,000 billion per year (Pimentel 2009).[1] Obtaining a more accurate estimate of the pest abundance could lead to the more timely use of a control action and ultimately reduce crop loss.

On the other hand an overestimate could lead to a control action being used unnecessarily. Application of pesticides is costly and brings considerable damage to the environment (Jepson and Thacker 1990). Pesticides are known to contribute to air, soil and water pollution whilst there is growing evidence linking their use to human illnesses (Alavanja et al. 2013; Pimentel and Greiner 1997). It has been estimated that less than 0.1 % of pesticides used reach their targeted pest, the remaining 99.9 % is absorbed by some means into the environment (Pimentel 1995). Some of the loss occurs during application with the spray drifting outside of the intended area, however once applied to a crop, pesticides can then vaporise into the air, end up in surface or groundwater, be absorbed by plants or ingested by non-target species, or indeed remain in the soil. Furthermore, unnecessary application of pesticides is undesirable from an economic perspective; around $40 billion is spent per year applying pesticides (Pimentel 2009).

It is obvious from the above that there is a significant need for reliable methods to accurately evaluate the pest population size in order to avoid making an unjustified decision about control action. It is worth noting here that the accuracy required by pest monitoring is not always very demanding as it differs according to the purpose. In routine monitoring an error range can be 20–100 % (Pascual and Kareiva 1996; Sherratt and Smith 2008), whereas monitoring for research purposes can demand a higher degree of accuracy of 10 % (e.g. see Pedigo and Rice 2009, p. 245).

Several means of optimising the accuracy of an estimate have been considered in the ecological literature. One way is to ensure that the size of the data set is large enough i.e. that enough sample units are taken. It follows from Eq. (8.1) that the exact value of the population size will be obtained for infinitely large number K. Hence we can expect better accuracy of the estimate when K gets larger. A pre-sample (or series of them) can be used to obtain a sample mean and sample variance from which an estimate of the number of sample units needed to achieve a specified precision can be calculated (e.g. see Binns et al. 2000; Dent 2000; Pedigo and Rice 2009). However there is a trade-off between the number of sample units needed to achieve sufficient accuracy and the number that can be practically afforded. For instance, if a trapping procedure is applied in ecological research, the number K of traps per given area can be made quite large, e.g. in the order of hundreds. Meanwhile in routine pest monitoring programmes K rarely exceeds 20 (Mayor and Davies 1976) per a typical agricultural field with a linear size of several hundred meters and, in some cases, it can be as small as one or a few traps per field (Northing 2009). There are several practical reasons why the number of traps cannot be made large. An increase in the number of sample units equates to an increase in the amount of labour and hence finances required. In any real-world scenario

[1]The work Pimentel (2009) refers to pests in the generic sense of the term, i.e. insects, plant pathogens and weeds.

there is a limit to such resources. Also, traps introduce a disturbance into the field and installing a large number of them can damage the corresponding agricultural product. Furthermore, trapping imposes a disturbance on the pests which can in turn affect the results of the trapping technique, therefore from this perspective the number of traps should be minimised.

The efficacy of a sampling technique is also important to the accuracy of an estimate of the pest abundance. Means of sampling a pest population are constantly being reviewed leading to sampling equipment being developed and improved (Birmingham et al. 2011; Taboada et al. 2012). Another key consideration is the sampling plan, that is, the prescribed locations at which samples are to be taken. For an estimate to be accurate the sample must capture sufficient information to adequately represent the true pest presence. If conditions are homogeneous across the field, insects can be randomly distributed, however they often exhibit an aggregated spatial distribution (Ferguson et al. 2000; Holland et al. 1999). The sampling plan thus becomes crucial; it is important to avoid bias stemming from samples being placed entirely in areas where the pests are clustered, or likewise, entirely in areas of zero density. Comparisons of various patterns e.g. random, transects, quadrats, etc. have been made in order to make recommendations (Alexander et al. 2005).

8.1.4 Goals and the Road Map

As the accuracy of evaluation of the pest abundance remains a crucial issue in IPM programmes, any new method that can increase the accuracy must be carefully studied and its advantages and disadvantages must be documented in order to decide whether or not the method can be used in routine monitoring. Although ensuring a sufficiently accurate estimate has been considered in the ecological literature as discussed above, to our best knowledge the focus has predominantly been on how the data is collected. In our paper we instead look at the way in which the data is processed and discuss numerical integration techniques that present an alternative approach to the existing statistical methods. In recent years intensive study of numerical integration methods for ecological applications has been carried out (Embleton and Petrovskaya 2013, 2014; Petrovskaya and Embleton 2013; Petrovskaya et al. 2013; Petrovskaya and Petrovskii 2010; Petrovskaya et al. 2012) and in this book chapter we summarize our experience with the application of numerical integration methods to ecological problems. We will focus our attention on a trapping procedure made in a single agricultural field and on the evaluation of the total pest population size from the information provided by trap counts, but the results of our discussion can be extended to other sampling techniques.

The main goal of the book chapter is twofold. Firstly, we would like to draw the attention of our readers to methods of numerical integration as a reliable alternative to a standard statistical method (8.1). We therefore explain a mathematical background for numerical integration techniques, elaborate on how to apply

them in ecological problems and demonstrate that advanced numerical integration methods can often be more effective in the evaluation of pest abundance than the method (8.1).

Secondly, we want to discuss the issues of accuracy for various methods of numerical integration and to identify the main factors that may affect the accuracy. It will be shown that the accuracy of numerical integration depends on the number of traps available in the problem and we therefore often have to deal with a numerical integration problem where the data are sparse (see Sect. 8.1.3). Meanwhile, if the number of traps is fixed in the problem, a spatial pattern of the pest density distribution remains the most crucial factor that affects the accuracy of numerical integration and this is another key topic that we discuss in this book chapter.

While most of our study with regard to the issues above will be done for regular grids of traps, we are also interested in the study of accuracy on quasi-irregular and random grids, as sampling patterns that result in such grids are backed by ecologists as mentioned in Sect. 8.1.3. It is worth noting that, although the spatial pattern of the sample units is considered important when collecting the data, an estimate of pest abundance based on the sample mean does not use this information directly. It can readily be seen that the expression for the sample mean (8.1) has no spatial dependence. Alternatively, an estimate formulated by means of numerical integration uses the spatial distribution information and we will see the implications of this approach.

The chapter is organised as follows. In the next section, we briefly explain basic information about the theory of numerical integration. In Sect. 8.3 we introduce a coarse grid problem that may hamper the use of numerical integration methods in ecological applications. In Sects. 8.2 and 8.3 we consider standard examples that have no ecological meaning but serve the purpose of illustrating numerical integration techniques well. We then demonstrate in Sect. 8.4 how to use methods of numerical integration in order to evaluate the total population size from discrete spatial data on regular grids. We also check the accuracy of various numerical integration methods by applying them to spatial population distributions of different complexity and conclude that knowledge of a spatial pattern is the most important requirement when accuracy of numerical integration is concerned. In Sect. 8.5, we discuss highly aggregated density distributions that present the most difficult case for numerical integration methods. In Sect. 8.6, we investigate the effect of a grid's irregularity on the population size estimation. Finally, in section "Concluding Remarks" we summarise our experience with the numerical integration problem in pest insect monitoring and control.

8.2 Theory of Numerical Integration

In this section we provide a brief discussion of methods of numerical integration and explain basic concepts related to this technique. We introduce a generic problem of numerical integration and elaborate on the accuracy of integration when various

methods are considered. For the sake of simplicity our discussion will mainly be focused on the one-dimensional case, but it can be readily extended to multi-dimensional problems.

8.2.1 Basic Concepts of Numerical Integration

Methods of numerical integration have to be applied when an integrand $f(x)$ defined over the interval $[a, b]$ is only given to us at a discrete set of points. This is a common situation when we make experimental measurements of the function $f(x)$ or when $f(x)$ is obtained as a result of computer simulation. If we consider the points $x_i, i = 1, \ldots, N+1$ where the function values $f_i \equiv f(x_i)$ are available, then computation of the integral

$$I = \int_a^b f(x)dx, \tag{8.3}$$

is reduced to computation of a weighted sum of the values f_i,

$$I \approx \tilde{I}(N) = \sum_{i=1}^{N+1} \omega_i f_i. \tag{8.4}$$

The basic problem of numerical integration is therefore to find weight coefficients ω_i such that the sum $\tilde{I}(N)$ will approximate the integral I with appropriate accuracy. The theory of numerical integration states that the weights ω_i in (8.4) depend on the number $N+1$ of points x_i where the function values f_i are available. Thus the accuracy requirement can be formulated for any numerical integration problem as

$$\tilde{I}(N) \to I, \text{as} N \to \infty, \tag{8.5}$$

and every time that the integration weights ω_i are defined in a new method of numerical integration, the condition (8.5) must be verified.

The condition (8.5) tells us that the weighted sum of function values (8.4) gets closer to the precise integral I when the number of points we use for integration increases. However, in order to come up with an efficient method of numerical integration we also want to know how fast the approximation $\tilde{I}(N)$ will approach the precise integral I when we increase N in (8.5). We have to introduce the concept of integration error in order to answer this question. Let us assume that the value I of the integral (8.3) is known to us. The integration error $E(N)$ is then defined as

$$E(N) = |I - \tilde{I}(N)|. \tag{8.6}$$

In many cases it is also convenient to consider the relative integration error,

$$e(N) = \frac{|I - \tilde{I}(N)|}{|I|}. \tag{8.7}$$

Consider now the unit interval $[0, 1]$. Let $x_1 = 0$ and equidistant points x_i, $i = 1, \ldots, N + 1$ be located over the interval, so that the distance between any two neighbouring points x_i and x_{i+1} is $h = 1/N = const < 1$. We refer to the set of points x_i, $i = 1, \ldots, N + 1$ as a *regular (or uniform) computational grid* of points. The points x_i are often called *grid nodes* and the distance h is referred to as *the grid step size*.

Once a computational grid has been generated, the integration error can be rewritten in terms of the distance h between neighbouring points as $E = E(h)$. We have $h \to 0$ as $N \to \infty$ and the condition (8.5) becomes

$$E(h) \to 0, \quad \text{as} \quad h \to 0, \tag{8.8}$$

where $E(h)$ is given by (8.6) after substituting $N = 1/h$. The formula (8.6) gives us a rigorous definition of the integration error, but it still remains unclear from (8.6) how we can check and control the condition (8.8), as the integral I is, of course, not available in real-life computations. Thus, instead of computing the exact value of $E(h)$ based on the exact value of the integral I, we make *an estimate* of the integration error in order to be able to check the condition (8.8). In the theory of numerical integration an integration error estimate is often considered in the following form Davis and Rabinowitz (1975)

$$E(h) = Ch^p, \tag{8.9}$$

where the constant C and the power p depend on a specific method of numerical integration used in the problem. The representation (8.9) of the integration error allows us to conclude about *the convergence rate*, i.e. to conclude how fast the error will decrease if we increase N. In other words, the formula (8.9) gives us the information on how fast $E(h) \to 0$, as $h \to 0$, and it is very important for our further discussion to emphasise here that h in the expression (8.9) is assumed to be small.

Let the integral be evaluated on a regular grid of $N_0 + 1$ points. The expression (8.9) reads that if we increase the original number N_0 as $N_1 = 2N_0$ then $h_1 = 1/N_1 = (1/2)h_0$ will be two times smaller, and the new error $E(h_1)$ will be 2^p times smaller. Obviously, the relative error (8.7) will exhibit similar behaviour. It is also obvious that the discussion above is true for any interval $[a, b]$ where the integrand $f(x)$ is considered. Indeed, any interval $[a, b]$ can be mapped onto the unit interval $[0, 1]$ by a linear transformation $x = (\hat{x} - a)/(b - a)$, where $x \in [0, 1]$ and $\hat{x} \in [a, b]$.

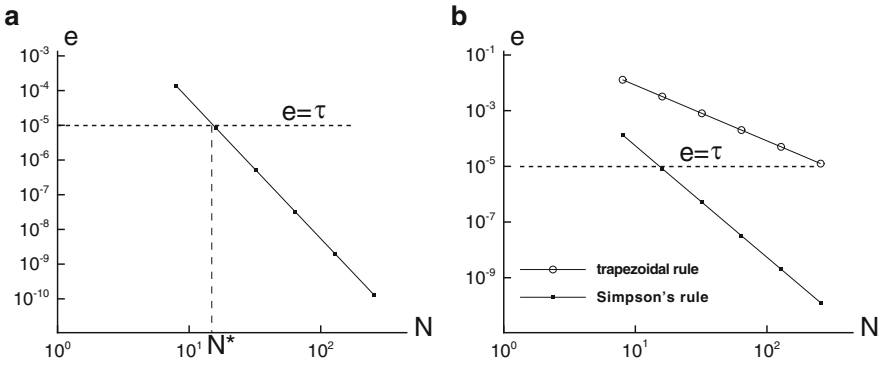

Fig. 8.1 The results of numerical integration of the function (8.10). (**a**) The convergence curve for the Simpson method of numerical integration. The relative integration error $e = e(N)$ is shown on the logarithmic scale. (**b**) Comparison of the convergence rate for the trapezoidal rule (*solid line*, *open circle*) and the Simpson rule (*solid line*, *closed square*)

From a practical viewpoint the concept of convergence means that we can control the accuracy of integral evaluation. This statement is illustrated in Fig. 8.1a, where the integral

$$I = \int_0^{\pi} \sin\, x dx \tag{8.10}$$

is evaluated by a selected method of numerical integration (composite Simpson's rule.[2]) Again, we assume that the function values are only available on a regular grid of $N + 1$ equidistant points. We start from the fixed number $N = 8$, and compute the approximate integral $\tilde{I} = \tilde{I}(N)$. As the precise integral $I = 2$ is known to us, we can compute the relative integration error (8.7). We then double the number N and repeat our computation of the error $e(N)$. After making this computation several times we obtain the error (8.7) as a function of N.

The graph $e(N)$ is shown in Fig. 8.1a on the logarithmic scale. It can be seen from the slope of the graph that the error decreases as h^4, where $h = 1/N$. The graph also gives us information about the threshold number N^* for which the following condition holds

$$e \leq \tau, \tag{8.11}$$

[2]The detailed description of this method is not important for our present discussion and will be provided later in the text.

where τ is a prescribed tolerance. If, for example, we choose $\tau = 10^{-5}$, then the accuracy (8.11) will be achieved for any $N \geq N^*$, where $N^* = 32$ (see Fig. 8.1a). Better accuracy requires a bigger number of points where function values are available, while larger τ (e.g., $\tau = 10^{-3}$) means that we can use a smaller number of points to evaluate the integral.

The convergence rate (8.9) of a particular method of numerical integration depends on the definition of the weight coefficients ω_i in the formula (8.4), and two different methods may therefore have different convergence rates. One example illustrating this statement is shown in Fig. 8.1b. In the figure we repeat the procedure previously explained for the graph in Fig. 8.1a, when another method of numerical integration (composite trapezoidal rule) is applied in the same problem. While we do not discuss here the definition of weight coefficients ω_i in each method, it can be readily concluded from Fig. 8.1b that the convergence rate of the trapezoidal rule is much slower than the convergence of the Simpson rule. The error in the composite trapezoidal rule decreases as h^2, while for the composite Simpson rule it decreases as h^4. Hence a much bigger number of points is required to achieve the accuracy $\tau = 10^{-5}$, if the composite trapezoidal rule is employed in the same problem of numerical evaluation of the integral (8.10).

The above discussion leads us to the conclusion that if we have several methods of numerical integration then the method that has the fastest convergence rate (8.9) must be employed in the problem and all other methods should be dismissed. Unfortunately, things are not so straightforward. Firstly, a fast convergence rate always comes at the price of the method's complexity, and methods that converge faster usually have more restrictions upon their implementation than the methods that converge slowly. The Simpson rule in the example above has a faster convergence rate, but it cannot be applied for an arbitrary number N and we should instead require that N is an even number in order to define weight coefficients for the Simpson rule. On the other hand, the trapezoidal rule has a slower convergence rate but it is more flexible and can be applied for arbitrary N. In practical applications the restrictions upon implementation of a specific method of numerical integration must be taken into account and that often results in the choice of a slower convergent method in the problem. Secondly, when we choose a method of numerical integration for the problem we solve, we need to understand how laborious the method is. In other words, it may happen that the desired accuracy will be achieved for a smaller number N but at the price of a very big number of computations, especially in multi-dimensional problems. In the latter case we should ask ourselves if we can come up with an alternative method of integral evaluation that may have a slower convergence rate but is easier to implement. Finally, and this is the most serious and difficult problem in numerical integration, the formula (8.9) may become invalid when the number $N + 1$ of points we have at our disposal is small. Other criteria should then be employed to compare two methods of numerical integration.

The above issues will be further discussed in the following sections. Their understanding will require us to give an explicit definition of the weight coefficients in numerical integration formulas. Below we consider the computation of weights ω_i in the integral approximation (8.4).

8.2.2 *Definition of Weight Coefficients in Various Methods of Numerical Integration*

Consider a regular computational grid of N sub-intervals in the domain $[a, b]$, i.e. consider points $x_1 = a$, $x_{i+1} = x_i + h$, $h = (b - a)/N$. As in the previous section we assume that the function values $f_i = f(x_i)$ are available at points x_i, $i = 1, \ldots, N + 1$. Numerical integration on regular grids with $h = const$ can be done by the application of well-known methods from the Newton-Cotes family of integration rules, the trapezoidal rule and the Simpson rule being, perhaps, the most famous. In this subsection we briefly review several methods of numerical integration that stem from various choices of weight coefficients ω_i in a generic formula (8.4) when regular grids are considered.

The problem of numerical integration is often thought of as a problem of finding the area under the curve $f(x)$. Thus the most straightforward and intuitively clear method is to take the function values $f_i \equiv f(x_i)$ at equidistantly spaced points x_i and to construct a rectangle with the sides $h = x_{i+1} - x_i$ and f_i. The area

$$a_i = hf_i, \tag{8.12}$$

gives us an approximation of the integral $I_i = \int_{x_i}^{x_{i+1}} f(x)dx$. Once the area a_i has been computed for each $i = 1, 2, \ldots, N$, the sum $S = \sum_{i=1}^{N} a_i$ is considered as an approximation of the integral $I = \int_a^b f(x)dx$. Such consideration is based on precise definition of a definite integral (8.3) as the limit of Riemann sums and the proof exists that the sum S will converge to the integral I as $N \to \infty$ (e.g. see Apostol 1974). It immediately follows from (8.4) and (8.12) that the weights are given by $\omega_i = h$ for any $i = 1, 2, \ldots, N$.

The approximation (8.12) is shown in Fig. 8.2a, where the function $f(x)$ is replaced by a constant $f_i \equiv f(x_i)$ on each subinterval $[x_i, x_{i+1}]$. It is clear that the approximation of the function by a constant is not very accurate, and we can improve it if we consider a straight line connecting points x_i and x_{i+1} (see Fig. 8.2b). The area a_i of each sub-interval is now given by

$$a_i = \frac{1}{2}h(f_i + f_{i+1}), \tag{8.13}$$

and again we compute the approximation to the integral as

$$I \approx S = \sum_{i=1}^{N} a_i. \tag{8.14}$$

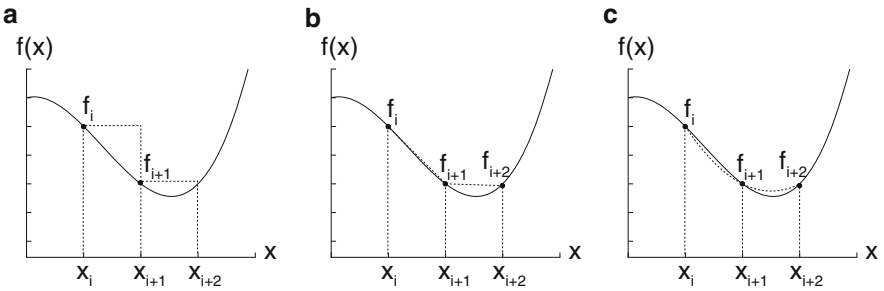

Fig. 8.2 Approximation of the function $f(x)$ by a polynomial of degree k. (**a**) Approximation by a constant ($k = 0$) over a subinterval $[x_i, x_{i+1}]$, (**b**) approximation by a straight line ($k = 1$), (**c**) three points x_i, x_{i+1} and x_{i+2} are required to approximate the function by a parabola ($k = 2$)

Substituting (8.13) into the sum (8.14) and re-arranging the terms, we arrive at the composite trapezoidal rule of integration,

$$I \approx S = \frac{h}{2}\left[f_1 + 2\sum_{i=2}^{N} f_i + f_{N+1} \right]. \tag{8.15}$$

The weight coefficients are now given by $\omega_1 = \omega_{N+1} = h/2$ and $\omega_i = h$, $i = 2, \ldots, N$.

Approximation of a function $f(x)$ by a straight line can be considered as replacing $f(x)$ by a linear polynomial on each subinterval $[x_i, x_{i+1}]$. If we go on with the idea of approximating the function by a polynomial of degree k, where $k = 0, 1, 2, 3, \ldots$, then our next step will be to consider $k = 2$ and to replace the integrand $f(x)$ by a quadratic polynomial. From a geometric viewpoint, this means drawing a parabola through three consecutive points where the function is defined. Clearly, we can use points x_i, x_{i+1}, x_{i+2} to define our quadratic polynomial as shown in Fig. 8.2c. The area under the curve is now approximated as the area a_i under the parabola passing through x_i, x_{i+1}, x_{i+2} and it is computed as

$$I_i = \int_{x_i}^{x_{i+2}} f(x)dx \approx \; a_i = \frac{1}{3}h(f_i + 4f_{i+1} + f_{i+2}). \tag{8.16}$$

The approximation (8.16) presents us with the well-known Simpson's rule of integration on the subinterval $[x_i, x_{i+2}]$.

Once the area a_i has been computed by the Simpson rule, the integral $I = \int_a^b f(x)dx$ is approximated as the sum of all integrals a_i,

$$\int_a^b f(x)dx \approx \frac{h}{3}\left[f_1 + 2\sum_{i=1}^{N/2-1} f_{2i+1} + 4\sum_{i=1}^{N/2} f_{2i} + f_{N+1} \right], \tag{8.17}$$

and we arrive at the composite Simpson's rule. It can immediately be seen from the formula (8.17) that the number N of grid sub-intervals must be even in order to apply the Simpson rule in the problem.

The above results can be further generalised as follows. Consider a polynomial $p_k(x)$ of degree k, where we require that $p_k(x_n) = f(x_n)$ for $n = i, i+1, \ldots, i+k$. In other words, we consider a polynomial passing through $k+1$ consecutive points where the function values are available. The area under the graph of the function $f(x)$ over a sub-interval $[x_i, x_{i+k}]$ is then approximated as

$$\int_{x_i}^{x_{i+k}} f(x)dx \approx a_i = \int_{x_i}^{x_{i+k}} p_k(x)dx,$$

and the resulting integral I is approximated by summation of all areas a_i.

Using local polynomials at each sub-interval $[x_i, x_{i+k}]$ with consecutive summation is known as the composite Newton-Cotes rules of numerical integration on regular grids (Davis and Rabinowitz 1975). The idea of interpolating the integrand function $f(x)$ by a polynomial $p_k(x)$ of degree k was pivotal in the development of the Newton-Cotes rules. The trapezoidal rule ($k = 1$) and the Simpson rule ($k = 2$) discussed above represent the first two rules in the Newton-Cotes family. They are, probably, the most well-known integration rules used in practical computations. The reason for their extensive use is twofold. Firstly, Newton-Cotes methods with $k > 2$ do not necessarily provide the most accurate estimate of the integral. For example, in the numerical integration problem considered in Davis and Rabinowitz (1975) increasing the polynomial degree k from $k = 2$ up to $k = 21$ resulted in a larger integration error in the latter case. Secondly, it is often difficult to apply a composite Newton-Cotes rule with $k > 2$ on a grid with an arbitrary number of grid sub-intervals, as the total number N of sub-intervals is required to be a multiple of k. That is why in many experimental applications the integral evaluation is restricted by the use of the composite trapezoidal rule (8.15) or the composite Simpson rule (8.17) and further in the text we consider the trapezoidal and Simpson rules only.

8.2.3 *Two-Dimensional Newton-Cotes Formulas*

Once the integration techniques have been understood in the one-dimensional $(1-d)$ case, they can be easily expanded to the two-dimensional $(2-d)$ case. Consider the unit square $D = [0,1] \times [0,1]$, where a regular grid is generated. Namely, let us consider a set of points $x_i, i = 1, \ldots, N+1$ on the interval $[0,1]$, where we require

that $x_1 = 0$, $x_{i+1} = x_i + h$, $i = 1, \ldots, N$, and the grid step size h is defined as $h = 1/N$. Similarly, we consider points y_j, $j = 1, \ldots, N+1$ on the interval $[0, 1]$ and generate a one-dimensional grid in the y-direction as $y_1 = 0, y_{j+1} = y_j + h, j = 1, \ldots, N$. The grid node position in the unit square is then given by (x_i, y_j) and we have a grid of square elements $c_{ij} = [x_i, x_{i+1}] \times [y_j, y_{j+1}]$.

A composite rule of integration in the $2-d$ case exploits the same idea as in the $1-d$ case. We have

$$I = \int_0^1 \int_0^1 f(x, y) dxdy = \sum_{i,j} I_{ij}, \tag{8.18}$$

where

$$I_{ij} = \int_{x_i}^{x_{i+1}} \int_{y_j}^{y_{j+1}} f(x, y) dxdy. \tag{8.19}$$

Hence, the integration problem is reduced to the integral evaluation in each subdomain c_{ij}. Integration on square elements can, in turn, be further reduced to consecutive application of the one-dimensional formulas. In other words, the integral (8.19) can be re-written as

$$I_{ij} = \int_{y_j}^{y_{j+1}} F(y) dy, \tag{8.20}$$

where

$$F(y) = \int_{x_i}^{x_{i+1}} f(x, y) dx.$$

We then employ $1-d$ Newton-Cotes formulas discussed in Sect. 8.2.2 in order to evaluate the function $F(y)$ in the square cell c_{ij}. Once the values of $F(y)$ have been computed, the same integration rule is applied to approximate the integral (8.20).

Different integration rules use different local approximation of the integrand $f(x, y)$ on a single grid cell c_{ij} (e.g., see Davis and Rabinowitz 1975). The simplest evaluation of the integral (8.19) can be done under the assumption that the function $f(x, y)$ is approximated by a constant on each grid cell. Such approximation results in the midpoint rule of integration:

$$I_{ij} \approx A_{ij} f(x_{i+1/2}, y_{j+1/2}), \tag{8.21}$$

where $A_{ij} = h^2$ and the node $(x_{i+1/2}, y_{j+1/2}) = (x_i + h/2, y_j + h/2)$ is the midpoint of the cell c_{ij}.

The trapezoidal rule of integration implies the approximation of $f(x, y)$ by a linear function on each sub-domain c_{ij}. Correspondingly, the integral I_{ij} is evaluated as

$$I_{ij} \approx \frac{h^2}{4}\left[f(x_i, y_j) + f(x_{i+1}, y_j) + f(x_i, y_{j+1}) + f(x_{i+1}, y_{j+1})\right]. \quad (8.22)$$

The Simpson rule of integration is a result of approximation of the integrand $f(x, y)$ by a quadratic polynomial in the square cell c_{ij}. The application of this rule in the cell c_{ij} requires that the data $f(x, y)$ are available at points (x_{i+q}, y_{j+r}), where $q = 0, 1, 2$ and $r = 0, 1, 2$. The function $f(x, y)$ is then integrated in the cell c_{ij} by the Simpson rule as

$$\begin{aligned} I_{ij} \approx \frac{h^2}{36}\big[&f(x_i, y_j) + f(x_i, y_{j+2}) + f(x_{i+2}, y_j) + f(x_{i+2}, y_{j+2}) \\ &+ 4\left(f(x_i, y_{j+1}) + f(x_{i+1}, y_j) + f(x_{i+2}, y_{j+1}) + f(x_{i+1}, y_{j+2})\right) \\ &+16 f(x_{i+1}, y_{j+1})\big]. \end{aligned} \quad (8.23)$$

Note that, like in the $1-d$ case, integration by the Simpson rule requires an even number N of grid sub-intervals in each direction x and y of a $2-d$ regular grid.

8.3 The Coarse Grid Problem

In this section we review a so called 'coarse grid' problem that was previously studied in detail in Petrovskaya and Petrovskii (2010), Petrovskaya et al. (2012), and Petrovskaya and Venturino (2011) because of its importance in ecological applications. For the sake of simplicity, the problem in this section is illustrated by $1-d$ examples, but the conclusions made in the $1-d$ case are also true for $2-d$ problems considered later in the text.

The coarse grid problem is closely related to the concept of the convergence rate discussed in Sect. 8.2. We know that, given the distance h between neighbouring points on a regular grid, the integration error (8.7) is controlled by the expression (8.9). However, we can only rely upon the error estimate (8.9) if the grid step size h is sufficiently small, i.e. if we deal with *fine* grids. Meanwhile if the distance h between grid nodes is not very small, it may happen that the error estimate (8.9) does not hold. In the latter case we cannot tell which integration method is better when we compare two integration methods based on their convergence rate (8.9). Correspondingly, a *coarse* grid is defined as a grid where one cannot apply the error estimate (8.9) to evaluate the integration error.

The above statement is illustrated in Fig. 8.3. We first consider the integrand

$$f(x) = \frac{e^x - 1}{e - 1}, \qquad x \in [0, 1], \quad (8.24)$$

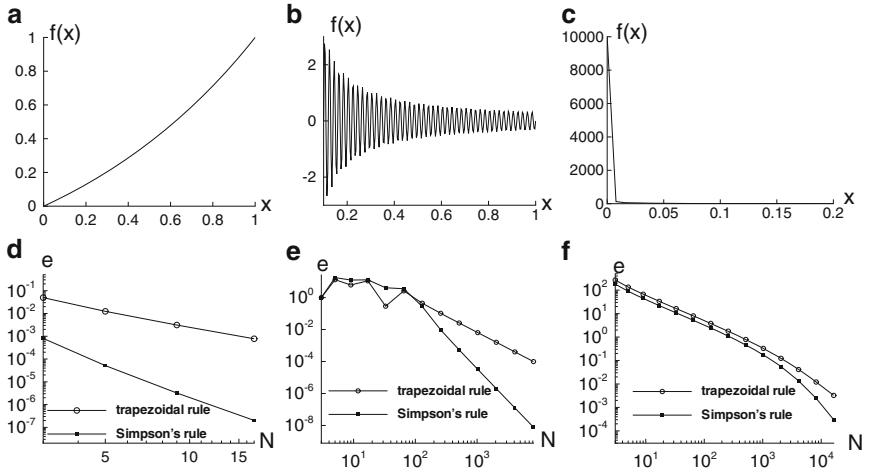

Fig. 8.3 The coarse grid problem: the comparison of the convergence rate for the trapezoidal rule (*solid line*, *open circle*) and the Simpson rule (*solid line*, *closed square*). (**a**) The integrand function (8.24) for $x \in [0, 1]$. (**d**) The convergence rate for the integrand (8.24) is as predicted by the error estimate (8.9). (**b**) The integrand function (8.25) over the interval $x \in [0.1, 1]$. (**e**) The convergence rate for the integrand (8.25). The error estimate (8.9) becomes true when the number N of grid sub-intervals is $N > N^* \approx 64$. (**c**) The integrand function (8.26). The function is shown at the sub-interval $[0, 0.2]$ for the sake of visualisation, while the integral is taken for $x \in [0, 1]$. (**f**) The convergence rate for the integrand (8.26). The error estimate (8.9) does not hold on coarse grids, unless at least one grid node is placed in the sub-region of the steep gradient

shown in Fig. 8.3a. The error graphs for the integrand (8.24) are shown in Fig. 8.3d, where the relative integration error (8.7) is computed for integration by the trapezoidal rule and the Simpson rule. It has been discussed in Sect. 8.2 that the convergence rate of the Simpson rule is much better than the convergence of the trapezoidal rule. Decreasing the grid step size from h_0 to $h_1 = h_0/2$ results in the error reduction $e(h_1) = (1/16)e(h_0)$ for the Simpson rule, while for the trapezoidal rule we have $e(h_1) = (1/4)e(h_0)$. It can be seen from Fig. 8.3d that in the case of the integrand function (8.24) this conclusion is true for any $N \geq 2$ considered in the problem.

Meanwhile, the above conclusion about the convergence rate does not hold for an arbitrary integrand function $f(x)$. Consider now a rapidly oscillating function

$$f(x) = \frac{\sin(100\pi x)}{\pi x}, \quad x \in [0.1, 1], \tag{8.25}$$

shown in Fig. 8.3b. The convergence of numerical integration methods, when the function (8.25) is integrated, is presented in Fig. 8.3e. The integration error on grids with $N \leq 64$ is very large for the both trapezoidal and Simpson's rule of integration. However, the most essential feature of the integration is that we cannot tell if the Simpson method is more accurate, unless we have the number of grid sub-intervals

$N > 64$, i.e. unless the grid step size becomes $h \approx 0.015$. The integration error of the Simpson rule remains approximately the same as the error of the trapezoidal rule on coarse grids with $N < N^* \approx 64$.

The coarse grid problem is further illustrated by consideration of the function

$$f(x) = \frac{1}{x + 0.0001}, \quad x \in [0, 1], \tag{8.26}$$

shown in Fig. 8.3c. It can be seen from the figure that the function (8.26) has a very narrow domain where the gradient is very steep. For the sake of illustration the function is shown on the sub-interval $x \in [0, 0.2]$, while the integration is carried out over the unit interval $x \in [0, 1]$. Our previous experience with the integrand (8.25) of Fig. 8.3b tells us that we can expect a big integration error when the number of grid nodes is not sufficient to resolve the domain of a steep gradient. This conclusion is confirmed by the convergence curve shown in Fig. 8.3f. The initial coarse grid with grid step size $h = 0.5$ cannot capture the sub-region of the steep gradient that has the width $w \sim 0.01$. Even when we make the grid step size smaller by halving each grid sub-interval, the whole sub-domain of the steep gradient remains 'invisible' to the integration method, as it is still located between two grid nodes where the function values are available. Hence both the trapezoidal and Simpson rules provide similar (and very inaccurate) results, unless we insert at least one grid node in the sub-region of the steep gradient. That happens when we have an unrealistically big number $N \approx 5{,}000$ of grid sub-intervals on a regular grid. Any grid with $N < N^*$ is a coarse grid where the error estimate (8.9) does not hold. Accordingly, any grid with $N > N^*$ is a fine grid where we can rely upon (8.9).

It was discussed in Petrovskaya and Petrovskii (2010) that the number N^* of grid subintervals when the grid becomes 'sufficiently refined', i.e.when we can rely upon the error estimate (8.9), can be evaluated from the knowledge of the shape of the integrand function. Let Δx be a characteristic width of a spatial heterogeneity described by a given integrand, e.g. the width of a single peak in (8.25). Then integration on a regular grid will give an inaccurate answer until at least one grid point falls into the heterogeneity region. We therefore have

$$N^* = s\frac{1}{\Delta x}, \tag{8.27}$$

where 1 in the numerator stands for the length of the domain of integration and $s \geq 1$ is a numerical coefficient depending on the type of the heterogeneity. If $f(x)$ is a monotone function on the interval $[x_1, x_2]$, then we consider the function values at two points, e.g., $x_1 + \delta$ and $x_2 - \delta$, where $0 < \delta < 0.5(x_1 + x_2)$, as the minimum 'amount of information' required to reconstruct $f(x)$ over $[x_1, x_2]$ as these data are sufficient for linear polynomial approximation of $f(x)$. Consequently, a sub-region of a steep gradient in (8.26) can be resolved by inserting into it just one grid point. Meanwhile, we need at least three grid points e.g., $x_1 + \delta$, x_2, and $x_3 - \delta$, to resolve a peak which spans the interval $[x_1, x_3]$, as that will result in linear approximation at each of subintervals $[x_1, x_2]$ and $[x_2, x_3]$ where $f(x)$ is a monotone function.

The most important conclusion that follows from the above consideration is that the grid coarseness should be evaluated in terms of the integration error rather than by the number of grid nodes. Hence the definition of a coarse grid depends strongly on the spatial pattern of the integrand function. It can immediately be seen from Fig. 8.3 that a grid considered as coarse for one integrand function can be a fine grid for another integrand. One way to improve very poor accuracy of integration on coarse grids would therefore be to use an irregular grid where most of the grid nodes would be concentrated in sub-regions that present difficulties in their numerical integration (i.e. peaks or sub-regions with a steep function gradient). Integration techniques on irregular grids are discussed in Sect. 8.6. However, in ecological applications it often is not possible to use irregular grids adapted to a spatial pattern of the density distribution because that pattern is usually not known a priori. On the other hand, coarse grids are widespread in ecological monitoring, as there are usually financial, ecological and other restrictions that do not allow for a big number of measurements and the data available in the problem are sparse. Thus the problem of accuracy control on coarse grids remains one of the most difficult problems in ecological monitoring and it is still far from being solved. We will discuss several particular examples of coarse grids in ecological applications further in the text.

8.4 Numerical Integration in Ecological Problems

In this section we consider the application of the methods reviewed in Sect. 8.2 to ecological monitoring and control. As we have already discussed in the introduction, one key problem of ecological monitoring is to obtain an accurate estimate $\tilde{I}(N)$ of the pest population size I in a given area under conditions when the population density is only known at $N + 1$ locations. It follows immediately from our study in Sect. 8.2 that the problem of evaluating the pest population size from discrete data can be considered as a problem of numerical integration. Indeed, installing traps in a domain where sampled data are collected and processing trap counts means that the discrete integrand function is defined at the nodes of a computational grid and methods (8.15) and (8.17) can be applied. However, several underlying assumptions should be made before we implement numerical integration rules in ecological problems.

8.4.1 Problem Statement and Underlying Assumptions

In our work we consider collecting information about a pest insect via trapping and we assume that a trapping procedure is done as described in the introduction. In this section we also assume that the traps are installed at the nodes of a regular grid, which is a common situation in ecological applications (Ferguson et al. 2000; Holland et al. 1999). Irregular grids will be discussed in Sect. 8.6.

As we already mentioned in the previous section, numerical integration techniques are essentially based on the underlying assumption that the integrand function is continuous. Meanwhile, if we consider an agricultural field, where pest insects are monitored, the distribution of the insects over the field is, of course, discrete. Hence, in order to apply numerical integration techniques in the problem we have to transform the discrete population distribution into a continuous function that we will refer to as "the population density". The population density can be obtained from the discrete distribution of the pest insects by allocating a certain area to each insect and assuming that only one insect can be found within that area at the fixed time t.

Another important underlying assumption is that the number of insects caught in each trap is an accurate representation of the absolute population density in its catchment area. The transformation techniques that allow one to link trap counts to the absolute density have been briefly discussed in the introduction. We also assume that the information about the population density at a given time and location can indeed be adequately obtained from trap counts, as depending on the biological and behavioural traits of the monitored species, the population density distribution can possibly change over the time of the traps' exposure. The spatial scale of variations in the population density distribution for walking insects usually sampled with pitfall traps is known to be 30–40 m (Holland et al. 1999). Meanwhile, typical dispersal distances for walking insects are estimated to be 1 m or less per day (Vinatier et al. 2010), which obviously corresponds to the spread area of the order of 1 m^2 per day. Hence the distance insects can move over 1 week (i.e. an average time of trap exposure) is $\sqrt{7} \approx 2.6$ m, which is about one order of magnitude less than the spatial scale of inherent variation. We conclude from the above that the spatial density distribution reconstructed from traps counts can approximately be relied upon as being static and methods of numerical integration can be applied.

Once the trap counts have been acquired, we can obtain the values of the population density at the nodes of a regular grid, i.e. at the trap locations, and we therefore can approximate the integral I, i.e. the total number of insects in the field, by a selected method of numerical integration. However, application of numerical integration in ecological monitoring and control is more difficult than a conventional integration problem. The standard numerical integration technique usually implies that a computational grid can be made sufficiently fine to provide the required accuracy. This requirement is not realistic in an ecological monitoring routine where the number of traps installed in a field cannot be made large. For example, a typical agricultural field in the United Kingdom has a characteristic size of the order of a few hundred meters. The number of traps installed over such a field very rarely exceed a few dozen (Blackshaw 1983; Ferguson et al. 2000; Holland et al. 1999). Moreover, we cannot increase the number of traps and repeat the trapping procedure if we are not happy with the accuracy of our original estimate, as a repeated trapping will inevitably be done under different conditions. Hence every time we compare the accuracy of several methods of numerical integration, we should keep in mind that in many ecological applications we may deal with numerical integration on coarse grids where the error estimate (8.9) cannot be applied. Further examples will be provided in the next sub-section.

8.4.2 Numerical Integration of Data Obtained from a Mathematical Model

Despite plenty of experimental data being available in the pest insect monitoring problem, we first apply our numerical integration techniques to the data obtained as a result of computer simulation. We use computer simulation for generating ecologically meaningful data because we want to subsequently increase the number of traps (i.e. the number of grid nodes) in order to investigate the integration error $e(N)$ for each integration method we employ in the problem. Thus we take our data from an ecologically sound mathematical model of population dynamics in order to be able to compute the function $e(N)$ for various N of our choice. Namely, we consider the spatially explicit predator-prey model with the Allee effect (Murray 1989; Turchin 2003). In dimensionless form the system is as follows:

$$\frac{\partial u(x,y,t)}{\partial t} = d\left(\frac{\partial^2 u}{\partial x^2} + \frac{\partial^2 u}{\partial y^2}\right) + \beta u(u-b)(1-u) - \frac{uv}{1+\Lambda u}\,, \tag{8.28}$$

$$\frac{\partial v(x,y,t)}{\partial t} = d\left(\frac{\partial^2 v}{\partial x^2} + \frac{\partial^2 v}{\partial y^2}\right) + \frac{uv}{1+\Lambda u} - mv\,, \tag{8.29}$$

where $x \in [0,1]$, $y \in [0,1]$, the functions $u(x,y,t)$ and $v(x,y,t)$ are the densities of prey and predator, respectively, at time $t > 0$ and position (x,y), d is the diffusion coefficient, and the other parameters have evident meaning (Murray 1989).

In order to obtain the population density distributions, the system (8.28–8.29) is solved numerically for a range of parameters, and the function $u(x,y,t)$ is then considered as the density of the pest insect in the problem. Solving the system (8.28–8.29) requires us to generate a regular spatial grid as described in Sect. 8.2. A discussion of the numerical solution along with the choice of the initial and boundary conditions has been provided in the paper Petrovskaya et al. (2012) where similar computer simulations have been done.

We begin our consideration from the simplest computational case where the pest insect population density is generated from the $1-d$ counterpart of the system (8.28–8.29). The parameters of the $1-d$ system of equations as well as the initial and boundary conditions required for its numerical solution are given in the paper Petrovskaya and Petrovskii (2010). The solution $u(x,t)$ of the $1-d$ system of equations is considered at fixed time $\hat{t}$ of our choice. We therefore have a $1-d$ spatial density distribution $u(x,\hat{t}) \equiv u(x)$ of the pest insect over the unit interval $x \in [0,1]$. This spatial density distribution is available to us at grid nodes x_i, $i = 1,2,\ldots,N+1$ only, but we can control the number $N+1$ of grid nodes in our computations by adding new nodes to a coarse grid or by removing them from a fine grid. Thus we first solve the $1-d$ system (8.28–8.29) on a grid with a very big number $N+1 = N_f + 1 = 2^{15}+1$ of nodes. Once the density distribution $u(x)$ has been obtained at fixed time $\hat{t}$ on an extremely fine grid of

$N_f + 1$ nodes, the integral $I = \int_0^1 u(x)dx$ is evaluated on that grid. The result $\tilde{I}(N_f)$ of that evaluation then is considered as the true integral I and is stored for further computations along with the spatial density $u(x)$ computed on a grid of $N_f + 1$ nodes. We then decrease the number of grid nodes and consider several approximations $\tilde{I}(N)$ for values $N \ll N_f$. Let us note that we do not re-compute the density function $u(x_i), i = 1, \ldots, N + 1$ every time that a new number N is chosen. The values of $u(x)$ are always taken from the 'exact solution' computed on a grid of $N_f + 1$ nodes at time $\hat{t}$, where we make a projection of the function $u(x_i), i = 1, \ldots, N_f + 1$ obtained on the fine grid to a coarse grid every time that we take a new, smaller number $N + 1$ of nodes. The details of this computational technique are provided in our previous work (Petrovskaya and Petrovskii 2010).

It is well-known (e.g., see Malchow et al. 2008; Petrovskii et al. 2003) that the properties of the spatial distribution $u(x)$ considered at a given time $\hat{t}$ are determined by the diffusion d. The density distribution can evolve into a monotone function if the diffusion d is of the order of 1 or larger. An example of a monotone density distribution is shown in Fig. 8.4a. For smaller values of $d \ll 1$ the initial conditions $u(x, 0),\ v(x, 0)$ evolve into an ensemble of irregular humps and hollows (see Fig. 8.4b), where the number of peaks gets bigger for smaller values of d. The density distributions from Fig. 8.4 present us with two somewhat extreme cases of ecologically meaningful integrand functions, while there can be one or two peaks in the domain for intermediate values of the diffusion coefficient d. Thus it is interesting to compare the accuracy of numerical integration for the two spatial patterns shown in the figure. Namely, we compare the results of the trapezoidal rule (8.15), the Simpson rule (8.17) and the results of the total population size evaluation by a statistical method.

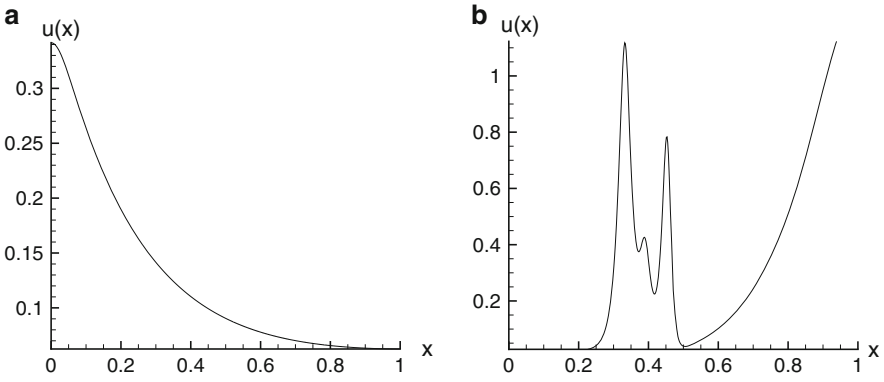

Fig. 8.4 Ecological test cases. (**a**) The spatial distribution of the pest population density $u(x)$ for the diffusivity $d = 10^{-4}$. Other parameters along with the initial and boundary conditions used to generate one-dimensional density distributions are discussed in Petrovskaya and Petrovskii (2010). (**b**) A 'multi-peak' density distribution obtained for the diffusion coefficient $d = 10^{-5}$

The statistical method commonly used in the evaluation of pest abundance is based on the computation of the sample mean pest population density (Davis 1994). The sample mean value $M(N)$ is given by a generic formula (8.1) where we have $K = N + 1$ in our problem. The expression (8.1) acts as an approximation to the true mean value. An approximation $\tilde{I}(N)$ to the actual pest population size I can then be found by multiplying the sample mean by the area of the field A, that is

$$I \approx \tilde{I}(N) = AM(N). \tag{8.30}$$

Consider the evaluation technique (8.30) in the $1-d$ case, so that the area A is given by the length $L = b - a$ of the interval $[a, b]$ where traps are installed. If the sampling positions x_i, $i = 1, \ldots, N + 1$, are equidistant, i.e. $x_{i+1} = x_i + h$ where $h > 0$ is constant, Eq. (8.30) can be written as

$$\tilde{I}(N) = \frac{L}{N+1} \sum_{i=1}^{N+1} u_i = \hat{h} \sum_{i=1}^{N+1} u_i = \sum_{i=1}^{N+1} \hat{h} u_i \approx \int_a^b u(x)dx, \tag{8.31}$$

where $u_i = u(x_i)$, $\hat{h} = L/(N + 1)$. It is readily seen that Eq. (8.31) coincides with the simplest method of numerical integration with weights $\omega_i = \hat{h}$. The convergence rate (8.9) of the integration rule (8.31) is $e = Ch$, where C is a constant (Davis and Rabinowitz 1975). Hence if the number of traps is big enough to resolve all features of the integrand function $u(x)$, the rule (8.31) should be inferior to more accurate integration methods such as the trapezoidal and Simpson rule.

The results of numerical integration of the density distributions shown in Fig. 8.4 are given in Table 8.1. It can be seen from the table that for the function $u(x)$ presented in Fig. 8.4a integration by the Simpson rule gives very accurate results even on a grid with a very small number of grid nodes. If we install three traps over the unit interval where the density measurements are made, evaluation of the total population size by the Simpson rule can be done with the error of 0.2 %, while the statistical rule provides us with an error over one hundred times bigger. Moreover, generally the error on each consecutive grid is smaller in comparison with the error on a previous grid.

Table 8.1 The relative integration error (8.7) for the $1-d$ density distributions of Fig. 8.4. The errors computed for the density distributions shown in Fig. 8.4a, b are marked with superscript (a) and (b), respectively. The first column gives the number $N + 1$ of the grid nodes. The error for each distribution (a) and (b) is computed by the statistical rule (8.31) (the column marked as e_{stat}), by the trapezoidal rule (8.15) (the column e_{TR}), and by the Simpson rule (8.17) (the column e_{SR})

$N+1$	$e^{(a)}_{stat}$	$e^{(a)}_{TR}$	$e^{(a)}_{SR}$	$e^{(b)}_{stat}$	$e^{(b)}_{TR}$	$e^{(b)}_{SR}$
3	0.283845	0.140895	0.002056	0.220479	0.056794	0.334066
5	0.132744	0.023493	0.015641	0.041373	0.245472	0.308365
9	0.064319	0.001141	0.006310	0.036879	0.138367	0.102665
17	0.033164	0.000373	0.000877	0.021570	0.025521	0.012094

Meanwhile, the situation is very different when we consider the density function shown in Fig. 8.4b. The application of the Simpson rule on grids with 3, 5 and 9 nodes does not have any advantage in comparison with the statistical rule. Clearly, in the case of the 'multi-peak' density distribution of Fig. 8.4b we have to deal with a 'coarse grid problem' where the density $u(x)$ is not well approximated on a grid with a small number of nodes. One important indicator of the coarse grid problem is that the error can oscillate between two grids, so that adding new nodes to the grid does not consistently make the error smaller until the integrand function is well resolved. An example is given by the error $e_{TR}^{(b)}$ of the trapezoidal rule on grids with $N = 3$ and $N = 5$ nodes.

It also is worth noting here that the statistical rule gives a more accurate answer on a grid of five nodes, while the error of the trapezoidal and the Simpson rule remains big on this grid. However, below we will see that even accurate results obtained on coarse grids are not reliable, as a slight change in the spatial pattern of the density function may result in a big jump in the integration error when the same numerical integration method is used in the problem.

8.4.3 *Numerical Integration of* $2-d$ *Data*

We now generate a $2-d$ density distribution $u(x, y)$ from numerical solution of the system of Eqs. (8.28–8.29). Let us fix the time t as $t = \hat{t} > 0$ and consider a snapshot $u(x, y) \equiv u(x, y, \hat{t})$ of a temporal-spatial density distribution $u(x, y, t)$. Numerical solution of (8.28–8.29) at any fixed time $\hat{t}$ provides us with the discrete density distribution $u_i \equiv u(x_i, y_j), i = 1, \ldots, N+1, j = 1, \ldots, N+1$, where grid nodes (x_i, y_j) are the points where traps are located. Similarly to the $1-d$ case we consider two density distributions whose spatial pattern is strongly different from each other. The density distribution shown in Fig. 8.5a presents a continuous front, while the density distribution of Fig. 8.5b is an example of a late stage of the patchy invasion (Petrovskii et al. 2005, 2002).

The computation carried out in the $1-d$ problem is repeated for the $2-d$ density distributions of Fig. 8.5. The results of numerical integration by the methods (8.30), (8.22) and (8.23) are shown in Table 8.2. It is readily seen from the table that the accuracy of integration depends again on the spatial pattern of the density function. Integration of the continuous front shown in Fig. 8.5a already gives a small integration error on grids with a small number of traps, the Simpson method being the most accurate method of integration. Let us recall that, in many ecological studies, a relative error of 100 % (i.e. $e(N) \sim 1$) is still regarded as acceptable, while the error $0.2 < e(N) < 0.5$ is considered as being good accuracy (Pascual and Kareiva 1996; Sherratt and Smith 2008). Hence numerical integration of the continuous front provides us with an accurate answer even on a grid with three grid nodes in each direction.

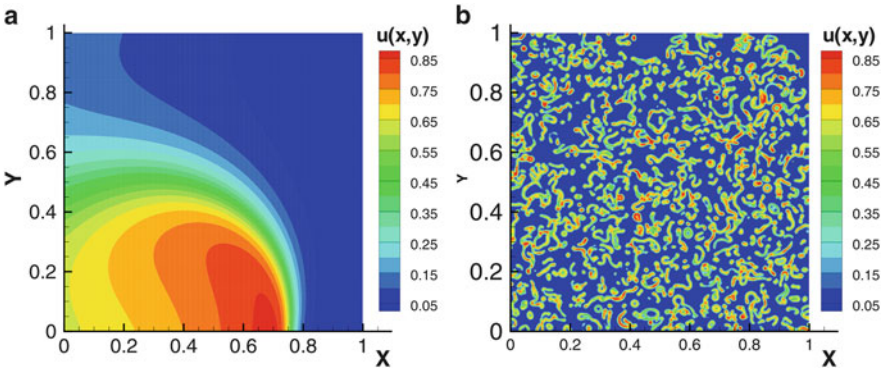

Fig. 8.5 Density function $u(x, y)$ as predicted by the population dynamics model (8.28–8.29) for different parameter values. (**a**) A snapshot of a continuous front. (**b**) A snapshot of the population density at a late stage of the patchy invasion

Table 8.2 The relative integration error (8.7) for the $2-d$ density distributions of Fig. 8.5. The errors computed for the density distribution shown in Fig. 8.5a, b are marked with superscript (a) and (b), respectively. The first column gives the number $N+1$ of the grid nodes in the direction x and y of a regular grid in the unit square. The error for each distribution (a) and (b) is computed by the statistical rule (8.31) (the column marked as e_{stat}), by the trapezoidal rule (8.22) (the column e_{TR}), and by the Simpson rule (8.23) (the column e_{SR})

$N+1$	$e_{stat}^{(a)}$	$e_{TR}^{(a)}$	$e_{SR}^{(a)}$	$e_{stat}^{(b)}$	$e_{TR}^{(b)}$	$e_{SR}^{(b)}$
3	0.1383	0.0506536	0.0255829	0.421591	0.496434	0.492878
5	0.064104	0.0142134	0.0221032	0.179808	0.263172	0.179825
9	0.032304	6.51693e-004	0.00389531	0.112412	0.111526	0.067423
17	0.017627	2.86861e-004	9.55669e-005	0.086713	0.064729	0.053797

Meanwhile, the more complex spatial structure of the density distribution of Fig. 8.5b requires a bigger number of grid nodes to provide the same level of accuracy. Moreover, on analysing the performance of the Simpson rule (8.23) on grids with $N+1<9$, we see that it is not more accurate than the other methods on coarse grids. On grids where the spatial pattern of the density function $u(x, y)$ is not well resolved it is hard to say which method is more accurate. This conclusion is further confirmed by numerous computations of approximate integrals made for various spatial distributions in the paper Petrovskaya et al. (2012).

8.4.4 Examples of Numerical Integration of Field Data

In this section we apply numerical integration techniques to field data of ecological monitoring. The aim of this study is to check what can be the smallest number of grid nodes (i.e. the number of traps in the agricultural field) used for accurate

evaluation of the pest insect population size, given the spatial distribution of the pest insect density. Obviously, density measurements made under real-life conditions cannot provide us with the data on a very fine grid. However, some experimental data contain information sufficient to extract a sequence of grids with a smaller number of nodes from the original grid and to compare the results of numerical integration on grids with various numbers of nodes.

We first illustrate our approach by considering data that have already been used in our earlier paper (Petrovskaya et al. 2012) where numerical integration techniques have been applied to experimental data collected for a New Zealand flatworm population (*Arthurdendyus triangulatus*) by Murchie and Harrison (2004). The data on flatworm abundance at different locations were collected by means of trapping where the traps were positioned at the nodes of a 12×12 regular grid. Spacing between two traps was 2 m in each direction. The traps were examined every week and the numbers of flatworms caught were counted. The various 12×12 grid trap systems caught 465–748 flatworms per sampling period (Murchie and Harrison 2004). Other details of the trapping procedure can be found in Murchie and Harrison (2004) and Petrovskaya et al. (2012).

Two examples of the density distributions obtained from trap counts are shown in Fig. 8.6. The trap counts have been linked to the local population density $u(x, y)$ by dividing the trap counts at each location by 4 m^2 (i.e. by the area of the grid cell) (Byers et al. 1989; Raworth and Choi 2001). For the sake of numerical integration, we have then extracted a sub-grid with $N + 1 = 11$ traps in each direction from the trap data originally collected in the field. This has been done because integration by the Simpson rule requires an odd number $N + 1$ of grid nodes. Having integrated the

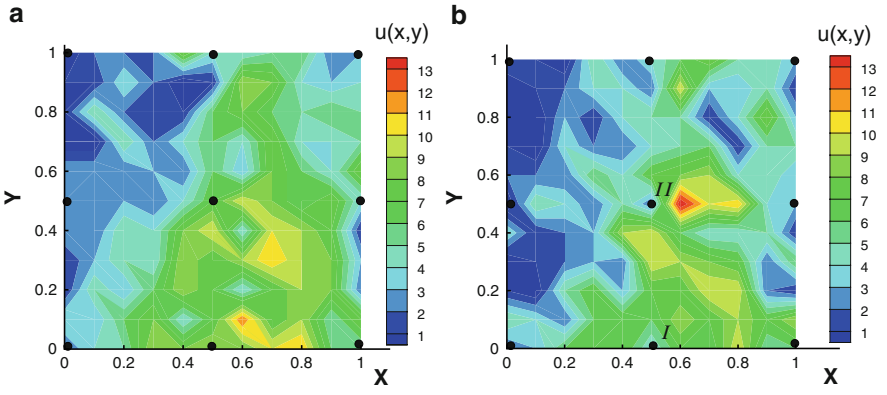

Fig. 8.6 Numerical integration of field data on a coarse grid of nine nodes. The nodes of a regular grid are shown as closed circles in the figure. The field data present flatworm spatial distributions over the study area (see Murchie and Harrison 2004; Petrovskaya et al. 2012 for more details).(**a**) Numerical integration of the density distribution gives good accuracy even on a grid with a very small number of nodes. (**b**) Two grid nodes (node *I* and node *II* in the figure) fall into small patches of different density on a coarse grid. Since the density values at those locations are not representative, numerical integration on a coarse grid results in a big integration error

Table 8.3 The approximation of the total population size and the integration error on a regular grid of 3×3 nodes for the field data taken from the paper Petrovskaya et al. (2012). The approximate integral is computed by the statistical rule (8.30) (the column I_{stat}), by the trapezoidal rule (8.22) (the column I_{TR}) and by the Simpson rule (8.23) (the column I_{SR}). The rows marked (a) and (b) in the table correspond to the density distributions shown in Fig. 8.6a, b, respectively

case	I	I_{stat}	e_{stat}	I_{TR}	e_{TR}	I_{SR}	e_{SR}
(a)	611	411	0.327	488	0.202	561	0.082
(b)	544	289	0.469	269	0.506	247	0.545

population density over the fine grid of $11 \times 11 = 121$ nodes, we have reproduced the total number I of collected insects. This number is further considered as the exact value of the population size.

Let us now compute the population size on a regular grid of $3 \times 3 = 9$ nodes and compare the population size obtained by numerical integration over this grid with the value I obtained for the density distributions shown in Fig. 8.6a and Fig. 8.6b on the original grid of 11×11 nodes. The 9 traps on a coarse grid are stationed as shown in Fig. 8.6 and we take the density values at those locations from the original grid.

The results of numerical integration on a grid of nine nodes are presented in Table 8.3. We compute the integral by the statistical rule (8.30) (the column I_{stat}), by the trapezoidal rule (8.22) (the column I_{TR}) and by the Simpson rule (8.23) (the column I_{SR}). We also compute the relative integration error (8.7) for each of the rules above (the columns marked as e_{stat}, e_{TR}, e_{SR}, respectively). The exact population size (i.e. the integral computed on a grid of 121 nodes) is $I^{(a)} = 611$ for the density distribution shown in Fig. 8.6a and $I^{(b)} = 544$ for the density distribution shown in Fig. 8.6b.

The results presented in the table confirm our previous conclusion that the accuracy of evaluation depends heavily on the spatial pattern of the density function $u(x, y)$. It is seen from the table that the integration of the density distribution shown in Fig. 8.6a gives good accuracy even on a grid with the number of nodes as small as nine nodes. This result lead us to the conclusion that robust information about the population size of pest insect population can be obtained using far fewer traps per unit area, provided that the spatial density pattern is not very patchy.

In the case of the density distribution in Fig. 8.6b some information about the density function $u(x, y)$ has been lost, as two grid nodes have fallen into small sub-regions (patches) where the density is strongly different from the density in the surrounding domain; see nodes *I* and *II* in the figure. The density values at those nodes made a misleading contribution to the sum (8.4) and that resulted in a big integration error. Meanwhile it is worth noting that even in the case (b) the relative error of the population size estimate still remains smaller than 55 % and such accuracy can still be considered as acceptable for large scale monitoring programmes (Northing 2009).

Let us also note that we had to transform the grid of 12×12 traps to conduct our computational study, as application of the Simpson method was not possible on a grid with an even number of nodes in each direction. Meanwhile, we would like to

Table 8.4 An example of trap count data for *Pterostichus melanarius* obtained by trapping with pitfall traps (The data are taken from the paper Alexander et al. (2005))

5	0	1	2	4	1	1	38	5	4	3	3	1	13	5	6
7	13	1	0	1	0	0	12	2	0	1	8	12	10	1	0
6	3	0	0	4	2	1	1	2	3	5	11	12	11	3	0
2	5	1	7	8	6	15	0	3	1	0	6	2	8	1	0
7	5	1	2	0	2	0	0	4	3	3	0	9	7	4	1
3	7	6	0	0	1	6	0	5	2	0	2	16	13	6	2
4	6	3	0	5	8	1	4	3	6	2	26	11	1	5	2
2	2	2	7	9	5	13	5	3	14	26	42	9	15	1	4
1	0	3	2	11	0	3	7	8	11	14	22	24	5	5	0
6	1	4	16	15	11	0	11	12	13	16	20	12	7	5	4
1	0	4	1	11	2	11	7	6	6	0	3	4	6	0	0
9	6	3	2	7	7	6	8	11	25	18	9	2	1	2	1
3	2	6	15	5	18	24	4	8	16	6	11	6	1	0	0
3	7	3	22	27	34	0	41	21	37	16	10	3	7	2	3
12	12	30	25	23	15	19	12	6	9	9	4	10	6	3	6
11	7	11	26	38	19	16	19	11	13	13	0	5	4	2	10

emphasise that application of so called higher order numerical integration methods can be made on grids with an arbitrary number of grid nodes in each direction. A numerical integration method that would have the same convergence rate as the Simpson method could be designed for the original grid of 12×12 nodes. The application of such a method, however, would be a much more difficult technical task and it is beyond the scope of our paper. Thus we only provide a brief discussion of more general methods of numerical integration in Sect. 8.6.

Our conclusion about the accuracy of numerical integration is further illustrated by another set of field data taken from the paper Alexander et al. (2005). The trap counts for beetles *Pterostichus melanarius* obtained by trapping with pitfall traps are presented in Table 8.4. Field sampling for data in the table was performed on a 16×16 regular grid of traps installed in a conventionally managed 4 ha winter wheat field in Devon, UK; see Alexander et al. (2005) for more details. The density distribution obtained from Table 8.4 is shown in Fig. 8.7a. Again, for the purpose of our study we have to transform the original grid of 16×16 nodes into a grid where the Simpson method of integration can be applied. In the case of Table 8.4 we found it more convenient to augment the table rather than extract a grid with a smaller number of nodes. Generating a 17×17 computational grid from the original data should allow us to compute the integration error on a sequence of regular grids of 3×3, 5×5 and 9×9 nodes and to compare the accuracy of integration on those grids. Thus we added another row and column to the original grid. Hypothetical data for that addition were generated under the requirement to keep the same structure of the spatial pattern as in the original density distribution (see Fig. 8.7b). The value of the integral (i.e. using the total number of trap counts) on the new grid of 17×17 nodes is $I = 1{,}980$.

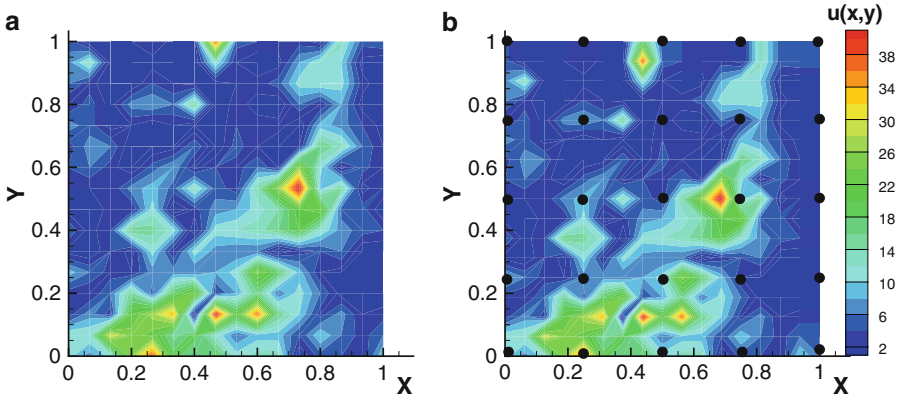

Fig. 8.7 The spatial density distribution obtained from the trap counts in Table 8.4. (**a**) The density function $u(x, y)$ based on the original data in Alexander et al. (2005). (**b**) Hypothetical data have been added to the original table in order to generate a 17×17 regular grid. The data have been generated to preserve the spatial structure of the original density distribution. An example of a regular grid (5×5 nodes) on which integral is computed is shown as a set of closed circles in the figure

It can be seen from Fig. 8.7b that the spatial pattern of the density distribution is similar to the spatial pattern of the $1 - d$ function (8.26) studied in Sect. 8.3. The density distribution is mostly homogeneous (cf. the function (8.26) on the interval $x \in [0.01, 1]$) with several small patches where the density is very high (cf. the function (8.26) for $x \in [0, 0.01]$). From the study of the convergence graph for the function (8.26) we predict that grids with 3×3, 5×5 and 9×9 nodes should be considered as coarse grids for the density distribution $u(x, y)$ of Fig. 8.7b, as small patches of the high density are not resolved on those grids. Hence the Simpson method will not have a visible advantage over the other integration methods employed in the problem. On the other hand, a big sub-domain where the density is almost homogeneous will be already well-resolved on coarse grids and integration over that sub-domain should give us an accurate contribution to the integral over the whole domain. Meanwhile, the number of patches with high density is not big and the density localised there is only approximately 30 times bigger than the density in the homogeneous sub-domain, while this ratio is approximately 5,000 for the function (8.26). Thus we expect a reasonably small integration error on coarse grids.

An example of a regular computational grid (a grid of 5×5 nodes) used in our computation is shown in Fig. 8.7b. The location of the nodes on a this grid confirms our analysis in the previous paragraph. Namely, all small patches of high density fall in between the grid nodes, but the density values on grid nodes are already representative enough to give accurate information about the density function in sub-domains where the density is an almost homogeneous function (see also Table 8.4). The results of numerical integration are shown in Table 8.5. The relative error is within 35 % even on a grid with three traps in each direction. However, as

Table 8.5 The approximate integral and the relative integration error (8.7) for the density distribution of Fig. 8.7b on a sequence of regular grids. The first column gives the number $N+1$ of the grid nodes in the direction x and y of a regular grid. The approximate integral and the error is computed on each grid by the statistical rule (8.30) (the columns marked as I_{stat} and e_{stat} in the table), by the trapezoidal rule (8.22) (the columns I_{TR} and e_{TR}), and by the Simpson rule (8.23) (the columns I_{SR} and e_{SR})

$N+1$	I_{stat}	e_{stat}	I_{TR}	e_{TR}	I_{SR}	e_{SR}
3	1,507	0.239	1,344	0.321	2,332	0.178
5	1,679	0.152	1,632	0.175	1,561	0.212
9	1,659	0.162	1,692	0.145	1,748	0.117

predicted, increasing the number of traps from three to nine in each direction does not significantly increase the accuracy of integration methods because small patches are still not resolved. Also, the Simpson method is not definitively superior to the statistical method and the trapezoidal rule, as the convergence rate (8.9) does not hold on coarse grids.

One important conclusion drawn from our consideration of $1-d$ and $2-d$ ecological distributions is that the accuracy of an estimation depends strongly on how the pest insects are dispersed across the agricultural field. The question of accuracy has been the focus of ecological research for a long time (Dent 2000; Vlug and Paul 1986; Ward et al. 1985). Reliable recommendations have been provided on the minimum number of traps required for obtaining an accurate estimate of a particular pest insect species based on the assumption that the pest insect density distribution is close to homogeneous (Binns et al. 2000; Karandinos 1976; Southwood and Henderson 2000). This assumption is true for many species, but as we could see in this section there also exist many ecologically important cases where the pest density is heterogeneous and can be aggregated into several patches (see also Barclay 1992; Ferguson et al. 2003). In the latter case we can anticipate an inaccurate estimate of the total pest population size, as a relatively small number of traps normally used in the trapping procedure may not be sufficient to resolve highly localised sub-domains of non-zero density. In the next section we discuss an extreme case of a single density patch in order to demonstrate that a conceptually different approach should be applied to evaluate the total population size for such spatial patterns.

8.5 Highly Aggregated Density Distributions

In this section we consider highly aggregated density distributions that we also refer to as peak functions. Namely, we discuss spatial patterns where the entire pest population is confined to a single sub-region (patch) within an agricultural field and the pest population is zero outside that patch. Such distributions have ecological significance as they present at an early stage of the biological invasion

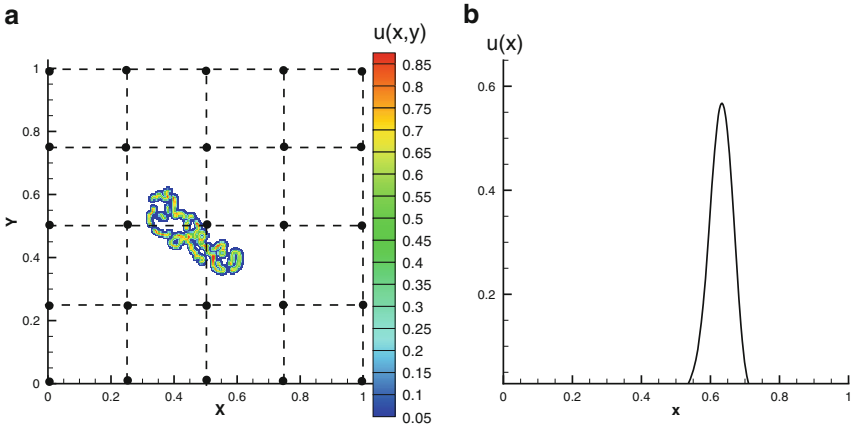

Fig. 8.8 (**a**) The pest population density distribution $u(x, y)$ at an early stage of patchy invasion. The highly aggregated density function $u(x, y)$ has been obtained from numerical solution of Eqs. (8.28–8.29). The traps used to measure the density $u(x, y)$ are installed at the nodes of a regular coarse grid as shown in the figure. (**b**) A one-dimensional counterpart of the density distribution of Fig. 8.9a

(Shigesada and Kawasaki 1997). It is clear that timely and accurate evaluation of the total number of pest insects at the beginning of biological invasion is beneficial for the cultivation of the agricultural product. At the same time the application of numerical integration methods to highly aggregated density distributions is a very difficult task, as the exact location of the high density sub-domain is normally not known in the problem. Thus, instead of installing the traps locally in the patch of the non-zero density in order to increase the accuracy of integration, traps have to be stationed at the nodes of a regular grid over the entire domain where monitoring is made. That, in turn, may result in the most unfavourable situation when the entire patch of non-zero density falls in between grid nodes.

Examples of highly aggregated density distributions are depicted in Fig. 8.8 where the density function was modelled by solving Eqs. (8.28–8.29) in the $2-d$ case (see Fig. 8.8a) and in the $1-d$ case (see Fig. 8.8b). It can be seen from Fig. 8.8a that the sub-region of non-zero density is entirely missed on a coarse grid of 5×5 nodes and we should significantly increase the number of nodes in order to resolve that sub-region. Given natural limitations on the number of traps that present in ecological applications, two basic questions arise. The first question is: What is the minimum number $N_t + 1$ of traps required to achieve desirable accuracy if a highly aggregated density distribution is numerically integrated? Also, we have to answer the related question: What can be an alternative measure of accuracy on a regular grid of traps where $N < N_t$?

The answer to the questions above were offered in the paper Petrovskaya and Embleton (2013). It has been shown there that a standard methodology does not work when the density of a highly aggregated pest population is measured by a trapping procedure with a small number $N + 1$ of traps installed. The uncertainty

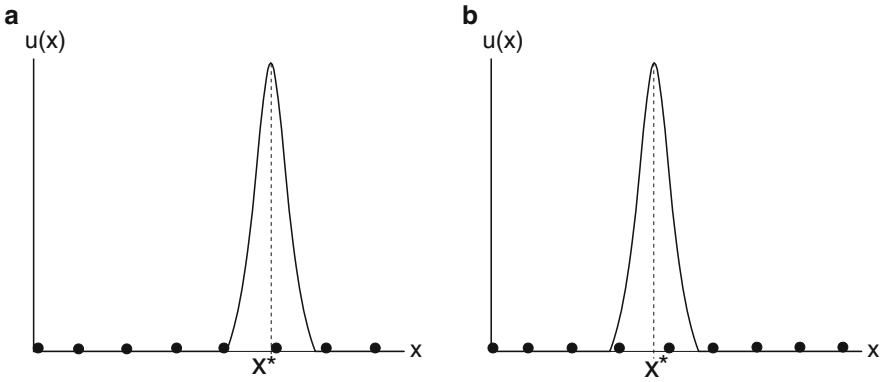

Fig. 8.9 Numerical integration of a highly aggregated density distribution. The accuracy of integration depends on the peak location x^* with respect to the nodes of a regular grid. (**a**) The peak sub-domain contains only one grid node. (**b**) The same peak is now located in a different region, so that two grid nodes lie within the peak sub-domain when the same regular grid is generated

in measurements made on coarse grids is so strong that an estimate $\tilde{I}(N)$ of the integral I becomes a random variable. As a result, the integration error also becomes a random variable with a high magnitude and we cannot control the accuracy of evaluation. In other words, we cannot consider the condition (8.11) for peak functions on grids with small N, as, depending on the peak location, we sometimes will obtain a very accurate answer and sometimes our answer on the same regular grid will be well beyond the accuracy range. An example illustrating this statement is shown in Fig. 8.9, where we have one grid node within the peak sub-domain in Fig. 8.9a. If we move the peak on the same grid, so that the location of the maximum x^* becomes different, two grid nodes will fall into the peak region (see Fig. 8.9b). As a result, the peak function will be better resolved and we will have a more accurate estimate of the integral.

Since the integration error is considered as a random variable on coarse grids where a location of the density patch is not known to us, it was therefore suggested in Petrovskaya and Embleton (2013) that we have to compute the probability of achieving an integration error within a certain accuracy range instead of computing the error itself. Namely, we compute the probability $p(h)$ (or $p(N)$ in some cases) that the condition (8.11) holds. The probability $p(h)$ is then considered an alternative measure of accuracy when we integrate a high aggregation density distribution on a regular grid with a small number of nodes.

Grids, where the integration error becomes a random variable because of the insufficient information about the integrand function and where we have to compute the probability of an accurate evaluation of the integral are referred to as *ultra-coarse* grids (Embleton and Petrovskaya 2013; Petrovskaya and Embleton 2013; Petrovskaya et al. 2012). It is clear that if we keep increasing the number of nodes on a regular grid, then sooner or later we are able to integrate the peak function with very good accuracy. We therefore have the threshold number N_t of

grid sub-intervals, where the desirable accuracy of pest population size evaluation cannot be guaranteed for any $N < N_t$. An immediate consequence of this result is that an estimate of the pest population size per se becomes unreliable if the number N of traps in the field is $N < N_t$.

The above results are illustrated by a simple example of a $1-d$ peak function. Consider the following density distribution (the Lorentzian) on the unit interval $x \in [0, 1]$,

$$u(x) = \begin{cases} \dfrac{\delta^2}{4}\dfrac{1}{4(x-x^*)^2+\delta^2/4} - \dfrac{1}{5}, & x \in [x^*-\delta/2, x^*+\delta/2], \\ 0, & otherwise, \end{cases} \tag{8.32}$$

where δ is the peak width and x^* is the location of the maximum point. Let us emphasise again that the location x^* is not known to us, so the peak can be located at any point of the sub-interval $[\delta/2, 1-\delta/2]$. The peak function (8.32) is shown in Fig. 8.10a for the peak width $\delta = 0.06$.

Consider now numerical integration of the function (8.32) by the trapezoidal rule (8.15). Let a regular grid of $N+1$ nodes be generated in the domain $[0, 1]$ as $x_1 = 0, x_{i+1} = x_i + h, i = 1, \ldots, N$, where the grid step size is $h = 1/N$. For the purpose of our study we require that the grid step size is $h > \delta/2$. We start from $h = 0.25$ (i.e., five equidistant grid nodes over the unit interval) and decrease h by adding new nodes to the grid until the grid step size is so small that the condition $h > \delta/2$ is broken. For each grid step size h we compute the probability $p(h)$ of getting an accurate estimate of the integral, provided that the peak is arbitrarily located in the domain. The accuracy we impose in the problem is $e(N) \le \tau_0 = 0.25$, where $e(N)$ is the relative integration error (8.7). The details of the computation of $p(h)$ can be found in Petrovskaya and Embleton (2013).

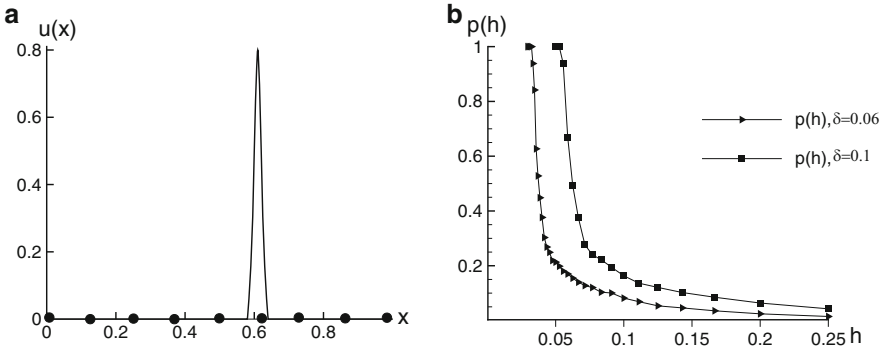

Fig. 8.10 (**a**) The peak function (8.32) with the peak width $\delta = 0.06$ on a regular grid of 9 nodes. (**b**) The probability curves $p(h)$ obtained for the function (8.32) with the peak width $\delta = 0.06$ (*solid line*, *closed right triangle*) and $\delta = 0.1$ (*solid line*, *closed square*)

Two probability curves $p(h)$ are shown in Fig. 8.10b for the function (8.32) with the peak width $\delta = 0.06$ and $\delta = 0.1$. It can be seen from the figure that for each probability curve there exists the threshold value h_t such that $p(h) = 1$ for any $h < h_t$. It was shown in Petrovskaya and Embleton (2013) that the grid step size h_t for which the error (8.7) becomes deterministic, that is $p(h_t) = 1$ and $p(h) < 1$ for any $h > h_t$, can be evaluated as

$$h_t = \alpha_t \delta, \tag{8.33}$$

where δ is the peak width and α_t is constant for any given tolerance τ in the accuracy condition (8.11). The value of α_t was computed in Petrovskaya and Embleton (2013) as $\alpha_t \approx 0.81$ for $\tau = 0.25$.

Let us, for example, integrate the function (8.32) with the peak width $\delta = 0.1$ on a regular grid with the grid step size $h = 0.1$ (i.e., a grid of 11 nodes). We have $h > h_t \approx 0.08$ and it follows from Fig. 8.10b that our chance $p(h)$ to evaluate the integral within the accuracy range $e(N) < 0.25$ is $p(h) \approx 0.2 = 20\,\%$. In other words, there is an 80 % chance that the error of our evaluation will be bigger than $\tau = 0.25$ when we evaluate the pest abundance for the peak function (8.32) on a regular grid of 11 nodes. Consider now a grid with $h = 0.07$ (15 grid nodes). Since the distance between nodes is now $h < h_t$, we will always have the error $e(N)$ of integral evaluation smaller than 0.25, no matter where the peak is located. The probability $p(h)$ of getting the error within the accuracy range $e(N) < 0.25$ is $p(h) = 1$.

In the $1 - d$ case the grid step size h is given by $h = 1/N$ and we can therefore evaluate the minimum number $N_t = 1/h_t$, such that the desirable accuracy of integration is guaranteed on a grid of $N_t + 1$ nodes. Furthermore, it has been discussed in Petrovskaya et al. (2013) that in ecological problems the width δ of the highly aggregated density distribution can be written as

$$\delta = \omega \sqrt{d}, \tag{8.34}$$

where d is the diffusion coefficient. Another coefficient ω in the expression (8.34) depends on the system's parameters. It was shown in Petrovskii and Malchow (2001) and Petrovskii et al. (2003) that the value ω is relatively robust to changes in the parameter values and can typically be considered as $\omega \approx 25$. Hence the threshold number N_t can be evaluated as

$$N_t = \frac{1}{\alpha_t \delta} \approx \frac{1}{\alpha_t \omega \sqrt{d}}. \tag{8.35}$$

For example, the ecologically meaningful density distribution of Fig. 8.8b was generated for the diffusion $d = 10^{-4}$. The estimate (8.35) gives us the grid step size as $h_t \approx 0.2$ and the corresponding number of grid nodes is $N_t + 1 \approx 6$.

Understanding accuracy requirements for highly aggregated density distributions is important when a sampling plan is designed for pest insect monitoring and control. As we already mentioned in the introduction, a standard procedure of the

risk evaluation in pest management is to compare an estimate of the total number of pest insects with a certain critical number and to make a decision based on that comparison. We discussed in the previous sections that the error in the estimation of pest abundance becomes worse as the number of samples decreases (see also Binns et al. 2000). However, consideration of the extreme case of a random error brings into the problem another risk factor related to the uncertainty in integral evaluation when the number $N + 1$ of traps is small. Taking this risk factor into account may constitute an important task in the whole process of designing an appropriate methodology for decision making in pest insect management.

8.6 Evaluating Pest Abundance on Irregular Grids

So far we have considered using methods of numerical integration to evaluate pest population abundance when the sampling plan is a regular grid, i.e. the samples are taken at regular spatial intervals. However, it may be that an irregular grid is prescribed in a pest monitoring programme. Furthermore, even if a regular grid has been selected as the intended sampling plan, taking samples at precisely regular intervals may not be possible in practise. The landscape of an agricultural field may have natural obstacles (e.g. a bush or a tree) that will make trap installation on the nodes of a regular grid impossible. One or many of the samples may then have to be taken at a location shifted from that which was intended due to an obstruction of some kind, hence the resulting grid of samples is irregular. We thus now investigate the accuracy of numerical integration methods formulated on an irregular grid. Our analysis is focused on a $1-d$ problem for the sake of simplicity, but, as in previous sections, our results can be readily extended to a $2-d$ problem.

8.6.1 Generation of Irregular Grids

We consider several types of grids with varying degrees of irregularity: a slightly irregular grid, a quasi-random grid, and a random grid. We use the term 'slightly irregular' to refer to a simple example of an irregular grid, whereby a single sampling location is shifted from the position prescribed by a regular sampling plan. We generate such a grid by first constructing a regular grid as was explained in Sect. 8.2. A single interior node x_i, for some $i = 2, \ldots, N$ is then perturbed according to the following transformation:

$$x_i^{irreg} = x_i + h\left(r - \frac{1}{2}\right), \tag{8.36}$$

where x_i is a node location on a regular grid, and $r \in (0, 1)$ is a uniformly distributed random variable. The transformation (8.36) is further illustrated in Fig. 8.11b.

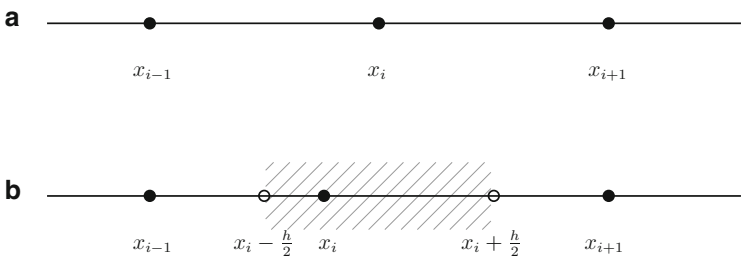

Fig. 8.11 (**a**) An interior grid node x_i for some $i = 2, \ldots, N$ is a fixed distance h from its neighbouring grid nodes in accordance with a regular sampling plan. (**b**) An interior grid node x_i^{irreg} which has been perturbed according to the transformation (8.36) (the superscript is omitted in the figure to make it consistent with Fig. 8.11a). The shaded region shows the possible locations for x_i^{irreg}, where this node is no longer an equal distance from its neighbouring nodes

A quasi-random grid has an increased level of irregularity whilst preserving some structure. Such grids are generated in a similar way to the method discussed above for the slightly irregular grids. The difference is that instead of a single interior node being perturbed, *all* interior nodes are perturbed. That is, the transformation (8.36) is applied to all interior nodes $x_i, i = 2, \ldots N$ of the regular grid. This form of grid is closely related to the so called 'centric systematic' sampling plan (e.g. see Milne 1959) whereby the field is divided into sections and a sample is taken from a random location within each section. Our version differs only in that we have fixed the boundary points so as to preserve the interval of integration as $[a, b]$.

A random sampling plan is often viewed favourably from a theoretical viewpoint as it is considered to avoid introducing bias into the estimate (Bliss 1941; Legg and Moon 1994; Reisen and Lothrop 1999; Silver 2008), the concern being that a systematic distribution of samples will somehow coincide with the distribution of the pests. We therefore take into consideration such a distribution of samples in our investigation and generate the points $x_i, i = 1, \ldots, N + 1$ as follows:

$$x_i = a + r(b - a), \qquad i = 1, \ldots, N + 1, \tag{8.37}$$

where $r \in (0, 1)$ is a uniformly distributed random variable. The points $x_i, i = 1 \ldots N + 1$ are then sorted into ascending order and the endpoints on a random grid are then replaced as

$$x_1 = a, \qquad x_{N+1} = b. \tag{8.38}$$

An example of a random grid is shown in Table 8.6. The grid of nine nodes presented in the table was generated over the interval $[0, \pi]$ using a standard function *rand*() in Visual C++.

Table 8.6 An example of random grid over the interval $[0, \pi]$

i	1	2	3	4	5	6	7	8	9
x_i	0.0	0.816881	1.05838	1.43716	1.489	1.58434	1.70697	1.74214	3.14159

8.6.2 Numerical Integration on Irregular Grids

We now look at the accuracy of pest abundance estimates obtained by methods of numerical integration on the grids outlined above. We will be using the statistical rule, the trapezoidal rule and Simpson's rule to evaluate the pest abundance. Since the statistical rule (8.31) has no spatial dependence it can be applied to regular and irregular grids alike.

Meanwhile, we must use different forms of the trapezoidal and Simpson's rules to those which have been mentioned above in order to be able to apply them to irregular grids. The Newton-Cotes formulas can, of course, be applied in the case that the integrand function $f(x)$ is defined on the nodes of an irregular grid. The idea remains the same: replace the integrand by a polynomial function and integrate the polynomial instead. However, we cannot use formulas (8.15) and (8.17) designed for regular grids and we have to take into account a grid's irregularity when the weight coefficients ω_i are computed.

The trapezoidal rule on irregular grids is given by

$$I \approx \tilde{I} = \sum_{i=1}^{N} h_i \frac{(f_i + f_{i+1})}{2}, \tag{8.39}$$

where N is the number of grid sub-intervals, and the grid step size $h_i = x_{i+1} - x_i$ is variable rather than fixed as in the formula for regular grids. We use the following adapted version of Simpson's rule to handle irregular grids

$$I \approx \tilde{I} = \sum_{i=1}^{\frac{N}{2}} \frac{h_{2i-1} + h_{2i}}{6} \left(f_{2i-1} + 4f_{2i} + f_{2i+1}\right), \tag{8.40}$$

which also relies on the variable grid step size $h_i = x_{i+1} - x_i$. As with the conventional Simpson's rule (8.17), the number of grid nodes $N + 1$ is required to be odd.

We illustrate the convergence on irregular grids by considering a sequence of grids, where each grid is generated according to the relevant procedure outlined above. The number of grid subintervals is set on the first grid in the sequence as $N = N_0$, an estimate is obtained by means of a chosen numerical integration method and the relative error (8.7) is calculated. The number of grid sub-intervals is then increased to $N_1 = 2N_0$, a new grid is generated, and the estimate and subsequent relative error is recalculated. This process is repeated until the number of grid sub-intervals reaches some chosen value $N = N_{final}$. In the case of the

slightly irregular grids, we want to determine how perturbing a single node affects the convergence rate of a method of numerical integration, rather than how the position of the grid node which is perturbed affects the accuracy. As such, in each generation of the slightly irregular grids, the same interior grid node is perturbed. We will begin all of our calculations on a grid of three grid nodes which has only one interior node. The unperturbed position of this node lies at $x = (a + b)/2$, therefore, it will always be this central node which is perturbed in the generation of each slightly irregular grid. For grids with a more significant level of irregularity i.e. the quasi-regular and random grids, each grid generation is repeated a total of n_r times thus providing n_r values of the error for any given grid of $N + 1$ nodes. The mean error on a grid of $N + 1$ nodes is then calculated as

$$\mu(e) = \frac{1}{n_r} \sum_{i=1}^{n_r} e_i \,. \tag{8.41}$$

We first consider a standard mathematical test case where the integral of the function (8.10) is evaluated over a sequence of increasingly refined irregular grids according to the procedure outlined above. For the slightly irregular grids, the corresponding relative errors are shown in Table 8.7. It can be seen from the table that very little difference is made to the accuracy by perturbing a single node as the results for the regular and slightly regular grids are close to each other.

For the random grids, the mean of $n_r = 10^4$ evaluations of the error have been plotted in Fig. 8.12. The convergence rate of errors calculated over increasingly refined regular grids has also been plotted in each graph for comparison purposes (see dashed line in the figure). Random perturbation of the interior nodes affects the convergence rate with varying degrees of prominence depending on the method of numerical integration employed as can be seen in the figure. The behaviour of the convergence curve for the statistical rule shown in Fig. 8.12a is different from the convergence for the trapezoidal rule (Fig. 8.12b) and the Simpson rule (Fig. 8.12c), as the convergence rate of the method (8.31) on irregular grids is slower in comparison with the convergence on regular grids. Meanwhile the randomness introduced to the computational grid causes the convergence curves

Table 8.7 The relative integration error (8.7) for the function (8.10) on slightly irregular grids where the central node is shifted from its position on the original regular grid. The first column gives the number $N + 1$ of grid nodes. The error (8.7) is computed on an irregular grid (marked as the superscript "irreg" in the table) and compared with the corresponding error on a regular grid (the superscript "reg"). The error is computed for the statistical rule (8.31) (the columns marked as e_{stat} in the table), the trapezoidal rule (8.39) (the columns e_{TR}), and the Simpson rule (8.40) (the columns e_{SR})

$N+1$	e_{stat}^{reg}	e_{stat}^{irreg}	e_{TR}^{reg}	e_{TR}^{irreg}	e_{SR}^{reg}	e_{SR}^{irreg}
3	4.764e−001	4.829e−001	2.146e−001	2.163e−001	4.720e−002	4.681e−002
5	2.416e−001	2.423e−001	5.194e−002	5.409e−002	2.280e−003	1.786e−003
9	1.226e−001	1.227e−001	1.288e−002	1.288e−002	1.346e−004	1.342e−004
17	6.185e−002	6.185e−002	3.215e−003	3.222e−003	8.296e−006	8.295e−006

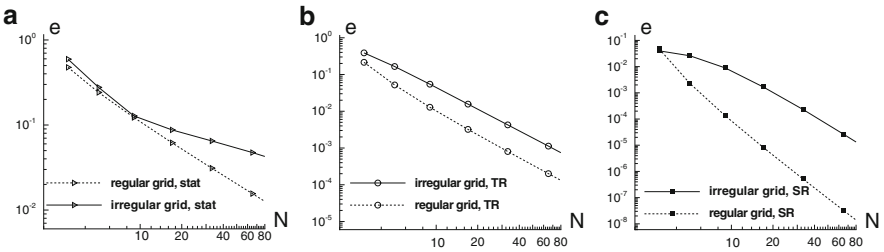

Fig. 8.12 Numerical integration of the function (8.10) on random grids. (**a**) The relative integration error (8.7) for the statistical rule (8.31) (*solid line*, *right open triangle*). The convergence curve is compared with the convergence on regular grids (*dashed line*, *right open triangle*). (**b**) Convergence curves for the trapezoidal rule (8.39) on random grids (*solid line*, *open circle*). The convergence curve for the method (8.15) on regular grids is shown as a *dashed line* in the figure. (**c**) Convergence curves for the Simpson rule (8.40) on random grids (*solid line*, *closed square*) and for the method (8.17) on regular grids (*dashed line*, *closed square*)

of the trapezoidal and Simpson's rules to be shifted upwards, that is, the resulting estimates are less accurate although they begin to converge at a similar rate to those formulated on regular grids as N increases. The higher the degree of the method applied, the more prominent the effect seems to be, although it should be noted that on average the accuracy still improves when a higher degree method is used.

8.6.3 Integration of Ecological Data on Irregular Grids

Let us now consider the accuracy of the numerical integration of ecologically significant data. Since we are required to perform repeated calculations over increasingly refined grids, we use simulated data as suitable field data is difficult to obtain. As earlier explained the simulated ecological population density functions were obtained through numerical solution of the $1-d$ system (8.28–8.29) on an extremely fine, regular grid of $N_f+1=2^{15}+1$ nodes on the interval $[a,b]=[0,1]$. Since the density functions are thus discrete rather than continuous, the method for generating the slightly irregular computational grid is now different to that outlined above although the fundamental ideas are the same.

We have available a fine grid of points $x_i^f, i=1,\ldots,N_f+1$ where

$$x_1^f = a = 0, \qquad x_i^f = x_{i-1} + \frac{b-a}{N_f}, \quad i=2,\ldots,N, \qquad x_{N_f+1}^f = b = 1.$$

To generate a slightly irregular grid of $N+1$ nodes, a regular grid is first obtained by extracting the required $N+1$ nodes from the available fine grid as

$$x_i = x_j^f, \qquad j = 1+(i-1)\left(\frac{N_f}{N}\right), \quad i=1,\ldots,N+1. \tag{8.42}$$

A single interior node must then be perturbed, however, it must be perturbed to a value for which the population density is available. This is achieved by replacing an interior grid node as

$$x_i = x^f_{j+r}, \qquad r \in \left[-\frac{N_f}{2N}, \frac{N_f}{2N}\right] \tag{8.43}$$

for some $i = 2, \ldots, N$, where j is as given in (8.42) and r is a uniformly distributed random integer.

The generation of quasi-random grids for use with simulated ecological data is as follows. The endpoints are fixed as

$$x_1 = x^f_1, \qquad x_{N+1} = x^f_{N_f+1}, \tag{8.44}$$

and the interior points are defined as

$$x_i = x^f_{j+r}, \qquad r \in \left[-\frac{N_f}{2N}, \frac{N_f}{2N} - 1\right], \qquad i = 2, \ldots, N. \tag{8.45}$$

Note that here the upper limit of the interval to which r belongs is one less than that in (8.43) so as to avoid any nodes coinciding.

To extract a random grid from the available data, the grid nodes of the fine grid $x^f_i, i = 1, \ldots, N_f + 1$ are first permuted randomly. We shall denote the resulting points as $\tilde{x}^f_i, i = 1, \ldots, N_f + 1$. We begin to form a random grid of $N + 1$ nodes by selecting the first $N + 1$ nodes from the permuted fine grid so we have

$$x_i = \tilde{x}^f_i, \qquad i = 1, \ldots, N + 1. \tag{8.46}$$

The nodes $x_i, i = 1, \ldots, N + 1$ are then sorted into ascending order and the endpoints are replaced as

$$x_1 = a = 0, \qquad x_{N+1} = b = 1. \tag{8.47}$$

Let us now consider the three-peak simulated ecological test case as shown in Fig. 8.4b. As above, we generate a sequence of increasingly refined grids and the relative errors are calculated according to (8.7). It should be noted that since the exact value of the integral is not available to us for such discrete data, we have taken the approximation obtained by applying the trapezoidal rule to the extremely fine, regular grid of $N_f + 1$ nodes to be the 'exact' value of the pest abundance I. For the quasi-random and random grids, $n_r = 10^4$ of each grid are generated and the mean of the errors is calculated.

Convergence curves for the slightly irregular grids, where one node is randomly shifted from its original location on a regular grid, are shown in Fig. 8.13. The integration error (8.7) computed for the statistical rule (8.31) is presented in

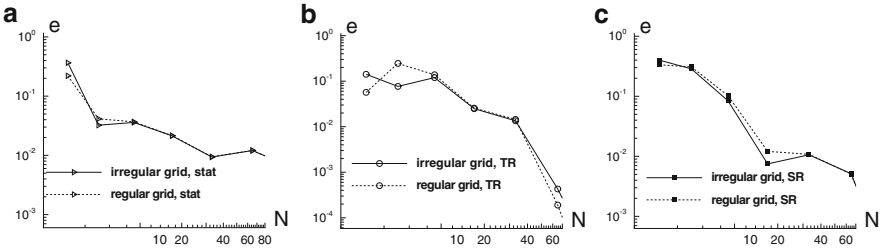

Fig. 8.13 Convergence curves on slightly irregular grids for the ecologically meaningful density distribution of Fig. 8.4b. Convergence on a sequence of grids where a central grid node is randomly shifted is compared to the convergence on regular grids. The figure legend is the same as in Fig. 8.12. (**a**) The statistical rule (8.31), (**b**) the trapezoidal rule (8.39), and (**c**) the Simpson rule (8.40) is implemented

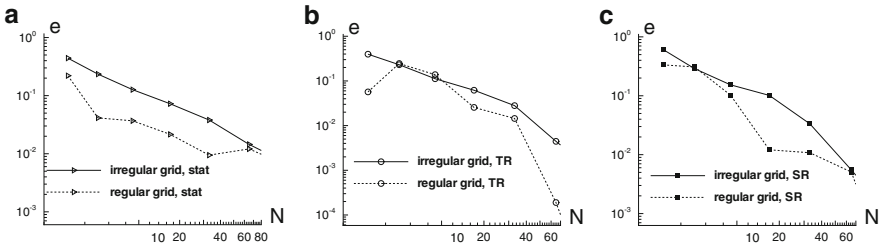

Fig. 8.14 Convergence curves on quasi-random grids for the ecologically meaningful density distribution of Fig. 8.4b. Convergence on a sequence of grids where each interior grid node is randomly shifted around its position on a regular grid is compared to the convergence on regular grids. The figure legend is the same as in Fig. 8.12. (**a**) The statistical rule (8.31), (**b**) the trapezoidal rule (8.39), and (**c**) the Simpson rule (8.40) is implemented

Fig. 8.13a, while the error for the trapezoidal rule (8.39) and the Simpson rule (8.40) is shown in Fig. 8.13b, c, respectively. The convergence results in the figure confirm our previous conclusion made for the function (8.10). A slight perturbation of grid regularity results in a slight perturbation in the integration error.

Let us now make a stronger perturbation of a regular grid and consider numerical integration on a sequence of quasi-random grids where each interior grid node is randomly shifted around its position on a regular grid. The corresponding convergence curves are shown in Fig. 8.14, where the figure legend is the same as in Fig. 8.12. It can be seen from the figure that increasing the degree of grid randomness in the problem results in a bigger integration error, no matter what integration method is used. This conclusion is further illustrated by consideration of the integration error on truly random grids; see Fig. 8.15. Again, the convergence curves shown in Fig. 8.15 for integration on regular grids always lie below convergence curves obtained for random grids for any integration rule employed in the problem.

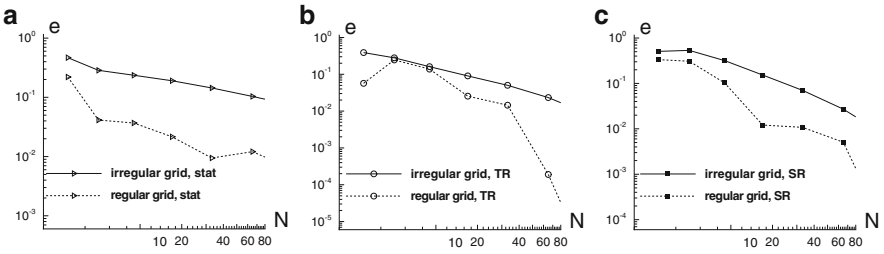

Fig. 8.15 Convergence curves on regular and random grids for the ecologically meaningful density distribution of Fig. 8.4b. The figure legend is the same as in Fig. 8.12. (**a**) The statistical rule (8.31), (**b**) the trapezoidal rule (8.39), and (**c**) the Simpson rule (8.40) is implemented

The results of our study demonstrate that grid randomisation leads to a bigger integration error on coarse and fine grids alike. Surprisingly, this conclusion is true even for the statistical method which has no spatial dependence. While further careful study of this issue is required, our first experience with the problem of numerical integration on random grids demonstrates that an equidistant distribution of traps is better than a random distribution.

8.7 Concluding Remarks

We considered the application of methods of numerical integration to the problem of evaluating pest insect abundance. Methods of numerical integration are well known and documented in the literature, but, to our best knowledge, they have never been applied in ecological problems. Meanwhile, employing advanced numerical integration techniques can be beneficial in the evaluation of total pest population size, as those techniques can help to improve the accuracy of evaluation. In our paper we studied a trapping procedure in an agricultural field and discussed how information about the pest population density at trap locations can be transformed into a numerical integration problem. However, our conclusions about the applicability of methods of numerical integration in ecological problems are general enough and therefore remain valid when the information about the local species density is obtained by another sampling technique.

The key idea behind numerical integration methods considered in the paper is to locally replace the existing density distribution by an approximated density distribution described by a polynomial function. The most straightforward way to apply numerical integration is to install traps at the nodes of a regular grid, but similar techniques can be designed for a random distribution of traps over an agricultural field. From a numerical integration viewpoint the method (8.31) widely used in ecological applications can be loosely interpreted as local approximation of the density function by a constant. While such approximation provides in some

cases rather poor accuracy, approximation by higher order polynomials (e.g. by a quadratic function) should result, according to the theory of numerical integration, in more accurate evaluation of pest abundance. It has been shown in the paper that advanced numerical integration techniques (e.g., the Simpson rule on regular grids) often provide a significantly more accurate estimate of the population size from trap data than the standard statistical approach (8.31). In many cases methods remain effective even when the distribution exhibit a complex spatial structure.

At the same time, it was discussed in the paper that the application of numerical integration methods in ecological problems may be restricted by the poor resolution of the density distribution on coarse grids. Our study demonstrated that numerical integration methods may become unreliable when pest abundance is evaluated from a heterogeneous density pattern on a coarse grid. For example, the accuracy of the Simpson method (8.17) is superior to the statistical rule (8.31) and the trapezoidal rule (8.15), but the Simpson method has no visible advantage over less accurate methods (8.31) and (8.15) when a strongly heterogeneous density distribution is considered on a coarse grid of traps. In the extreme case when the total population is localised in a small sub-domain, an estimate of the total population size becomes a random variable, and we cannot even tell whether or not the estimate is within a given accuracy range.

The coarse grid problem remains, in our opinion, the main obstacle to the implementation of numerical integration methods in IPM programmes. It was shown in the paper that grid coarseness is not defined by the number of traps available in the problem. For any fixed number of traps, that number can be considered as a grid with good resolution for one density pattern, while the same grid of traps can appear as a coarse grid, where the accuracy of evaluation is poor, for another density distribution. Our study confirmed that grid coarseness is directly related to the degree of heterogeneity, highly aggregated density distributions being the most difficult case for numerical integration. Meanwhile, ecologists and farmers often have to deal with pest insect density distributions that have a considerable degree of aggregation (Comins et al. 1992; Malchow et al. 2008; Okubo 1986). Thus an important conclusion that stems from our results is that any information about the spatial pattern of the pest insect density distribution must be used to its fullest extent (cf. Perry 1996; Perry and Hewitt 1991) in order to decide whether or not we can expect to obtain an accurate estimate of pest abundance. This conclusion is true for any numerical integration technique including the method (8.31), as examples studied in the paper reveal that an estimate of the mean density on coarse grids can be very far away from its true value. Let us also note that the unreliability of results on coarse grids should, in our opinion, be taken into account as another risk factor when a sampling plan is designed, and results of large-scale ecological monitoring should be interpreted accordingly.

Summarising the above, the main recommendation from our study is to implement methods of numerical integration that are based on approximation of the density distribution by higher order polynomials (e.g. the Simpson method). If heterogeneity in a spatial pattern is not well resolved, no method of numerical integration has an advantage over the other methods, as all of them will give equally

unreliable results. However, as soon as the heterogeneity is resolved, approximation of the density distribution by higher order polynomials will provide a more accurate estimate of the total pest population size.

Our study leaves a number of open questions. The most difficult and crucial issue is, of course, the question of how to get information about a spatial pattern of the density distribution in order to be able to predict the accuracy of integration. Another important issue related to the question above is the optimisation of trap locations. Grid adaptation to the spatial pattern can be made if we have the information about patches of high density. Numerical integration on an adapted grid should result in an improvement in accuracy, but its application requires further discussion of the technical details. Also, numerical integration techniques can be extended to domains of arbitrary shape, but resolution of a curvilinear boundary remains a topic for future research.

Finally, we would like to emphasise that numerical integration techniques still have to be validated for a broad variety of ecological test cases before they can be routinely used in ecological monitoring and control. However, identification and clear understanding of all theoretical aspects of numerical integration techniques can accelerate and simplify further incorporation of those techniques into IPM programmes and the issues that have been in the focus of this paper are important milestones along the way.

References

Alavanja MCR, Ross MK, Bonner MR (2013) Increased cancer burden among pesticide applicators and others due to pesticide exposure. CA Cancer J Clin 63:120–142

Alexander CJ, Holland JM, Winde L et al (2005) Performance of sampling strategies in the presence of known spatial patterns. Ann Appl Biol 146:361–370

Alyokhin A, Baker M, Mota-Sanchez D et al (2008) Colorado potato beetle resistance to insecticides. Am J Potato Res 85:395–413

Apostol TM (1974) Mathematical analysis. Addison-Wesley, Reading

Ausden M (1996) Invertebrates. In: Sutherland WJ (ed) Ecological census techniques: a handbook. Cambridge University Press, Cambridge

Barclay HJ (1992) Modelling the effects of population aggregation on the efficiency of insect pest control. Res Popul Ecol 34:131–141

Bates SL, Zhao JZ, Roush RT, Shelton AM (2005) Insect resistance management in GM crops: past, present and future. Nat Biotechnol 23:57–62

Binns MR, Nyrop JP, Van Der Werf W.(2000) Sampling and monitoring in crop protection: the theoretical basis for designing practical decision guides. CABI Publishing, Wallingford

Birmingham AL, Kovacs E, Lafontaine JP et al (2011) A new trap and lure for Drosophila melanogaster (Diptera: Drosophilidae). J Econ Entomol 104:1018–1023

Blackshaw RP (1983) The annual leatherjacket survey in Northern Ireland, 1965–1982, and some factors affecting populations. Plant Pathol 32:345–349

Bliss CI (1941) Statistical problems in estimating populations of Japanese beetle larvae. J Econ Entomol 34:221–232

Browde JA, Pedigo LP, Degooyer TA et al (1992) Comparison of sampling techniques for grasshoppers (Orthoptera: Acrididae) in soybean. J Econ Entomol 85:2270–2274

Burn AJ, Coaker TH, Jepson PC (1987) Integrated pest management. Academic, New York

Byers JA, Anderbrant O, Löfqvist J (1989) Effective attraction radius: a method for comparing species attractants and determining densities of flying insects. J Chem Ecol 15:749–765
Christou P, Capell T, Kohli A et al (2006) Recent developments and future prospects in insect pest control in transgenic crops. Trends Plant Sci 11:302–308
Comins HN, Hassell MP, May RM (1992) The spatial dynamics of host-parasitoid systems. J Anim Ecol 61:735–748
Davis PM (1994) Statistics for describing populations. In: Pedigo LP, Buntin GD (eds) Handbook of sampling methods for arthropods in agriculture. CRC Press, Boca Raton, pp 33–54
Davis PJ, Rabinowitz P (1975) Methods of numerical integration. Academic, New York
Dent D (2000) Insect pest management. CABI Publishing, Wallingford
Embleton NL, Petrovskaya NB (2013) On numerical uncertainty in evaluation of pest population size. Ecol Complex 14:117–131
Embleton NL, Petrovskaya NB (2014) A novel approach to evaluation of pest insect abundance in the presence of noise. Bull Math Biol 76:718–743. doi:10.1007/s11538-014-9940-z
Ester A, van Rozen K (2005) Monitoring and control of Agriotes lineatus and A. obscurus in arable crops in the Netherlands. IOBC Bull Insect Pathog Insect Parasit Nematodes Melolontha 28:81–86
Evans EW, Rogers RA, Opfermann DJ (1983) Sampling grasshoppers (Orthoptera: Acrididae) on burned and unburned tallgrass prairie: night trapping vs. sweeping. Environ Entomol 12: 1449–1454
Ferguson AW, Klukowski Z, Walczak B et al (2000) The spatio-temporal distribution of adult Ceutorhynchus assimilis in a crop of winter oilseed rape in relation to the distribution of their larvae and that of the parasitoid Trichomalus perfectus. Ent Exp Appl 95:161–171
Ferguson AW, Klukowski Z, Walczak B et al (2003) Spatial distribution of pest insects in oilseed rape: implications for integrated pest management. Agric Ecosyst Environ 95:509–521
Gatehouse AMR, Ferry N, Edwards MG, Bell HA (2011) Insect-resistant biotech crops and their impacts on beneficial arthropods. Philos Trans R Soc B Biol Sci 366:1438–1452
Gwinner J, Harnisch R, Mück O (1996) Manual of the prevention of post-harvest grain losses. GTZ, Eschborn
Hagler JR, Jackson CG (2001) Methods for marking insects: current techniques and future prospects. Ann Rev Entomol 46:511–543
Higley LG, Pedigo LP (1996) Economic thresholds for integrated pest management. University of Nebraska Press, Lincoln
Hokkanen HMT (1991) Trap cropping in pest management. Ann Rev Entomol 36:119–138
Holland JM, Perry JN, Winder L (1999) The within-field spatial and temporal distribution of arthropods in winter wheat. Bull Entomol Res 89:499–513
Hutchins SH (1994) Techniques for sampling arthropods in integrated pest management. In: Pedigo LP, Buntin GD (eds) Handbook of sampling methods for arthropods in agriculture. CRC, Boca Raton, pp 73–97
Jepson PC, Thacker JRM (1990) Analysis of the spatial component of pesticide side-effects on non-target invertebrate populations and its relevance to hazard analysis. Funct Ecol 4:349–355
Karandinos MG (1976) Optimum sample size and comments on some published formulae. Bull Entomol Soc Am 22:417–421
Kogan M (1998) Integrated pest management: historical perspectives and contemporary developments. Ann Rev Entomol 43:243–270
Legg DE, Moon RD (1994) Bias and variability in statistical estimates. In: Pedigo LP, Buntin GD (eds) Handbook of sampling methods for arthropods in agriculture. CRC, Boca Raton, pp 55–69
Liebman M, Dyck E (1993) Crop rotation and intercropping strategies for weed management. Ecol Appl 3:92–122
Louws FJ, Rivard CL, Kubota C (2010) Grafting fruiting vegetables to manage soilborne pathogens, foliar pathogens, arthropods and weeds. Scientia Horticulturae 127:127–146
Malchow H, Petrovskii SV, Venturino E (2008) Spatiotemporal patterns in ecology and epidemiology: theory, models, and simulations. Chapman & Hall/CRC, London

Mayor JG, Davies MH (1976) A survey of leatherjacket populations in south-west England, 1963–1974. Plant Pathol 25:121–128
Metcalf RL, Luckmann WH (eds) (1982) Introduction to insect pest management. Wiley, London
Milne A (1959) The centric systematic area-sample treated as a random sample. Biometrics 15:270–297
Murchie AK, Harrison AJ (2004) Mark-recapture of 'New Zealand flatworms' in grassland in Northern Ireland. In: Proceedings crop protection in Nothern Britain: 2004, Association for Crop Protection in Northern Britain, Dundee, Scotland
Murray JD (1989) Mathematical biology. Springer, Berlin
Northing P (2009) Extensive field based aphid monitoring as an information tool for the UK seed potato industry. Aspects Appl Biol 94:31–34
Oerke EC (2006) Crop losses to pests. J Agric Sci 144:31–43
Okubo A (1986) Dynamical aspects of animal grouping: swarms, schools, flocks, and herds. Adv Biophys 22:1–94
Pascual MA, Kareiva P (1996) Predicting the outcome of competition using experimental data: Maximum likelihood and Bayesian approaches. Ecology 77:337–349
Pedigo LP, Rice ME (2009) Entomology and pest management. Pearson Prentice Hall, Upper Saddle River
Perry JN (1996) Simulating spatial patterns of counts in agriculture and ecology. Comput Electron Agric 15:93–109
Perry JN, Hewitt M (1991) A new index of aggregation for animal counts. Biometrics 47: 1505–1518
Petrovskaya NB, Embleton NL (2013) Evaluation of peak functions on ultra-coarse grids. Proc R Soc A 469:20120665. http://dx.doi.org/10.1098/rspa.2012.0665
Petrovskaya NB, Embleton NL, Petrovskii SV (2013) Numerical study of pest population size at various diffusion rates. In: Lewis MA et al (eds) Dispersal, individual movement and spatial ecology. Lecture notes in mathematics. Springer, Berlin/Heidelberg 2071:355–386
Petrovskaya NB, Petrovskii SV (2010) The coarse-grid problem in ecological monitoring. Proc R Soc A 466:2933–2953
Petrovskaya NB, Petrovskii SV, Murchie AK (2012) Challenges of ecological monitoring: estimating population abundance from sparse trap counts. J R Soc Interface 9:420–435
Petrovskaya NB, Venturino E (2011) Numerical integration of sparsely sampled data. Simul Model Pract Theory 19:1860–1872
Petrovskii SV, Bearup D, Ahmed DA, Blackshaw RP (2012) Estimating insect population density from trap counts. Ecol Complex 10:69–82
Petrovskii SV, Li B-L, Malchow H (2003) Quantification of the spatial aspect of chaotic dynamics in biological and chemical systems. Bull Math Biol 65:425–446
Petrovskii SV, Malchow H (2001) Spatio-temporal chaos in an ecological community as a response to unfavorable environmental changes. Adv Complex Syst 4:227–250
Petrovskii SV, Malchow H, Hilker FM, Venturino E (2005) Patterns of patchy spread in deterministic and stochastic models of biological invasion and biological control. Biol Invasions 7:771–793
Petrovskii SV, Morozov AY, Venturino E (2002) Allee effect makes possible patchy invasion in a predator-prey system. Ecol Lett 5:345–352
Pimentel D (1995) Amounts of pesticides reaching target pests: environmental impacts and ethics. J Agric Environ Ethics 8:17–29
Pimentel D (ed) (1997)Techniques for reducing pesticide use: economic and environmental benefits. Wiley, New York
Pimentel D (2009) Pesticides and pest control. In: Peshin R, Dhawan AK (eds) Integrated pest management: innovation-development process, vol 1. Springer, Berlin, pp 83–87
Pimentel D, Greiner A (1997) Environmental and socio-economic costs of pesticide use. In: Pimentel D (ed) Techniques for reducing pesticide use: economic and environmental benefits. Wiley, New York, pp 51–78
Pimentel D, Pimentel M (2008) Food, energy and society. CRC, Boca Raton

Raworth DA, Choi MJ (2001) Determining numbers of active carabid beetles per unit area from pitfall-trap data. Ent Exp Appl 98:95–108

Reisen WK, Lothrop HD (1999) Effects of sampling design on the estimation of adult mosquito abundance. J Am Mosq Control Assoc 15:105–114

Ruberson JR (ed) (1999) Handbook of pest management. Marcel Dekker, New York

Sherratt JA, Smith M (2008) Periodic travelling waves in cyclic populations: field studies and reaction diffusion models. J R Soc Interface 5:483–505

Shoffner AV, Tooker JF (2013) The potential of genotypically diverse cultivar mixtures to moderate aphid populations in wheat (Triticum aestivum L.) Arthropod-Plant Interact 7:33–43

Shigesada N, Kawasaki K (1997) Biological invasions: theory and practice. Oxford University Press, Oxford

Silver JB (2008) Mosquito ecology: field sampling methods. Springer, New York

Smigocki AC, Ivic-Haymes S, Li H, Savić J (2013) Pest protection conferred by a beta vulgaris serine proteinase inhibitor gene. PLoS ONE 8:e57303. doi:10.1371/journal.pone.0057303

Snedecor GW, Cochran WG (1980) Statistical methods. The Iowa State Iniversity Press, Ames

Sohrabi F, Shishehbor P, Saber M, Mosaddegh MS (2013) Lethal and sublethal effects of imidacloprid and buprofezin on the sweetpotato whitefly parasitoid Eretmocerus mundus (Hymenoptera: Aphelinidae). Crop Protection 45:98–103

Southwood TRE, Henderson PA (2000) Ecological methods. Blackwell Science, Oxford

Stern VM (1973) Economic thresholds. Ann Rev Entomol 18:259–280

Stern VM, Smith RF, van den Bosch R, Hagen KS (1959) The integration of chemical and biological control of the spotted alfalfa aphid. Part I. The integrated control concept. Hilgardia 29:81–101

Taboada A, Pérez-Aguirre C, Assmann T (2012) A new method for collecting agile tiger beetles by live pitfall trapping. Ent Exp Appl 145:82–87

Turchin P (2003) Complex population dynamics: a theoretical/empirical synthesis. Princeton University Press, Princeton

Vinatier F, Chailleux A, Duyck P-F et al (2010) Radiotelemetry unravels movements of a walking insect species in heterogeneous environments. Anim Behav 80:221–229

Vlug HJ, Paul H (1986) Sampling leatherjackets. Med Fac Landbouww Rijksuniv Gent 51:939–942

Ward SA, Rabbinge R, Mantel WP (1985) The use of incidence counts for estimation of aphid populations. 1. Minimum sample size for required accuracy. Neth J Plant Pathol 91:93–99

Chapter 9
Models for Overdispersed Data in Entomology

Clarice G.B. Demétrio, John Hinde, and Rafael A. Moral

Abstract Entomological data are often overdispersed, characterised by a larger variance than assumed by simple standard models. It is important to model overdispersion properly in order to avoid incorrect and misleading inferences. Outcomes of interest are often in the form of counts or proportions and we present extended models that incorporate overdispersion, methods to assess its impact and model goodness-of-fit, and techniques to test treatment differences in the presence of overdispersion.

Keywords Overdispersion • Statistical models • Count data • Proportion data • Zero-inflated data

9.1 Introduction

Outcomes of interest for entomological data are often in the form of counts or proportions and as a first step we might analyse these using standard Poisson and binomial models. These are both specific examples of generalized linear models (McCullagh and Nelder 1989) and hence our focus here on this class of models. However, in general, the data are overdispersed, characterised by a larger variance than assumed by these simple standard models. It is important to adapt models to take account of overdispersion in order to avoid incorrect and misleading inferences (Hinde and Demétrio 1998). In this chapter we will consider some general approaches for doing this and illustrate with specific examples.

C.G.B. Demétrio (✉) • R.A. Moral
Departamento de Ciências Exatas, Escola Superior de Agricultura "Luiz de Queiroz", Piracicaba, São Paulo, Brazil
e-mail: clarice.demetrio@usp.br; rafael.moral@usp.br

J. Hinde
School of Mathematics, Statistics and Applied Mathematics, National University of Ireland Galway, Galway, Ireland
e-mail: john.hinde@nuigalway.ie

C.P. Ferreira, W.A.C. Godoy (eds.), *Ecological Modelling Applied to Entomology*, Entomology in Focus 1, DOI 10.1007/978-3-319-06877-0_9

There are many different possible causes of overdispersion and in specific situations a number of these could be involved. Some common possibilities in entomological studies are:

1. **Variability of experimental material** – this can be thought of as individual variability of the experimental units and may give an additional component of variability that is not accounted for by the basic response model. For example, in dose-response experiments, the insects used will typically have differing susceptibilities to the substance which will affect propensity to respond.
2. **Correlation between individual responses** – in biological assays involving batches of insects we may expect to see some correlation between insects from the same batch since they may be genetically similar. There may also be correlation due to shared experimental environments or through observing a group of insects over time.
3. **Cluster and multistage sampling** – often, instead of a simple random sample, the insects under study may be structured into some hierarchy with sampling sequentially from each level. For example, we may consider insects within metapopulations within ecosystems. In our sampling we may take a random sample of ecosystems, then from these selected ecosystems we may pick a random sample of metapopulations, and, finally, take our observational units from a random sample of insects in these selected metapopulations. This structured hierarchical sampling can lead to complex dependencies between the individual level responses and certainly we are likely to see correlation between the responses within a given metapopulation.
4. **Aggregation** – here the individual level responses are grouped into a response at a higher, aggregate, level. The aggregation process may be known, but more generally it is not completely specified and leads to a compound distribution for the observed responses. For example, in biological control studies we may observe total numbers of insects emerged from larvae parasitised by a number of females, but given that generally every female can lay a different number of eggs per host the observed totals of insects will be a combination of the number of females that parasitised the larvae and the distribution of the number of eggs per female; any modelling may more sensibly apply to the numbers of insects from the same female, but this is not observed, only the total number of insects emerged from a number of parasitised larvae.
5. **Omitted unobserved variables** – in some sense the above categories are all special cases of this, but generally in a rather complex way. Our models will often be formulated with the notion of some omitted variable to account for possible underlying, but unobserved, structure. This is particularly relevant in the regression modelling context.

In some circumstances the cause of the overdispersion may be apparent from the nature of the data collection process. Although, it should be noted that different explanations of the overdispersion process can lead to the same model. In general, it is difficult to infer the precise cause, or underlying process, leading to the overdispersion. However, the causes mentioned above provide a useful framework

for thinking about overdispersion in practical applications, even if the distinctions are not always sharp. This will become apparent in the subsequent development of overdispersion models and some applications.

However overdispersion may arise, its presence will be apparent through some failure of the basic model assumptions. In this chapter we will begin by considering how to detect these model failures in categorical and count data and then consider model extensions to account for overdispersion. We will also illustrate the effect of ignoring overdispersion on key questions of interest, such as treatment comparisons.

9.2 Models for Proportion Data

One of the simplest forms of data in entomology consists of observing a number of insects and counting the number that respond to some stimulus, with the aim of possibly comparing different treatments or environments, or perhaps studying a dose-response relationship. In this context our variable of interest is an observed (counted) proportion y/m, where we have y insects responding out of a group of size m. If we assume that each individual insect has the same chance of responding and they act independently then the binomial distribution gives a natural starting point for data analysis.

9.2.1 Binomial Model

Outcomes which can be classified as response/non-response can be thought of as arising from a Bernoulli trial.[1] Taking a group of m independent Bernoulli outcomes with constant response probability π and counting the total number of insects that respond, y, leads to the binomial probability model

$$\Pr(Y = y) = \binom{m}{y} \pi^y (1-\pi)^{m-y} \quad y = 0, 1, \ldots, m \tag{9.1}$$

denoted by Binomial(m, π). This is simply the distribution of the sum of m independent Bernoulli random variables. The binomial coefficient $\binom{m}{y}$ arises from the number of possible sequences of m Bernoulli trials that give rise to y responses.

If we extend this to a sample of n groups of observations, we obtain a set of random variables Y_i, $i = 1, \ldots, n$, with possibly different response probabilities

[1] A Bernoulli trial is a random experiment with exactly two possible outcomes, "success" and "failure", in which the probability of success is the same every time the experiment is conducted.

π_i, representing counts of responses from samples of size m_i. We can summarise this as the model $Y_i \sim \text{Binomial}(m_i, \pi_i)$, where Y_i has mean

$$\text{E}(Y_i) = \mu_i = m_i \pi_i,$$

and variance

$$\text{Var}(Y_i) = m_i \pi_i (1 - \pi_i) = \mu_i \left(1 - \frac{\mu_i}{m_i}\right). \tag{9.2}$$

In general we will be interested in modelling the π_is in terms of p observed explanatory variables, $\mathbf{x}$, which may include continuous variates (e.g. doses) and/or sets of $0/1$ dummy variables to represent one or more factors that classify the data into groups (e.g. treatments, species). (We will also assume that $\mathbf{x}$ includes a constant term to account for the overall response rate.) This is conveniently done through the framework of generalized linear models which allow us to model the expected proportions π_i in terms of explanatory variables $\mathbf{x}_i$ through a transformed linear function

$$g(\pi_i) = \boldsymbol{\beta}^T \mathbf{x}_i = \eta_i$$

where g is some suitable function, called the *link* function and $\boldsymbol{\beta}$ is a vector of p unknown parameters.

It is important to note that although we are modelling the mean response through the π_is, the variance of Y_i is a simple fixed function of the mean which constrains how the model can account for the observed variability in proportion data. In general, for real data sets the observed variance is larger than that implied by the binomial model – observed overdispersion.

To complete the binomial regression model specification we need to consider the choice of the link function g. The usual (canonical) link function for the binomial distribution is the logit link

$$g(\mu_i) = \log\left(\frac{\mu_i}{m_i - \mu_i}\right) = \log\left(\frac{\pi_i}{1 - \pi_i}\right)$$

which corresponds to modelling on the log-odds scale with regression parameters corresponding to log odds-ratios. Other common choices of link function for proportion data are the probit

$$g(\mu_i) = \Phi^{-1}(\mu_i / m_i) = \Phi^{-1}(\pi_i),$$

based on an underlying normal tolerance distribution for the probability of a positive response, and the complementary log-log (CLL) link

$$g(\mu_i) = \log\{-\log(1 - \mu_i / m_i)\} = \log\{-\log(1 - \pi_i)\}.$$

The probit and logit links are very similar and are symmetric in π and $1-\pi$, while the CLL link is not symmetric and can lead to rather different fits in certain cases and can be useful in experiments where over time the insect population becomes increasingly resistant to the insecticide, see Mallet (1989). The probit has a long history in biological assays and dose-response studies, see Finney (1971), although in general the logit is now preferred. A common feature of all of these link functions is that they transform the response probability π from $[0, 1]$ to the real line where the linear regression model $\boldsymbol{\beta}^T\mathbf{x}$ can be sensibly applied – direct modelling of π can lead to non-sensical fitted values and should be avoided.

Inference for generalized linear models proceeds in the same way as for standard normal linear regression models. Testing an individual term in the regression model can be based on the parameter estimate and associated standard error, while tests for groups of terms (e.g. a factor) and model comparison are based on the *analysis of deviance* from Nelder and Wedderburn (1972), which generalizes the ideas in standard ANOVA. Here, the usual residual sum of squares is replaced by the residual deviance, a measure that compares a fitted model to a saturated model (with n regression parameters) that reproduces the observed data. For the binomial model this deviance is given by

$$D_B = 2\sum_{i=1}^{n}\left[y_i \log\left(\frac{y_i}{\hat{\mu}_i}\right) + (m_i - y_i)\log\left(\frac{m_i - y_i}{m_i - \hat{\mu}_i}\right)\right],$$

where $\hat{\mu}_i$, $i = 1, 2, \ldots, n$, are the fitted values for the model of interest. The deviance D_B can be viewed as a measure of goodness-of-fit of the fitted model with p estimated parameters. A more traditional goodness-of-fit statistic is the Pearson X^2 statistic, which for binomial data takes the form

$$X_B^2 = \sum_{i=1}^{n}\frac{(y_i - \hat{\mu}_i)^2}{\widehat{\mathrm{Var}}(Y_i)} = \sum_{i=1}^{n}\frac{(y_i - \hat{\mu}_i)^2}{\hat{\mu}_i\left(1 - \frac{\hat{\mu}_i}{m_i}\right)}.$$

For data with large sample sizes m_i, D_B and X_B^2 are equivalent and under the null hypothesis of an adequate model both have an approximate χ^2 distribution on $n-p$ degrees of freedom (df). However, Jørgensen (2002) recommends using X_B^2 rather than D_B as a measure of goodness-of-fit, based on numerical and analytical studies which show that the limiting χ^2 distribution is approached faster (as the sample sizes m_i increase) for the X^2 statistic than for D. So, for a well-fitting (adequate) model we would expect X_B^2 to be consistent with the χ^2_{n-p} distribution and at a significance level α we would require $X_B^2 < \chi^2_{n-p;(1-\alpha)}$, the upper α-percentage point of the χ^2_{n-p} distribution. More informally, we may simply check to see if $X_B^2 \approx n-p$, that is if the observed value is of the same order as the mean of the χ^2_{n-p}. An incorrect, or inadequate, model with unexplained variation (overdispersion) will lead to much larger observed values of X_B^2 (and D_B).

In addition to providing a measure of fit, the deviance plays a central role in comparing different nested models and hence testing groups of one or more effects. The choice of the deviance for this, rather than the Pearson X^2, is because it has the same sort of additive breakdown that the sum of squares has in standard regression and analysis of variance. For example, suppose that we consider dropping some variables from our original p-variate model to give a sub-model with only $q < p$ variates – this corresponds to setting the β-coefficients of the $p-q$ eliminated terms to zero. Writing D_p for the residual deviance of the full model and D_q as that for the reduced model, then under the null hypothesis that true coefficient values of omitted terms really are zero the change in deviance $D_q - D_p$ should have a χ^2_{p-q} distribution. So a formal test at significance level α will reject the null hypothesis if $D_q - D_p > \chi^2_{p-q;(1-\alpha)}$ indicating that some, or all, of the omitted terms need to be retained (this actually corresponds to a likelihood-ratio test for comparing the nested models). A model selection process involves a combination of such tests for terms of possible interest and the use of the goodness-of-fit to check that any selected models are adequate descriptions of the data.

To complete the checking of a model, in addition to the global goodness-of-fit, it is useful to use some diagnostic plots to detect specific aspects of possible model failure. The procedures typically compare the observed and fitted values for the individual observations through some type of *residual* and the simplest forms of these are the n individual contributions to the X^2 and D statistics giving the Pearson and deviance residuals, respectively. Typical plots may include:

- Observed and fitted values versus continuous explanatory variables to examine overall model fit;
- Residuals (deviance or Pearson) versus fitted values to check model adequacy, detect outliers and other unusual features;
- (Half-)normal plot of the residuals, with an added model-based simulation envelope (Hinde and Demétrio 1998), to check that the residuals are consistent with the variation implied by the model.

The whole process of modelling proportion data is most easily illustrated through example analyses. We will begin with a situation where the binomial model is found to be appropriate. Subsequently, we will see that the same general approach applies not only for proportion data where the binomial model is not adequate but also for other data types within the generalized linear modelling framework.

Example 1: Dose-response model

The neuropteran *Chrysoperla externa* (Neuroptera: Chrysopidae) is a predator that acts as a natural enemy of the brown citrus aphid, *Toxoptera citricida* (Hemiptera: Aphididae), which is among the most important citrus pests worldwide. A substance called "lime sulphur" is a product made of calcium polysulphides and used to control fungi, bacteria and insects that live on trees. A possible strategy to control *T. citricida* populations would be to use lime sulphur and the *C. externa* predator in combination which may be beneficial as long as the lime sulphur has less

Table 9.1 *Chrysoperla externa* lime sulphur mortality data (table entries: dead/number of larvae, y_i/m_i)

Concentration (ppm)	Replicates					
0	0/2	0/5	1/4	0/5	0/3	0/6
60	0/6	2/6	0/5	0/5	0/4	1/5
600	1/3	1/5	2/3	2/6	1/5	0/4
6,000	0/1	0/5	1/5	2/4	3/7	2/5

effect on the predator than the prey. To explore this Battel (2012) conducted an experiment with first-instar larvae of *Chrysoperla externa* exposed to different levels of lime sulphur. Specifically, 24 Orange Jessamine (*Murraya paniculata*) plants were sprayed with different concentrations (`conc`) of lime sulphur and up to 7 first-instar larvae (m_i) were placed on each plant. The experiment was set up in a completely randomized design with four treatments: lime sulphur concentrations at 0 ppm (water control), 60 ppm, 600 ppm, and 6,000 ppm. The plants were observed until the predators reached the second instar and the number of larvae that died on each plant (y_i) was recorded. The data is presented in Table 9.1.

We now consider fitting a standard binomial logit model in R (R Core Team 2013). Here, the concentrations are proportional to powers of 10 and so it is more natural to use the logarithm of the concentrations in our models and because of the control at 0 ppm we add 1 before taking the log (this is rather arbitrary and alternatives could be explored if the model is poor, such as allowing for natural mortality). The full R-code to do this is given below (in subsequent examples we will omit data input details as the full code will be available as "Electronic Supplementary Material").

```
# set-up data
dead <- c(0, 0, 1, 0, 0, 0, 0, 2, 0, 0, 0, 1,
          1, 1, 2, 2, 1, 0, 0, 0, 1, 2, 3, 2)
alive <- c(2, 5, 3, 5, 3, 6, 6, 4, 5, 5, 4, 4,
           2, 4, 1, 4, 4, 4, 1, 5, 4, 2, 4, 3)
conc <- rep(c(0,60,600,6000),each=6)
lconc <- log(conc+1)
resp <- cbind(dead, alive)
total <- dead + alive
# fit model using conc levels both on log-scale and
  as a factor
# to produce simple analysis of deviance
model <- glm(cbind(dead, alive) ~  lconc +
                  factor(conc), family=binomial)
anova(model, test="Chisq")
# test adequacy of factor model using deviance and X2
1-pchisq(deviance(model), df.residual(model))
(X2 <- sum(residuals(model, type="pearson")^2))
1-pchisq(X2, df.residual(model))
```

Table 9.2 Analysis of deviance for the *Chrysoperla externa* mortality data, using a binomial logit model

Source	df	Deviance	p-value	X^2	p-value
Linear trend	1	8.73	< 0.01		
Non-linearity	2	0.91	0.63		
Residual	20	21.95	0.34	20.77	0.41

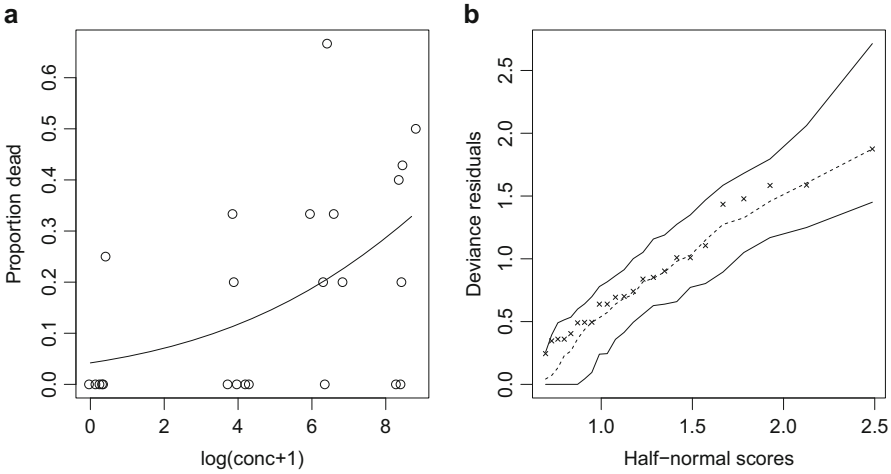

Fig. 9.1 *Chrysoperla externa* mortality data, log-dose binomial logit model: (**a**) fitted curve with observed proportions; (**b**) half-normal plot: × – data; —- – simulated envelope

This produces an analysis of deviance with a term by term breakdown as follows:

```
             df Deviance Resid. df Resid. Dev Pr(>Chi)
NULL                                23     31.594
lconc         1   8.7310         22     22.863 0.003129 **
factor(conc)  2   0.9141         20     21.949 0.633138
```

For convenience we have re-summarised this together with the goodness-of fit values in Table 9.2. The added contribution of specifying concentration as a (4-level) factor gives a test for non-linearity of the log-dose response.

For the factor model the values of the residual deviance $D_B = 21.95$ and Pearson statistic $X^2_B = 20.77$ are similar and consistent with a χ^2_{20} distribution as they are close to the mean value of 20 and considerably less than $\chi^2_{20,0.95} = 31.41$. This suggests an adequate model, but as there is also no evidence of non-linearity in the dose response we can use this linear trend model, which has a residual deviance of 22.86 on 22 df. We now refit this and produce some simple diagnostic plots presented in Fig. 9.1; a plot of the observed proportions with the fitted dose-response curve and a half-normal plot of the deviance residuals. The R-code is as follows:

```
model1 <- glm(resp ~ lconc, family=binomial)
par(mfrow=c(1,2), cex=1.4)
plot(jitter(lconc), dead/total, ylab="Proportion dead",
     xlab="log(conc+1)", main="(a)")
```

```
x <- seq(0, 8.7, .1)
pr <- predict(model1, data.frame(lconc=x), ty="response")
lines(x, pr)
# half-normal plot
hnp(model1, xlab="Half-normal scores",
    ylab="Deviance residuals", pch=4, main="(b)")
```

Neither of these show anything particularly unusual and in the half-normal plot the residuals lie completely within the simulated envelope, based on a binomial model, indicating the adequacy of the binomial modelling assumption. (Note that the simulated envelope is randomly generated and will be slightly different each time the function is called.)

Here, the interest is in finding a level of lime sulphur that is not too toxic to the predator, so the fact that the maximum estimated death proportion is only around 0.3 is not a problem. (In general dose-response studies we may want to select concentration level to give response proportions over the [0,1] range.) A common use of such fitted models is to determine a concentration level that kills some specified proportion, p, of the target insects, referred to as the $100p\,\%$ lethal (effective) concentration and denoted by LC_{100p}. For this example we might be interested in estimating a concentration level that kills *no more* than, say, 10 % of the predators, the LC_{10}, and its associated confidence interval. This involves using the fitted curve to read back from a specified proportion to the associated dose and can be done using the `dose.p` function in the R-package `MASS` (Venables and Ripley 2002).

```
require(MASS)
dose.p(model1, p=.10)
```

```
               Dose       SE
p = 0.1: 3.353481 1.49095
```

The above estimated dose is on the log-scale and converting this back to ppm gives $LC_{10} = 27.60$. While the simplest way to obtain a confidence interval is to construct an interval on the log-scale using the estimate and standard error from `dose.p` and then converting this interval back to the ppm scale, this approach is not optimal and other intervals include Fieller and profile-likelihood intervals, see Morgan (1992). Adopting the simple approach here gives an approximate 95 % confidence interval for LC_{10} of $[0.45, 563.18]$, although of course in this particular application a one-sided lower interval may be more appropriate.

9.2.2 Overdispersion Models

Now we will turn to look at an example where the assumption of the binomial model is less satisfactory and consider a first simple approach to allowing for overdispersion.

Example 2: Corn damage

A major pest of stored maize in Brazil is *Sitophilus zeamais* (Coleoptera: Curculionidae). In an experiment to assess the insecticide action of organic extracts of *Annona mucosa* (Annonaceae) Petri dishes containing 10 g of corn were treated with extracts prepared with different parts of the plant (seeds, leaves and branches) at a concentration of 1,500 mg/kg or just water (control), using a completely randomized design with 10 replicates. Then 20 *Sitophilus zeamais* adults were placed in each Petri dish and, after 60 days, the numbers of damaged and undamaged corn grains were counted, see Ribeiro et al. (2013). The data are given in Table 9.3.

We begin by fitting a standard binomial logit model with the different extracts and inspect the analysis of deviance and goodness-of-fit given in Table 9.4.

```
model1 <- glm(cbind(y, m-y) ~ extract, family=binomial)
anova(model1, test="Chisq")
hnp(model1, pch=4, main="Binomial: Logit",
    xlab="Half-normal scores", ylab="Deviance residuals")
```

Here, there is clear evidence from the residual deviance and X^2 values that the model does not fit – the replicates are more variable than we would expect under a binomial model. This can also be seen in the half-normal plot of the deviance residuals shown in Fig. 9.2a.

So having established that a particular dataset may exhibit overdispersion, how can we extend our basic model to take account of this? As we have discussed there are many different possible causes of overdispersion and consequently a number of different models and associated estimation methods have been proposed (see Hinde and Demétrio 1998 for a review). For binomial data, Collett (2003) gives a good practical introduction to some of these methods, following the work of Williams (1982, 1996). We will begin by considering a quasi-likelihood approach to accommodate increased variability.

Table 9.3 Corn damage data (table entries: damaged/no. of grains, y_i/m_i)

Extract	Replicates									
Leaf	26/35	25/36	21/38	18/38	30/39	8/38	12/34	33/38	23/36	18/37
Branch	28/36	29/35	26/37	19/37	28/36	29/37	22/39	10/37	26/34	18/35
Seed	0/35	1/35	0/36	0/34	1/35	0/37	0/35	0/35	2/36	0/35
Control	20/37	25/35	31/35	28/35	31/35	35/36	23/34	32/32	33/35	28/37

Table 9.4 Analysis of deviance for the corn damage data, using a binomial logit model

Source	df	Deviance	p-value	X^2	p-value
Extracts	3	636.04	< 0.01		
Residual	36	165.92	< 0.01	158.75	< 0.01

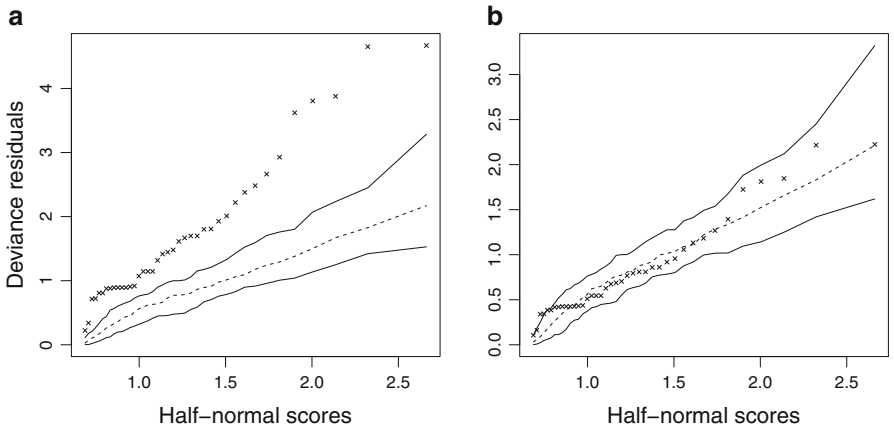

Fig. 9.2 Corn damage data – Half-normal plots with simulated envelopes of deviance residuals for (**a**) binomial and (**b**) quasi-binomial logit models

9.2.2.1 Quasi-likelihood

One of the simplest means to allow for overdispersion is to replace the mean-variance function of the original model by a more general form, typically involving additional parameters.

A constant overdispersion binomial model replaces (9.2) by

$$\mathrm{Var}(Y_i) = \phi m_i \pi_i (1 - \pi_i), \tag{9.3}$$

where the overdispersion factor $\phi\,(>\ 1)$ indicates that the increased variation for observation y_i depends on neither the sample size m_i nor the true response probability π_i. This is often referred to as the heterogeneity factor model, see Finney (1971).

Here, estimation of the regression parameters $\boldsymbol{\beta}$ is based on maximum quasi-likelihood (Wedderburn 1974) and for this constant overdispersion model the estimates $\hat{\boldsymbol{\beta}}$ are identical to those from the binomial model. (This arises as the key mean-variance relationship is of the same form for the binomial and quasi-binomial models; the constant scale factor ϕ is irrelevant here in the same way that the variance σ^2 does not affect parameter estimates in the usual normal regression model.) However, the assumed greater variability in (9.3) does have an impact on the standard errors of $\hat{\boldsymbol{\beta}}$ and these are inflated by a factor of $\sqrt{\phi}$ compared to those of the binomial ($\phi = 1$) model. To obtain an estimate for ϕ we can proceed analogously to estimating σ^2 in a normal model fit and use some measure of residual variation. Obvious candidates are our goodness-of-fit measures, the residual deviance or the

Pearson X^2, and the use of both is discussed in McCullagh and Nelder (1989) with X^2 being preferred. For our overdispersed binomial model we estimate ϕ using

$$\tilde{\phi} = \frac{X_B^2}{n-p} = \frac{1}{(n-p)} \sum_{i=1}^{n} \frac{(y_i - m_i\hat{\pi}_i)^2}{m_i\hat{\pi}_i(1-\hat{\pi}_i)},$$

and use this estimated value to obtain the standard errors of $\hat{\boldsymbol{\beta}}$.

We also need to take account of our assumed extravariability in the assessment of effects using analysis of deviance tables. We can no longer assess significance by reference to χ^2 distributions, but again proceed as for the normal regression model and use F-tests for *scaled* deviances (for this simple constant overdispersion model these are merely the binomial model deviances divided by the estimated scale parameter $\tilde{\phi}$).

Example 2 (ctd): Corn damage

For the corn damage data fitting a quasi-binomial logit model the estimated value for ϕ is $\tilde{\phi} = 4.41$ ($= 158.75/36 = X_B^2/\text{df}$). This is easily obtained in R using the `quasibinomial` family in `glm` and the analysis of deviance with associated F-tests is given by `anova`.

```
model2 <- glm(cbind(y, m-y) ~ extract,  family=quasibinomial)
summary(model2)$dispersion
[1] 4.409755
anova(model2, test="F")
        df Deviance Resid. df Resid. Dev      F    Pr(>F)
NULL                       39     801.96
extract  3   636.04        36     165.92 48.078 1.127e-12 ***
```

Here, there is no overall goodness-of-fit test available as the residual variation has been used to estimate ϕ. However, half-normal plots can still be used with a simulated envelope that takes account of the extravariability assumed in (9.3). The plot presented in Fig. 9.2b shows no strong evidence of an inadequate model with most of the observed residuals lying within the simulated envelope.

The F-test for extracts has an observed value of 48.08, which is large when compared to $F_{3,36;0.05} = 2.87$, and so we reject the null hypothesis of no extract effect, even allowing for additional variability. To further explore the differences between extracts we can consider the parameter estimates and standard errors as given in Table 9.5, where we see the same estimates for the binomial and quasibinomial models and standard errors scaled by $\sqrt{4.41} = 2.10$.

What can we say about differences between the extracts? In Table 9.5 the parameter estimates and standard errors give us comparisons between extracts and the default baseline, `extract1` the leaf extract. Here it might have been more sensible to use the control group as the baseline, which could be done by redefining the levels of the factor `extract` (easily done by using `relevel(extract,4)` in the `glm` call). However, for summary purposes and to allow for multiple

Table 9.5 Corn damage data: parameter estimates, standard errors

	Binomial		Quasi-binomial	
Source	Estimate	se	Estimate	se
(Intercept)	0.3226	0.1055	0.3226	0.2215
extract2	0.2850	0.1523	0.2850	0.3198
extract3	−4.7913	0.5138	−4.7913	1.0789
extract4	1.1591	0.1732	1.1591	0.3638

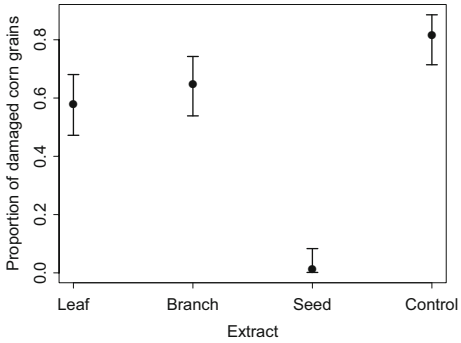

Fig. 9.3 Corn damage data – Plot of fitted proportions with quasi-binomial confidence intervals

comparisons between the treatments, we will obtain the fitted linear predictors and standard errors for each of the four treatments.

```
summary(update(model2,.~.-1))

Coefficients:
         Estimate Std. Error
extract1   0.3226     0.2215
extract2   0.6076     0.2307
extract3  -4.4688     1.0560
extract4   1.4816     0.2886
```

These estimates, $\hat{\gamma}_j$, $j = 1, \ldots, 4$ can then be converted back to the probability scale to give fitted proportions, $\exp(\hat{\gamma}_j)/\{1 + \exp(\hat{\gamma}_j)\}$. Interval estimates can be constructed by first forming intervals on the linear predictor scale (approximately $\hat{\eta} \pm 2 * se(\hat{\eta})$, or refinements of this such as replacing 2 by the appropriate t-value and possible multiple comparison type corrections) and again transforming back to the probability scale. A plot of the fitted proportions (here identical to the overall observed proportions for each extract) with approximate 95 % quasibinomial confidence intervals is given in Fig. 9.3. It is clear that the extract prepared with seeds of *Annona mucosa* gives better protection against *Sitophilus zeamais* than the other extracts, which are little better than the non-active control.

9.2.2.2 Beta-Binomial

An alternative approach to account for overdispersion is to adopt a two-stage model, allowing the probability of response, π_i, in the binomial model to vary according to some distribution. We can represent this as taking the conditional distribution of Y_i given its response probability to be binomial, $Y_i|P_i \sim \text{Binomial}(m_i, P_i)$, and assuming that the P_is are now themselves random variables with some distribution. By assuming different distributions for the P_is we can in principle obtain a range of different models, however treating the P_is as continuous we can assume that they follow a beta distribution, a highly flexible family of distributions on $[0, 1]$. Specifically, if we take $P_i \sim \text{Beta}(a_i, b_i)$ with $a_i + b_i$ constant, then unconditionally Y_i has a beta-binomial distribution with

$$\text{E}(Y_i) = m_i \pi_i$$

and

$$\text{Var}(Y_i) = m_i \pi_i (1 - \pi_i)[1 + \phi(m_i - 1)]. \tag{9.4}$$

where $\pi_i = a_i/(a_i + b_i)$ and $\phi = 1/(a_i + b_i + 1)$ is the additional dispersion parameter. For applications where all of the m_i are equal, the variance function in (9.4) will be of the same form as the quasi-binomial in (9.3), although the beta-binomial model differs in that it corresponds to a fully specified probability distribution for which full maximum likelihood estimation is available. In the following example we have m_i varying from 2 to 44 and so the two approaches will not be identical.

Example 3: **Wolbachia** ***bacteria***
The bacteria *Wolbachia* is commonly found in various insect species and has the ability to change reproductive aspects of its host. When it infects the wasp *Trichogramma galloi* (Hymenoptera: Trichogrammatidae) it is known to induce thelythokous parthenogenesis, i.e., only females are produced from unfertilized eggs. In Brazil, *Trichogramma galloi* is the most important egg parasitoid of *Diatraea saccharalis* (Lepidoptera: Crambidae), a sugarcane pest. Souza (2011) conducted an experiment to assess the effects of *Wolbachia* on the viability of *T. galloi* eggs. Around 100 *D. saccharalis* eggs were offered to infected ($^+$) or non-infected ($^-$) parasitoid couples or virgin females every day until the death of the female. The parasitised eggs, (m_i), easily identifiable because they become dark, were then kept on moist filter paper for 20 days when counts (y_i) were then made of the number of eggs that had an orifice, which meant that an adult parasitoid had emerged and thus the parasitoid was viable, see Table 9.6. Note that this is an example of aggregated data as the number of parasitised eggs (m_i) is the sum over the (unrecorded) numbers of eggs parasitised each day, and the lifespan of the females also varied. This same aggregation process will also apply to the number of viable parasitoids (y_i) and may contribute additional variability to the data.

Table 9.6 *Wolbachia* bacteria data (table entries: viable/no. of parasitised eggs y_i/m_i)

Treatment							
M^+F^+	M^+F^-	F^+		M^-F^+	M^-F^-	F^-	
28/35	30/38	11/13	14/15	22/25	20/27	4/4	2/12
16/26	21/35	12/13	5/7	28/37	3/9	12/12	2/9
13/17	22/27	11/13	21/22	30/30	19/21	5/6	4/6
16/16	20/28	17/18	2/2	34/39	26/33	11/12	3/15
25/30	17/22	3/8	4/4	10/14	14/22	2/2	3/18
25/28	23/23	8/8	10/11	27/33	21/27	7/7	
13/21	26/29	11/13	15/15	9/16	22/44	4/5	
14/21	13/17	7/7	10/14	22/22	27/28	5/6	
18/18	12/18	12/13		26/34	34/38	7/9	
36/36	27/34	19/20		28/33	25/25	8/14	
14/29	23/23	16/17		43/43	23/26	3/13	
28/30	18/18	14/14		37/37	17/28	5/6	
32/32	27/28	8/10		39/39	21/21	6/8	
	31/31	16/17		37/37	16/16	8/14	
	27/27	8/9			27/27	6/13	
		8/10			13/14	4/11	
		5/6			24/27	4/5	

Table 9.7 Analysis of deviance for the *Wolbachia* data, using a binomial logit model

Sources of variation	df	Deviance	p-value	X^2	p-value
Treatments	5	109.00			
Residual	100	435.08	< 0.01	386.61	< 0.01

We begin as before by fitting a standard binomial logit model.

```
model1 <- glm(cbind(y, m-y) ~ treat, family=binomial)
anova(model1, test="Chisq")
sum(resid(model1, ty="pearson")^2)
```

The resulting analysis of deviance in Table 9.7 shows a clear lack of fit even for the full model. This is confirmed by looking at the half-normal plot in Fig. 9.4a, where the deviance residuals are completely outside of the simulated binomial envelope. Turning to a quasi-binomial model the estimated overdispersion parameter is $\tilde{\phi} = 386.61/100 = 3.866$. The treatment factor is still significant with an F-value of 5.64 (109.0/5/3.866), however the half-normal plot in Fig. 9.4b still indicates an inappropriate model.

We now consider fitting the beta-binomial model making use of the `aods3` package (Lesnoff and Lancelot 2013).

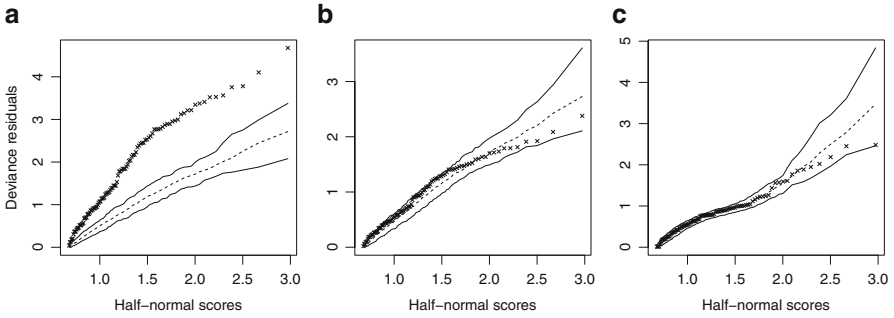

Fig. 9.4 *Wolbachia* bacteria data – Half-normal plots of deviance residuals for (**a**) binomial, (**b**) quasi-binomial and (**c**) beta-binomial logit models with different fitted probabilities for each treatment

Fig. 9.5 *Wolbachia* bacteria data – Plot of the fitted proportions with approximate 95 % confidence intervals, using a beta-binomial logit model

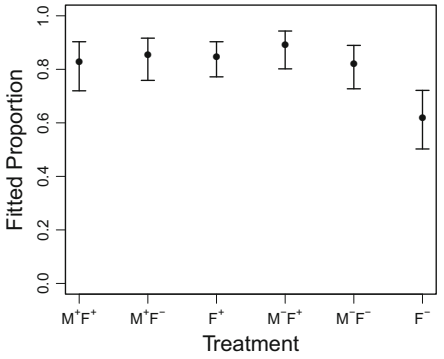


```
require(aods3)
model3<-aodml(cbind(y, m-y) ~ treat, family='bb',
              data=wolbachia)
summary(model3)
hnp(model3)
```

The estimated value for ϕ is $\hat{\phi} = 0.18$ and the half-normal plot presented in Fig. 9.4c looks reasonable and suggests that the beta-binomial model is to be preferred over the quasi-binomial model. The latter has constant overdispersion while for the beta-binomial the additional variability depends upon the number of parasitised eggs, m_i.

Working from the beta-binomial model we can now consider testing for any treatment difference. A plot of the fitted proportions from the treatment factor model with associated approximate 95 % confidence intervals is given in Fig. 9.5. This suggests that the only real difference here is for the F^- group of non-infected virgin females, whose eggs are less viable than those from females receiving the other treatments.

To explore this formally, we can fit nested submodels firstly grouping the first five treatments to contrast them against the F^- group (most easily done by using a single

0/1 dummy variable for the F^- group), and then the null no treatment difference model. One issue to consider here is the estimation of the overdispersion parameter ϕ and there are two strategies that can be used: (i) re-estimating ϕ in each model, or (ii) fixing ϕ at the value from the full treatment model. Strategy (i) corresponds to standard maximum likelihood estimation of the different beta-binomial models and comparisons can be made using likelihood ratio tests. However, a possible difficulty with this is that the estimate of the ϕ parameter can increase and absorb treatment differences into the extravariability of the beta-binomial model. Strategy (ii) is more akin to the usual approach in regression and analysis of variance where the variance is estimated from some full model (or from replication) and is what was done for the quasi-binomial model. Adopting this strategy here the change in deviance ($-2\times$ log-likelihood) for treatment of 20.83 on 5 df decomposes into 1.96 on 4 df for the first 5 treatments and 18.67 on 1 df for the F^- group. The conclusion is clear that only the F^- group is different, even allowing for extravariation. In this case strategy (i) gives identical conclusions with the overall treatment deviance of 18.31 on 5 df decomposing into 1.95 and 16.36, respectively. The ϕ estimates change very little, only increasing to 0.23 for the null model – here there are sufficient replicates to constrain the estimate of ϕ. Note that performing the same tests with the inappropriate binomial model would lead to the erroneous conclusion that there are significant differences between many of the treatments.

9.2.2.3 Logistic/Probit-Normal

The beta-binomial model assumes that the P_is have a beta distribution. Another possibility is to assume that the linear predictor, η_i, has some continuous distribution. If this distribution is taken to be in the location-scale family then this corresponds to including an additive random effect in the linear predictor and we can write

$$\eta_i = \mathbf{x}_i^T \boldsymbol{\beta} + \sigma Z_i$$

where Z_i is assumed to be from the standardized form of the distribution. Most commonly Z_i is taken to be normally distributed leading to the logistic-normal and probit-normal models. The probit-normal has a particularly simple form as the individual binary responses can be considered as arising from a threshold model for a normally distributed latent variable, see McCulloch (1994).

The model for Y again has

$$\mathrm{E}(Y_i) = m_i \pi_i$$

and the variance can be approximated by

$$\mathrm{Var}(Y_i) \approx m_i \pi_i (1 - \pi_i)[1 + \sigma^2 (m_i - 1)\pi_i (1 - \pi_i)]. \tag{9.5}$$

Williams (1982) refers to this as a type III variance function (the beta-binomial variance in (9.4) is similarly sometimes referred to as type II) and proposes a quasi-likelihood type of estimation procedure that just depends upon these first two moments and hence only on the variance, σ^2, of the observation level random effect. By specifying the distribution for Z_i, typically as normal, it is possible to use full maximum likelihood estimation for $\boldsymbol{\beta}$ and σ and there are several R packages that provide this option, here we will use `lme4`.

Example 4: **Diaphorina citri *mortality***

The Citrus psyllid *Diaphorina citri* (Hemiptera: Psyllidae) is a vector of Huanglongbing, known as greening disease. An alternative to chemical control is to use solutions of fungi conidia as a biological control strategy. D'Alessandro (2014, unpublished data, private communication) conducted a completely randomized experiment to assess how different conidia concentrations (10^4, 10^5, 10^6, 10^7 and 10^8 conidia.ml^{-1}) of two fungi species, *Beauveria bassiana* and *Isaria fumosorosea*, infected *D. citri* adults. Each experimental unit consisted of around 20 *D. citri* adults, which were placed on *Citrus limonia* plants. The insects were pulverized with the solutions and after 10 days the number of dead insects and dead insects due to fungus infection were observed, see Table 9.8. Note that in this case the conidia concentrations are obtained in successive dilutions and therefore small variations in the number of conidia per ml may contribute additional variability to the data. Such additional variability may be accounted for in the model by including an additive random effect in the linear predictor.

We begin by fitting a standard binomial logit model with different dose-response curves (using log(concentration)) for each species.

```
model1 <- glm(cbind(y, m-y) ~ lconc*species,
       family=binomial)
anova(model1, test="Chisq")
sum(resid(model1, ty="pearson")^2)
```

Table 9.8 *Diaphorina citri* mortality data (table entries: dead due to fungus infection/no. of dead insects, y_i/m_i)

Species	Concentration (conidia/ml)	Replicates		
	10^4	3/19	6/10	0/19
	10^5	2/15	2/3	1/10
B. bassiana	10^6	6/14	5/18	10/16
	10^7	10/17	6/15	9/13
	10^8	14/16	12/16	12/13
	10^4	5/17	2/18	2/11
	10^5	5/15	8/20	13/24
I. fumosorosea	10^6	12/13	15/17	17/17
	10^7	14/16	20/21	11/13
	10^8	13/13	12/14	13/13

Table 9.9 Analysis of deviance for the *Diaphorina citri* mortality data, using a binomial logit model

Sources of variation	df	Deviance	p-value	X^2	p-value
log(concentration)	1	128.14			
Species	1	36.64			
Species:log(concentration)	1	7.23	0.007		
Residual	26	56.25	< 0.01	62.99	< 0.01

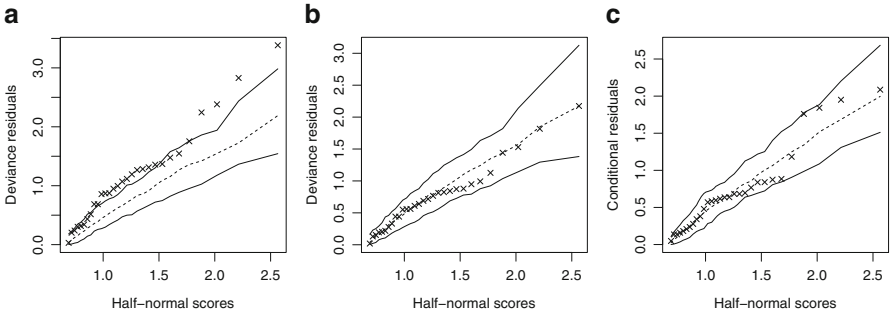

Fig. 9.6 *Diaphorina citri* mortality data – Half-normal plots of deviance residuals for (**a**) binomial and (**b**) quasi-binomial models and conditional residuals for (**c**) the logistic-normal model

The resulting analysis of deviance in Table 9.9 shows a clear lack of fit even for the full model.

This is confirmed by looking at the half-normal plot in Fig. 9.6a, where most of the deviance residuals are outside of the simulated binomial envelope. Turning to a quasi-binomial model the estimated overdispersion parameter is $\tilde{\phi} = 62.99/26 = 2.42$. Now, the interaction factor is no longer significant with an F-value of 2.98 (7.23/1/2.42) on 1 and 26 df. The half-normal plot in Fig. 9.6b shows no evidence of an inadequate model with all of the observed residuals lying within the simulated envelope. However, a practical explanation for the extra-variation could be the random variation of conidia concentration leading naturally to a logistic-normal model. We now consider fitting this model making use of the `lme4` package (Bates et al. 2013).

```
require(lme4)
model3 <- glmer(cbind(y, m-y) ~ lconc*species + (1|ind),
                family=binomial, data=fungi)
summary(model3)
hnp(model3)
```

The estimated value for σ is $\hat{\sigma} = 0.33$ and the half-normal plot presented in Fig. 9.6c looks reasonable and suggests that the logistic-normal model is also an adequate model to analyse this data set. The quasi-binomial model has constant overdispersion while for the logistic-normal model the additional variability depends upon an observation level random effect.

Working from the logistic-normal model, we can now consider testing for parallelism of the lines on the logistic scale. Here, again one issue to consider is the estimation of the overdispersion parameter σ and as for the beta-binomial model in Sect. 9.2.2.2 there are two strategies that can be used: (i) re-estimating σ in each model, or (ii) fixing σ at the value from the maximal model. Adopting strategy (i) here the change in deviance ($-2\times$ log-likelihood) for parallelism is 3.38 on 1 df, showing no strong evidence against a simpler adequate model. The σ estimate for the parallel lines model changes very little only increasing to 0.49.

```
model4 <- glmer(cbind(y, m-y) ~ lconc + species + (1|ind),
                family=binomial, data=fungi)
anova(model4,model3)
```

Note that performing the same tests with the inappropriate binomial model would lead to the erroneous conclusion that the distinct dose-response curves model is necessary. A plot of the fitted proportions from the parallel lines model (on the logit against log-dose scales) is given in Fig. 9.7.

An approximate way of calculating the lethal doses that kill $100\,\%\,p$ insects is to use the expression

$$\log_{10}(LD_p) = \frac{\log \frac{p}{1-p} - \hat{\beta}_0}{\hat{\beta}_1}$$

where $\hat{\beta}_0$ and $\hat{\beta}_1$ are, respectively, the estimated intercept and slope from the linear predictor. For the *D. citri* mortality data, the median lethal doses are $10^{4.84}$ and $10^{6.25}$ conidia/ml, respectively, for *I. fumosorosea* and *B. bassiana*, showing that *I. fumosorosea* is more than $10^{6.25}/10^{4.84} \approx 25$ times as potent as *B. bassiana*.

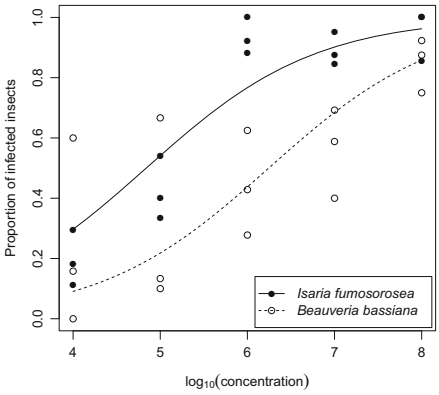

Fig. 9.7 *Diaphorina citri* mortality data – Plot of the fitted proportions, using a parallel lines logistic-normal model

9.2.3 Zero-Inflated Models

In many entomological applications involving proportion data there is often an excess of zero observations. This could be due to various reasons. Most commonly, it may be the case that a subgroup of the individuals under study are incapable of responding and so will always give a zero. This situation can be described by a two component mixture model for the subgroup that always gives zero responses and the subgroup that may, or may not, respond in the usual way for quantal responses – this corresponds to the *zero-inflated model* described below. An alternative approach to modelling data of this form is to use a two-stage model; one stage for division into zero/non-zero data and the other for the response within the non-zero data – this is sometimes referred to as a *hurdle model* and requires the use of a zero-truncated distribution for the non-zero part.

To modify the basic binomial distribution to allow for extra zeros using a *zero-inflated binomial* (ZIB) distribution, we augment the probability of zero by a proportion ω giving

$$\Pr(Y_i = y_i) = \begin{cases} \omega + (1-\omega)(1-\pi_i)^{m_i} & y = 0 \\ (1-\omega)\binom{m_i}{y_i}\pi_i^{y_i}(1-\pi_i)^{m_i - y_i} & y_i = 1, \ldots, m_i. \end{cases}$$

The mean is now $\mathrm{E}(Y_i) = m_i(1-\omega)\pi_i$ and the variance can be written as

$$\begin{aligned} \mathrm{Var}(Y_i) &= (1-\omega)\left\{m_i\pi_i(1-\pi_i) + \omega(m_i\pi_i)^2\right\} \\ &= m_i(1-\omega)\pi_i\left\{1-(1-\omega)\pi_i\right\} + m_i\pi_i^2\omega(1-\omega)(m_i-1). \end{aligned}$$

Since the latter term is non-negative, we see that, unless $\omega = 0$, this model is overdispersed compared to a binomial model, indeed, zero-inflation can be a common source of observed overdispersion. In general, we could specify regression models for both ω and π, although the simplest form of model takes ω to be constant. There are some other obvious variants of this model that could be considered, For example, in the counted proportion context we could also have excess numbers of total response (m out of m), or of 1 out of m responses, and similarly modified models can be used. We can also consider combining zero-inflation with other models, such as the beta-binomial, etc., to give zero-inflated overdispersed binomial models.

Example 5: Biological control of **Diatraea saccharalis**

Applied biological control is an important branch of entomology, which seeks methods to control pests without damage to the environment and the ecosystem, using natural enemies of the pest (parasitoids and/or predators). Sugarcane borer

Table 9.10 *Trichogramma galloi* DA biotype data (table entries: no. of parasitised eggs out of 128, y_i)

Number of females	Replicates									
2	0	0	0	0	0	50	65	30	62	48
4	0	0	0	0	0	0	0	62	3	1
8	0	0	0	0	0	49	19	22	51	65
16	0	0	0	0	0	57	35	52	37	58
32	0	0	0	0	0	120	90	86	102	95
64	0	0	0	0	0	0	57	77	105	99
128	0	0	0	0	38	21	82	42	90	81

(*Diatraea saccharalis*), the main pest in sugar cane cultivation in Brazil, has been controlled using egg parasitoids, such as *Trichogramma galloi*. This requires large numbers of parasitized eggs for inundative release in the sugarcane fields. As part of a study on the efficient production of parasitized eggs, experiments were conducted to compare two different *T. galloi* biotypes and to determine the optimal number of females needed to maximize parasitized egg production. In a completely randomized experiment, these two biotypes of the parasitoid, namely AA and DA, were put to parasitize 128 eggs of *Anagasta kuehniella* (Lepidoptera: Pyralidae), an economically suitable alternative host, using different numbers of female parasitoids $(2, 4, 8, \ldots, 128)$, with 10 replicates of each combination. The AA biotype was adapted to the alternative host while the DA biotype was adapted to the natural host, however, in the experiment, both were set to parasitize the alternative host. The response variable is the number of parasitized eggs out of the 128 available, see Table 9.10 for DA biotype data.

A plot of the observed proportions is given in Fig. 9.8 and shows that for DA biotype there are large numbers of zero observations across the whole range of different parasitoid numbers. The observed pattern of non-zero response for DA is also rather unusual. Here to illustrate modelling of zero-inflated data we will restrict our analyses to the DA biotype and to focus on the modelling of the zeros and the overdispersion we will use the numbers of females as a 7-level factor in the model. Further modelling might include using some smooth function over these parasitoid numbers to determine the optimal value, see Vieira et al. (2000).

A binomial model is clearly inadequate here with a residual deviance of 4,045.9 on 63 df indicating huge overdispersion. This is confirmed by looking at the half-normal plot in Fig. 9.9a. Using this model, it is suggested that the factor `female` is significant, but this is based on a blatantly incorrect variance function. We can see that the overdispersion may be due to the approximately 50 % of zero observations at each level and also possibly greater than binomial variation for the non-zero observations. We will now fit a range of models to explore these aspects. A simple quasi-likelihood model has an estimated scale parameter $\tilde{\phi} = 57.4$ and the factor `female` is now not significant, with an F-statistic of 1.56 on 6 and 63 df. However, the half-normal plot of the deviance residuals shows that this simple overdispersion

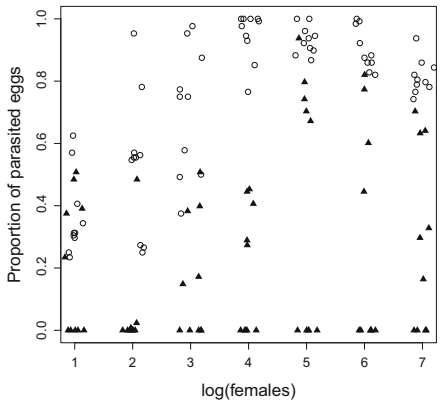

Fig. 9.8 *Trichogramma galloi* biotype data – Plot of observed proportions against number of female parasites ($\log_2$-scale) with jittering of points: ∘ biotype AA, ▲ biotype DA

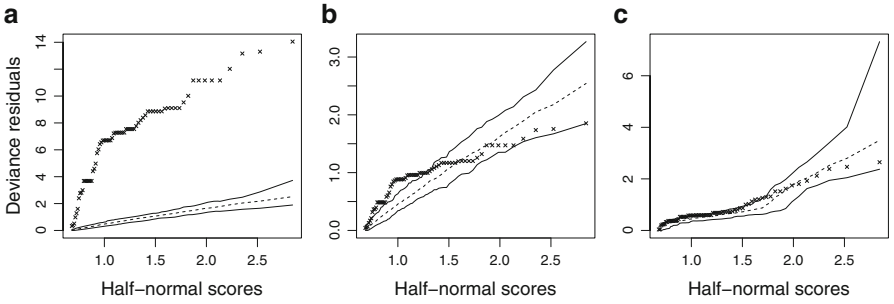

Fig. 9.9 *Trichogramma galloi* DA biotype data – Half-normal plots of deviance residuals for (**a**) binomial, (**b**) quasi-binomial and (**c**) beta-binomial models

model fails to capture the true pattern of variation here, see Fig. 9.9b. Fitting a beta-binomial model, the results are similar (see Fig. 9.9c) with the same conclusion about the non-significance of `female`. This is as we might expect since the sample sizes $m_i = 128$ for all of the observed proportions and so the beta-binomial overdispersion, $1 + \phi(m_i - 1)$, is also constant, although the details of the fits differ as the beta-binomial uses full maximum likelihood.

Turning to zero-inflated models, we initially fit a zero-inflated binomial model with constant zero-inflation using the R package `glmmADMB` (Skaug et al. 2013).

```
require(glmmADMB)
fase2s1.ZIB <- glmmadmb(cbind(peggs, 128-peggs)
               ~factor(female),
               family="binomial", zeroInflation=T,
               data=fase2s1)
summary(fase2s1.ZIB)
```

This model gives an estimate for the proportion of extra-zeros of $\hat{\omega} = 0.61$. The change in deviance from the binomial model is 3,599.6 on 1 df, showing that

the zeros accounted for much of the lack of fit of the binomial model. However, the residual deviance is 446.3 on 62 df, which still suggests considerable overdispersion. The package `glmmADMB` also allows the fitting of a zero-inflated beta-binomial distribution.

```
fase2s1.ZIBB <- glmmadmb(cbind(peggs, 128-peggs)
            ~factor(female),
            family="betabinomial", zeroInflation=T,
            data=fase2s1)
summary(fase2s1.ZIBB)
anova(fase2s1.bin,fase2s1.ZIB,fase2s1.ZIBB)
anova(fase2s1.bin,fase2s1.bb,fase2s1.ZIBB)
```

This gives a further reduction in the residual deviance of 231.4 on 1 df, showing evidence of some additional overdispersion. However, the estimate of the zero-inflation parameter is reduced to $\hat{\omega} = 0.51$. Note that the overall change in deviance of 3,831 on 2 df from the binomial to the zero-inflated beta-binomial model does not give a unique decomposition into zero-inflation and overdispersion, as is made clear in the two different analysis of deviance tables. Indeed, going from a binomial to a beta-binomial model gives a deviance change of 3,769.4 on 1 df, leaving only 61.6 on 1 df for the additional effect of zero-inflation. This makes clear the links between these two aspects; the presence of zero-inflation results in overdispersion and overdispersion models can often accommodate an excess of zeros, however, it is possible for both features to be present. In this extended model, the factor `female` remains significant with a deviance of 34.6 on 6 df (compared to a deviance of 536.9 for the original binomial model), although much of the variation between the different levels would no longer be significant and a simpler (smooth) model could be considered.

While, in principle, half-normal plots could be used to check the fit of these complex models, simulating from something like a zero-inflated beta-binomial model can lead to datasets for which the fitting algorithm fails and hence construction of the simulated envelope can be problematic. Refinements to avoid these difficulties are the subject of ongoing work.

9.3 Models for Count Data

The other form of data frequently collected in entomology is that of a simple count, with common examples being the number of insects on plants or in fixed areas, and the number of eggs laid. Again, interest may focus in how these counts vary under different treatments, for different host plants, in different environments, etc. Specific examples include:

– Ecological diversity studies using numbers of insect species in quadrats at different locations;

– Physiology experiments, assessing fecundity using number of eggs laid per female;
– Behavioural studies to analyse reproduction patterns using number of matings;
– Biological control studies using numbers of attacks by predators on prey.

The simplest underlying process assumes that counts arise at some average rate with the variability in the observed counts coming from independent, random variation over time, space, individual, etc. The response variable of interest is now simply an observed count, y, and the Poisson distribution provides a starting point for data analysis.

9.3.1 Poisson Models

For counts over time or space a very simple model is to assume that events happen independently, singly, and at random at some constant underlying rate. Considering events over time, if we write λ for the average rate per unit time, then, under these assumptions, the distribution for the number of events, $Y(t)$, in an interval of length t is Poisson(λt) with probabilities

$$\Pr(Y(t) = y) = \frac{e^{-\lambda t}(\lambda t)^y}{y!}, \qquad y = 0, 1, 2, \ldots . \tag{9.6}$$

The mean and variance are $\mathrm{E}(Y(t)) = \lambda t$ and $\mathrm{Var}(Y(t)) = \lambda t$ and are equal. This is an important practical characterisation of the Poisson distribution and can be checked empirically by assessing approximate equality of sample means and variances. A similar model applies for counts over space, with the parameter λ giving the rate per unit area or volume.

In many simple applications, counts will be observed over identical time periods, areas, etc. In this case, we can use a standard Poisson(μ) distribution for a count Y with

$$\Pr(Y = y) = \frac{e^{-\mu}\mu^y}{y!}, \qquad y = 0, 1, 2, \ldots \tag{9.7}$$

where μ is the rate for the period/region of observation and we have

$$\mathrm{E}(Y) = \mathrm{Var}(Y) = \mu. \tag{9.8}$$

This equality is often expressed in terms of the variance-to-mean-ratio, or *index of overdispersion*, $\mathrm{Var}(Y)/\mathrm{E}(Y)$, which is 1 for the Poisson distribution. Of course, in practice this is very restrictive and overdispersion in our counts, for reasons outlined in Sect. 9.2, means that the Poisson distribution may not provide a good fit for most real count data and we need to consider more general distributions with an index of overdispersion greater than 1.

To apply the Poisson distribution in a modelling framework, we proceed as for the Binomial in Sect. 9.2.1. For a random sample of n counts $Y_i, i = 1, \ldots, n$, with possibly different underlying rates μ_i, we have $Y_i \sim \text{Poisson}(\mu_i)$ where μ_i can be modelled in terms of p observed explanatory variables $\mathbf{x}$ (again assumed to include a constant term). Since the Poisson parameter μ_i is constrained to be positive ($\mu_i > 0$) the most widely used (canonical) link function for the Poisson distribution is the *log link*, so the Poisson regression model specification is completed by taking

$$\log \mu_i = \boldsymbol{\beta}^T \mathbf{x}_i = \eta_i$$

where $\boldsymbol{\beta}$ is a vector of p unknown parameters.

Note that this model easily incorporates the possibility of counts being observed over different times, areas, etc. Returning to the Poisson distribution for different time intervals in (9.6), we have $\mu_i = \lambda_i t_i$ where t_i are the known periods of observation and our regression model becomes

$$\log \mu_i = \log(\lambda_i t_i) = \log(\lambda_i) + \log(t_i) = \boldsymbol{\beta}^T \mathbf{x}_i + \log(t_i) = \eta_i$$

where the model $\boldsymbol{\beta}^T \mathbf{x}_i$ is for the rates λ_i. The known t_i's are included in the linear predictor η_i as a fixed term $\log(t_i)$, commonly referred to as an *offset*, and this provides a natural and simple way of analysing rate data.

The deviance for the Poisson model is given by

$$D_P = 2 \sum_{i=1}^{n} \left[y_i \log \left(\frac{y_i}{\hat{\mu}_i} \right) - (y_i - \hat{\mu}_i) \right]$$

where $\hat{\mu}_i$, $i = 1, 2, \ldots, n$, are the fitted values for the model of interest. The deviance D_P can be viewed as a measure of goodness-of-fit of the fitted model with p estimated parameters. For log-linear models (log link) which include an intercept, the deviance reduces to

$$D_P = 2 \sum_{i=1}^{n} \left[y_i \log \left(\frac{y_i}{\hat{\mu}_i} \right) \right]$$

since the fitted model reproduces the overall total, i.e. $\sum_i \hat{\mu}_i = \sum_i y_i$. The alternative measure of overall fit, the Pearson X^2 statistic, takes the familiar form

$$X_P^2 = \sum_{i=1}^{n} \frac{(y_i - \hat{\mu}_i)^2}{\widehat{\text{Var}}(Y_i)} = \sum_{i=1}^{n} \frac{(y_i - \hat{\mu}_i)^2}{\hat{\mu}_i}.$$

For large expected counts (μ_i), D_P and X_P^2 are equivalent and under the null hypothesis of an adequate model both have an approximate χ^2 distribution on $n - p$

df. As the Poisson log-linear model is a standard generalized linear model, model comparisons and model checking proceed in the same way as for the Binomial distribution and will be illustrated in the following examples.

Example 6:* Sitophilus zeamais *progeny

We return to the experiment described in Example 2 on the maize pest *Sitophilus zeamais*. Petri dishes containing 10 g of corn were treated with extracts prepared with different parts of the plant *Annona mucosa* (seeds, leaves and branches) at a concentration of 1,500 mg/kg or just water (control), using a completely randomized design with 10 replicates. Then 20 *S. zeamais* adults were placed in each Petri dish and the focus now is on the numbers of emerged insects (progeny) after 60 days, see Ribeiro et al. (2013). The data are given in Table 9.11.

We begin by fitting a standard Poisson log-linear model with the different extracts and inspect the analysis of deviance and goodness-of-fit given in Table 9.12.

```
model1 <- glm(y ~ extract, family=poisson)
anova(model1, test="Chisq")
hnp(model1, pch=4, main="Poisson: log-linear",
    xlab="Half-normal scores", ylab="Deviance
       residuals")
```

Here, there is clear evidence from the residual deviance and X^2 values that the model does not fit – the replicates are more variable than we would expect under a Poisson model. This can also be seen in the half-normal plot of the deviance residuals shown in Fig. 9.10a. As for proportion data, we will turn to look at models to be used to analyse data where the assumption of the Poisson model is less satisfactory and consider approaches to allowing for overdispersion.

Table 9.11 *Sitophilus zeamais* data (table entries: no. of emerged insects, y_i)

Treatment	Replicates									
Leaf extract	19	20	36	32	18	47	38	31	32	40
Branch extract	20	34	41	29	31	15	31	33	45	20
Seed extract	4	0	1	1	1	0	2	0	2	0
Control	35	26	41	34	23	29	39	34	16	38

Table 9.12 Analysis of deviance for the *Sitophilus* data, using a Poisson log-linear model

Sources of variation	df	Deviance	p-value	X^2	p-value
Extracts	3	444.68			
Residual	36	89.77	< 0.01	85.15	< 0.01

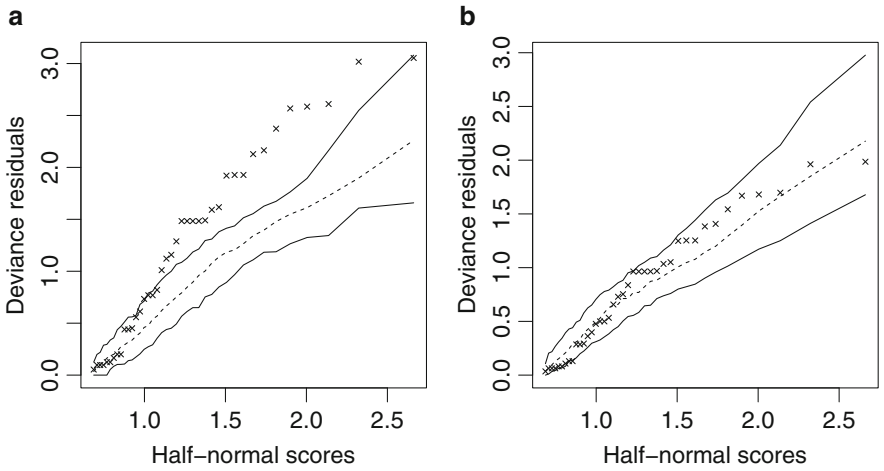

Fig. 9.10 *Sitophilus zeamais* progeny data – Half-normal plots with simulated envelopes of deviance residuals for (**a**) Poisson and (**b**) quasi-Poisson log-linear models

9.3.2 Overdispersion Models

Models for overdispersed count data move away from the strict Poisson assumption of equal mean and variance (index of dispersion = 1). There is a long history of accounting for overdispersion in count data, including Breslow (1984) and Lawless (1987) and more general discussions are also to be found in McCullagh and Nelder (1989) and Lindsey (1995). We will begin by considering a quasi-likelihood approach to accommodate increased variability.

9.3.2.1 Quasi-likelihood

As for the quasi-binomial model in Sect. 9.2.2.1, here a constant overdispersion model replaces (9.8) by

$$\text{Var}(Y_i) = \phi\mu_i. \tag{9.9}$$

and the overdispersion parameter factor ϕ (>1) indicates that the increased variation for observation y_i does not depend on the μ_i. Again this is referred to as the heterogeneity factor model, see Finney (1971).

Estimation of the regression parameters $\boldsymbol{\beta}$ using maximum quasi-likelihood (Wedderburn 1974) proceeds in the same way as for the quasi-binomial model and for this constant overdispersion model the estimates $\hat{\boldsymbol{\beta}}$ are identical to those from the Poisson model. (Again the key mean-variance relationship is of the same form for the Poisson and quasi-Poisson models, up to the constant scale factor ϕ.) However,

the assumed greater variability in (9.9) inflates the standard errors of $\hat{\boldsymbol{\beta}}$ by a factor of $\sqrt{\phi}$ compared to those of the Poisson ($\phi = 1$) model. For the overdispersed Poisson model (9.9) we estimate ϕ using

$$\tilde{\phi} = \frac{X_P^2}{n-p} = \frac{1}{(n-p)} \sum_{i=1}^{n} \frac{(y_i - \hat{\mu}_i)^2}{\hat{\mu}_i}$$

and use this estimated value to obtain the standard errors of $\hat{\boldsymbol{\beta}}$.

We also need to take account of our assumed extra-variability in the assessment of effects using analysis of deviance tables and again use F-tests for *scaled* deviances (for this simple constant overdispersion model these are just the Poisson model deviances divided by the estimated scale parameter $\tilde{\phi}$).

Example 6 (ctd):* Sitophilus zeamais *data

For the *Sitophilus zeamais* data fitting a quasi-Poisson model the estimated value of ϕ is $\tilde{\phi} = 2.36$ ($= 89.77/36 = X_P^2/\text{df}$). This is easily obtained in R using the `quasipoisson` family in `glm` and the analysis of deviance with associated F-tests is given by `anova`.

```
model2 <- glm(y ~ extract, family=quasipoisson)
summary(fm2)$dispersion
[1] 2.365385
anova(model2, test="F")
        df Deviance Resid. df Resid. Dev      F    Pr(>F)
NULL                       39     534.44
extract  3   444.68        36      89.77 62.664 2.303e-14 ***
```

As for the quasi-binomial model in Sect. 9.2.2.1, there is no overall goodness-of-fit test available, as the residual variation has been used to estimate ϕ. However, half-normal plots can still be used with a simulated envelope that takes account of the extravariability assumed in (9.9). The plot presented in Fig. 9.10b shows no strong evidence of an inadequate model, with most of the observed residuals lying within the simulated envelope.

The F-test for extracts has an observed value of 62.66, which is large when compared to $F_{3,36;0.05} = 2.87$, and so we reject the null hypothesis of no extract effect, even allowing for additional variability. To further explore the differences between extracts, we can consider the parameter estimates and standard errors as given in Table 9.13, where we see the same estimates for the Poisson and quasi-Poisson models and standard errors scaled by $\sqrt{2.36} = 1.54$.

In Table 9.13, the parameter estimates and standard errors give us comparisons between extracts and the default baseline, `extract1` the leaf extract. Here, as in Example 2, it might have been more sensible to use the control group as the baseline, which could be done by redefining the levels of the factor `extract`. However, for summary purposes and to allow for multiple comparisons between the treatments, we will obtain the fitted linear predictors and standard errors for each of the four treatments.

Table 9.13 *Sitophilus zeamais* progeny data: parameter estimates, standard errors

	Poisson		Quasi-Poisson	
Source	Estimate	se	Estimate	se
(Intercept)	3.4436	0.0565	3.4436	0.0869
extract2	−0.0458	0.0809	−0.0458	0.1244
extract3	−3.3483	0.3068	−3.3483	0.4718
extract4	0.0064	0.0798	0.0064	0.1227

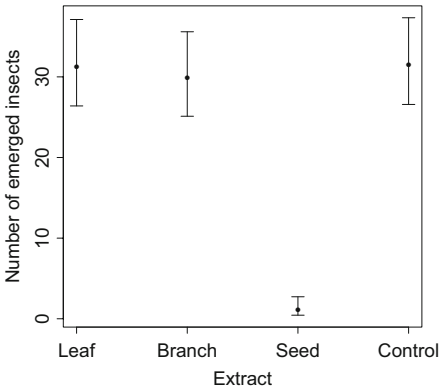

Fig. 9.11 *Sitophilus zeamais* progeny data – Plot of fitted counts with quasi-Poisson confidence intervals

```
summary(update(model2,.~.-1))
Coefficients:
         Estimate Std. Error
extract1  3.44362    0.08693
extract2  3.39786    0.08894
extract3  0.09531    0.46371
extract4  3.44999    0.08666
```

These estimates, $\hat{\gamma}_j$, $j = 1, \ldots, 4$ can then be converted back to the mean scale to give fitted counts, $\exp(\hat{\gamma}_j)$. Interval estimates can be constructed by first forming intervals on the linear predictor scale (approximately $\hat{\eta} \pm 2 * se(\hat{\eta})$, or refinements of this such as replacing 2 by the appropriate t-value and possible multiple comparison type corrections) and transforming back to the mean scale. A plot of the fitted counts (here identical to the overall observed means for each extract) with approximate 95 % quasi-Poisson confidence intervals is given in Fig. 9.11. It is clear that the extract prepared with seeds of *Annona mucosa* gives better protection against *S. zeamais* than the other extracts, which are each no better than the non-active control.

9.3.2.2 Negative Binomial

An alternative approach to account for overdispersion in the Poisson model is to adopt a two-stage model, allowing the Poisson mean, T_i, to vary according to some distribution. We can represent this by writing the conditional distribution of Y_i given

its mean, $Y_i|T_i \sim \text{Poisson}(T_i)$, and assuming that the T_is are now themselves random variables with some distribution. If we treat T_i as continuous, since it must also be positive, a natural and flexible family of distributions on $(0, \infty)$ is given by the gamma distribution. Specifically, if we take $T_i \sim \text{Gamma}(\theta, \lambda_i)$, i.e. fix the shape parameter θ, then unconditionally Y_i has a negative binomial distribution with $\text{E}(Y_i) = \theta/\lambda_i = \mu_i$ and

$$\text{Var}(Y_i) = \mu_i + \mu_i^2/\theta = \mu_i(1 + \mu_i/\theta). \tag{9.10}$$

This is sometimes referred to as Negative Binomial type II to distinguish it from negative binomial distributions with different mean-variance relationships. An advantage of using a fixed value of θ is that the resulting distribution for Y_i is in the exponential family and so we are still in the generalized linear modelling framework.

Note that by assuming a different form for the gamma mixing distribution we can obtain different overdispersed Poisson-Gamma models. For example, taking a $\text{Gamma}(\theta_i, \lambda)$ distribution for T_i leads to

$$\text{Var}(Y_i) = \mu_i + \mu_i/\lambda \equiv \phi\mu_i, \tag{9.11}$$

the constant overdispersion model, referred to as Negative Binomial type I. However, the resulting distribution for Y_i is not in the exponential family and so will not be considered here; see Nelder and Lee (1992) for details of maximum likelihood estimation.

Example 7: **Diaphorina citri** ***oviposition***

In an experiment to assess the effect of three agricultural oils on the oviposition of *Diaphorina citri*, 70 Orange Jessamine (*Murraya paniculata*) plants were sprayed with solutions of the mineral oils Oppa and Iharol, and the vegetable oil Nortox. The experiment used the oils in concentrations of 0.5 % and 1.0 % and a control of plain water set out in a completely randomized design with ten replicates. Following treatment, when the plants were dry, ten pregnant females of *D. citri* were released on each plant. After 5 days, the insects were removed and the total number of eggs on each plant was observed, see Amaral et al. (2012). The data are given in Table 9.14. This is another example of aggregated data as the number of eggs (y_i) is the sum over the (unrecorded) numbers of eggs deposited each day and the possibility of day to day variation may contribute additional variability to the recorded counts.

We begin as before by fitting a standard Poisson log linear model.

```
model1 <- glm(y ~ oil, family=poisson)
anova(model1, test="Chisq")
sum(resid(model1, ty="pearson")^2)
```

The resulting analysis of deviance in Table 9.15 shows a clear lack of fit even for the full model.

Table 9.14 *Diaphorina citri* oviposition data (table entries: no. of eggs, y_i)

Treatment	Replicates									
Control	137	20	105	1	102	10	61	148	69	56
Oppa (0.5 %)	127	124	121	1	15	131	1	69	68	49
Oppa (1.0 %)	11	49	67	2	43	38	25	67	12	82
Iharol (0.5 %)	159	129	67	24	12	112	46	17	51	3
Iharol (1.0 %)	25	16	7	53	75	1	53	5	101	151
Nortox (0.5 %)	114	29	125	117	13	86	15	43	210	11
Nortox (1.0 %)	1	3	4	12	3	12	1	3	17	1

Table 9.15 Analysis of deviance for the *Diaphorina citri* oviposition data, using a Poisson log-linear model

Sources of variation	df	Deviance	p-value	X^2	p-value
Treatments	6	944.35			
Residual	63	2,523.10	<0.01	2,290.85	<0.01

This is confirmed by looking at the half-normal plot in Fig. 9.12a, where the deviance residuals are completely outside of the simulated Poisson envelope. Turning to a quasi-Poisson model the estimated overdispersion parameter is $\tilde{\phi} = 2{,}290.85/63 = 36.36$. The treatment factor (`oil`) is still significant with an F-value of 4.33 (944.35/6/36.36). However, the half-normal plot in Fig. 9.12b still indicates a possibly inappropriate model with many of the residuals lying outside of the quasi-Poisson envelope and the noticeable curvature of the observed residuals makes it clear that we do not have constant overdispersion here.

We now consider fitting the negative binomial model making use of the `MASS` package.

```
require(MASS)
model3 <- glm.nb(y ~ oil)
summary(model3)
```

The estimated value for θ is $\hat{\theta} = 1.09$ (s.e. 0.18) and implies considerable overdispersion. The half-normal plot presented in Fig. 9.12c looks reasonable and suggests that the negative binomial model is to be preferred over the quasi-Poisson model. The latter has constant overdispersion, while for the negative binomial the additional variability depends upon the mean number of eggs (μ_i), as shown in the variance expression (9.10), and is better at capturing the observed overdispersion.

Working from the negative binomial model we can now consider testing for any treatment difference. A plot of the fitted means from the treatment factor model with associated approximate 95 % confidence intervals is given in Fig. 9.13. This suggests that the only real difference here is for Nortox at a 1 % concentration, which is more effective than the other treatments at inhibiting oviposition.

To explore this formally, we can fit nested submodels. We begin by grouping the first six treatments to contrast them against Nortox at a 1 % concentration, and

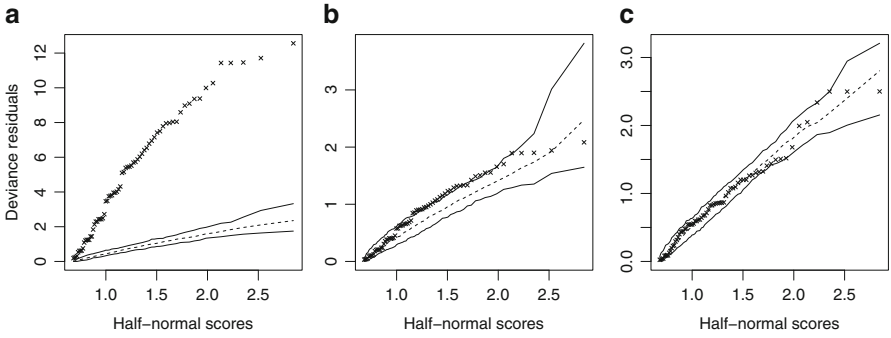

Fig. 9.12 *Diaphorina citri* oviposition data – Half-normal plots of deviance residual for (**a**) Poisson, (**b**) quasi-Poisson and (**c**) negative binomial log-linear models

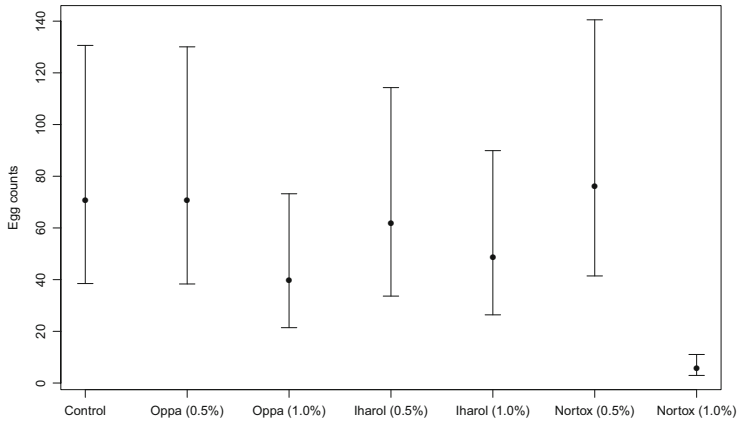

Fig. 9.13 *Diaphorina citri* oviposition data – Plot of the fitted proportions with approximate 95 % confidence intervals, using a negative binomial model

then fit the null model of no treatment difference. One issue to consider here is the estimation of the overdispersion parameter θ and, as for the beta-binomial model in Sect. 9.2.2.2, there are two strategies that can be used: (i) re-estimating θ in each model, or (ii) fixing θ at the value from the full treatment model. Fixing $\theta = \hat{\theta} = 1.09$ (strategy (ii)) the change in deviance ($-2\times$ log-likelihood) for treatment of 32.25 on 6 df decomposes into 3.30 on 5 df for the first 6 treatments and 28.95 on 1 df for Nortox at 1 % concentration. The conclusion is clear that only 1 % Nortox is different, even allowing for the extravariation of the negative binomial model. In this case strategy (i) gives the same conclusions with the overall treatment deviance of 27.40 on 6 df decomposing into 3.23 and 24.17, respectively. The θ estimates change little with a value of 0.78 for the null model – this smaller value indicates greater overdispersion for this constant mean model, which is to be expected as some of the variation between treatments has been accounted for by additional overdispersion.

Note that performing the same tests with the inappropriate Poisson model would lead to the erroneous conclusion that there are significant differences between many of the treatments.

9.3.2.3 Poisson-Normal

We can also consider extending the Poisson model by including a random effect in the linear predictor. Indeed, the negative binomial model can be viewed in this way by the addition of a log-gamma random effect. However, since we may think of this additional random effect as a combination of many unexplained things, it may be natural to assume that it has a normal distribution. Taking a Poisson log-linear model and a normally distributed random effect leads to the Poisson-normal model, see Hinde (1982). The model can be specified as

$$Y_i|Z_i \sim \text{Poisson}(\lambda_i) \quad \text{with} \quad \log \lambda_i = \mathbf{x}_i^T \boldsymbol{\beta} + \sigma Z_i$$

where $Z_i \sim N(0,1)$. This unfortunately has no closed form for the distribution of Y_i. Using standard results on conditional moments, we obtain

$$\begin{aligned} \text{E}(Y_i) &= e^{\mathbf{x}_i^T \boldsymbol{\beta} + \frac{1}{2}\sigma^2} := \mu_i \\ \text{Var}(Y_i) &= e^{\mathbf{x}_i^T \boldsymbol{\beta} + \frac{1}{2}\sigma^2} + e^{2\mathbf{x}_i^T \boldsymbol{\beta} + \sigma^2}(e^{\sigma^2} - 1) = \mu_i + k'\mu_i^2, \end{aligned}$$

which is the same form of quadratic variance function as for the negative binomial distribution. In fact, with a log-link function and an additive continuous random effect in the linear predictor, we always obtain a variance function of approximately this form, see Nelder (1985). Because of the identical forms of variance function, approximate quasi-likelihood estimates are the same for both the negative binomial and Poisson-normal models. However, full maximum likelihood estimates will differ; see Hinde (1982) for details of maximum likelihood estimation for the Poisson-normal model based on using Guassian-quadrature to integrate over the random effect.

Example 8: Coffee berry borer trapping

The coffee berry borer, *Hypothenemus hampei* (Coleoptera: Scolytidae), is a major pest of commercial coffee. The insect directly attacks the coffee fruit in development causing severe losses in bean production and quality. The wingless male stays inside the fruit during its entire life cycle. The females, after being fertilized, lay some of their eggs and in adequate environmental conditions (low atmospheric pressure) leave the fruit to form another colony in a different fruit. Behavioural aspects of the pest may be taken into account to develop alternative control strategies for pesticide application. For example, it is known that this beetle is attracted by ethanol and by the color red. To explore this, Mota (2013) conducted an experiment randomizing three types of traps ("SF", "F", "CV") in each of four equidistant lines (blocks) of a

Table 9.16 Coffee berry borer trapping data (table entries: no. of trapped insects, y_i)

	Block I			Block II			Block III			Block IV		
Week	SF	F	CV	SF	F	CV	SF	F	CV	SF	F	CV
1	5	22	126	55	57	95	15	19	166	9	59	99
2	2	1	6	1	4	11	1	3	25	0	1	9
3	1	8	39	5	3	113	1	8	22	1	10	110
4	5	14	65	8	25	80	7	28	258	58	38	95
5	5	4	70	8	16	42	8	17	149	45	9	24
6	32	36	169	55	61	163	43	56	551	94	68	171
7	15	11	31	11	9	24	0	35	61	6	1	8
8	57	104	110	38	57	150	37	23	230	29	98	148
9	36	28	56	10	19	116	3	36	103	15	16	83
10	5	17	96	1	5	217	12	67	49	4	5	212
11	5	5	14	3	4	85	0	22	10	4	1	67
12	16	21	134	41	19	176	4	54	72	6	10	353
13	2	4	26	4	5	46	0	16	9	3	10	86
14	0	0	12	0	2	27	4	8	17	5	3	29
15	0	2	5	1	0	11	0	2	2	0	0	7
16	1	4	6	3	2	22	1	1	2	2	2	6
17	0	0	3	1	1	16	1	2	5	0	1	14
18	0	0	4	0	3	3	0	1	0	1	2	4
19	3	0	4	0	1	3	0	2	0	0	2	3
20	17	7	77	26	25	246	4	57	40	26	6	66
21	5	3	12	9	0	28	0	25	8	8	5	15
22	4	8	7	5	10	31	3	17	4	9	2	37
23	0	3	17	0	0	15	3	2	47	0	4	59
24	10	0	10	4	3	6	8	3	40	0	4	53

coffee field. Each week, over a 24 week period, the insects were removed from the traps and counted. The data is presented in Table 9.16 and it is clear from Fig. 9.14 that the "CV" type trap collects more insects than the other two types.

We begin by fitting a standard Poisson log-linear model with the factors block, trap and week as fixed effects and inspect the analysis of deviance and goodness-of-fit for the full model given in Table 9.17.

```
model1 <- glm(count ~ block + trap * factor(week),
                    data=trap.data, family=poisson)
anova(model1, test="Chisq")
sum(resid(model1, ty="pearson")^2)
```

Here, there is clear evidence from the residual deviance and X^2 values that the model does not fit – the replicates are more variable than we would expect under a Poisson model. This can also be seen in the half-normal plot of the deviance residuals shown in Fig. 9.15a, where the deviance residuals are completely outside

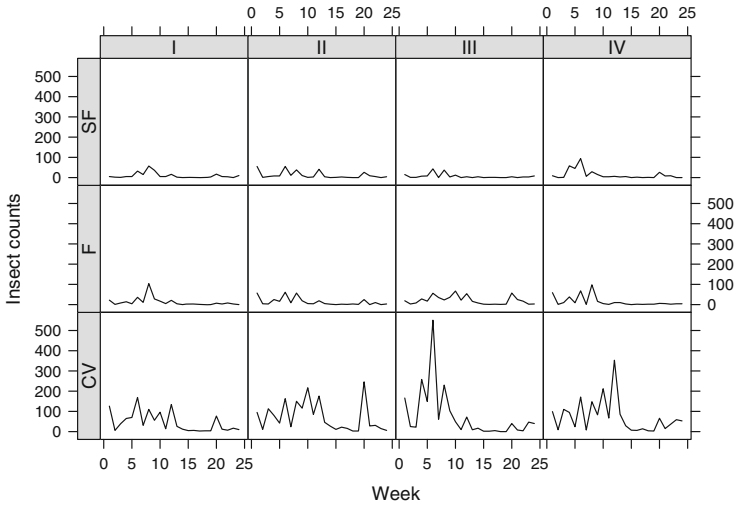

Fig. 9.14 Coffee berry borer trapping data – Plot of the observed counts for each trap and block over 24 weeks

Table 9.17 Analysis of deviance for the coffee berry borer trapping data, using a Poisson log-linear model

Sources of variation	df	Deviance	p-value	X^2	p-value
Block	3	243.6			
Trap	2	5,721.4			
Week	23	8,539.4			
Week:Trap	46	454.3			
Residual	213	2,729.5	<0.01	2,695.7	<0.01

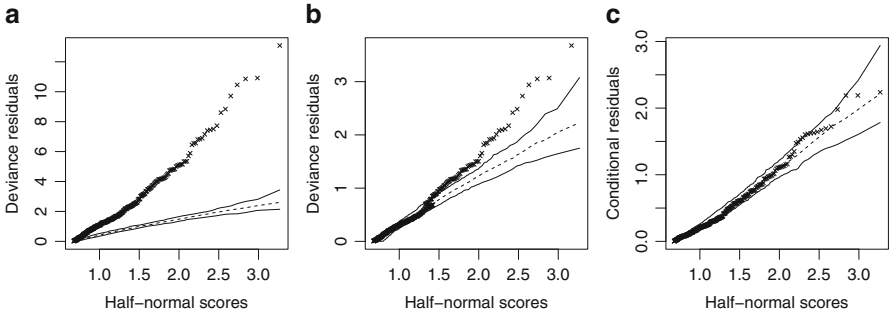

Fig. 9.15 Coffee berry borer trapping data – Half-normal plots of deviance residual for (**a**) Poisson and (**b**) quasi-Poisson models and conditional residuals for (**c**) the Poisson-normal model

of the simulated Poisson envelope. Turning to a quasi-Poisson model the estimated overdispersion parameter is $\tilde{\phi} = 2{,}695.7/213 = 12.65$ and the interaction is no longer significant with an F-value of 0.78 (454.3/46/12.65). However the half-normal plot in Fig. 9.15b suggests that the constant overdispersion assumption is inappropriate.

We now consider fitting a Poisson-normal model making use of the R package `lme4`. For these data we can think of including two normal random effects, one at trap-block combination level ($Z_{ij} \sim N(0, \sigma_Z^2)$) to account for the correlation between counts taken on the same trap and block over time and another at observation level ($W_{ijk} \sim N(0, \sigma_W^2)$) to model overdispersion. These two random effects will account for part of the variability caused by environmental conditions.

```
z <- factor(c(rep(1:12,each=24)))
w <- factor(1:nrow(trap.data))
model3 <- glmer(count ~ block + trap*factor(week)
                + (1|z) + (1|w), family=poisson,
                   data = trap.data,
              control=glmerControl(optCtrl=list
                (maxfun=50000)))
```

The estimated values for σ_Z^2 and σ_W^2 are $\hat{\sigma}_Z^2 = 0.0377$ and $\hat{\sigma}_W^2 = 0.3270$. The half-normal plot presented in Fig. 9.15c looks reasonable and suggests that the Poisson-normal model is adequate to analyse this data set.

Working from the Poisson-normal model, we now consider testing for the trap by week interaction. Here, as for the logistic-normal model in Sect. 9.2.2.3, we proceed, using strategy (i), re-estimating σ_Z^2 and σ_W^2.

```
model4 <- glmer(count ~ block + trap + factor(week)
          + (1|z) + (1|w), family=poisson, data
          = trap.data) anova(model3,model4)
```

The change in deviance for no interaction effect is 60.84 on 46 df, showing no evidence of a significant effect, although this value also reflects the change in the estimates $\hat{\sigma}_Z^2 = 0.0343$ and $\hat{\sigma}_W^2 = 0.4323$ and the extra dispersion associated with the increased value for σ_W^2 may have accounted for some of the interaction variation. The half-normal plot, not presented here, indicates that this is also an adequate model fit. Testing now for no trap effect the change in deviance is 31.69 on 2 df, showing evidence of a significant effect of traps, and note that this value also reflects the change in the variance estimates $\hat{\sigma}_Z^2 = 0.8485$ and $\hat{\sigma}_W^2 = 0.4322$ with σ_Z^2 now much larger and also accounting for some of the between trap variation. So clearly we need to include `trap` in our model. A plot for the average predicted and observed values from the additive model is given in Fig. 9.16. Figure 9.17 shows the averages of the fitted values for traps with approximate 95 % confidence intervals and suggests that the only real difference here is for trap "CV" which collects more insects.

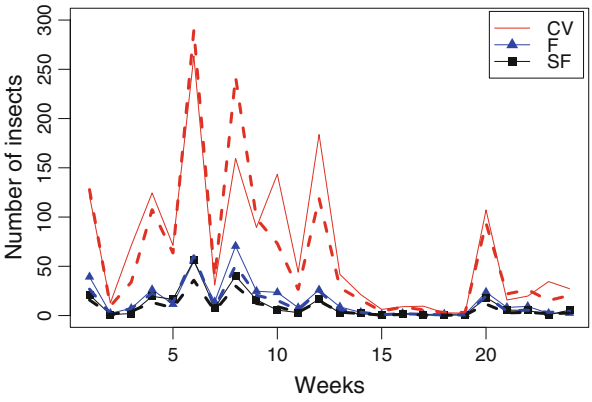

Fig. 9.16 Coffee berry borer trapping data – Plot of average predicted and observed counts over the 24 weeks, using a Poisson-normal model

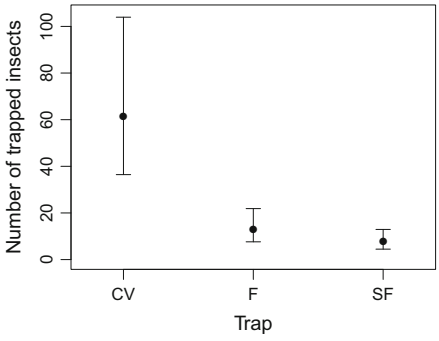

Fig. 9.17 Coffee berry borer trapping data – Plot of fitted counts for traps with Poisson-normal confidence intervals

9.3.3 Zero-Inflated Models

As for proportion data in Sect. 9.2.3, count data often show a higher incidence of zero counts than would be expected if the data were Poisson distributed, see Ridout et al. (1998). To modify the basic Poisson distribution to allow for extra zeros using a *zero-inflated Poisson* (ZIP) distribution, we augment the probability of zero by a proportion ω giving

$$\Pr(Y = y) = \begin{cases} \omega + (1-\omega)e^{-\theta} & y = 0 \\ (1-\omega)\dfrac{e^{-\theta}\theta^y}{y!} & y = 1, 2, \ldots \end{cases}$$

The mean is now $\mu = \mathrm{E}(Y) = (1-\omega)\theta$, while the variance is

$$\mathrm{Var}(Y) = (1-\omega)\theta(1+\omega\theta) = \mu + \mu^2\frac{\omega}{(1-\omega)}$$

which is greater than μ, unless $\omega = 0$, and has the same quadratic form as the negative binomial and Poisson-normal variances. In this sense we may think of it as a model for overdispersed count data, but data in which the overdispersion arises in a very specific way, through an excess of zeros. Zero-inflated forms of other count distributions, such as the negative binomial, can be defined similarly. For zero-inflated models it is also possible to include random effects in the linear predictor to account for overdispersion, correlation between measurements due to cluster sampling, longitudinal data, etc. As an alternative to zero-inflated models we can also consider the two-part hurdle model, with a logistic model for the occurrence/non-occurrence of zeros and a zero-truncated model for the non-zero counts.

In R, some of those models can be fitted using different packages as follows:

- `pscl` (Zeileis et al. 2008) allows the fitting of zero-inflated and hurdle Poisson and negative binomial models with regression models for both components, but without additional random effects;
- `glmmADMB` (Skaug et al. 2013) allows the fitting of mixed Poisson and negative binomial models, with constant zero-inflation;
- `gamlss` (Rigby and Stasinopoulos 2005) includes the fitting of mixed Poisson and negative binomial models, with zero-inflation modelled with covariates.

With regression modelling of both the core model linear predictor and, possibly, also of the zero-inflated and overdispersion parameter, these models can provide a flexible framework, but their application is not without problems, both in terms of model fitting and inference. As we saw with the zero-inflated overdispersed binomial model, there can be a substantial trade-off between zero-inflation and overdispersion making such models difficult to interpret.

9.4 Discussion

The aim of this chapter has been to demonstrate the utility of generalized linear models as the basis of a coherent and unified framework for the analysis of various types of entomological data. However, as we have seen, the core binomial and Poisson models for proportion and count data, respectively, are rarely adequate for data as encountered in practice, due to the presence of additional variability. Extensions to these models have been considered to allow for both structured and unstructured components of extravariation, including the presence of additional zeros. The basic ideas used to extend our core models can be further combined and generalized but the model fitting principles and approach to data analysis stay essentially the same, albeit with further levels of complication. We have tried to indicate some of the range of software available to fit these models, specifically in terms of R packages, although similar extended functionality exists in many other statistical software systems, such as SAS, Stata and Genstat. However, while we intended to show the practicising entomologist how to apply some of these

models, it is perhaps clear that it is not always straightforward – consultation and collaboration with a statistician may well be necessary for more complex datasets and analyses, most usefully at the beginning when designing the experiment. A completely different approach to the modelling discussed here would be through Bayesian statistical modelling and MCMC (Markov Chain Monte Carlo). We intend to present this in a future review chapter or article.

References

Amaral FSA, Poltronieri AS, Alves EB, Omoto C (2012) Efeito de óleos agrícolas no comportamento de oviposição e viabilidade de ovos de *Diaphorina citri* Kuwayama (Hemiptera: Psyllidae). In: XX Simpósio Internacional de Iniciação Científica da Universidade de São Paulo, 2012, Pirassununga

Bates D, Maechler M, Bolker B, Walker S (2013) lme4: linear mixed-effects models using Eigen and S4. R package version 1.0-5. http://CRAN.R-project.org/package=lme4

Battel, APMB (2012) Dinâmica de predação e resposta funcional em *Chrysoperla externa* (Neuroptera: Chrysopidae) sobre *Toxoptera citricida* (Hemiptera: Aphididae) aplicada à citricultura orgânica. Master's dissertation, ESALQ-USP, Piracicaba, São Paulo, Brazil

Breslow NE (1984) Extra-Poisson variance in log-linear models. J R Stat Soc Ser C Appl Stat 33:38–44

Collett D (2003) Modelling binary data. Chapman and Hall, London

Finney DJ (1971) Probit analysis. University Printing House, Cambridge

Hinde J (1982) Compound Poisson regression models. In: Gilchrist R (ed) GLIM 82: Proceedings of the international conference on generalized linear models, London. Springer, Berlin, pp 109–121

Hinde J, Demétrio CGB (1998) Overdispersion: models and estimation. Comput Stat Data Anal 27:151–170

Lawless JF (1987) Negative binomial and mixed Poisson regression. Can J Stat Rev Can Stat 15:209–225

Lesnoff M, Lancelot R (2013) aods3: analysis of overdispersed data using S3 methods. aods3 package version 0.4-1. http://CRAN.R-project.org/package=aods3

Lindsey JK (1995) Fitting parametric counting processes by using log-linear models. J R Stat Soc Ser C Appl Stat 44:201–212

Jørgensen B (2002) Generalized linear models. In: El-Shaarawi AH, Piegorsch WW (eds) Encyclopedia of environmetrics, vol 2. Wiley, Chichester, pp 873–880

Mallet J (1989) The evolution of insecticide resistance: have the insects won? Trends Ecol Evol 4:336–340

McCullagh P, Nelder J (1989) Generalized linear models. Chapman and Hall, London

McCulloch CE (1994) Maximum likelihood variance components estimation in binary data. J Am Stat Assoc 89:330–335

Morgan B (1992) Analysis of quantal response data. Chapman and Hall, London

Mota LHC (2013) Desenvolvimento de armadilha de auto-inoculação para o controlde de *Hypothenemus hampei* (Ferrari, 1867) (Coleoptera: Curculionidae) com *Beauveria bassiana* (Bals.) Vuil (Ascomycota: Hypocreales) em tecido sintético. Master's dissertation, ESALQ-USP, Piracicaba, São Paulo, Brazil

Nelder J (1985) Quasi-likelihood and glim. In: Gilchrist R, Francis B, Whittaker J (eds) Generalized linear models. Springer, Berlin, pp 120–127

Nelder J, Lee Y (1992) Likelihood, quasi-likelihood and pseudo-likelihood: some comparisons. J R Stat Soc Ser B Stat Methodol 54:273–284

Nelder J, Wedderburn R (1972) Generalized linear models. J R Stat Soc Ser A Stat Soc 135: 370–384

R Core Team (2013) R: a language and environment for statistical computing. R Foundation for Statistical Computing, Vienna. http://www.R-project.org

Ribeiro LP, Vendramin JD, Bicalho KU, Andrade MS, Fernandes JB, Moral RA, Demétrio CGB (2013) *Annona mucosa* Jacq. (Annonaceae): A promising source of bioactive compounds against *Sitophilus zeamais* Mots. (Coleoptera: Curculionidae). J Stored Prod Res 55:6–14

Ridout MS, Demétrio CGB, Hinde JP (1998) Models for count data with many zeros. In: International biometric conference 1998, Cape Town, pp 179–190

Rigby RA, Stasinopoulos DM (2005) Generalized additive models for location, scale and shape. J R Stat Soc Ser C Appl Stat 54:507–554

Skaug H, Fournier D, Nielsen A, Magnusson A, Bolker B (2013) Generalized linear mixed models using AD Model Builder. R package version 0.7.7. http://glmmadmb.r-forge.r-project.org/

Souza AR (2011) A interação *Wolbachia* – *Trichogramma galloi* Zucchi, 1988 (Hymenoptera: Trichogrammatidae). Master's dissertation, ESALQ-USP, Piracicaba, São Paulo, Brazil

Venables WN, Ripley BD (2002) Modern applied statistics with S. Springer, New York

Vieira A, Hinde J, Demétrio CGB (2000) Zero-inflated proportion data models applied to a biological control assay. J Appl Stat 27:373–389

Wedderburn R (1974) Quasi-likelihood functions, generalized linear models and the Gauss-Newton method. Biometrika 61:439–447

Williams DA (1982) Extra-binomial variation in logistic linear models. J R Stat Soc Ser C Appl Stat 31:144–148

Williams DA (1996) Overdispersion in logistic-linear models. In: Morgan B (ed) Statistics in toxicology. Clarendon Press, Oxford

Zeileis A, Kleiber C, Jackman S (2008) Regression models for count data in R. J Stat Softw 27:1–25. http://www.jstatsoft.org/v27/i08/

Index

A
Abiotic effects, 39–78
Aedes aegypti, 39, 40, 42, 81–105
Anthropogenic impacts, 111, 112, 114–118, 122, 123
Aquatic networks, 109–123
Autonomous model, 42, 46–48, 52–57, 63, 69, 77

B
Beta binomial, 232–236, 238, 239, 241, 242, 251
Binomial model, 219, 221–230, 232–235, 237–242, 246, 250–252, 257
Bioassessment, 110–114
Biocontrol model, 128
Biodiversity, 110, 112–114, 123
Biological control, 3, 130–135, 173, 220, 236, 239–243
Biomonitoring, 6, 109–123

C
Climate change, 3, 35, 82, 93, 110, 142
Coarse grid, 178, 187–193, 195–198, 200–203, 214
Community structure, 112, 113, 127, 128
Conservation, 2, 3, 6, 110, 113, 114, 123
Count data, 199, 221, 242–257

D
Demography, 2, 5, 11–36, 40, 44, 135
Dengue, 3, 6, 39–78, 81, 82, 89, 97, 102, 105
Dengue epidemiology, 56, 59
Density-dependence, 2, 4
Dispersal, 2, 6, 12, 13, 15, 16, 19–21, 23–28, 31–36, 112, 113, 115–117, 119–123, 142–147, 151, 152, 156, 160, 164, 166, 191

E
Ecological data, 210–213
Ecological modelling, 4, 6, 18, 28, 30, 32
Ecological monitoring, 190, 192, 196, 214, 215
Entomology, 5, 6, 12, 40–43, 48, 58, 60–77, 82, 88, 102, 105, 139, 144, 219–258
Environmental factors, 26, 102, 121, 143
Equilibrium, 5, 15, 33, 45–47, 52–54, 56, 57, 91, 94–100, 132, 158

F
Fitness, 88
Food web, 6, 12, 127–130, 132–135, 138
Foraging behaviour, 13, 27, 28, 35
Functional response, 12, 128–131, 136

H
Host-parasitoid dynamics, 12–20, 22, 27, 33, 36
Hydrographic networks, 113–114

C.P. Ferreira, W.A.C. Godoy (eds.), *Ecological Modelling Applied to Entomology*,
Entomology in Focus 1, DOI 10.1007/978-3-319-06877-0

I
Insect(s)
behaviour, 6, 143
population model, 1, 5, 62, 68, 138
Integrated pest management (IPM), 130–135, 166, 172–175, 177, 215
Interaction models, 35, 139

L
Landscape structure, 13, 36
Lattice model, 141–166
Life-cycle mosquitoes, 105
Long term dynamics, 132

M
Macroinvertebrates, 110, 111, 114
Mathematical modelling, 1–7, 42
Metacommunities, 6, 109–123
Metapopulation, 21, 22, 24–26, 28, 33, 34, 220
Monitoring, 6, 134, 173–178, 190–192, 196, 198, 202, 205, 206, 214, 215
Mosquitoes, 3, 6, 39–78, 81–105, 143

N
Negative binomial model, 250–252, 257
Non-linearity, 226
Numerical integration, 6, 177–188, 190–204, 206, 208–210, 213–215

O
Overdispersed data, 6, 219–258
Overdispersion model, 221, 227–238, 242, 246–256

P
Patch dynamics, 26, 112, 113
Patchy invasion, 195, 196, 202
Pest
abundance, 6, 172–178, 194, 205–214
control, 134, 173
management, 6, 130–135, 166, 172–174, 206
Physiological parameters, 82
Poisson model, 243–248, 250, 252, 253, 257
Population dynamics, 2, 4–6, 13, 24, 34, 39–78, 96, 127–139, 192, 196
Public health, 3

Q
Quantitative ecology, 4, 128

R
Repellents, 91, 142, 143, 153–157, 162, 166
Reproductive strategy, 13, 26–34, 36, 128
River In Vertebrate Prediction And Classification System (RIVPACS), 111, 114–123

S
Sex ratio, 2, 12, 13, 15–18, 22, 26–35
Spatial dynamics, 112
Spatial structure, 11–36, 113, 114, 121, 122, 144–150, 196, 200, 214
Spatio-temporal dynamics, 144, 150
Spreadable particles, 142
Statistical modelling, 110, 258
Subpopulations, 19, 24, 25, 32, 33, 51, 94

T
Temperature, 3, 6, 40–53, 58, 59, 61, 63–78, 81–105
Traps, 172, 174, 176–178, 190–192, 194–204, 206, 213–215, 252–256
Trophic interactions, 4, 6, 25, 127–139, 142

Z
Zero-inflated models, 239–242, 256–257